

Study on Trajectory Planning of Surgical Manipulator  
Considering Visualization and Operability in Narrow  
Workspace for Pediatric Surgery

小児外科における狭い空間での視野確保と操作性を  
考慮したマニピュレータの動作計画に関する研究

February, 2015

Quanquan LIU



Study on Trajectory Planning of Surgical Manipulator  
Considering Visualization and Operability in Narrow  
Workspace for Pediatric Surgery

小児外科における狭い空間での視野確保と操作性を  
考慮したマニピュレータの動作計画に関する研究

February, 2015

Department of Integrative Bioscience and Biomedical Engineering  
Graduate School of Advanced Science and Engineering  
Waseda University

Quanquan LIU



*To my dear family and my friends*



# ACKNOWLEDGMENTS

*“We can't solve problems by using the same kind of thinking we used when we created them.”*

*-Albert Einstein*

This research had been performed in Waseda University, Japan, from 2011 to 2014. Without supports by many people, I cannot successfully complete this thesis. Therefore, I would like to express my honest thanks here. My deepest gratitude goes first and foremost to my supervisor, Prof. Masakatsu G. Fujie who is a professor in Waseda University, for his constant encouragement and guidance. He is a knowledgeable, insightful professor, has taught me not only scientific knowledge, but also the generous man's life way. Without his consistent and warm-hearted instruction for my research life in Japan, my study would not be continued abroad. In my whole life, I will be proud that I was a member of Fujie laboratory.

I also would like to express my heartfelt gratitude to Prof. Atsuo Takanishi, Prof. Shigeki Sugano, Prof. Tomiyuki Miyashita, Prof. Toshio Chiba who are the sub-supervisors for my study. They give suggestions to guide me to complete my thesis with great deal of patience and professionalism. With their valuable guidance, I could successfully finish this thesis and make it more desirable.

In Fujie laboratory, I would like to express my sincere thanks to Associate Prof. Yo Kobayashi, Assistant Prof. Kazuya Kawamura in Chiba University, Secretary Ms. Masami komiya, Ms. Harumi Miyata, and my senior colleagues: Dr. Takeharu Hoshi, Dr. Bo Zhang, Dr. Takao Watanabe, Dr. Masatoshi Seki, Dr. Hiroki Watanabe, Dr. Jun Inoue, Dr. Elgezua Inko, and Dr. Songha Song, Dr. Yasutaka Nakashima. During the Ph.D studying course, I received

many kind helps and valuable suggestions for my research and life in Japan. I would like to express my special thanks to Associate Prof. Yo Kobayashi and Dr. Bo Zhang for their help to me with technical discussion during my writing thesis.

I would like to thank my peers: Dr. Jing Ye, Dr. Nozomu Yamazaki. Without your help, I cannot smoothly carry on the graduation process. And also thank doctoral course students: Ms. Xiaowei Lu, Ms. Mariko Tsukune, Mr. Satoshi Miura, Mr. Yuya Matsumoto, Mr. Yang Cao, Master's graduates: Ms. Aiko Jeannette. I wish good luck to all members in Fujie laboratory.

Before and during my study in Japan, I have received many helps from Prof. Weiguang Li, Prof. Liangzhong Jiang, and Dr. Chunbao Wang from South China University of Technology, China. You are the initiators for my research on robotics and automatics field. I would like to express my deep appreciation to you.

In here, I would like to express my sincere thanks to China Scholarship Council (CSC), China and Global COE (Centers of Excellence) Program "Global Robot Academia", from the Ministry of Education, Culture, Sports, Science and Technology of Japan, without your financial support, I cannot focus on my research in Japan.

Above all, I would like to appreciate my family. Firstly, I would like to express my hearty thanks to my three elder sisters. They are always solid united and take care of our family no matter what happens. Without their sincere dedication, I cannot wholeheartedly leave hometown and study abroad. Lastly, I would gratefully appreciate my parents with all my heart. Although they are just common farmer in China, my parents have taught me how to be an honest, brave, upright and persistent man since my childhood. They selfless dedicate everything for their daughters and son. Their encouragement is my motivation to face with the reality and unswervingly pursue my dream. I would like to express the best appreciation to them repeatedly.

I dedicate this thesis to my dear family and people who care and help me.

2015.2.10 at Tokyo

Quanquan Liu



# ABSTRACT

Minimally invasive surgery (MIS) is a particular way of performing surgery by using smaller instruments and smaller incisions than traditional surgical methods. The goal of the MIS is to perform operations through very small incisions, a relatively smaller size of the incisions than that used in traditional surgery with equal or superior clinical outcomes and less impact on a patient's body and organs. Generally, surgical instruments and endoscope approach the surgical site through small incisions in the MIS process. In order to arrange the instruments and endoscope at the surgical site, an inflated cavity is usually created via an artificial pneumoperitoneum at the beginning of the MIS. This method takes advantages of using the elastic sealed cavity of human body, such as the abdomen, to build the pneumoperitoneum. Generally, a 40~50 mm incision is created for adult esophageal atresia repair surgery. However, to pediatric patient, such as the congenital esophageal atresia surgery, the workspace is about 30x30x30 mm near the fourth intercostal of the right side of chest, which is very tight to place two or three manipulator and an endoscope simultaneously. Furthermore, the surgical manipulator can easily to block endoscopic vision during performing surgical procedures in the narrow space.

The robotic assistance technologies extended the capabilities of surgeons by progress of computer-aided technology and dexterous manipulator. Compared with the traditional MIS, utility of robotic assistance surgical system breaks the law that surgeon must perform operation besides operating table. In order to smoothly operate in narrow workspace, forceps manipulator should be designed with small size and high rigidity. Compact surgical manipulator with multiple Degree of Freedoms (DoFs) is becoming hot issue used for tissue intervention. In the robotic assisted system, remote control is commonly employed to map the

movement of a user input to the surgical manipulator. Remote control, also known as master-slave control, is widely used in robotic surgical systems. It provides beneficial results via taking advantages of less restriction by space in operation room (OR), reduced fatigue to operators because of ergonomic input devices, reduced surgical trauma to patients with dexterous instruments. Based on the configuration of manipulators, mapping relation between master input device and slave actuator would be mathematical computed. Surgeon steer two user inputs to control the slave manipulators through master-slave control architecture during operation, while guided by visual feedback from a visual module. However, although the multi-DoF surgical manipulator improves the dexterity on operation, it poses new challenges on the robotic control. Generally, with the consideration of ergonomics, the master input and the slave manipulator are isomeric, therefore, the surgical manipulator in the slave side cannot complete map the posture of the overall master mechanism. The user of the robotic system mainly pays attention to the position and posture of the forceps of the surgical manipulator during operation. In order to obtain good eye-hand coordination, the posture of master handle in surgeon's vision and that of the surgical manipulator tip in the endoscopic view should be identical. To the redundant serial manipulator, there are many solutions for the redundant joints in the inverse kinematics computation, even though the position and posture of the forceps of the manipulator is unique. In order to select out the optimal solution, the constraints of surgery will be considered. In the pediatric surgery, the MIS can reduce the geometric cut size on the body surface, but increase the risk of hurting pediatric organ by pneumoperitoneum.

In this study, we aim to design a robotic system to assist pediatric Congenital Esophageal Atresia (CEA) surgery. Pediatric CEA is a birth defect that affects the alimentary tract, occurs in approximately 1 in 4400 live births. Pediatric CEA takes several different forms often involving one or more fistulas connecting the trachea to the esophagus. In approximately 85% of cases, the esophagus ends in a blind-ended pouch, rather than connecting normally to the stomach. Without treatment, the infant will soon die due to malnutrition. Currently, the most immediate and effective treatment in the majority of pediatric CEA is a surgical repair to close the fistulas and reconnect the two ends of the esophagus to each other in a 30x30x30 mm workspace. However, current robotic system exposed obvious drawbacks: manipulator with small geometric dimension (diameter  $\leq 5$ mm) is danger due to high risk of damaging pediatric tender organ; manipulator with large geometric dimension (diameter  $\geq 10$  mm) is difficult to operate in narrow space due to the

vision shielded by manipulator in endoscopic surgery. In this thesis, the author indicates a compact surgical robot for pediatric surgery. It can realize dexterous operation by two slave manipulators, each with an external diameter of 8 mm at the forceps. In order to reduce the shelter of vision caused by manipulator during operation, an algorithm to control redundant manipulator is developed to map the trajectory while the forceps of manipulator tracking the position and posture of the user input, maintaining triangle formation between slave manipulators and endoscope.

This thesis consists of 6 chapters.

In chapter 1, the author introduces the state of the art of minimally invasive surgery (MIS) as well as the utility of surgical robot, especially in pediatric surgery. The author also presents the remaining problem and technique issue of current robotic system, and states the purpose of this research and the research flow.

In chapter 2, the author describes the typical control method of computer-aided robotic system, and states the control strategy of remote-control robot system. Since this research needs to map the trajectory relation between user input and slave manipulator, the author considers the influence of the mechanism configuration of surgical robot in the control strategy for performing intervention in narrow workspace on surgery.

In chapter 3, the author presents the mechatronics design of pediatric surgical robot. The surgical robot consists of a master console and slave manipulators. The master console is composed of Phantom Omni and foot pedals to generate input signals. In the slave side of surgical robot, it consists of two isomorphic slave manipulators, with total 18 DoFs. Each slave manipulator is composed of a positioning manipulator and a surgical tool manipulator. The positioning manipulator has 4 DoFs, which can achieve translational movements in spatial movement. The surgical tool manipulator employs double screw drive (DSD) mechanism to achieve bendable movements. A single surgical tool manipulator with 5 DoFs and an external diameter of 8 mm consists of two bendable joints and a rotatable forceps. Each bendable joint can realize two bending movements in two orthogonal planes. The rotatable forceps is composed of a rotatable joint and a clipper with opening and closing movement. In this chapter, the kinematics of the slave manipulator is calculated. The simulation results show the overlapped area of two positioning manipulator covers a 30x30 mm zone; and the distal of the surgical tool manipulator can achieve an arbitrary bending movement in 40x40x13 mm workspace by two bendable joints. By integrating tool manipulator with positioning manipulator, the robot system can perform surgical intervention

in a 30x30x30 mm workspace in pediatric surgery. The inverse kinematics for calculating active rod's length illustrated that the rod's deviation of bending linkage is less than 3 mm. The experiment to measure the flexible shaft's rigidity show the flexible shaft could keep high rigidity when loaded within 200 g.

In chapter 4, the author proposes a shape optimal algorithm to map the relation between master input and the slave manipulator. The purpose of this algorithm aims to construct a triangle formation between endoscope and the slave manipulators to provide good operability and visualization for robot user. Due to the heterogeneous configuration between the master input and the slave manipulator, the posture of each joint in the master input cannot complete match with the slave mechanism chain. Therefore, the master input just directly control the position and posture of the distal of the manipulator, the redundant joints of manipulator will be controlled by the proposed algorithm. In the first step, the relation between the robot joint's inverse kinematics solution and the disturbance at redundant joint is established. The verification simulation shows that the robotic arm with the inverse kinematic algorithm can accurately track the input ( $\Delta_{simulator} < 0.5mm$ ). Subsequently, a shape optimal algorithm considering the visualization and operability is developed to construct a triangle formation between slave manipulators and endoscope in workspace. Given a tolerable error ( $\varepsilon = 0.001$ ), the adjacent angle deviation between two bendable joints among the 4 quadrants satisfy that  $\Delta_{angle\_deviation} < 0.5^\circ$ . The experimental result of position tracking with the shape optimal algorithm demonstrated that the distal of the manipulator could achieve position error  $\Delta_{position\_error} < 1mm$  when loaded within 50 g in two-dimensional plane or loaded within 20 g in three-dimensional space. Therefore, the pediatric surgical robot satisfies the precision requirement of tissue intervention in pediatric CEA surgery.

In chapter 5, the author presents a novel application for reducing operating difficulty to the master-slave robot user. Generally, human being have dexterous hand than the other, therefore, they are willing to use their dexterous hand for important manipulation, even though their both hands are needed in normal operation. The author extends the algorithm referred in chapter 4 by using two endoscopes in the pediatric surgical robot. The two endoscopes located at both sides with respect to the plane, where the both slave manipulators located. Therefore, there are two solutions by combining a single endoscope and two slave manipulators. In addition, the correspondence between the master input and the slave manipulator can be exchanged based on the selection of combination between the endoscope and the slave manipulator. The algorithm guarantees the operator of this robot system to use their dexterous

hands for important operation even performing suture task on both sides of a cut. The experimental results show that the time taken for the same task with the handedness control obviously improves user's performance and the feasibility of suture on an esophagus model by using the developed algorithm.

In chapter 6, the author concludes this research and discusses future work, such as the evaluation of pediatric surgical robot through *in vivo* experiments, and the clinical applications of using pediatric surgical robot as well as the control algorithm in serial robotic manipulator.

In this overall research, the author establishes a compact robot system for pediatric surgery. Considering the narrow space of pediatric surgery, the author proposes an algorithm to control the trajectory of redundant manipulator. From this research, the author establishes a way to perform tissue intervention with surgical robot in narrow workspace for pediatric surgery.

# TABLE OF CONTENTS

- Chapter 1 Introduction.....1**
- 1.1 Background..... 1
  - 1.1.1 Minimally Invasive Surgery..... 1
  - 1.1.2 Surgical Robot System ..... 4
- 1.2 Robot-assisted Pediatric Surgery..... 9
- 1.3 Technical Issue for Robot-assisted Pediatric Surgery ..... 11
  - 1.3.1 Current Limitation in Robot-assisted Pediatric Surgery ..... 11
  - 1.3.2 Technical Issue for Robot-assisted Pediatric Surgery ..... 12
- 1.4 Research Objective and Motivation ..... 12
  - 1.4.1 Pediatric Congenital Esophageal Atresia..... 12
  - 1.4.2 Motivation..... 13
- 1.5 Structure of this Thesis ..... 14
  
- Chapter 2 Control Strategy of Redundant Robotic Manipulator.....19**
- 2.1 Introduction ..... 19
- 2.2 Control Method of Redundant Robotic Manipulator ..... 20
- 2.3 Discussion..... 22
- 2.4 Comparison between Current Surgical Robotic System and the Proposed System..... 25
  
- Chapter 3 Mechatronics Design of Pediatric Surgical Robot.....27**
- 3.1 Introduction ..... 27
- 3.2 Overview of Pediatric Surgical Robot..... 28

3.3 Configuration of the Left Slave Arm.....	29
3.3.1 Mechanism Type Selection for Compact Design .....	30
3.3.2 Positioning Manipulator .....	34
3.3.3 Surgical Tool Manipulator.....	37
3.3.4 Visual Module Design .....	40
3.4 Forward Kinematics of the Left Slave Arm .....	42
3.4.1 Nomenclature of the Feature Points .....	42
3.4.2 Forward Kinematics.....	45
3.5 Inverse Kinematics of the Left Slave Arm .....	51
3.6 Rod's Length Computation .....	57
3.7 Transmission Medium .....	61
3.8 Discussion.....	63

## **Chapter 4 Control Strategy of Redundant Robotic Manipulator in Narrow**

<b>Workspace.....</b>	<b>65</b>
4.1 Introduction .....	65
4.2 Inverse Solutions corresponding to Disturbance.....	66
4.2.1 Inverse Solution Algorithm .....	66
4.2.2 Algorithm Verification .....	69
4.3 Visualization in Narrow Workspace.....	77
4.4 Operability in Narrow Workspace.....	80
4.5 Motion Modeling and Parameterization .....	82
4.5.1 Nomenclature of Robot Bending.....	82
4.5.2 Shape Optimization of Tool Manipulator Configuration .....	83
4.5.3 Shape Optimization of Slave Arm Configuration .....	90
4.5.4 Example Simulation.....	93
4.6 Experiments with Pediatric Surgical Robot.....	101
4.6.1 Accurate Control of Bendable Joints.....	101
4.6.2 Trajectory Control in Narrow Workspace .....	110
4.6.3 Manipulation without/with Redundant DoF Control Algorithm.....	117
4.7 Discussion.....	121

<b>Chapter 5 Handedness Control with Pediatric Surgical Robot.....</b>	<b>123</b>
5.1 Introduction .....	123
5.2 Handedness Control.....	124
5.2.1 Handedness .....	124
5.2.2 Hypothesis .....	124
5.2.3 User Interface and System Control.....	126
5.3 Handedness Control Experiment with Pediatric Surgical Robot .....	128
5.3.1 Handedness Control for Ring Transfer Task .....	128
5.3.2 Handedness Suture Manipulation in Narrow Workspace.....	132
5.4 Discussion.....	135
<b>Chapter 6 Conclusion and Future Work.....</b>	<b>137</b>
6.1 Conclusion.....	137
6.1.1 Master-slave Pediatric Surgical Robot for Narrow Workspace.....	137
6.1.2 Control Strategy of Redundant Manipulator in Narrow Workspace .....	138
6.1.3 Handedness Control with Pediatric Surgical Robot .....	139
6.2 Future Work.....	139
<b>Appendix A Aurora System .....</b>	<b>141</b>
A.1 Description .....	141
A.2 Important Feature .....	141
A.3 System Component.....	142
A.4 Measurement Volume .....	143
A.5 Aurora System Accuracy.....	143
<b>Appendix B Super Extra Fine 2.9 mm Borescope .....</b>	<b>145</b>
B.1 Description.....	145
B.2 Main Feature .....	145
B.3 Specification .....	146
<b>Appendix C Phantom Omni .....</b>	<b>147</b>
C.1 Description.....	147



C.2 Highlighted Feature .....	147
C.3 Specification .....	148
<b>Reference .....</b>	<b>149</b>
<b>Research Achievement.....</b>	<b>161</b>

# LIST OF ABBREVIATIONS

MIS	Minimally Invasive surgery
CEA	Congenital Esophageal Atresia
ICEA	Infant Congenital Esophageal Atresia
DoF	Degree of Freedom
SCARA	Selective Compliance Assembly Robot Arm
DH	Denavit-Hartenberg
SPS	Single Port Surgery
OR	Operation Room
TEF	Trachea-Esophageal Fistula
NOTES	Natural Orifice Translumenal Endoscopic Surgery
VFs	Virtual Fixtures
PQs	Proximity Queries
DACs	Dynamics Active Constraints
SPAS	Single Port Access Surgery
MRI	Magnetic Resonance Imaging
CT	Computerized Tomography
LS	Laparoscopic Surgery
OS	Open Surgery
DSD	Double Screw Drive

# LIST OF FIGURES

Figure 1.1 Configuration of laparoscope and instruments in myomectomy of fibroids removing surgery [5].....	2
Figure 1.2 ROBODOC® .....	5
Figure 1.3 Neuromate® .....	5
Figure 1.4 ZEUS® .....	6
Figure 1.5 da Vinci® robot system. ....	7
Figure 1. 6 Insertable robotic effector platform for single access surgery [32]. ....	8
Figure 1.7 NOTES robot in USGI Medical® [34].....	8
Figure 1.8 General case of congenital esophageal atresia (CEA).....	13
Figure 1.9 Structure of this thesis.....	17
Figure 2. 1 Triangle formation of bimanual surgical manipulation. ....	23
Figure 2.2 da Vinci Si® .....	23
Figure 2.3 Manipulation with both hands (right hand preferred).....	24
Figure 2.4 The proposed method.....	25
Figure 3.1 Overview of pediatric surgical robot. ....	28
Figure 3. 2 Schematic diagram of a compact robot located on pediatric patient. ....	30
Figure 3. 3 Location between pediatric patient and the surgical robot. ....	31
Figure 3. 4 Mechanism type proposal for positioning manipulator.....	33
Figure 3.5 Overview of the positioning manipulator. ....	35

Figure 3.6 Drive principle of SCARA mechanism. ....	36
Figure 3.7 Overview of the surgical tool manipulator. ....	38
Figure 3.8 Mechanical configuration of bendable joints,.....	39
Figure 3.9 Mechanism of gripper .....	40
Figure 3.10 Configuration of the visual module in the surgical robot system.....	41
Figure 3. 11 Relation between length T4 and the bending angle $\theta$ .....	43
Figure 3. 12 Mechanism of the visual module in the surgical robot system.....	43
Figure 3.13 Nomenclature of the left arm. ....	44
Figure 3.14 Workspace of the positioning manipulator. ....	48
Figure 3.15 Nomenclature of the tool manipulator. ....	50
Figure 3. 16 Workspace of the tool manipulator.....	51
Figure 3. 17 Feature points for rod's length calculation. ....	57
Figure 3. 18 Relation of rod's length and bending angle in segment I. ....	60
Figure 3.19 Relation of rod's length and bending angle in segment II. ....	61
Figure 3. 20 Components of flexible shaft.....	61
Figure 3. 21 Experimental platform for verifying transmission accuracy of flexible shaft. ...	62
Figure 3. 22 Relation between motor's rotation angle and deviation of screw-nut driven by flexible shaft. ....	63
Figure 4. 1 Movement of redundant joint when disturbance at point B3.....	67
Figure 4. 2 Modeling the surgical robot in Adams. ....	70
Figure 4. 3 Control diagram of simulator in Matlab. ....	71
Figure 4. 4 Surgical robot in the simulator. a). isometric view, b) top view, c) front view. ....	72
Figure 4. 5 Expect value and the measured value in the simulator of translational joint $\theta_{1s}$ of the positioning manipulator.....	73
Figure 4. 6 Expect value and the measured value in the simulator of rotary joint $\theta_{2s}$ of the positioning manipulator.....	73
Figure 4. 7 Expect value and the measured value in the simulator of rotary joint $\theta_{4s}$ of the positioning manipulator.....	74

Figure 4. 8 Expect value and the measured value in the simulator of rotary joint $\theta_{3s}$ of the positioning manipulator.....	74
Figure 4. 9 Expect x axial position and the measured value in the simulator of the distal of the tool manipulator. ....	75
Figure 4. 10 Expect y axial position and the measured value in the simulator of the distal of the tool manipulator. ....	75
Figure 4. 11 Expect z axial position and the measured value in the simulator of the distal of the tool manipulator. ....	76
Figure 4. 12 Expect Mag position and the measuredvalue in the simulator of the distal of the tool manipulator. ....	76
Figure 4. 13 The positional relation between endoscope and surgical cavity.....	77
Figure 4. 14 Triangle formation of bimanual surgical operation. ....	80
Figure 4. 15 Relation between the tool manipulator and the surgical cavity's edge.....	81
Figure 4. 16 Shape illustration of tool manipulator. ....	84
Figure 4. 17 Deviation between $\angle P1P2P3$ and $\angle P2P3P4$ within the range for searching optimal bending state in the 1 <sup>st</sup> quadrant.....	86
Figure 4. 18 Deviation between $\angle P1P2P3$ and $\angle P2P3P4$ within the range for searching optimal bending state in the 2 <sup>nd</sup> quadrant.....	87
Figure 4. 19 Deviation between $\angle P1P2P3$ and $\angle P2P3P4$ within the range for searching optimal bending state in the 3 <sup>rd</sup> quadrant. ....	88
Figure 4. 20 Deviation between $\angle P1P2P3$ and $\angle P2P3P4$ within the range for searching optimal bending state in the 4 <sup>th</sup> quadrant. ....	89
Figure 4. 21 Configuration of the robot and the surgical cavity for collision avoidance algorithm. ....	95
Figure 4. 22 Joint value of SCARA manipulator with/without collision avoidance algorithm ( $\Delta x=5, \Delta y=0$ ).....	95
Figure 4. 23 Joint value of SCARA manipulator with/without collision avoidance algorithm ( $\Delta x=3, \Delta y=0$ ).....	96
Figure 4. 24 Joint value of Tool manipulator with/without collision avoidance algorithm ( $\Delta x=5, \Delta y=0$ ).....	96

Figure 4. 25 Joint value of Tool manipulator with/without collision avoidance algorithm ( $\Delta x=3, \Delta y=0$ ).....	97
Figure 4. 26 Joint value of SCARA manipulator with/without collision avoidance algorithm ( $\Delta x=3, \Delta y=3$ ).....	97
Figure 4. 27 Joint value of tool manipulator with/without collision avoidance algorithm ( $\Delta x=3, \Delta y=3$ ).....	98
Figure 4. 28 The visuable ratio of tool manipulator corresponding to different $\Delta x$ and $\Delta y$ when bent angle = $50.2^\circ$ .....	99
Figure 4. 29 The visuable ratio of tool manipulator corresponding to different $\Delta x$ and $\Delta y$ when bent angle = $50.0^\circ$ .....	99
Figure 4. 30 Visible ratio of the tool manipulator under collision avoidance algorithm. ....	100
Figure 4. 31 Ratio deviation caused by $\Delta y$ corresponding to differience of $\Delta x$ .....	100
Figure 4. 32 Experimental platform for accuracy verification. ....	101
Figure 4. 33 Experiment sence of accuracy during bendable movement.....	102
Figure 4. 34 Experimental results without compensation algorithm when the tip bent from $45^\circ$ to $90^\circ$ .....	103
Figure 4. 35 Experimental results with compensation algorithm when the tip bent from $45^\circ$ to $90^\circ$ .....	104
Figure 4. 36 Experiment setup of bent motion with load.....	105
Figure 4. 37 Position tracking of sensor 3 at the 2 <sup>nd</sup> bendable joint in xoz plane.....	106
Figure 4. 38 Position tracking of sensor 2 at the 1 <sup>st</sup> bendable joint in xoz plane.....	106
Figure 4. 39 Position tracking of sensor 2 at the 1 <sup>st</sup> bendable joint when the manipulator's tip bent $30^\circ$ and rotated $30^\circ$ simultaneously in 3D space.....	107
Figure 4. 40 Position tracking of sensor 3 at the 2 <sup>nd</sup> bendable joint when the manipulator's tip bent $30^\circ$ and rotated $30^\circ$ simultaneously in 3D space.....	108
Figure 4. 41 Illustration of experiment 2.....	110
Figure 4. 42 Experimental platform for robot trajectory planning.....	111
Figure 4. 43 Manipulation sence when the right arm actuated..	112
Figure 4. 44 Simulation and experimental data in sensor 1..	113
Figure 4. 45 Simulation and experimental data in sensor 2..	114

Figure 4. 46 Simulation and experimental data in sensor 3..	115
Figure 4. 47 Relation between tip's bent angle and the distance that tool manipulator to the surgical cavity.	116
Figure 4. 48 Experimental platform for ring transfer.	117
Figure 4. 49 Ring transfer task by left surgical manipulator.	118
Figure 4. 50 Manipulation scenes with surgical robot for ring transfer task by left surgical manipulator.	119
Figure 4. 51 Manipulation scenes with surgical robot for ring transfer task by right surgical manipulator.	120
Figure 4. 52 Manipulation scenes with surgical robot for ring transfer task between both hands.	121
Figure 5. 1 Correspondence between master input and the slave manipulator in the master-slave robotic system.	125
Figure 5. 2 Expected manipulation manner at unnatural work task.	125
Figure 5. 3 Mode switch when working at unnatural state	126
Figure 5. 4 Control frame for handedness control with surgical robot. left U: left user input; right U: right user input; left S: left slave manipulator; right S: right slave manipulator.	127
Figure 5. 5 Experiment setup.	128
Figure 5. 6 Image of ring transfer task by user's preferred hand (yellow frames are endoscopic view).	129
Figure 5. 7 Configuration of ring transferring task with handedness control.	129
Figure 5. 8 Manipulation scene after exchange of the correspondence between the master, the slave and visual modules.	130
Figure 5. 9 Time taken to complete the three tasks by five trails.	131
Figure 5. 10 Experimental setup of handedness control for suture task.	132
Figure 5. 11 Suture manipulation on the right side by right slave manipulator with right Phantom Omni.	133

Figure 5. 12 Suture manipulation on the left side by left slave manipulator with right Phantom Omni.....	134
Figure 5.13 Suture result on the esophageal model by the left slave manipulator.....	135
Figure A. 1 Aurora system.....	142
Figure A. 2 Aurora system measurement volumes.....	143
Figure A. 3 System accuracy (6 DoFs sensor).....	144
Figure B. 1 Super extra fine 2.9 mm industrial video borescope.....	146



# LIST OF TABLES

Table 1- 1 Comarison between open surgery and laparoscopic surgery on typical surgical operation.....	2
Table 1- 2 Comparision between open surgery and laparoscopic surgery in pediatric surgery [1] .....	3
Table 1- 3 Robotically assisted procedures for children [36] .....	9
Table 1- 4 Comparison between robot-assisted pediatric surgery and open/conventional laparoscopic surgery [36] .....	10
Table 2- 1 Comparison between current surgical robotic system and the proposed system....	26
Table 3- 1 Comparison among three typic robots [86][87][88][89] .....	34
Table 3- 2 Geometric dimension of links in the SCARA .....	36
Table 3- 3 Specifications of Maxon motor (EC-max 16 type 283835) [90] .....	37
Table 3- 4 Specification of Reduction (CSF-5-30-1U) [91] .....	37
Table 3- 5 Geometric dimension and joint range of the visual module .....	42
Table 3- 6 Geometric dimension of the slave arm .....	45
Table 3- 7 DH parameter of the positioning manipulator .....	46
Table 3- 8 Kinematics parameter of the tool manipulator .....	49

Table 4- 1 Coordinate of the feature point in the left arm.....	69
Table 4- 2 The given value mapped from master input to the left arm.....	71
Table 4- 3 Steps of shape optimal algorithm for searching bending solutions .....	86
Table 4- 4 Inverse solution of bendable joint based on shape optimal algorithm in the 1 <sup>st</sup> quadrant.....	87
Table 4- 5 Inverse solution of bendable joint based on shape optimal algorithm in the 2 <sup>nd</sup> quadrant.....	88
Table 4- 6 Inverse solution of bendable joint based on shape optimal algorithm in the 3 <sup>rd</sup> quadrant.....	89
Table 4- 7 Inverse solution of bendable joint based on shape optimal algorithm in the 4 <sup>th</sup> quadrant.....	90
Table 4- 8 Steps for computing the inverse solution of the redundant manipulator .....	93
Table 4- 9 Nomenclature points and master input .....	94
Table 4- 10 Deviation conditions for computing new solutions .....	94
Table A- 1 Cube volume- position errors.....	143
Table A- 2 Cube volume- orientation errors .....	143
Table B- 1 Specification of HNL-2.9 CAM.....	146
Table C- 1 Specifications of Phantom Omni .....	148

# LIST OF SYMBOLS

## Chapter 2

$q$	$(n \times 1)$ vector of joint variables
$x$	$(m \times 1)$ vector of task variables
$J$	$(m \times n)$ Jacobian matrix

## Chapter 3

$L_{si}$	Link length of SCARA mechanism
$S_i$	Geometric dimension of the visual module
$T_i$	Joint range of the visual module
$L_i$	Geometric dimension of the slave manipulator
$d_n$	Linkage length of the slave manipulator
${}^{i-1}T_i$	Homogeneous transformation matrix
$\theta_{pi}$	Joint variables of the positioning manipulator
$\theta_i$	Joint variables of the tool manipulator
$(P_x, P_y, P_z)$	Position of distal in the tool manipulator
$T_{up}$	Homogeneous transformation matrix of the distal of the tool manipulator
$M_i$	Rotary point of the universal joint in the segment I

$N_i$	Rotary point of the universal joint in the segment II
$S$	Translational distance of nut

## Chapter 4

$\theta_{iN}$	Joint variables of the tool manipulator after deviation
$\theta_{iS}$	Joint variables of the positioning manipulator after deviation
$\lambda$	Visible ratio of tool manipulator under endoscopic vision
$f_{(R,d)}$	Deviation of tool manipulator and surgical cavity boundary
$d_{M_1M_3\_E_1E_3}$	Distance between skew line $M_1M_3$ and $E_3E_4$
$q_c$	Bent angle of the distal segment corresponding to horizontal plane
$\varphi$	Rotary angle of the distal segment along z-axis
$\varepsilon$	Tolerable error
$\Delta_{angle\_deviation}$	Angle deviation between the two adjacent bendable joints in the tool manipulator
$\Delta(x, y, z)$	Total deviation of the distal of the positioning manipulator
$\theta_{com}$	Angle for compensation of backlash in the bending motion of the universal joint
$\Delta_{position\_error}$	Position tracking error of the manipulator's tip during bent motion

# Chapter 1

## Introduction

### 1.1 Background

#### 1.1.1 Minimally Invasive Surgery

Minimally invasive surgery (MIS), typically known as laparoscopic surgery, has obvious advantages to patients, such as less postoperative pain, decreased inflammatory response, shorter hospital stay and convalescence, improved cosmesis [1]. The emerging of new technologies (e.g. advanced machining technologies, innovative laparoscopes, special materials and efficient energy sources) pushed forward rapid development and popularization in MIS [2].

In the classical way to perform a surgery, generally, an open incision is created in the skin and the underlying tissues. The surgeon can directly reach the tissue to be operated on with their hands through the open incision. In this way, the surgeon has directly tactile feeling about the handled tissue and unrestricted view on the operating field. However, the open surgery brings much damage to healthy tissue, such as tear healthy tissue, accidentally destroy healthy organs. MIS is a special way of performing surgery by using smaller surgical apparatus and smaller incisions than that used in traditional surgical process, as shown in Fig. 1.1. The goal of MIS is to perform operations with equal or superior clinical outcomes and less

## 1. Introduction

negative impact on a patient's body and healthy organs by using special instruments. In 1910, Hans *et al.* reported the first laparoscopic operation in human being, by using a special trocar and a 14-cystoscope for endoscopy [3]. In the subsequent several decades, a great deal of individuals contributed the approach further for laparoscopy. In the early 1970s, Tarasconi from the University of Passo Fundo used laparoscopy to perform organ resection for the first time [4]. Subsequently, laparoscopy to remove appendicitis, ovarian cyst enucleation, myomectomy for fibroids and vaginal hysterectomy on adult patient were reported [5][6]. The comparison between open surgery and laparoscopic surgery on typical surgical operation are listed in table 1-1.

Table 1- 1 Comparison between open surgery and laparoscopic surgery on typical surgical operation

Type	Laparoscopic surgery (LS) VS open surgery (OS)
Inguinal hernioplasty	LS is safe and effective, however, the recurrence rates are a little higher than that happened in OS [7]
Cholecystectomy	LS benefits from shorter hospital stay, less pain [8]
Splenectomy	LS is suffered from longer operative time, benefited from less blood loss, shorten recovery [9]
Esophageal surgery	Similar symptomatic and physiologic outcomes, but LS gets better quality-of-life outcomes [10] [11]

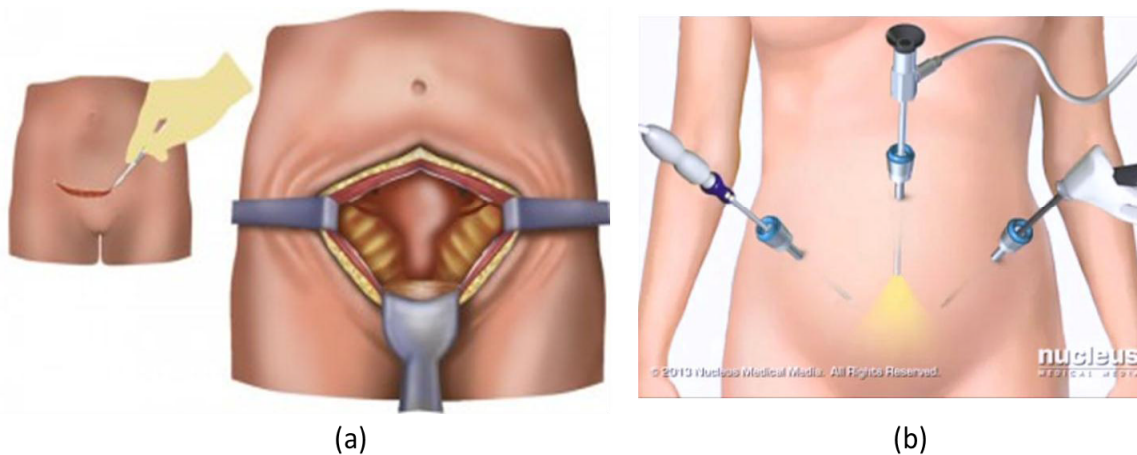


Figure 1.1 Configuration of laparoscope and instruments in myomectomy of fibroids removing surgery [5]. (a) open surgery; (b) laparoscopic surgery.

Similar as the popular utility of MIS in adult patients, the population of paediatrics using MIS is also rapidly increasing. However, paediatricians maybe face with a dilemma: whether the children can enjoy such techniques. Since the paediatrics have small geometric body dimension, the selection of surgery is important for paediatric patients. Table 1-2 shows the comparison between open surgery and laparoscopic surgery in paediatric surgical operation.

Table 1- 2 Comparision between OS and LS in paediatric surgery [1]

procedure	Upper gastrointestinal surgery			
	Gastro-esophageal reflux	Esophageal atresia	Achalasia	Idiopathic infantile pyloric stenosis
Open surgery		Recommend		
Laparoscopic surgery	Recommend[12]		Recommend[13]	No obvious advantages [14] [15] [16]
	Hepato-biliary surgery			
	Cholelithiasis	Choledochal cyst	Spherocytosis	
Open surgery				
Laparoscopic surgery	Recommend[17]	No obvious advantages	Recommend[18]	
	Surgery of the body wall and diaphragm			
	Inguinal hernia	Diaphragmatic hernia	Pectus excavatum	
Open surgery				
Laparoscopic surgery	No obvious advantages [19]	No obvious advantages	No obvious advantages	

There are many procedures of pediatric surgery where the surgeon can use minimally invasive techniques. However, there are still some procedures where surgeons are recommended to use open surgery, especially in the complex surgery. Until now, there is no a single procedure that one technique can prove stronger benefits than the other for pediatric surgery. To the current pediatric surgeries that are still recommended to use open surgery, the best way is to find a balance point that can integrate the advantages of minimally invasive techniques and open surgery.

### 1.1.2 Surgical Robot System

Robotic assisted technologies extend the performance of surgical operation via dexterous manipulation, high precision and good operability. According to the different functions of surgical robot, surgical robot could be subdivided into treatment surgical robot and surgical assisted robot.

Generally, a treatment surgical robot system is integrated with three parts: (a) navigation system, (b) trajectory planning system, and (c) robotic manipulation system. Firstly, the robot system gets the coordinate information of surgical scene by magnetic resonance imaging (MRI), computerized tomography (CT) or camera. In the controller, based on the specification of hardware of robot, the trajectory of surgical tool will be calculated correspondence to surgical demands. Subsequently, the controller sends the approximate order to the relative actuator for manipulation.

In 1992, the first pure surgical robot was reported by using ROBODOC<sup>®</sup> (Integrated Surgical Systems Inc.) for human hip surgery, as Fig. 1.2. It uses a computer station to accurately examine a patient's bone's position and size by CT image, and performs a pre-operative plan prior to total hip replacement surgery [20][21]. Mitsubishi *et al.* developed an orthopedic milling system, which could monitor the cut force and milling temperature during operation [22]. Neuromate<sup>®</sup> (Renishaw Inc.) uses a 6 degree of freedom robot arm to perform deep brain stimulation. At first, with the help of MRI, patient's brain tumor will be positioned and the trajectory of needle insertion will be planned, then, based on the planned trajectory, the needle will be inserted for therapy [23][24], as shown in Fig. 1.3. In the recent years, [25][26][27][28][29][30] *et al.* developed navigation-based robot system, which



introduced real-time compensation for accurately operation. These systems used CT or MRI image to guide the manipulator's movement, while real-time to compare the real trajectory of manipulator with the planned trajectory. By calculating the deviation between the real trajectory and the planned trajectory, the controller real-time amend manipulator's trajectory.

In the past decades, robot-assisted surgery had rapidly developed. By means of the

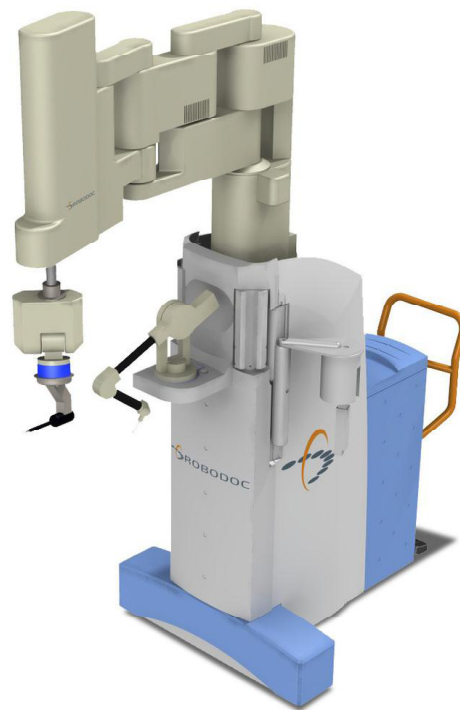


Figure 1.2 ROBODOC® [19].



Figure 1.3 Neuromate® [21].

## 1. Introduction

---

dexterous manipulator, the surgeon can reach tiny space where their hands cannot directly approach. For example, in the minimally invasive surgery, only several key holes (each diameter < 10 mm) are created in patient's skin. It is impossible for human being to put their hands through these key holes for tissue intervention. Because of these limitations, robotic manipulator to assist surgeon's operation is necessary.

The common solution for overcoming these limitations is to develop master-slave robot system. User bimanual steer master input for intended motion, the controller analyze the data of master input, and map these instructions to slave manipulator. In 1997, the robot system ZEUS<sup>®</sup> (Computer Motion Inc., merged into Intuitive Surgical Inc. at 2013.6) successfully performed cholecystectomy [31]. In 2001, the ZEUS<sup>®</sup> system got the certification from food and drug administration (FDA) from USA, could be used for abdominal surgery. It consists of two separated systems – master console and slave robotic manipulators. The master console is used for receiving user's instruction, and slave manipulator is responsible for tissue intervention. The ZEUS<sup>®</sup> system is shown in Fig. 1.4. In 2001, da Vinci<sup>®</sup> robot system got the certification from FDA, mainly used to assist for abdominal surgery, as shown in Fig. 1.5. Da Vinci system is composed of three parts: master input at the console, slave manipulators, and visual module. The distal of manipulator can achieve four

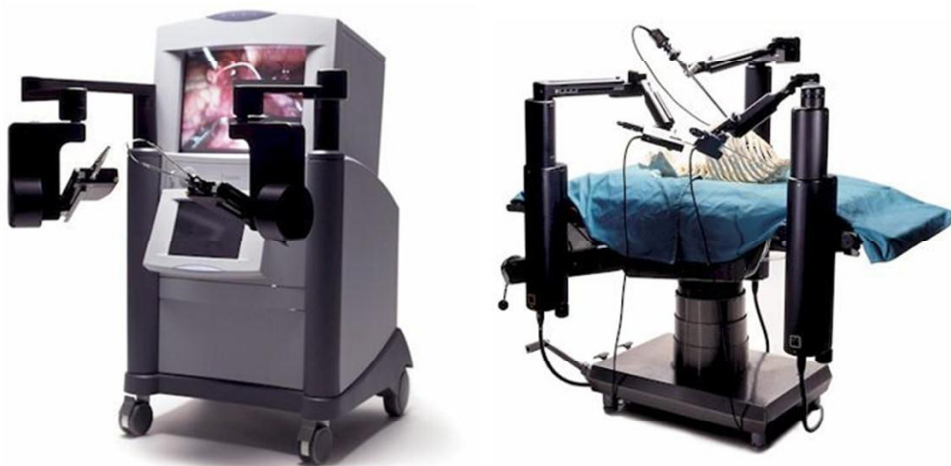


Figure 1.4 ZEUS<sup>®</sup> [26].

degree of freedoms (yaw, pitch, roll, grasp), which used for tissue intervention, as Fig. 1.5(c). During surgery, a surgeon sit at the console side, manipulate the dual artificial hands to control the movement of slave manipulators. By 2013, more than 2,000 units of da Vinci robot system had been sold worldwide, and tens of thousands of surgeries had been recorded by using da Vinci system in the past decades [32]. However, current da Vinci robot system still suffered by the less degrees of freedom of slave manipulators, which led to obscured vision by manipulators on surgery.

In order to improve the dexterity of manipulation, many researchers had been focusing on development of new flexible manipulators. Simaan *et al.* presented a snake-like manipulator with high elasticity central backbone tube. The manipulator can obtain arbitrary orientational bending motion by pulling and pushing four flexible tubes, which are located at the circumumn of a circle [33]. Dupont *et al.* reported a robot assembled by a concentric combination of pre- cured elastic tube. This robot can achieve Omni-directional bending



Figure 1.5 da Vinci<sup>®</sup> robot system [27].

## 1. Introduction

---

movements by rotating and extending the tubes [34]. Yang *et al.* described an articulated robotic manipulator, which features its tip with several independently controllable DoFs. Each joint of the manipulator is actuated by an embedded motor fitted with a gearbox [35][36]. Based on the feature of dexterous manipulator and requirement of MIS, single port access surgical (SPAS) robot and natural orifice transluminal endoscopic surgical (NOTES) robot had been developed [37] [38] [39] [40] [41] [42]. During surgery, SPAS robot can be inserted through a single incision, and deploy its manipulators guided by the visual feedback. However, limited by the geometric configuration of manipulators and visual module, SPAS robot need enough workspace to extend its manipulator and visual module, as Fig. 1.6. NOTES robot, as shown in Fig. 1.7, can pass through irregular pass to access surgical object, what makes the least damage to human's skin. However, due to the small external geometry,



Figure 1. 6 Insettable robotic effector platform for single access surgery [32].

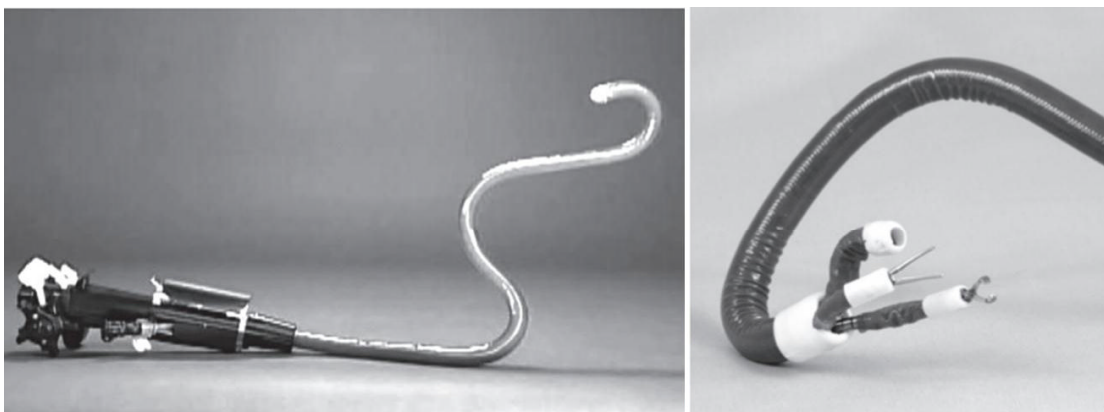


Figure 1.7 NOTES robot in USGI Medical® [34].

the inserted manipulators and flexible endoscope in the NOTES robot owns low dexterity, restricted by the size of inner channels, the insertable tool manipulators are weak in rigidity.

## 1.2 Robot-assisted Pediatric Surgery

Although the robot-assisted surgeries had proved their advantages in minimally access surgery, the clinic benefits in pediatric surgery is still unclear [43]. The main use of robotic surgical system in the pediatric surgical literature is Zeus robotic surgical system (formerly Computer Motion, Inc., now operated by Intuitive Surgical, Inc.) and the da Vinci Surgical System (Intuitive Surgical, Inc.) [44] [45] [46] [47]. Table 1-3 shows the currently robotically assisted procedures for paediatrics.

Table 1- 3 Robotically assisted procedures for paediatrics [48][49]

Routine procedures	Complex procedures
Nissen fundoplication	Reoperative pyeloplasty
Dismembered pyeloplasty	Mullerian and wolffian duct remnant removal
PDA closure	Seminal vesicle cyst removal
Nephrectomy	Bochdalek congenital repair
Calyceal diverticulectomy	Kasai portoenterostomy
Antireflux surgery	Choledochal cyst excision
	Lithotomy
	Atrial septal defect closure
	Ureteral reimplantation
	Partial nephrectomy
	Bladder augmentation
	Mitrofanoff procedure

## 1. Introduction

Table 1-4 lists the comparison between robot-assisted pediatric surgery and conventional minimally access surgery.

Table 1- 4 Comparison between robot-assisted pediatric surgery and open/conventional laparoscopic surgery [50][51][52]

Specification			
Procedures	average age (years) (100 samples)	Average weight (kg) (100 samples)	Utility of robotic surgical system
General surgery, urology, and cardiothoracic surgery	7.8 years 1 day ~ 23 years	24.2 kg 2.2kg -103kg	da Vinci® and Zeus®
Performance comparison			
	Operating time and learning curve	complications	Postoperative data
Robot-assisted surgery	No fixed regulation, depending on the detailed surgery [53] [54]	Overall rates of reported were low [55]	Shorten hospital stay, less pain [56]
Open or conventional laparoscopic surgery			

From the table 1-3, the body suitable for pediatric robotic surgery is still small. However, the available studies demonstrate that a number of robotically assisted surgeries are feasible and safe when performed by surgeons who are experienced in the techniques. Generally, compared with traditional laparoscopic and open surgery, robotic surgery provides superior clinical outcomes. However, procedures such as the repair operation of esophageal atresia, ureteral reimplantation, and protoenterostomy in minimally access surgery are still extremely challenging.

## 1.3 Technical Issue for Robot-assisted Pediatric Surgery

### 1.3.1 Current Limitation in Robot-assisted Pediatric Surgery

Compared with the clinic performance of typical surgical operation, published experiments have demonstrated the potential to enable the robot-assisted technologies for pediatric surgery. However, there are still a number of technological limitations specific to pediatric surgery that restricts their wide use:

1. the overall dimension of the robotic systems.

Compared with many pediatric surgical patients, the geometric dimension of the robotic systems such as the Zeus modular robotic arms and the da Vinci surgical cart are overwhelming in OR. It puts forward a big problem that the bulky cart make it is difficult for a surgical assistant to access the patient while the operation procedure needed manipulator exchange or other procedure needed to access [57].

2. the geometric size, and variety of available robotic instruments is restricted compared with those offered for standard laparoscopy.

The most commonly instruments used in the commercial surgical robotic system such as Da Vinci® system is with a diameter of 8~10 mm. Recently, 5 mm instruments with 7 degrees of freedom has been introduced for use with this system. However, the number of instruments offered for other special use is still limited.

3. the snake-like constructure instruments needs a slightly larger amount of intracorporeal working space to deploy their redundant joints. Specifically, a >10 mm distance needed from the distal to articulating joint in the intracorporeal cavity.

4. compared with the comedy incision, however, a little longer operating times, higher costs.

Robotic surgery does not currently represent a general alternative to conventional or minimally invasive surgery.

### **1.3.2 Technical Issue for Robot-assisted Pediatric Surgery**

In the MIS, the approach for robot-assisted pediatric surgery is similar to that of its adult counterpart. However, compared with the size of adult, the workspace is limited in children and the abdominal wall is generally thinner, proper positioning of ports is highly important [58]. In the intracorporal, the camera and manipulators are mapping the relation of human's eye and hands. Furthermore, a pneumoperitoneum is needed before MIS, which generally would create an inflated to take full advantage of their enhanced dexterity. Therefore, the small working space poses a higher risk of inadvertent visceral injury with the positioning of ports and manipulation instruments.

According to the specification of pediatric surgery, “dexterity”, “safety” and “good operability” are necessary elements in the design of robotic-assist system.

## **1.4 Research Objective and Motivation**

As shown in table 1-3, pediatric congenital repair surgery such as congenital esophageal atresia repair is still a tricky thing by using current robot-assisted system for surgeon. This research aims to develop a robot-assisted system for pediatric esophageal atresia repair surgery.

### **1.4.1 Pediatric Congenital Esophageal Atresia**

Pediatric congenital esophageal atresia (CEA) is a congenital medical condition (birth defect) that affects the alimentary tract. It occurs in approximately 1 in 4400 live births [59] Pediatric CEA takes several different forms, often involving one or more fistulas connecting the trachea to the esophagus. In approximately 85% of cases, the esophagus ends in a blind-ended pouch, rather than connecting normally to the stomach, therefore, the food cannot drain into the stomach. Without treatment, the pediatric patient will soon die due to malnutrition. Recently, the most immediate and effective treatment in the majority of pediatric CEA is a surgical repair to close the fistulas and reconnect the two separated ends of the esophagus to each other. However, there are several factors affecting the surgical procedure, such as the state of the patient's health [60] and the size of the esophageal gap [61]. Generally, neonates



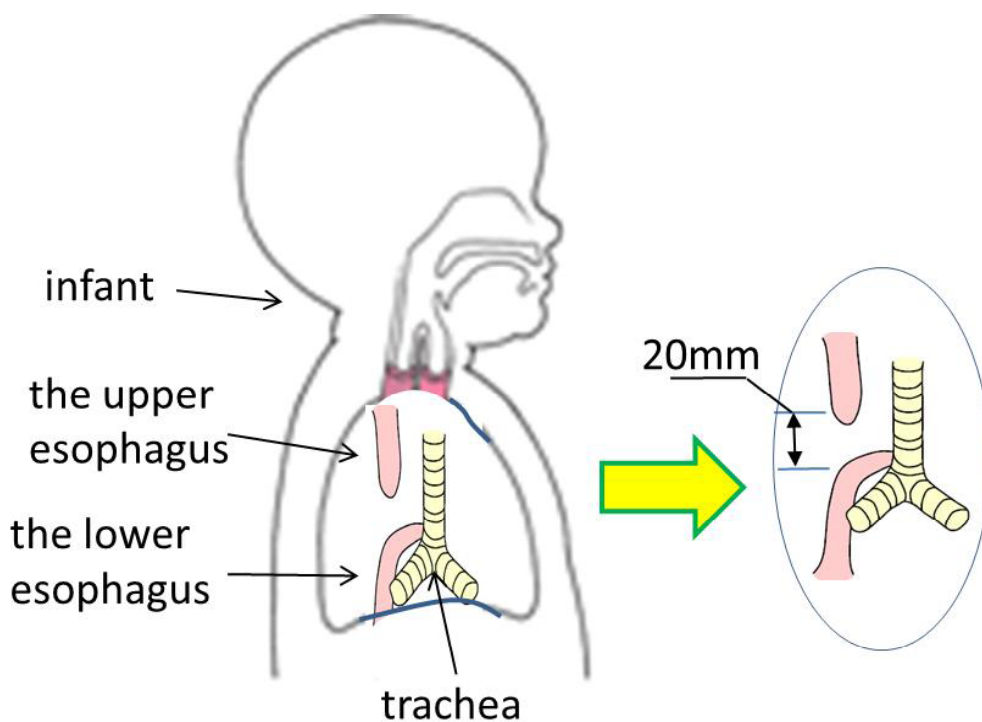


Figure 1.8 General case of congenital esophageal atresia (CEA).

are suffering from the CEA symptoms shown in Fig. 1.8. Esophagus generally located below the ribs 30 mm, and the mean gap between the upper esophagus and the lower esophagus is typically about 20 mm [62], and the average chest measurement of the neonate is about 31 cm [63], therefore, the width of chest is 100 mm on average.

### 1.4.2 Motivation

The traditional operation in pediatric CEA surgery includes several steps: exploration of operative field, stripping esophagus, ligation of tracheoesophageal fistula, and esophageal anastomosis. Compared with the thoracoscopic surgical method, open surgery with small incision can avoid the side effect of pneumoperitoneum. In this research, the surgeon manually explores the esophagus segments, then performs esophagus anastomosis via robot assisted system.

The semi-prone position is recommended during pediatric CEA surgery, with the right side elevated at  $45^\circ$  and right arm placed over the head [64]. *Atkins* reported a 40~50 mm

incision for dissection of the upper thoracic and stellate ganglia in adult patient [65]. However, the 40~50 mm cut brings much hurt to pediatric patient. In order to reduce the harm, a 30x30x30 mm narrow space near the fourth intercostal of the right side will be created. Our objective is to develop a compact robot assisted system to support surgeon perform surgical intervention in the 30x30x30 mm workspace.

## 1.5 Structure of this Thesis

As the author states in the preview sections, this research aims to develop a surgical robot system to assist the pediatric congenital esophageal atresia surgery. Because the geometric specification of infant is small, we design a compact surgical robot, which approach the target esophagus through a 30x30 mm incision. Due to the pediatric thinner tissue, the designed robot should be accurate manipulation. In order to provide good visual feedback for navigating surgeon's operation, the manipulator should avoid blocking camera's vision while tracking the master instruction.

This thesis consists of 6 chapters. The structure of this thesis is presented as Fig. 1.9. The summarization of each chapter is described as follow.

### ■ **Control strategy of robot in constrained condition (chapter 2)**

In this chapter, the author describes the general control mode of compute-control assisted robotic system, and states the control strategy of remote robot system. Since this research needs to map the trajectory relation between user input and slave manipulator, the author considers the influence of the mechanism configuration of surgical robot in the control strategy for performing operation in narrow workspace during surgery.

### ■ **Mechatronic design of pediatric surgical robot (chapter 3)**

In this chapter, the author presents the mechatronics design of pediatric surgical robot. The surgical robot consists of a master console and two slave manipulators. The master console is composed of Phantom Omni and foot pedals to generate input signals. In the slave side, it consists of two isomorphic slave manipulators, with total 18 DoFs. Each slave manipulator is composed of a positioning manipulator and a

surgical tool manipulator. The positioning manipulator has 4 DoFs, which can achieve translational movements in spatial movement. The surgical tool manipulator employs DSD mechanism to achieve bendable movements. A single surgical tool manipulator with 5 DoFs and an external diameter of 8 mm consists of two bendable joints and a rotatable forceps. Each bendable joint can realize two bending movements in two orthogonal planes. The rotatable forceps is composed of a rotatable joint and a clipper with opening and closing movement. In this chapter, the kinematics of the slave manipulator is calculated. The simulation results show the overlapped area of two positioning manipulator covers a 30x30 mm zone; and the distal of the surgical tool manipulator can achieve an arbitrary orientational bending movement. The results guarantee pediatric surgical robot can perform surgical intervention in a 30x30x30 mm workspace in pediatric surgery. The inverse kinematics for calculating active rod's length illustrated that the rod's deviation of bending linkage is less than 3 mm. The experiment to measure the flexible shaft's rigidity shows that the flexible shaft could keep high rigidity when loaded within 200 g.

■ **Control strategy of redundant robotic manipulator in narrow space (chapter 4)**

In this chapter, the author proposes a shape optimal algorithm to map the relation between master input and the slave manipulator. The purpose of this algorithm aims to construct a triangle formation between endoscope and the slave manipulators to provide good operability and visualization for robot user. Due to the heterogeneous configuration between the master input and the slave manipulator, the posture of each joint in the master input cannot complete match with the slave mechanism chain. Therefore, the master input just directly control the position and posture of slave manipulator's tip, the redundant joints of manipulator will be controlled by the proposed algorithm. In the first step, the relation between the robot joint's solution and the disturbance at redundant joint is established. The verification simulation shows that the robotic arm with inverse kinematics algorithm can accurately track the input ( $\varepsilon < 0.5mm$ ). In the next step, a shape optimal algorithm considering the visualization and operability is developed to construct a triangle formation between slave manipulators and endoscope in workspace. Given a tolerable error ( $\varepsilon = 0.001$ ), the

adjacent angle deviation between two bendable joints among 4 quadrants is less than  $0.5^\circ$ . The experiment result of position tracking with shape optimal algorithm demonstrated that the distal of slave manipulator could achieve position error  $< 1$  mm during trajectory planning when loaded within 50 g in 2D plane or 20 g in 3D space.

### ■ **Handedness control with pediatric surgical robot (chapter 5)**

In this chapter, the author presents a novel application for reducing operating difficulty to the master-slave surgical robot user. Generally, human being have dexterous hand than the other, therefore, they are willing to use their dexterous hand for important manipulation, even though their both hands are needed in normal operation. The author extends the algorithm referred in chapter 4 by using two endoscopes in the pediatric robot system. The two endoscopes located at both sides with respect to the plane, where the both slave manipulators located. Therefore, there are two solutions for combining a single endoscope and two slave manipulators. In addition, the correspondence between the master input and the slave manipulator can be exchanged based on the selection of combination between the endoscope and the slave manipulator. The algorithm guarantees the robot operator use their dexterous hands for important operation even performing suture task on both sides of a cut. The experimental results show that the time taken for the same task with the handedness control obviously improves user's performance and the feasibility of suture on an esophagus model by using the developed algorithm.

### ■ **Conclusion and future work (chapter 6)**

In this chapter, the author concludes this research and discusses future work, such as the evaluation of pediatric surgical robot through *in vivo* experiments, and the clinical applications of using pediatric surgical robot as well as the control algorithm in serial robotic manipulator.

The flow chart of this research is shown in Fig. 1.9.

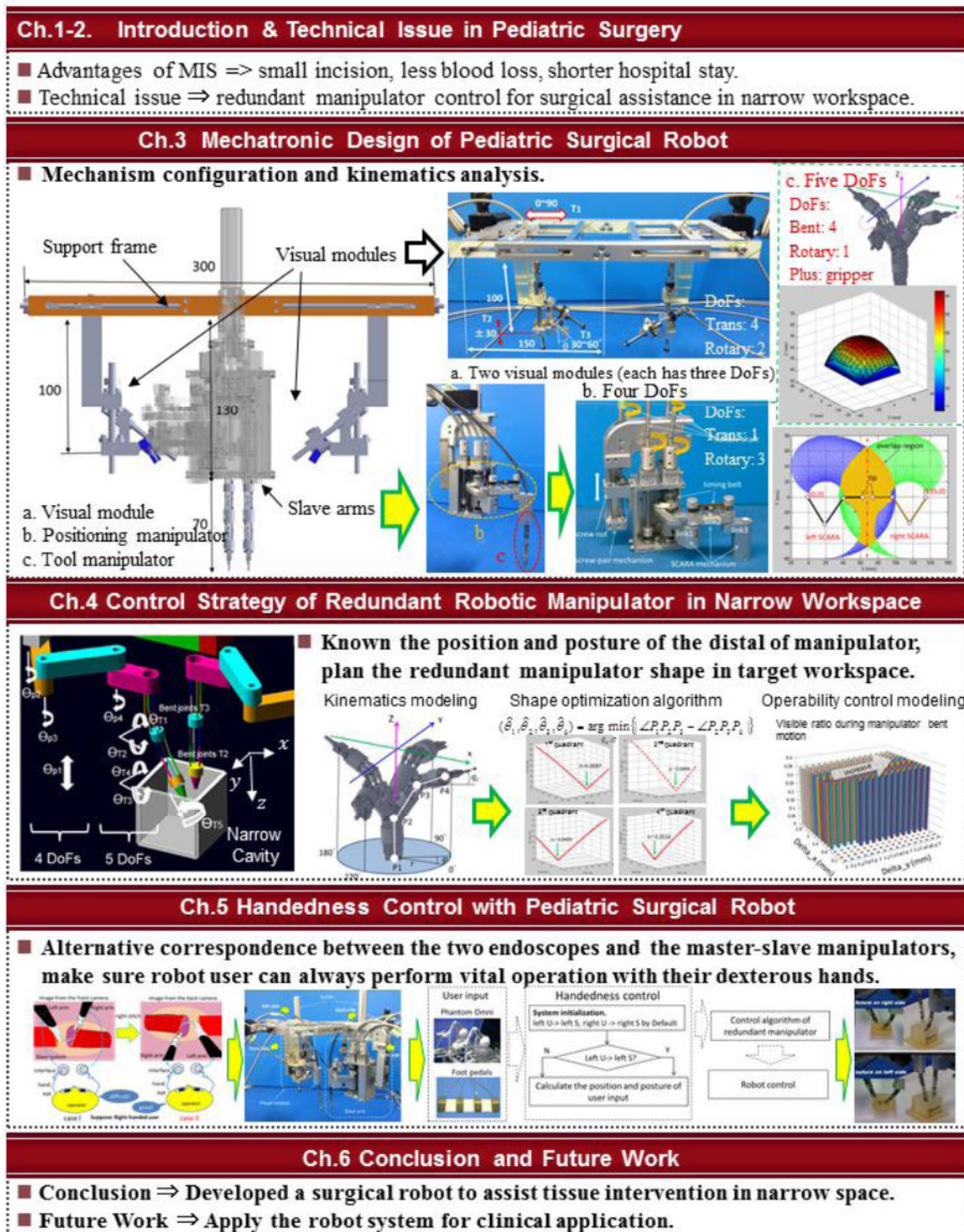


Figure 1.9 Structure of this thesis.



## **Chapter 2**

# **Control Strategy of Redundant Robotic Manipulator**

## **2.1 Introduction**

Master-slave architecture can retrieve surgeon from the patient bed and may achieve good operability. However, in some surgical occasion, the advantages of the minimally invasive access surgery are weakened by complex instrument manipulation due to the difficulty of approaching target anatomical region through irreguate path. The development of slave manipulator with small geometric dimension and multiply DoFs can improve the operability in narrow workspace. Especially, redundant manipulator significantly highlights the benefit. Redundancy means that a manipulator possesses more degrees of freedom than the minimum number required to excute a given task. Generally, a manipulator with actuators for three position coordinates and three orientations is necessary to achieve essential movements in spatial space. However, a six degree-of-freedom manipulator mechanism has many kinematic flaws such as limited joint ranges, workspace obstructions and kinematic singularities [66]. Therefore, redundant manipulator could competent for tasks that deficient or normal manipulator cannot carry out in narrow space, such as in irregular fistula or narrow

surgical cavity. Nevertheless, redundancy also poses challenge at inverse kinematics problem, which is affected by DoFs' distribution, shape conformance, and external constraints.

## 2.2 Control Method of Redundant Robotic Manipulator

In chapter 1, there are many dexterous manipulator were introduced. The presence of a large amount of DoFs enhances the flexibility and dexterity of the robotic platform, however, the control of redundant structure pose much difficulty due to the coordination of the large number of possible joint configuration. To a redundant manipulator, it is possible that the inverse kinematic problem admits infinite solutions. It means that for a given redundant manipulator, the manipulator can demonstrate different posture even the manipulator's end-effector located at the same position and posture.

Many solution techniques for solving the kinematic control problem for redundant manipulators have been suggested by researchers. Most traditional approaches are based on the calculation of the manipulator's Jacobian matrix. The process of computing the inverse kinematic problem is equivalent to that calculating the joint angle ( $q$ ) based on the task position and orientation ( $x$ ). The relation between  $q$  and  $x$  can be given

$$\begin{aligned} x &= f_{(q)} \\ \dot{x} &= J_{(q)} \dot{q} \end{aligned} \quad (2.1)$$

Where,  $x$  is the  $(m \times 1)$  vector of task variables,  $q$  is the  $(n \times 1)$  vector of joint variables.  $f$  is a differentiable nonlinear vector function whose structure and parameters are "brige" between the angular velocities from joint space and the target velocities in task space.  $J$  is the  $(m \times n)$  Jacobian matrix. Generally, for a given trajectory in the task space  $x_{(t)}$ , the inverse kinematic computation is formulated to find a joint space  $q_{(t)}$  that satisfied the equation  $x_{(t)} = f_{(q_{(t)})}$ . Since the manipulator is redundancy, therefore, the task variables and joint variables meet the relation  $m < n$ , which means the inverse kinematic resolution is not unique. In order to filter the prefer solution, [67] presented a method for avoiding obstacles based on



pseudoinverse. However, the computation of Moore-Penrose pseudoinverse is subject to the path reconstruction error. Furthermore, when the Jacobian is rank deficient, the approach of inverse kinematic have to face the singularities problem, which would lead to unpredictable jump in the joint space [68]. [69] reported a singularities avoidance approach for the optimal path planning of redundant robot manipulators. It induced proper bounds to avoid singularitis by changing the transformation between the joint speeds and end-effector target velocities. The observation of proper bounds reduces the efficiency that the end-effector tracks planned trajectory. [70][71][72][73] illustrated a gradient projection method that modified the Moore-Penrose pseudoinverse matrix to (2-2),

$$\dot{q} = J^+_{(q)} \dot{x} + [I - J^+_{(q)} J_{(q)}] \dot{q}_0 \quad (2.2)$$

The above techniques focus on avoiding the singularities, however, they are impractical for on-line feedback control, due to the heavy computational reuquirements [74].

Other methods, such as augmented Jacobian[75], extended Jacobian [76] and [77] assigned additional constraint task to complete the Jacobian's rank, therefore, the space of redundancy is entirely exploited. However, these methods are still subject to algorithmic singularities which are the singularities associated with the augmented Jacobian matrix [78].

For the control proceduces such as redundant manipulators, the use of the constraints to guide tissue manipulation is important. When a redundant manipulator is used for such application, the major technical hurdles include

- 1) shape comformance to required constraints;
- 2) motion modeling and parameterization to ensure the ease control of the redundant manipulator.

Recent advances [79], [80] in considering potential anatomical changes of the model have enabled haptic guidance under active constraints or virtual fixtures (VFs). A perquisite of these procedures is the computation of proximity queries (PQs), which is a challenging problem for haptic rendering because of its intrinsic complexity and high update rate required (>1 kHz) [81]. Well-known methods such as [82], [83] require object representation as convex polyhedral to gurantee global convergence. It addresses a dynamic active constraints (DACs) to navigate generic articulated MIS instrument using accurate forward kinematics. It reported a PQ formulation to compute the deviation of the robot outside the constraint

pathway defined by a 3D anatomical model, and navigate the endoscope in the distal of the manipulator for panoramic exploration.

### 2.3 Discussion

In the master-slave architecture of the surgical robot system, the control framework of the redundant manipulation consists of 1) shape conformance condition; and 2) motion modeling, parameterization and control.

Generally, in the master-slave system, the structure of the master input and the slave manipulator are isomeric. It means that the master input cannot directly control every joint of the slave manipulator for motion navigation. The common way of mapping the master input to the slave manipulator is that the master input controls the position and the posture of the distal of the slave manipulator, and the redundant DoFs follows the control optimization algorithm. In the bimanual master-slave surgical system, the manipulation image is shown in Fig. 2.1 [84]. For achieving comfortable and natural manipulation, the surgeon bimanual the dual handles with angle of  $60\sim 120^\circ$ , while the surgeon's eye, surgical target, and the monitor lies in a straight line. The configuration of the two slave manipulators guarantee to provide a good visualization for visual feedback. However, in some surgical task, such as suture, the surgical symptoms needs the operator do suture at both sides of the cut. Therefore, it poses a big challenge to single handed user. To right-handed operator, when do left suture task, the user could use his/her right hand to catch the needle and the left hand to support the suture task. However, when do right suture task, the user must drive his/her right hand for inverse suture or his/her left hand to catch the needle. Fig. 1.5 shows the only commercial bimanual operation robotic system, Da vinci<sup>®</sup> system, the coorspondence between the master handles and the slave manipulator is fixed before operation (the left master handle coorsponds to the left slave manipulator and the right master handle coorsponds to the right manipulator). Furthermore, in the latest version of the Da vinci<sup>®</sup> system (Da vinci *Si*), shown in Fig. 2.2, the coorspondence between the master and the slave still cannot be changed during operation (the coorspondence between the master and the slave are swapped). Therefore, it cannot resolve the problem encountered at bimanual operation, especially the robot user is only familiar with

## 2. Control Strategy of Redundant Robotic Manipulator

---

one hand (Fig. 2.3). Therefore, when novel operator use his/her unpreferred hands for do dexterous manipulation, the performance is difficult to be guaranteed.

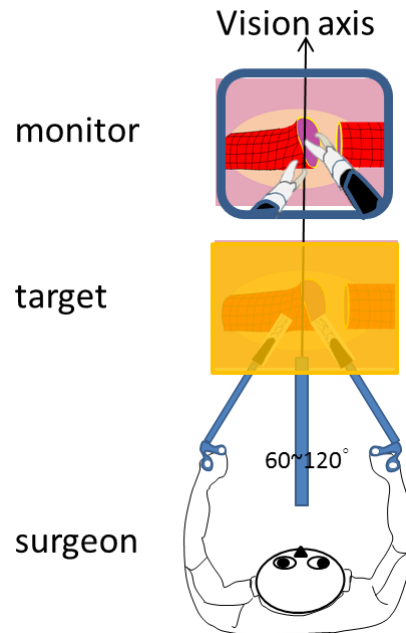


Figure 2. 1 Triangle formation of bimanual surgical manipulation.

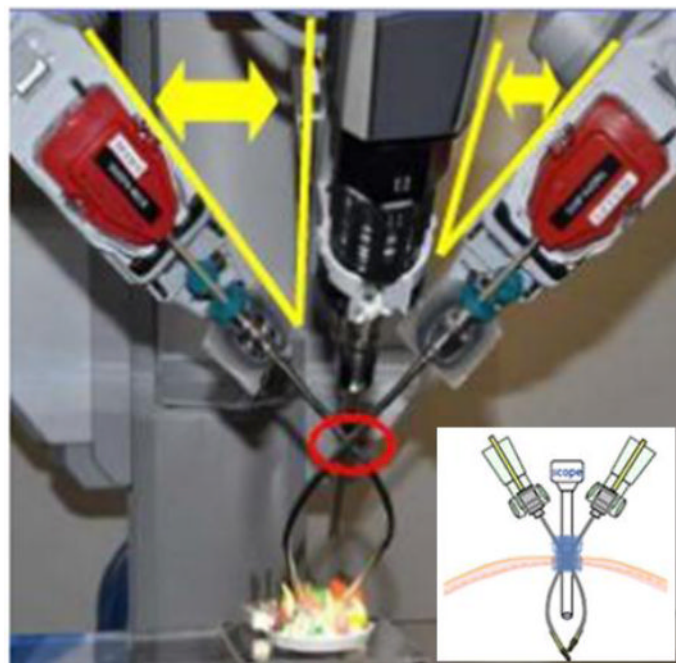


Figure 2.2 da Vinci Si<sup>®</sup> [27].

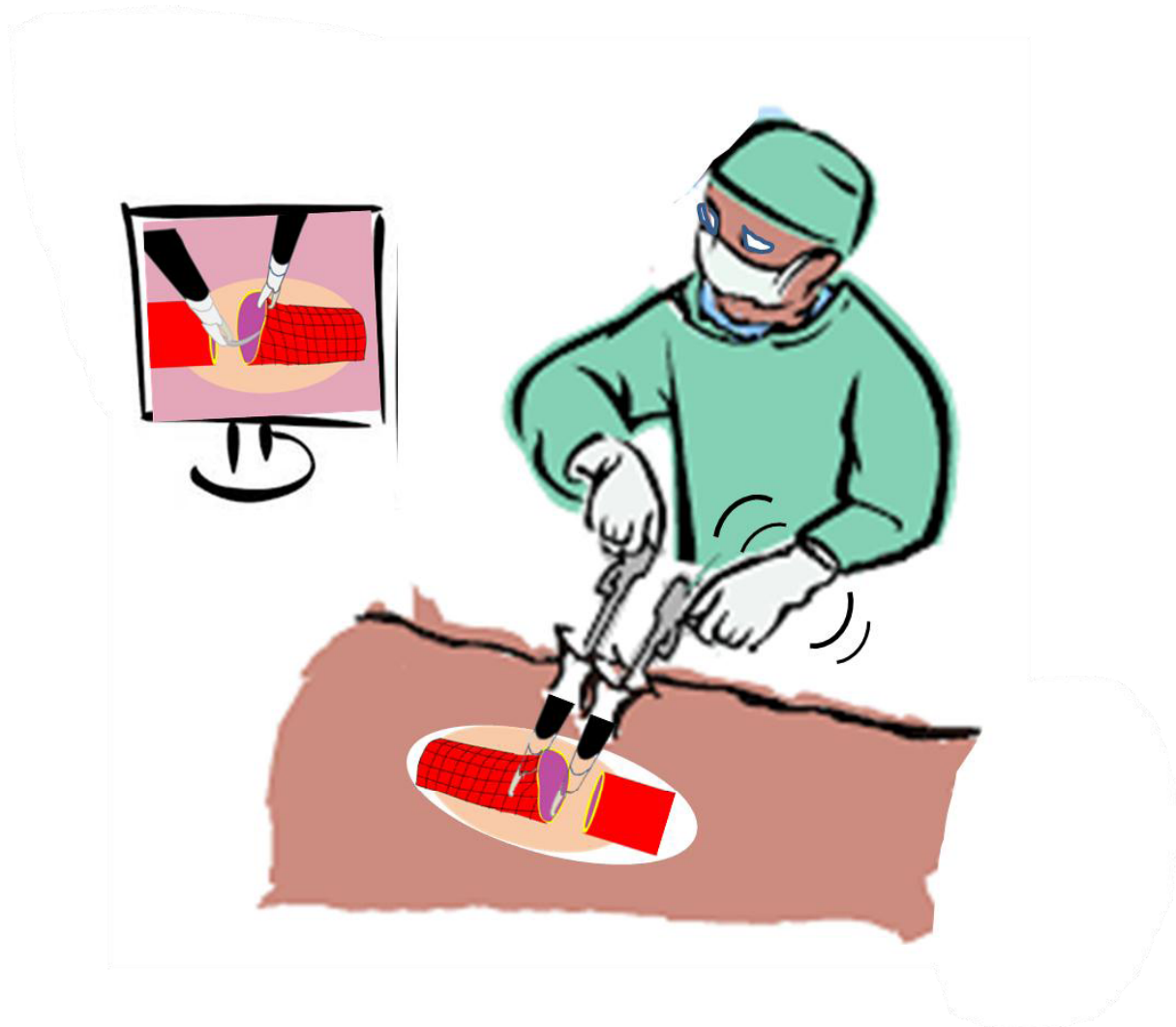


Figure 2.3 Manipulation with both hands (right hand preferred).

Recent advances in robot mechanism design (single port access surgical robot, shown in Fig. 1.6 and Natural Orifice Transluminal Endoscopic Surgery, shown in Fig. 1.7) could access the surgical site through smaller incision or natural orifice such as mouth and anal. However, in the current configuration, the correspondence between the master and the slave manipulator also is fixed before operation.

In this thesis, the author proposes a novel robotic system, which consists of two visual modules except the master handles and the slave manipulators. The two visual modules located at the both sides of the frame, where the two slave manipulators located. Therefore, there are two combinations between the visual module and the slave manipulator, the

configuration between the visual module and the slave manipulators ensure that the robot user can maintain the preferred hand-use even do both suture task needed inverse manipulation. The implementation of this system is shown in Fig. 2.4.

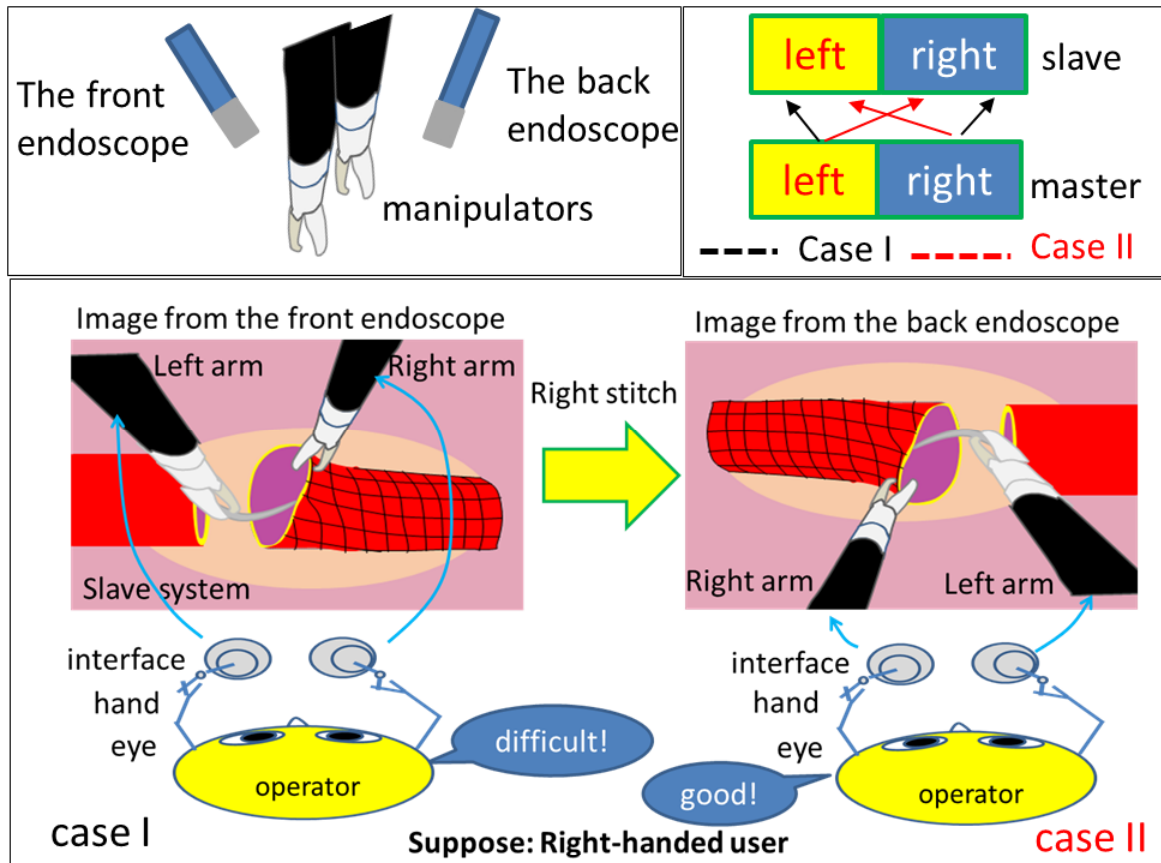


Figure 2.4 The proposed method.

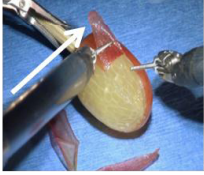


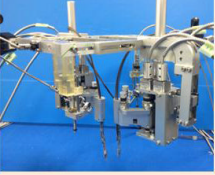
## 2.4 Comparison between Current Surgical Robotic System and the Proposed System

Table 2-1 shows the comparison between current surgical robotic systems and the proposed robotic system. The author focuses to establish the visualization and operability into the master-slave surgical robot system. Where, the visualization means that the redundant joints in the robotic system should block endoscopic view as small as possible, while the

## 2. Control Strategy of Redundant Robotic Manipulator

distal of the manipulator tracking the master input. The operability means the endoscope and the redundant slave manipulators should follow eye-hand triangle coordination when both hands are needed in surgical tasks.

Table 2- 1 Comparison between current surgical robotic system and the proposed system

Category	Multi-port Access Surgery (MAS) (Da Vinci <sup>®</sup> )	Single Port Access Surgery (SPAS) (Columbia Univ.)	Natural Orifice Transluminal Endoscopic Surgery (NOTES) (ICL)	Pediatric surgical robot (Waseda Univ.)
	Dexterous wrist and straight stem 	Tube-actuated snake-like 	Serial U-joints 	Serial U-joints + separated endoscope 
Master-slave consistent	○	○	○	○
Trajectory planning in narrow space	×	×	○	○
Preferred hand operation	×	×	×	○

## Chapter 3

# Mechatronics Design of Pediatric Surgical Robot

### 3.1 Introduction

In this research, the author develops a compact surgical robot system, which can perform tissue intervention in the target workspace. The surgical robot uses master-slave control architecture, which can translate the intention of master input and reproduce that through slave manipulator. The master-slave control architecture of surgical robot system could benefit both surgeon and patient through:

(a). Liberate surgeon from hospital bed, which could relieve surgeon's pressure by designing ergonomics user interface.

(b). Optimize the configuration of operation room (OR). The utility of robotic manipulator replacing the attend of surgeon near hospital bed can reduce the colliding probability between surgeon and physician assistant.

(c). Make the remote operation become possible, which can introduce global surgery via internet.

(d) The utility of robotic manipulator could bring out the equal or superior clinical outcomes and less impact on a patients' organ and body.

## 3.2 Overview of Pediatric Surgical Robot

According to the introduction of robotic-assisted pediatric surgery in section 1.4, the pediatric robot is fixed above a pediatric body by fixator. The pediatric congenital esophageal atresia repair surgery could be divided into five steps [85]: ①create an incision at the right axillary of pediatric patient and explore the 4<sup>th</sup> and 5<sup>th</sup> ribs; ②create the workspace between the 4<sup>th</sup> and 5<sup>th</sup> ribs for manipulator entering; ③distinguish the esophagus from other tissue; ④suture the trachea-esophageal fistula (TEF); ⑤esophageal anastomosis. Since the created incision is 30x30x30 mm, therefore, the anastomosis in this narrow workspace provides much challenge to surgeon, the purpose of this designed robot is aiming to assist surgeon for suture

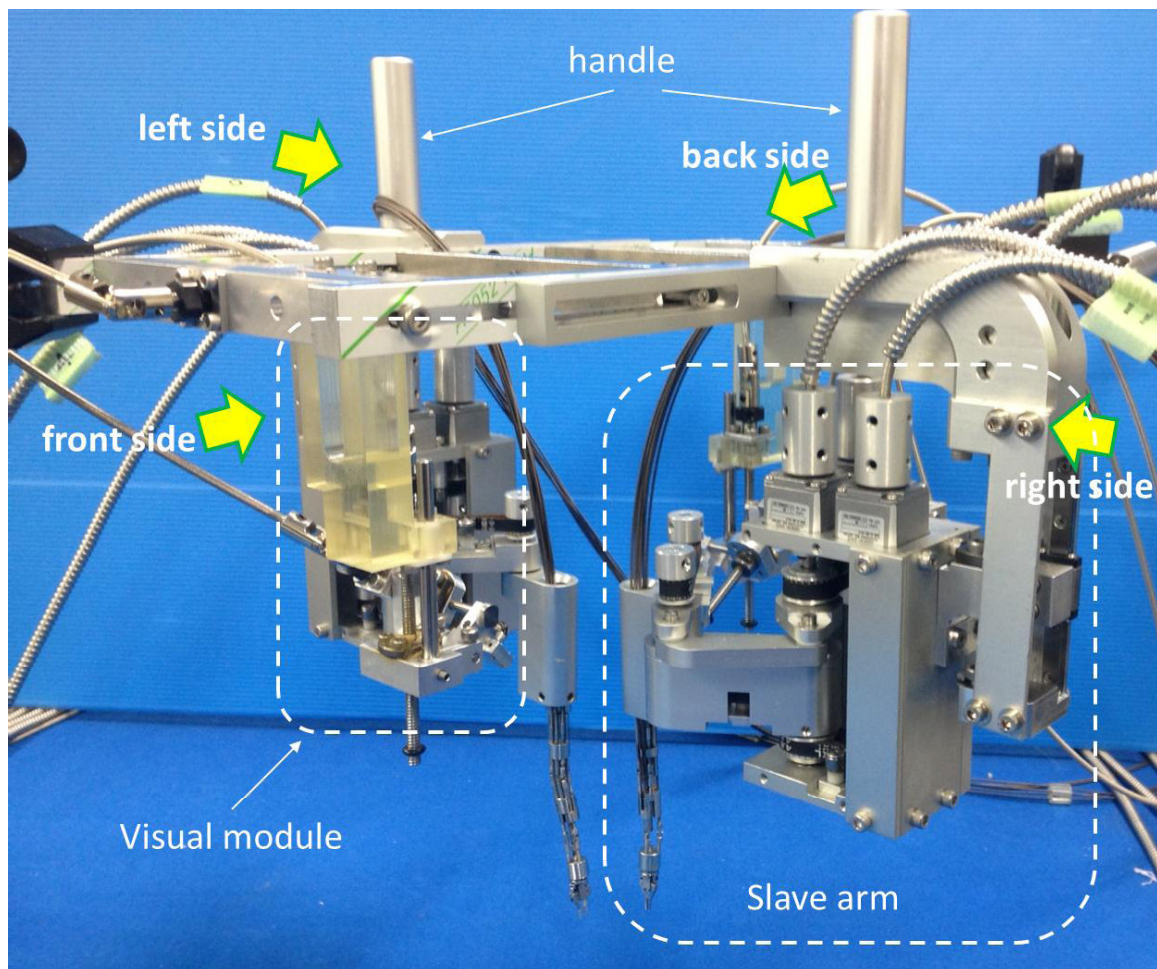


Figure 3.1 Overview of pediatric surgical robot.



operation. Fig. 3.1 depicts an overview of the pediatric robot. It consists of four parts: two slave arms and two sets of visual module, which are alternatively located along the square frame. The two slave arms are located at the left side and the right side respectively; and the two sets of visual module are located at the front side and the backside respectively. There are two combinations between the slave arms and the two visual modules. The front side visual module with the two slave arms and the back side visual module with the two slave arms, respectively. The utility of two combinations will be described in the Section 5.1. Since the two slave arms and the two visual modules are symmetrical, only the left slave arm and the front side visual module are illustrated.

## 3.3 Configuration of the Left Slave Arm

The slave arm in surgical robot is used to substitute surgeon's hand to perform tissue intervention directly. Generally, there are two typical mechanical structures to realize dexterous manipulation: serial manipulator and parallel manipulator. Compared with parallel manipulator, serial manipulator may achieve large workspace. The workspace of serial manipulator is limited by the geometrical and mechanism limits of the design (such as the collisions between legs and the singularities). However, parallel manipulator may easily obtain high rigidity and high precision with small mass of the manipulator (compared with serial manipulator structure).

The slave arm in this thesis consists of a positioning manipulator and a tool manipulator [86]. The positioning manipulator plays in a coordinated manner for translating the tool manipulator in 3D spatial space. The surgical tool manipulator, attached to the tip of the positioning manipulator, is used to perform tissue intervention. The author employs serial structure for designing positioning manipulator. In order to overcome the low rigidity of serial manipulator, a selective compliance assembly robot arm (SCARA) is employed. To the design of tool manipulator, in order to improve the dexterity and the rigidity, a hybrid (serial-parallel architecture) is used.

### 3.3.1 Mechanism Type Selection for Compact Design

Compare to the geometric size of a pediatric patient, a compact robot mechanism will be a best choice in OR. Referred in section 1.1.4, the average chest measurement of pediatric patient is 31 cm [56], since the pediatric patient lay on surgical table with semi-prone position while the right side tilted  $45^\circ$  with operation table and the right arm put over the head, therefore, the general width of pediatric body on operation table is 100 mm. Corresponding to the geometric dimension of pediatric chest, the base of the proposed robot should cover 100~200 mm parallel with the cross section of pediatric body. In order to adjust endoscope and fix the robot, the length of the robot's base that parallel with pediatric body stem is better within 350 mm. The location scheme is shown in Fig. 3.2.

Our purpose is to develop a compact surgical robot to assist surgeon perform surgical intervention. The surgical robot will locate at the above of the pediatric patient. Considering the narrow size of surgical cavity, only the distal of the manipulator will be inserted into

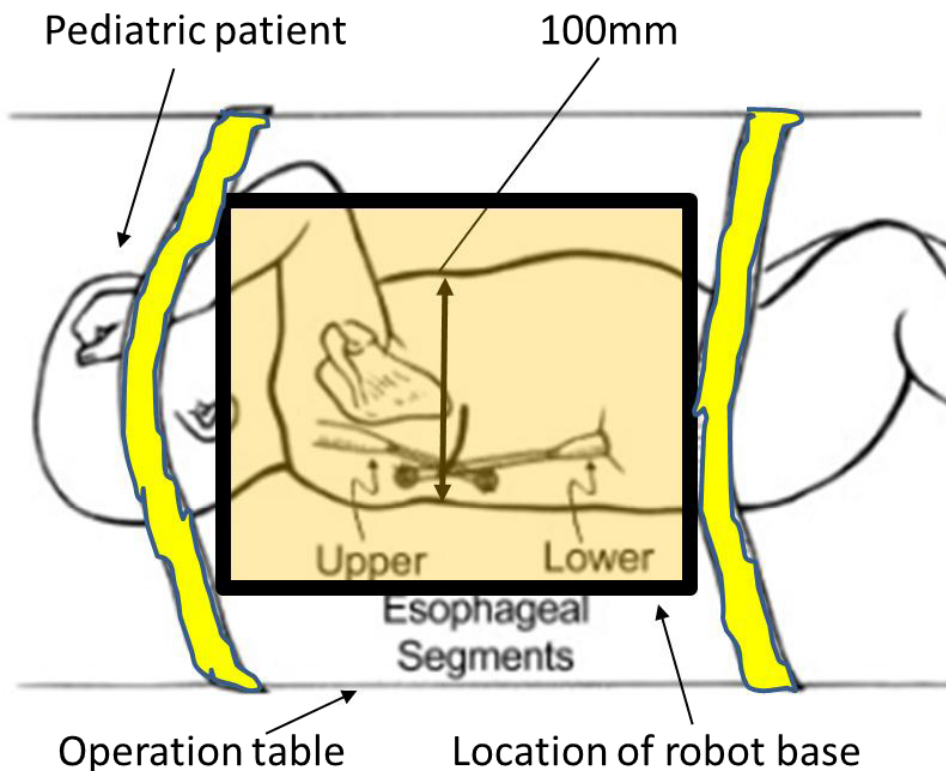


Figure 3. 2 Schematic diagram of a compact robot located on pediatric patient.

surgical cavity. The location between surgical robot and pediatric patient is shown in Fig. 3.3. During operation, surgeon will perform tissue pull, push and grab tasks. Therefore, the tip of the proposed robot must be adjusted for different postures and positions. Since the surgical cavity is about 30x30x30 mm, therefore, the requirement of moveable range of the distal of the manipulator is small. Considering the procedure of surgery, the surgical robot should be setup at first, then, the distal segment of robot will be driven to surgical cavity. Thus, the surgical robot should contain a coarse positioning mechanism. After the distal of the robot reaching the surgical sence, the tip would be controlled for tissue intervention. Based on the surgical requirement, the proposed robotic manipulator consists of a positioning manipulator and a tool manipulator.

There are many mechanism types to satisfy the positioning requirement, such as Cartesian robot, six-axis robot, parallelogram mechanism and SCARA.

#### 1) Cartesian robot

Cartesian robot has three specified directions X, Y and Z. the main advantages of Cartesian robot is that the tip of robot could be actuated in multiple linear directions and easy to program. Generally, the Cartesian robot is designed with gantrical structure, therefore, it

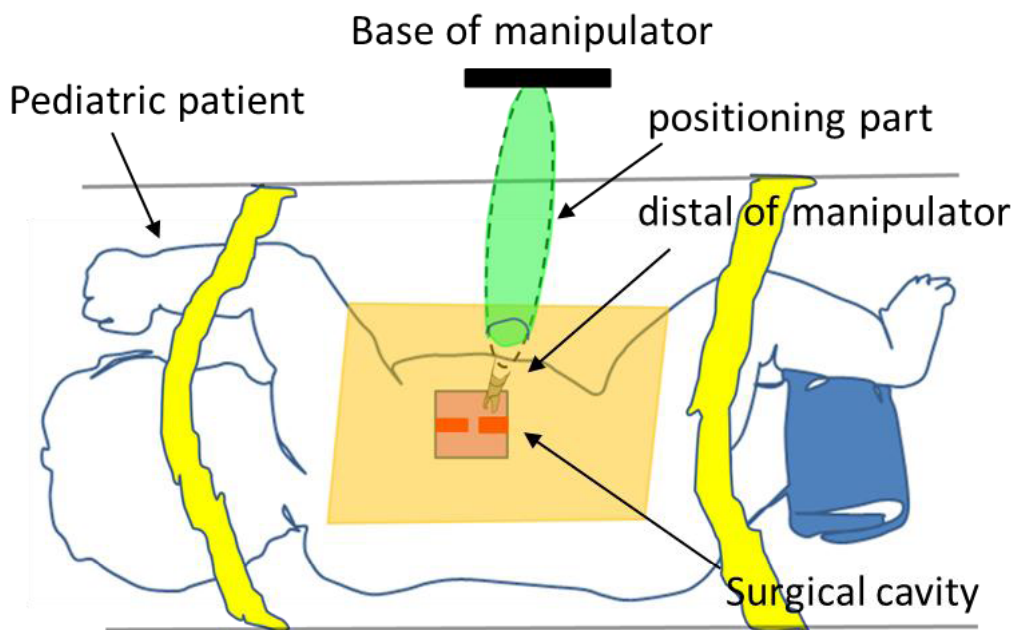


Figure 3. 3 Location between pediatric patient and the surgical robot.

### 3. Mechatronics Design of Pediatric Surgical Robot

---

can have the most rigid robotic structure for a given length. Due to the X, Y, and Z axial platform are independent, therefore, the tip of the robot could achieve a very high precision when use ball bearing. Cartesian robot however, the main disadvantage is that the Cartesian robot occupies a large volume of space to operate, furthermore, linear rail is usually directly mounted at each joint, which make the front part bulky.

#### 2) Six-axis robot

Six-axis robot can move translational along three coordinate axis, and achieve yaw, pitch, roll rotary DoFs corresponding to three coordinate axis. It is suitable to handle complex actions such as reaching under barrier to grab a part and so on. Six-axis robot simulate as human arm that it can handle parts or tools at various angles and positions. Furthermore, the serial structure of six-axis robot occupies a small volume by enveloping its links. The disadvantage is that the cumulative error caused by the serial structure.

#### 3) Parallelogram mechanism

Parallelogram mechanism can arrange a 2D motion by driving two adjacent active levers in a parallelogram. By control the angle between the two adjacent levers, the distal diagonal point corresponding to the cross point of two active levers will be shifted. The parallelogram mechanism can take advantage of lightweight, compact size when all levers are folded. However, the active levers will be unfolded for deploying the distal point to target position. Therefore, it may collide with other parts of the robot, such as the adjacent endoscope.

#### 4) SCARA (Selective Compliance Assembly Robot Arm)

Typical SCARA is used to arrange a tool header in an X-Y-Z envelope. The SCARA is also a mechanism type of serial structure, unlike a six-axis robot, a robotic SCARA mechanism is more limited in movement (rotary movement). The main advantage of SCARA is that higher moving speed. Furthermore, by using timing belt, the transmission medium can be hidden inside the links. Therefore, the SCARA could keep its “slim” links while deploying the serial links in the workspace. The work precision is effected by the workload.

The mechanism type selection for positioning part is shown in Fig. 3.4.

The comparison among these four robot types are listed in table 3-1.

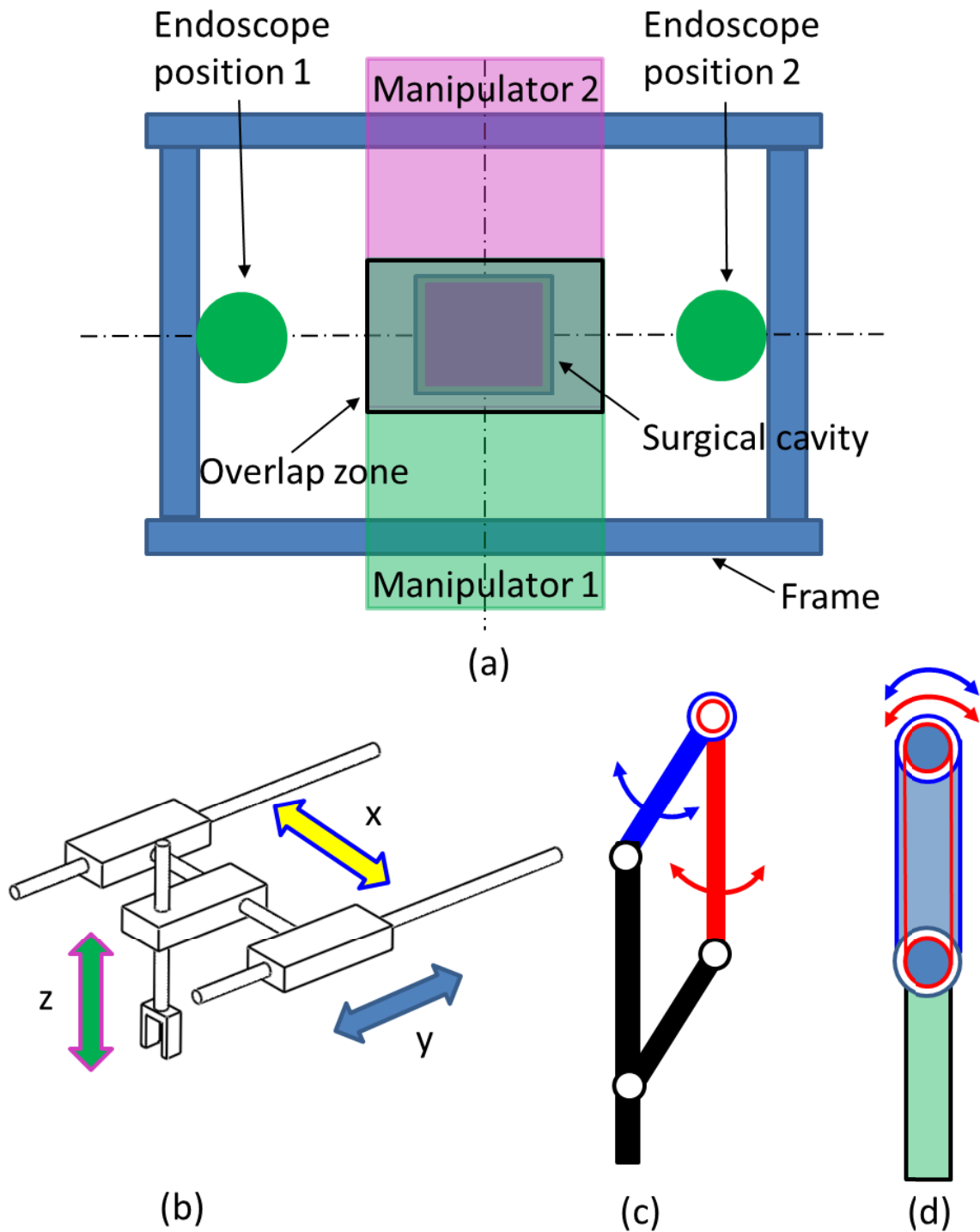


Figure 3. 4 Mechanism type proposal for positioning manipulator. (a) Location between manipulator, endoscope in the proposed surgical robot; (b) Cartesian robot; (c) parallelogram mechanism; (d) SCARA mechanism.

Table 3- 1 Comparison among three typic robots [87][88][89][90]

type	Cartesian robot	Six-axis robot	Parallelogram links	SCARA
Merit	High rigidity; High precision;	Dexterous; compact;	Lightweight; High stiffness; A simple structure;	High speed; compact; light weight
Demerit	Big volume; costly;	Low load capability; Cumulative error; Costly;	Occupy much volume when two active levers unfolded;	Cumulative error; Low load capability;

The mechanism of the proposed robot should be compact and lightweight, since the surgical objective is aim to perform at the pediatric esophageal tissue, therefore, the workload at the robotic plier is light. Compared with the four robot types in table 3-1, due to the requirement of compact design, we chose SCARA mechanism as the positioning manipulator in our robot. In order to reduce the load of the 1<sup>st</sup> joint in the SCARA, we use timing belt to transmit power from the base to the distal of the robot, and attach pretension pulley on the timing belt, therefore, the SCARA mechanism can achieve high position precision when the workload at the distal is light.

#### 3.3.2 Positioning Manipulator

1) *Objective*: The positioning manipulator was designed to control the translational displacement of the tool manipulator.

2) *Distribution of degree of freedom (DoF)*: Generally, three DoFs are required to determine a point in spatial space. Redundant DoFs can be used to improve operative dexterity. The designed positioning manipulator is composed of four DoFs: vertical translational joint of the surgical tool manipulator (one DoF), horizontal translational joint of the surgical tool manipulator (three DoFs). One redundant DoF of the horizontal translational joint is used to set the initial posture of the tool manipulator.

3) *Mechanism*: the positioning manipulator consists of a SCARA mechanism and a screw pair mechanism. It can achieve three dimensions motion in 3D space. The tool manipulator is held at the distal of the SCARA mechanism, and the SCARA mechanism is fixed on the screw nut (shown in Fig. 3.5). Because the SCARA mechanism and the tool manipulator are lightweight, the SCARA and the tool manipulator can easily achieve a translational movement along the screw rotational axis. In the SCARA mechanism, timing belts are employed to transmit power from the base coordinate frame to the corresponding link, since each power transmission path is independent of each other (shown in Fig. 3.6), therefore, link 1, link 2 or link 3 could keep its original pose in the base coordinate system,

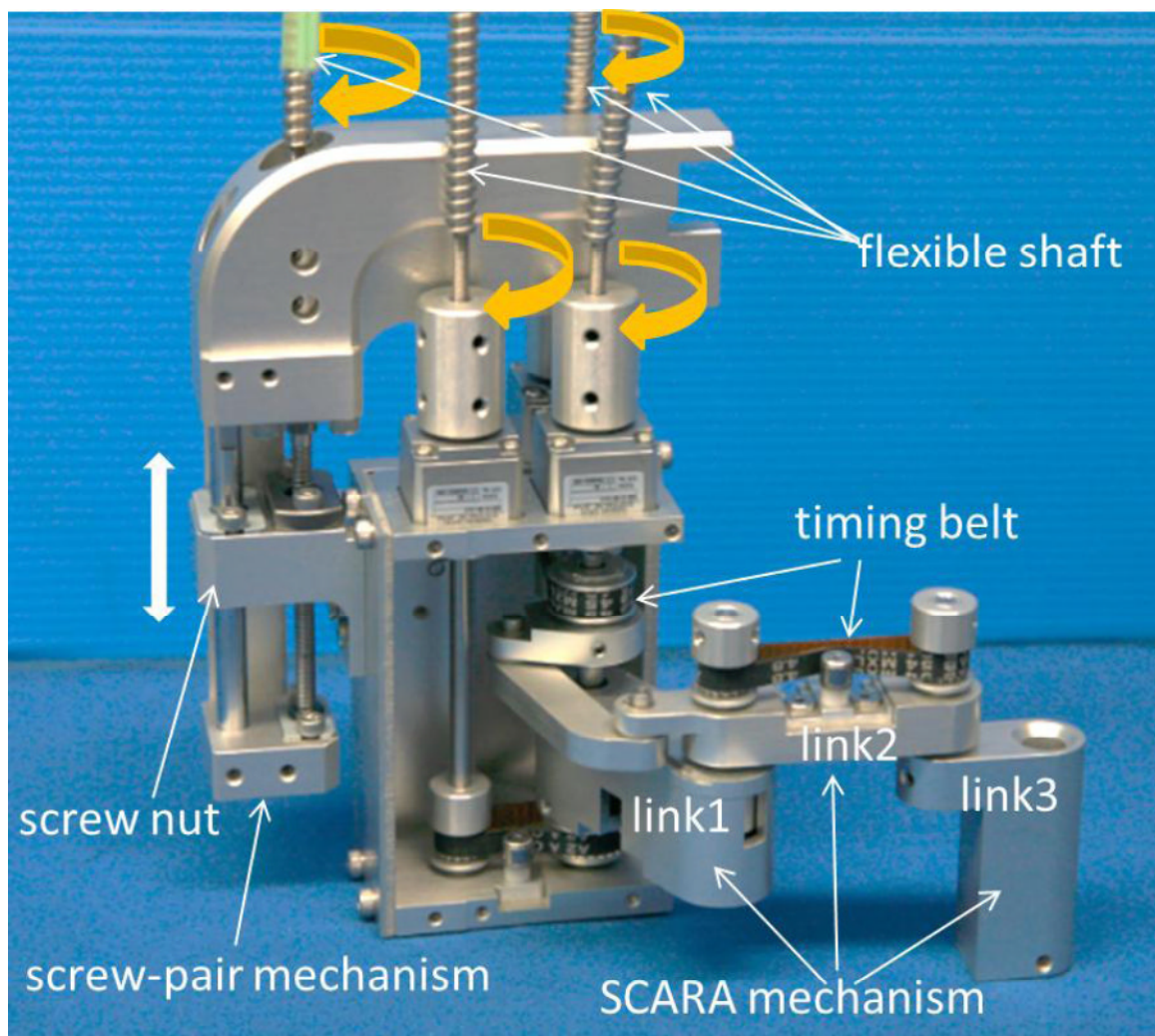


Figure 3.5 Overview of the positioning manipulator.

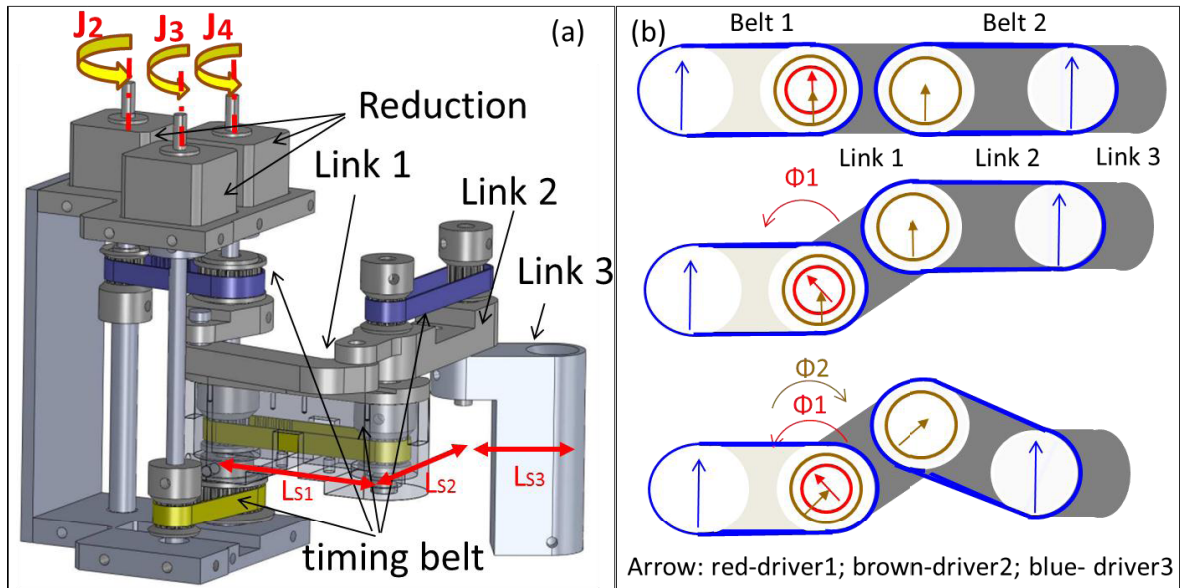


Figure 3.6 Drive principle of SCARA mechanism.

even other links moved. Thanks to this configuration, the positioning manipulator could be easily deployed for adjusting the position of the tool manipulator. Because the link 3 moves in a panel that paralleled with the horizontal plane, thus, the SCARA mechanism can bear large vertical load, which is important in lifting tissue on surgery. The geometric dimension of positioning manipulator is listed in table 3-2. In order to improve the mobility of distribution of motor unit, the motor and joint are not connected with each other directly, alternatively, “motor + flexible shaft + joint” structure is used to transmit motor power to the corresponding rotary joint. We choose Maxon motor as actuator, shown in table 3-3. In order to improve the drive capability of each rotary joint, a reduction (table 3-4) is used to connect with each actuator. Flexible shafts are used for the power transmission elements, which may reduce the overall weight of the robot and decrease the assembly difficulty.

Table 3- 2 Geometric dimension of links in the SCARA

Link No.	Ls1	Ls2	Ls3
Length (mm)	40	40	20



Table 3- 3 Specifications of Maxon motor (EC-max 16 type 283835) [91]

Nominal Voltage	V	24
No load speed (rpm)	rpm	11900
No load current (mA)	mA	31.9
Nominal speed (rpm)	rpm	7360
Nominal torque (max. continuous torque)	mNm	8.19
Nominal current (max. continuous current)	A	0.461
Stall torque	mNm	22.0
Starting current	mA	1.17
Max. efficiency	%	71

Table 3- 4 Specification of Reduction (CSF-5-30-1U) [92]

Output	shaft
reduction	30
Rated torque (N.m)	0.25
Starting torque (N.m)	0.5
Average input speed (r/min)	6500
Max input speed (r/min)	10000
Inertia moment (kgcm <sup>2</sup> )	$2.5 \times 10^{-4}$

### 3.3.3 Surgical Tool Manipulator

1) *Objective:* The surgical tool manipulator is designed for tissue manipulation. The tool manipulator acts as a surgical slave hand for surgical intervention. To realize this task,

the tool manipulator fitted with a forceps as end-effector.

2) *Required DoFs*: In our proposal, the tool manipulator aims to mime human's upper limb. It consists of bendable arm, rotatable wrist and forceps. Generally, more DoFs can achieve higher dexterity. Simultaneously, the tool manipulator should provide sufficient rigidity for tissue operation. Considering the trade-off between dexterity and rigidity, the tool manipulator comprises two segments of bendable joint (improved dexterity), one rotary wrist and a forceps for the opening and closing motion.

3) *Mechanism* [93][94]: Generally, hinge could easily to achieve rotational movement by attaching a motor at the rotary axis. And several hinges with serial architecture may obtain high dexterity. However, this manner poses a big challenge for minimizing the volume of manipulator due to the motor's size. In order to make compact design, wire-driven structure may improve the compactness. Nevertheless, the auxiliary for preloading the wire make the whole mechanism cumbersome. In order to overcome these disadvantages, a "double screw drive (DSD) + universal joint" structure is used to realize the bending motion, referred in [95] [96] [97]. The overview of the tool manipulator is shown in Fig. 3.7.

a). *Bendable joints*

We define the group of a left-handed screw, a right-handed screw and a universal joint as "bending linkage", the group of a universal joint, a support rod as "base linkage". Fig. 3.5 shows the bendable mechanism. It consists of two segments (segment 1 and segment 2), each segment includes two bending linkages and one base linkage, operation of any of the two

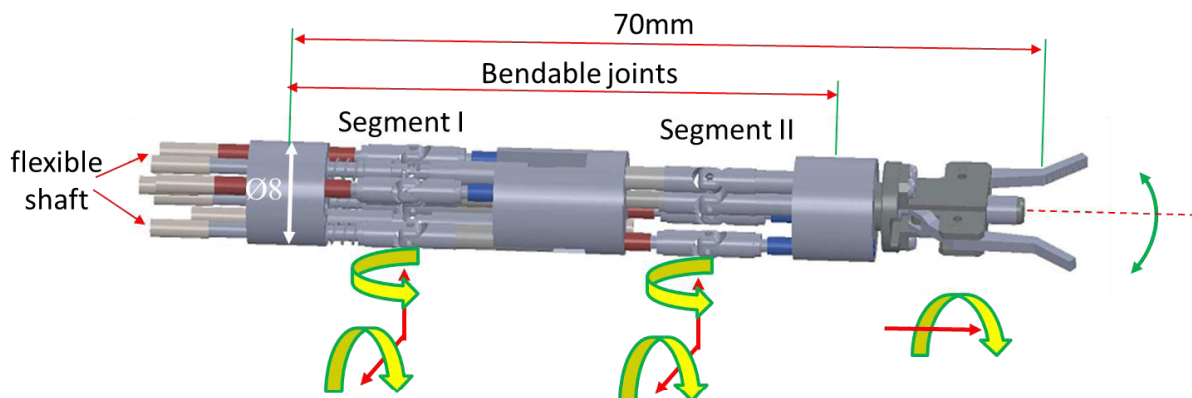


Figure 3.7 Overview of the surgical tool manipulator.

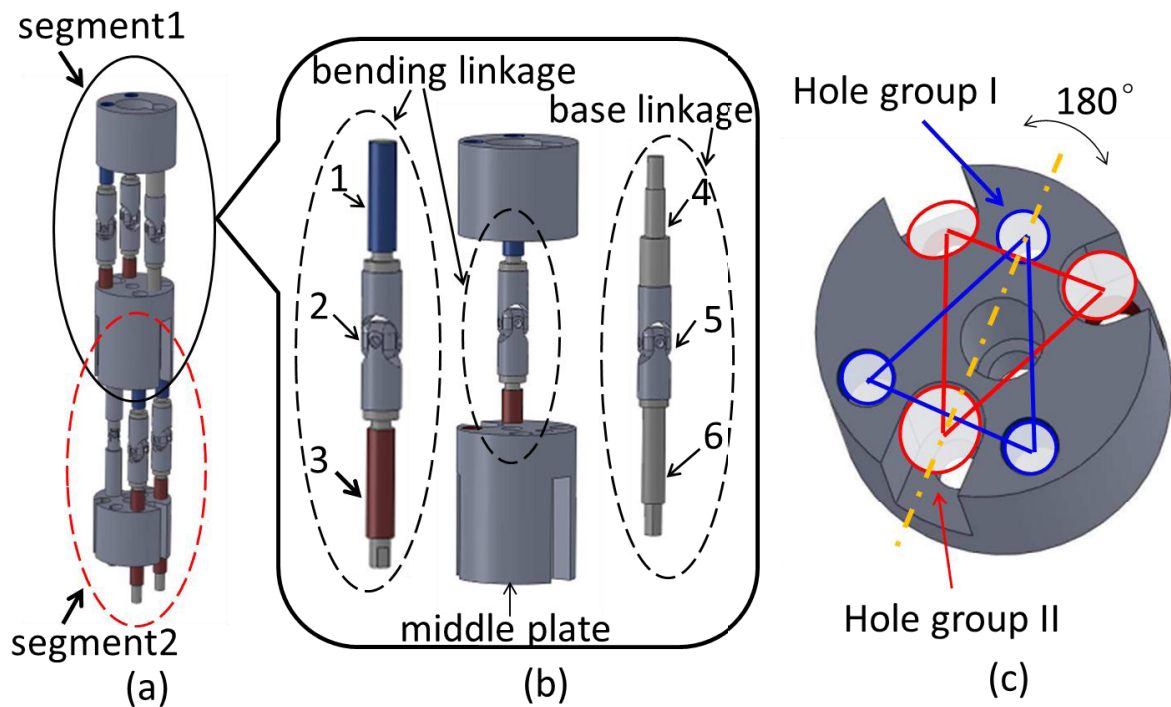


Figure 3.8 Mechanical configuration of bendable joints, (a) bendable joints, (b) nomenclature of mechanical parts, (c) the distribution of channels in the middle frame. 1) Left-handed screw, 2,5) universal joint, 3) right-handed screw, 4,6) support rod.

bending linkages will create an arbitrary orientation bending motion.

In the bending mechanism, two segments structure was adopted, which can realize a big bending angle. Segment 1 and segment 2 can be controlled respectively, which improves the operational dexterity during surgery. In order to transmit rotation between segment1 and segment2, the distribution of linkages on the middle disk is shown in Fig.3.8(c). The angle of distribution between linkages in segment1 and segment2 is  $180^\circ$ , the distribution of base linkages can provide high rigidity for surgical intervention.

#### b) Rotatable gripper

On surgery, the gripper should assist surgeon for tissue grasping and suture operation, the gripper must adjust the posture for proper surgical intervention. In our proposal, a gripper with 1-DoF rotation, opening and closing forceps was designed. The gripper is shown in Fig.3.9.

The gripper consists of a rotation part and a forceps. Rotation actuator rotates along its axial line. Meanwhile, the forceps will rotate along spindle's axial line. A flexible shaft is connected to the gripper actuator, the rotation of the flexible shaft will be transmitted to the spindle, that drives the tip to open or close the forceps.

#### 3.3.4 Visual Module Design

There are two sets of visual modules in this robotic system, shown in Fig. 3.10. The two visual modules located at the different side of the slave tool manipulators. Combination of any visual module with the two slave tool manipulators, a triangle relation of eye-hand coordinate system could be set up. Since the visual module is used to capture surgical information, therefore, the position and posture of the visual module should be adjusted for matching good eye-hand coordination.

A single visual module consists of three degree of freedoms, two translational joints for position adjustment; a single rotary joint for posture adjustment. In the chapter II, the position between the operator, endoscope and the symmetric axis of the slave manipulator should lie in the same line. Therefore, in the design of the visual module, we just attained two translational movements (along x axis and z axis) [94].

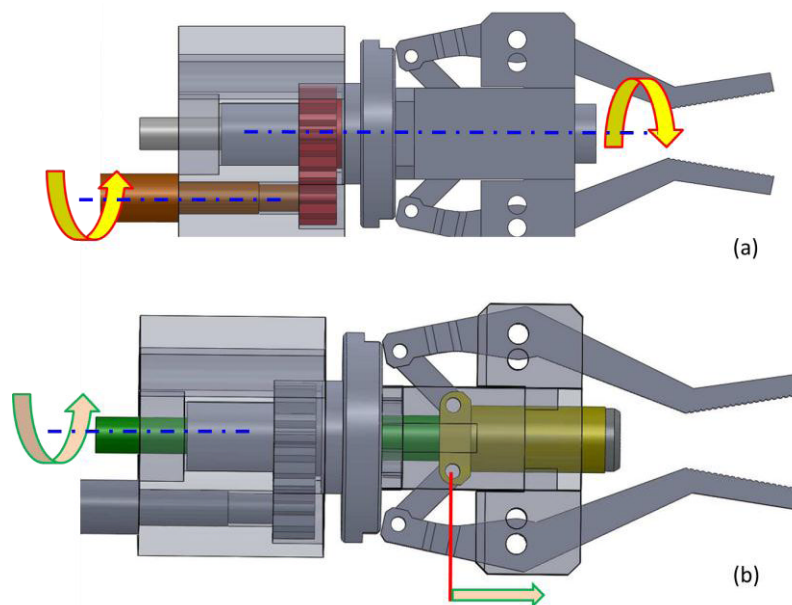


Figure 3.9 Mechanism of gripper, (a) illustration of rotary joint, (b) illustration of gripper

Because the triangle formation between the manipulation axis and the visual axis for comfortable operation is  $30^\circ$  to  $60^\circ$  [83]. The translational distance  $T_4$  base on angle  $\theta$  can be calculated based on the following,

$$\cos \alpha = \frac{(S_3^2 + S_4^2) + S_5^2 - T_4^2}{2S_5\sqrt{S_3^2 + S_4^2}} \quad (3-1)$$

$$\text{tg}^{-1} \frac{S_3}{S_4} + \alpha + \theta = 180^\circ \quad (3-2)$$

Where,

$$T_4 = \sqrt{S_5^2 + S_3^2 + S_4^2 - 2S_5\sqrt{S_3^2 + S_4^2} \cos(\text{tg}^{-1} \frac{S_3}{S_4} + \theta)} \quad (3-3)$$

Based on the geometric dimension of the visual module in the table 3-5, the value can

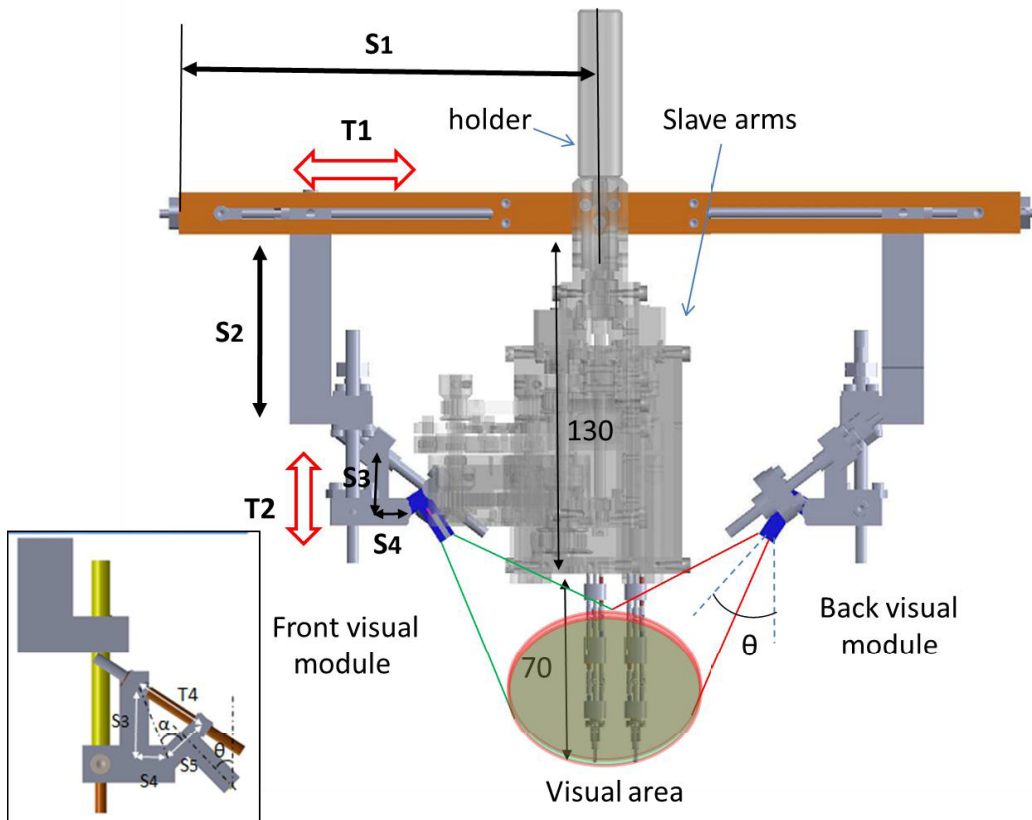


Figure 3.10 Configuration of the visual module in the surgical robot system..

be computed.

Table 3- 5 Geometric dimension and joint range of the visual module

Geometric dimension					
S <sub>1</sub> (mm)	S <sub>2</sub> (mm)	$\theta$ (°)	S <sub>3</sub> (mm)	S <sub>4</sub> (mm)	S <sub>5</sub> (mm)
150	70	45 (initial)	22	8	14.5
Joint range					
T <sub>1</sub> (mm)	T <sub>2</sub> (mm)	T <sub>3</sub> (°)	T <sub>4</sub> (mm)		
0~90	-30~30	30~60	18~25.5		

From Table 3-5, the relation between distance T<sub>4</sub> and the bending angle  $\theta$  is shown in Fig. 3.11.

The mechanism of the visual module is shown in the Fig. 3.12. Considering the compact size, an extra fine endoscope (SPI Engineering, Japan) is attached for catching visual feedback.

## 3.4 Forward Kinematics of the Left Slave Arm

### 3.4.1 Nomenclature of the Feature Points

In this section, we will describe the necessary nomenclature for the formulation of the kinematics of the slave manipulator. As shown in Fig. 3.13, the parameters needed for computation procedure are presented as follows.

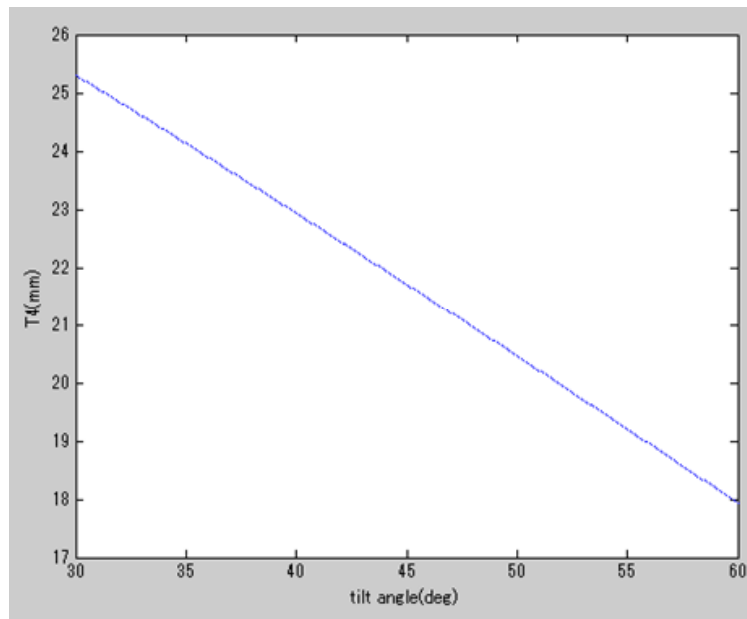


Figure 3.11 Relation between length  $T_4$  and the bending angle  $\theta$ .

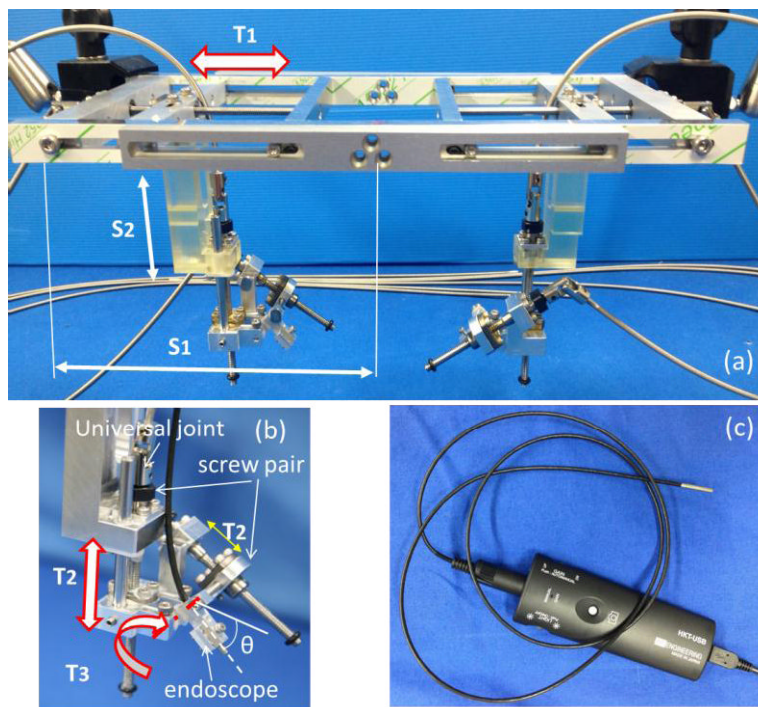


Figure 3.12 Mechanism of the visual module in the surgical robot system. (a) geometric dimension of the visual module; (b) joint configuration; (c) endoscope (SPI Engineering, Japan)

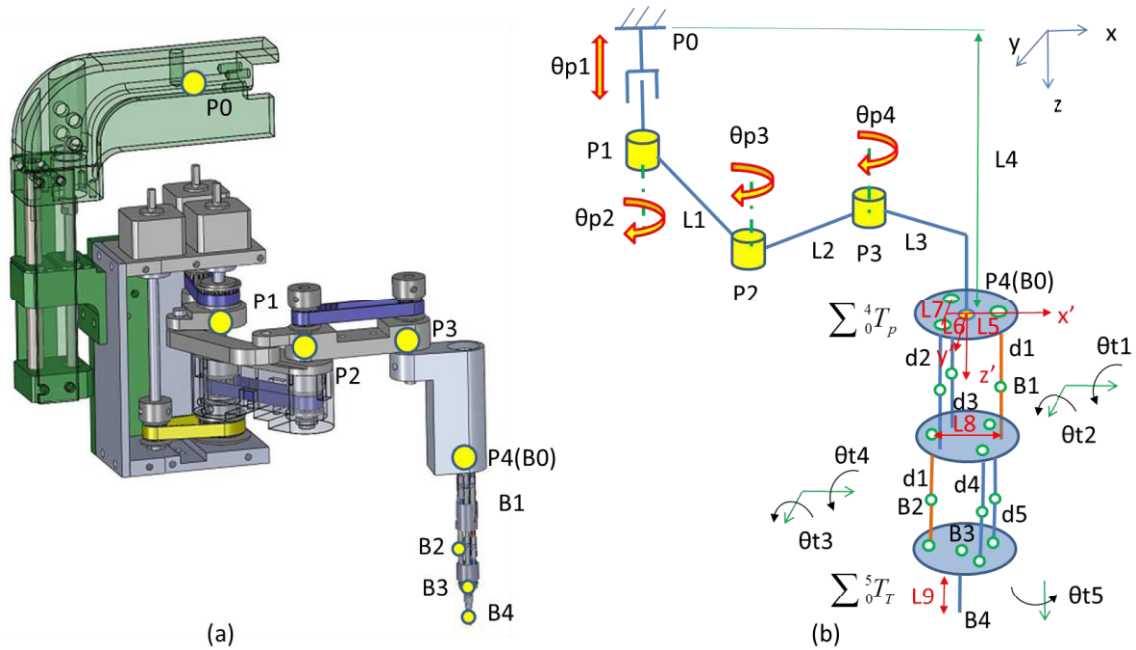


Figure 3.13 Nomenclature of the left arm,  
 (a) definition of feature points, (b) coordination chain.

- $P_i$  ( $i=0\sim4$ ) is the feature point in the joint of positioning manipulator;  $B_i$  ( $i=0\sim4$ ) is the feature point of tool manipulator. Since the tool manipulator is attached at the tip of the positioning manipulator, therefore, point P4 and B0 are coincidence.
- $\theta_{p_i}$  ( $i=1\sim4$ ) illustrates the amount of movement of the positioning manipulator, while  $\theta_{p_1}$  is the translational displacement;  $\theta_{p_2}$ ,  $\theta_{p_3}$ ,  $\theta_{p_4}$  are the rotary displacements of the SCARA mechanism.  $\theta_{t_i}$  ( $i=1\sim5$ ) illustrates the amount of movement of the tool manipulator, while  $\theta_{t_1}$ ,  $\theta_{t_2}$  are located in the two orthogonal plane of segment I;  $\theta_{t_3}$ ,  $\theta_{t_4}$  are located in the two orthogonal plane of segment II; the combination of  $\theta_{t_1}$ ,  $\theta_{t_2}$  and  $\theta_{t_3}$ ,  $\theta_{t_4}$  could achieve  $45^\circ$  bending movement in arbitrary orientation, respectively. The combination of bending movement of segment I and segment II could obtain  $90^\circ$  in Omni-direction.
- $L_n$  ( $n=1\sim9$ ) is the geometric dimension of slave manipulator.  $L_1$ ,  $L_2$  and  $L_3$  are the lengths of the SCARA links;  $L_4$  describes the initial distance between the reference coordinate and the base of the tool manipulator. Parameters  $L_n$  ( $n=5\sim9$ ) describe the geometry of tool manipulator.  $L_5$  presents the distance between point  $P_4$  and



base linkage;  $L_6$  presents the distance between point  $P_4$  and bending linkage;  $L_7$  presents the distance between two bending linkages in a single segment;  $L_8$  presents the distance between two base linkages in the middle frame;  $L_9$  presents the length of forceps.

- $d_n$  ( $n=1\sim5$ ) describes the length of the linkages in tool manipulator.  $d_1$  is length of the base linkage;  $d_2$  and  $d_3$  are the length of bending linkages of segment I in manipulator;  $d_4$  and  $d_5$  are the length of bending linkages of segment II in the tool manipulator.

According to the nomenclature of parameters in the slave manipulator, the geometric dimensions of the slave manipulator are listed in table 3-6.

Table 3- 6 Geometric dimension of the slave arm

Positioning manipulator					
$L_1$ mm	$L_2$ mm	$L_3$ mm	$L_4$ mm		
40	40	20	145		
Tool manipulator					
$L_5$ mm	$L_6$ mm	$L_7$ mm	$L_8$ mm	$L_9$ mm	$d_1$ mm
2.4	2.1	4.2	4.8	11	15

### 3.4.2 Forward Kinematics

From the figure 3.13, the positioning manipulator can just affect the position of the distal of the manipulator. The tool manipulator is mainly for adjusting for tip'orientation. Corresponding to this characteristics, the calculation of the position and orientation of the tool

manipulator's tip can be divided into two parts,  $\sum_{i=1}^5 {}^{i-1}T_p$  and  $\sum_{j=1}^5 {}^{j-1}T_t$ . The kinematics matrix

of the tool manipulator can be calculated by,

$${}^0T = \sum_{i=1}^5 {}^{i-1}T_p \cdot \sum_{j=1}^5 {}^{j-1}T_t \quad (3.4)$$

### 3. Mechatronics Design of Pediatric Surgical Robot

Where,  $\sum_{i=1}^5 {}^{i-1}T_p$  - the kinematics chain of the positioning manipulator;

$\sum_{j=1}^5 {}^{j-1}T_t$  - the kinematics chain of the tool manipulator.

DH matrix is used to express the kinematics chain of the manipulator. Since the DH matrix cannot directly describe the two adjacent orthogonal transforms, therefore, only the positioning manipulator use DH matrix transmission, while, the tool manipulator directly use transfer matrix for kinematics transmission.. Table 3-7 shows the DH parameters of the positioning manipulator.

Table 3- 7 DH parameter of the positioning manipulator

i	$\alpha_{i-1}$ (°)	$a_{i-1}$ (mm)	$d_i$ (mm)	$\theta_i$ (°)
1	0	0	$\theta_{p1}$ (-30~30)	0
2	0	0	0	$\theta_{p2} + 90$ (-90~90)
3	0	$L_1$	0	$\theta_{p3} - 90$ (0~150)
4	0	$L_2$	0	$\theta_{p4}$ (-90~240)
5	0	$L_3$	$L_4$	0

Where,  $L_1 = 40$  mm,  $L_2 = 40$  mm,  $L_3 = 20$  mm,  $L_4 = 145$  mm.

Equation (3.2) shows the homogeneous transformation matrix for each joint of our manipulator joint i to i-1 [98].

$${}^{i-1}T_i = \begin{bmatrix} c\theta_i & -s\theta_i & 0 & a_{i-1} \\ s\theta_i \cdot c\alpha_{i-1} & c\theta_i \cdot c\alpha_{i-1} & -s\alpha_{i-1} & -d_i \cdot s\alpha_{i-1} \\ s\theta_i \cdot s\alpha_{i-1} & c\theta_i \cdot s\alpha_{i-1} & c\alpha_{i-1} & d_i \cdot c\alpha_{i-1} \\ 0 & 0 & 0 & 1 \end{bmatrix} \quad (3.5)$$

Where,  $s\theta_i = \sin\theta_i$ ,  $c\theta_i = \cos\theta_i$ .

Substituting the parameters of table 3-4 into (3.5), get

$$\begin{aligned}
 {}^0T_p &= \begin{bmatrix} 1 & 0 & 0 & 0 \\ 0 & 1 & 0 & 0 \\ 0 & 0 & 1 & \theta_{p1} \\ 0 & 0 & 0 & 1 \end{bmatrix} & {}^1T_p &= \begin{bmatrix} -s\theta_{p2} & -c\theta_{p2} & 0 & 0 \\ c\theta_{p2} & -s\theta_{p2} & 0 & 0 \\ 0 & 0 & 1 & 0 \\ 0 & 0 & 0 & 1 \end{bmatrix} \\
 {}^2T_p &= \begin{bmatrix} s\theta_{p3} & c\theta_{p3} & 0 & L_1 \\ -c\theta_{p3} & s\theta_{p3} & 0 & 0 \\ 0 & 0 & 1 & 0 \\ 0 & 0 & 0 & 1 \end{bmatrix} & {}^3T_p &= \begin{bmatrix} c\theta_{p4} & -s\theta_{p4} & 0 & L_2 \\ s\theta_{p4} & c\theta_{p4} & 0 & 0 \\ 0 & 0 & 1 & 0 \\ 0 & 0 & 0 & 1 \end{bmatrix} \\
 {}^4T_p &= \begin{bmatrix} 1 & 0 & 0 & L_3 \\ 0 & 1 & 0 & 0 \\ 0 & 0 & 1 & L_4 \\ 0 & 0 & 0 & 1 \end{bmatrix} & & & & & & & & & & (3.6)
 \end{aligned}$$

Therefore, the position and orientation of the distal of the positioning manipulator can be expressed as,

$${}^0T_p = \prod_{i=1}^5 {}^{i-1}T_p \quad (3.7)$$

Since the positioning manipulator mainly for adjusting the positioning of the tool manipulator and both positioning manipulator are symmetrical, therefore, substituting the range of each joint, the workspace of the SCARA mechanism is shown in Fig. 3.13. The green area and the the blue area are the workspace of the left SCARA and the right SCARA, respectively. The yellow area is the overlap region of the two SCARA mechanisms. The purple area describes a 30x30 workspace for surgery. From Fig. 3.14, it shows the SCARA mechanisms are competent for arranging the tool manipulators in the narrow workspace.

In the tool manipulator, it consists of two bendable joints, a rotary gripper. Each bendable joint use universal joint as fulcrum, can achieve bending movement in two orthogonal orientations. As shown in Fig. 3.15, the corresponding joint axes of both bendable joints are parallel to each other when the manipulator is in a straight state (rotary axis  $\theta_{i1}$  and  $\theta_{i4}$ ,  $\theta_{i2}$  and  $\theta_{i3}$  are parallel with each other, respectively). The isotropic actuations of the dual bendable joints generate a planar motion. These two motion planes are orthogonal to each other.

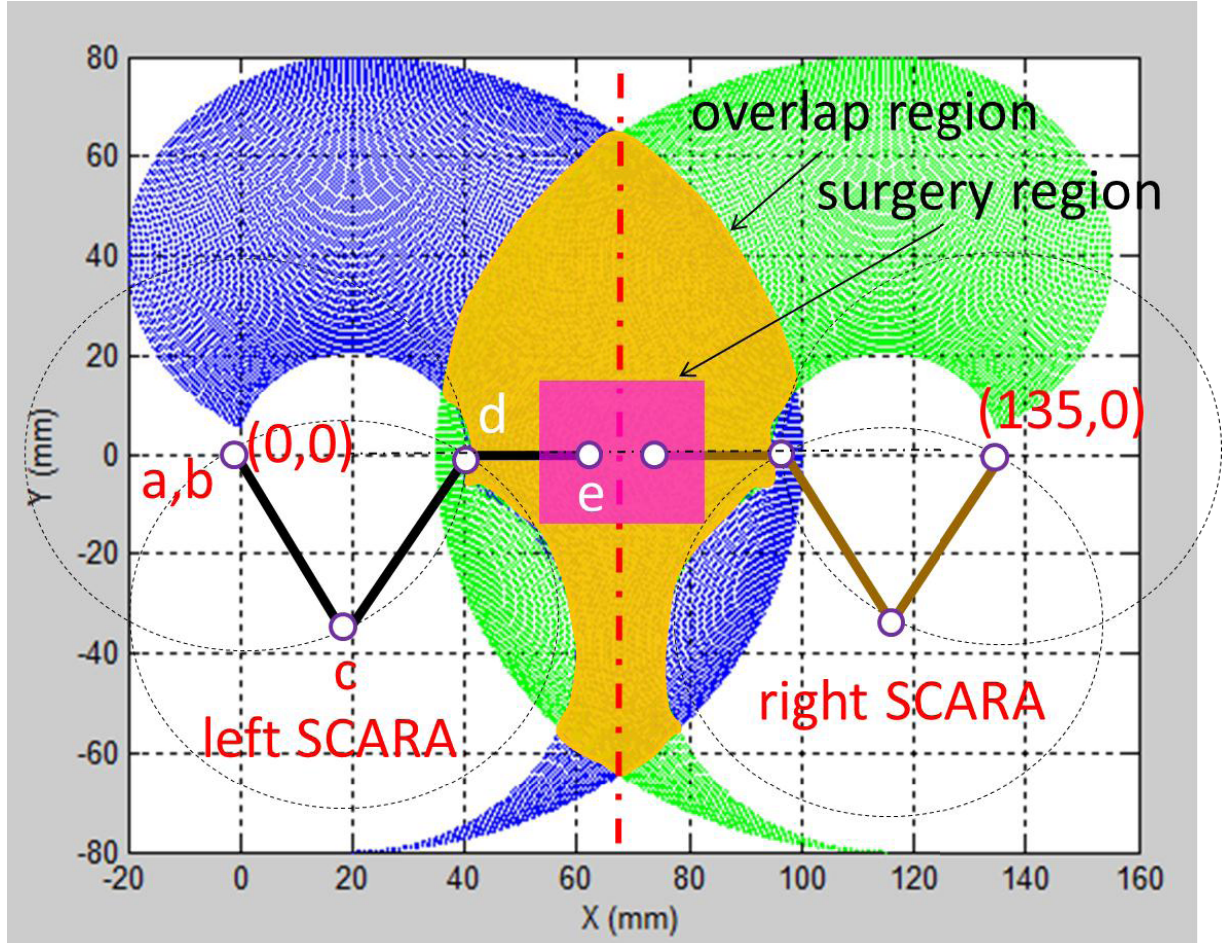


Figure 3.14 Workspace of the positioning manipulator.

In this thesis, we employ  $xyyx$  orders to describe the kinematics chain of the tool manipulator, therefore, in the computation, the bending motion of tool manipulator follow the order of  $\theta_{i1} \rightarrow \theta_{i2} \rightarrow \theta_{i3} \rightarrow \theta_{i4}$ . The kinematics parameters of the tool manipulator are listed in table 3-8. By combining with the translational joint of the positioning manipulator, the transfer matrix of the tool manipulator can be calculated,

$${}^0T_1 = \begin{bmatrix} 1 & 0 & 0 & L_5 \\ 0 & 1 & 0 & 0 \\ 0 & 0 & 1 & d_1 + \theta_{p1} \\ 0 & 0 & 0 & 1 \end{bmatrix} {}^1T_2 = \begin{bmatrix} 1 & 0 & 0 & 0 \\ 0 & c\theta_{i1} & -s\theta_{i1} & 0 \\ 0 & s\theta_{i1} & c\theta_{i1} & 0 \\ 0 & 0 & 0 & 1 \end{bmatrix} {}^2T_3 = \begin{bmatrix} c\theta_{i2} & 0 & s\theta_{i2} & 0 \\ 0 & 1 & 0 & 0 \\ -s\theta_{i2} & 0 & c\theta_{i2} & 0 \\ 0 & 0 & 0 & 1 \end{bmatrix}$$

Table 3- 8 Kinematics parameter of the tool manipulator

i	$\theta_x$	$\theta_y$	$\theta_z$	$\Delta x$	$\Delta y$	$\Delta z$
1	0	0	0	$L_5 (2.4)$	0	$d_1 (15)$
2	$\theta_{t1}$	0	0	0	0	0
3	0	$\theta_{t2}$	0	0	0	0
4	0	0	0	$-L_8(-4.8)$	0	$2 d_1 (30)$
5	0	$\theta_{t3}$	0	0	0	0
6	$\theta_{t4}$	0	0	0	0	0
7	0	0	0	$L_5(2.4)$	0	$d_1(15)$
8	0	0	$\theta_{t5}$	0	0	0

$$\begin{aligned}
 {}^3T_4 &= \begin{bmatrix} 1 & 0 & 0 & -L_8 \\ 0 & 1 & 0 & 0 \\ 0 & 0 & 1 & 2d_1 \\ 0 & 0 & 0 & 1 \end{bmatrix} &
 {}^4T_5 &= \begin{bmatrix} c\theta_{t3} & 0 & s\theta_{t3} & 0 \\ 0 & 1 & 0 & 0 \\ -s\theta_{t3} & 0 & c\theta_{t3} & 0 \\ 0 & 0 & 0 & 1 \end{bmatrix} &
 {}^5T_6 &= \begin{bmatrix} 1 & 0 & 0 & 0 \\ 0 & c\theta_{t4} & -s\theta_{t4} & 0 \\ 0 & s\theta_{t4} & c\theta_{t4} & 0 \\ 0 & 0 & 0 & 1 \end{bmatrix} \\
 {}^6T_7 &= \begin{bmatrix} 1 & 0 & 0 & L_5 \\ 0 & 1 & 0 & 0 \\ 0 & 0 & 1 & d_1 \\ 0 & 0 & 0 & 1 \end{bmatrix} &
 {}^7T_8 &= \begin{bmatrix} c\theta_{t5} & -s\theta_{t5} & 0 & 0 \\ s\theta_{t5} & c\theta_{t5} & 0 & 0 \\ 0 & 0 & 1 & L_9 \\ 0 & 0 & 0 & 1 \end{bmatrix} &
 & (3.8)
 \end{aligned}$$

Therefore, the position and orientation of point  $B_4$  can be calculated

$${}^0T_8 = \prod_{i=1}^8 {}^{i-1}T_i \quad (3.9)$$

By substituting (3.8) into (3.9), the transfer matrix is given,

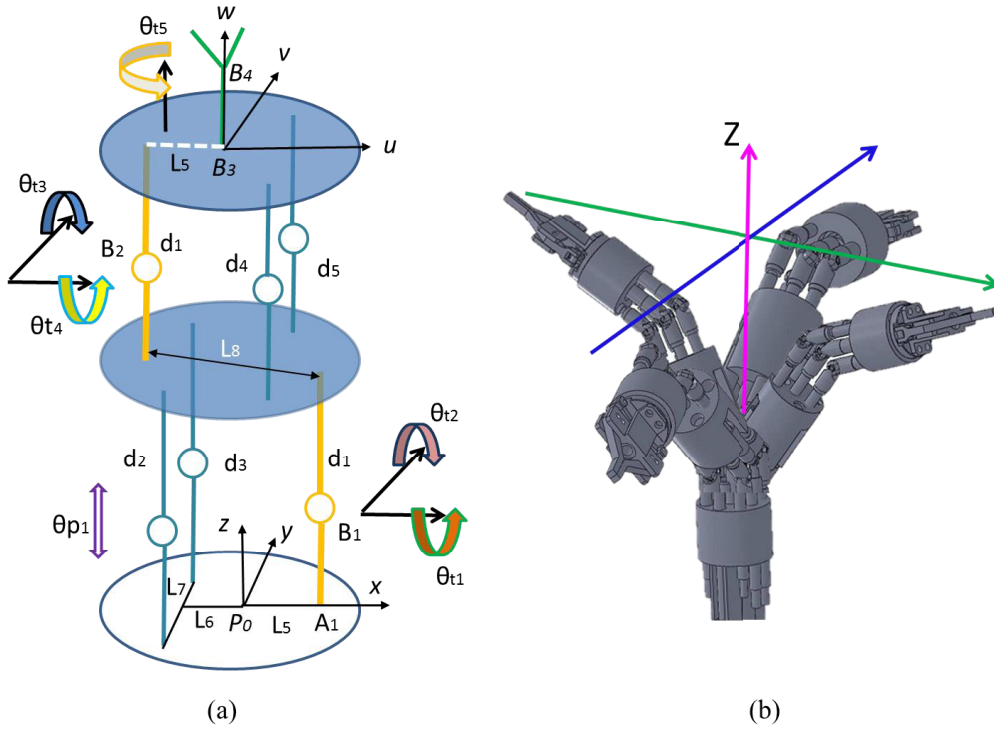


Figure 3.15 Nomenclature of the tool manipulator. (a) feature points and distribution of DOFs; (b) schematic movement of tool manipulator.

$${}^0T_i = \begin{bmatrix} c\theta_{i2+i3} & s\theta_{i4}s\theta_{i2+i3} & c\theta_{i4}s\theta_{i2+i3} & P_x \\ s\theta_{i1}s\theta_{i2+i3} & c\theta_{i1}c\theta_{i4} - s\theta_{i1}s\theta_{i4}c\theta_{i2+i3} & -c\theta_{i4}s\theta_{i1}c\theta_{i2+i3} - c\theta_{i1}s\theta_{i4} & P_y \\ -c\theta_{i1}s\theta_{i2+i3} & s\theta_{i1}c\theta_{i4} - c\theta_{i1}s\theta_{i4}c\theta_{i2+i3} & c\theta_{i1}c\theta_{i4}c\theta_{i2+i3} - s\theta_{i1}s\theta_{i4} & P_z \\ 0 & 0 & 0 & 1 \end{bmatrix}$$

(3.10)

Where,

$$\begin{aligned} P_x &= 2d_1s\theta_{i2} - 2L_5c\theta_{i2} + L_5c\theta_{i2+i3} + d_1c\theta_{i4}s\theta_{i2+i3} + L_5 \\ P_y &= -d_1s\theta_{i1}c\theta_{i4}c\theta_{i2+i3} - d_1c\theta_{i1}s\theta_{i4} - 2L_5s\theta_{i1}s\theta_{i2} - 2d_1c\theta_{i2}s\theta_{i1} + L_5s\theta_{i1}s\theta_{i2+i3} \\ P_z &= d_1c\theta_{i1}c\theta_{i4}c\theta_{i2+i3} - d_1s\theta_{i1}s\theta_{i4} + 2L_5c\theta_{i1}s\theta_{i2} + 2d_1c\theta_{i2}c\theta_{i1} - L_5c\theta_{i1}s\theta_{i2+i3} + d_1 + \theta_{p1} \end{aligned}$$

(3.11)

Where,  $s\theta_i = \sin \theta_i$ ,  $c\theta_i = \cos \theta_i$ ,  $s\theta_{i+j} = \sin(\theta_i + \theta_j)$ ,  $c\theta_{i+j} = \cos(\theta_i + \theta_j)$ .

In the bendable joints, the rigid manipulator links are connected by universal joints, each providing two-degree-of-freedom rotational movement within  $\pm 45^\circ$ . The workspace of

the tool manipulator is shown in Fig. 3.16. It covers a 40x40x13 mm by bendable joints.

### 3.5 Inverse Kinematics of the Left Slave Arm

In session 3.4, substituting (3.6) into (3.7), we can obtain the tip position of positioning manipulator,

$$\begin{aligned} x_{p4} &= L_2 \cos(\theta_{p2} + \theta_{p3}) - L_1 \sin \theta_{p2} + L_3 \cos \theta_{p4} \cos(\theta_{p2} + \theta_{p3}) - L_3 \sin \theta_{p4} \sin(\theta_{p2} + \theta_{p3}) \\ y_{p4} &= L_2 \sin(\theta_{p2} + \theta_{p3}) + L_1 \sin \theta_{p2} + L_3 \cos \theta_{p4} \sin(\theta_{p2} + \theta_{p3}) + L_3 \sin \theta_{p4} \cos(\theta_{p2} + \theta_{p3}) \end{aligned} \quad (3.12)$$

Combining (3.11) and (3.12), the position of the tip of the slave arm refer to the world coordinate frame can be given

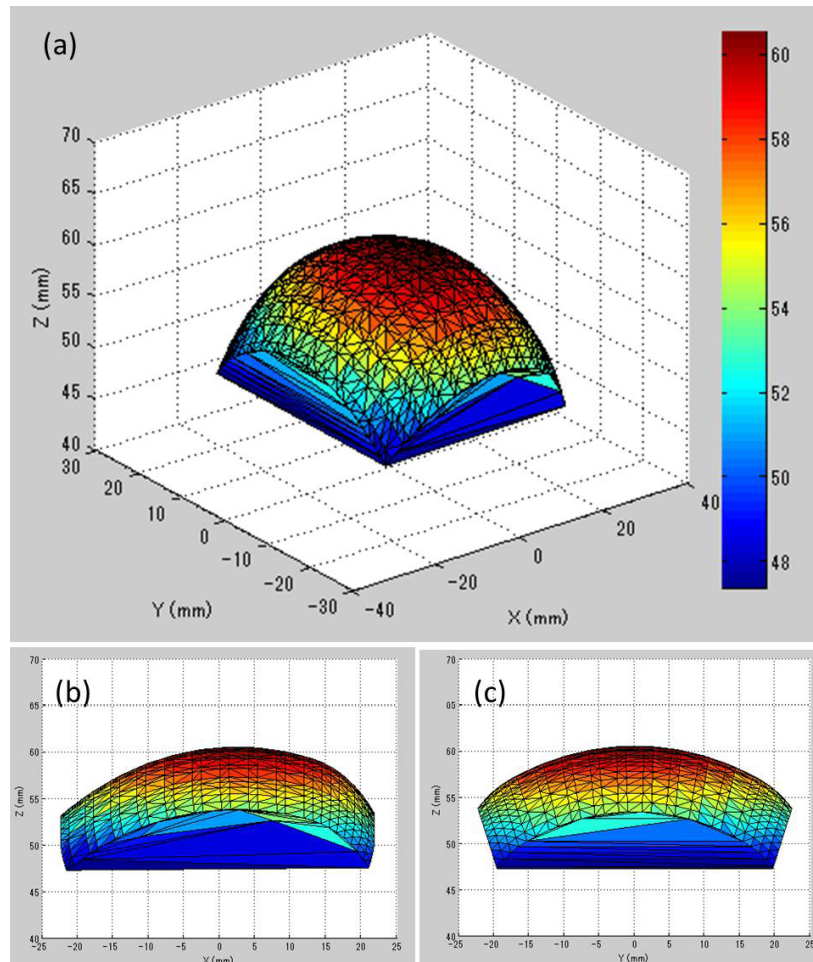


Figure 3. 16 Workspace of the tool manipulator,  
(a) the isometric view, (b) the XZ view, (c) the YZ view.

### 3. Mechatronics Design of Pediatric Surgical Robot

$$\begin{aligned}
P_{tip\_x} &= L_2 \cos(\theta_{\rho_2} + \theta_{\rho_3}) - L_1 \sin \theta_{\rho_2} + L_3 \cos \theta_{\rho_4} \cos(\theta_{\rho_2} + \theta_{\rho_3}) - L_3 \sin \theta_{\rho_4} \sin(\theta_{\rho_2} + \theta_{\rho_3}) + \\
&\quad 2d_1 s \theta_{i_2} - 2L_5 c \theta_{i_2} + L_5 c \theta_{i_2+i_3} + d_1 c \theta_{i_4} s \theta_{i_2+i_3} + L_5 \\
P_{tip\_y} &= -d_1 s \theta_{i_1} c \theta_{i_4} c \theta_{i_2+i_3} - d_1 c \theta_{i_1} s \theta_{i_4} - 2L_5 s \theta_{i_1} s \theta_{i_2} - 2d_1 c \theta_{i_2} s \theta_{i_1} + L_5 s \theta_{i_1} s \theta_{i_2+i_3} + \\
&\quad L_2 \sin(\theta_{\rho_2} + \theta_{\rho_3}) + L_1 \sin \theta_{\rho_2} + L_3 \cos \theta_{\rho_4} \sin(\theta_{\rho_2} + \theta_{\rho_3}) + L_3 \sin \theta_{\rho_4} \cos(\theta_{\rho_2} + \theta_{\rho_3}) \\
P_{tip\_z} &= d_1 c \theta_{i_1} c \theta_{i_4} c \theta_{i_2+i_3} - d_1 s \theta_{i_1} s \theta_{i_4} + 2L_5 c \theta_{i_1} s \theta_{i_2} + 2d_1 c \theta_{i_2} c \theta_{i_1} - L_5 c \theta_{i_1} s \theta_{i_2+i_3} + d_1 + \theta_{\rho_1}
\end{aligned} \tag{3.13}$$

In (3.13), the input variables include  $\theta_{\rho_1}, \theta_{\rho_2}, \theta_{\rho_3}, \theta_{i_1}, \theta_{i_2}, \theta_{i_3}, \theta_{i_4}$ . The output variables include  $P_{tip\_x}, P_{tip\_y}, P_{tip\_z}$ . Therefore, the Jacobian matrix of the slave arm can be calculated,

$$J_{tip}(\theta_{\rho_1}, \theta_{\rho_2}, \theta_{\rho_3}, \theta_{i_1}, \theta_{i_2}, \theta_{i_3}, \theta_{i_4}) = \begin{bmatrix} \frac{\partial P_{tip\_x}}{\partial \theta_{\rho_1}} & \frac{\partial P_{tip\_x}}{\partial \theta_{\rho_2}} & \frac{\partial P_{tip\_x}}{\partial \theta_{\rho_3}} & \frac{\partial P_{tip\_x}}{\partial \theta_{i_1}} & \frac{\partial P_{tip\_x}}{\partial \theta_{i_2}} & \frac{\partial P_{tip\_x}}{\partial \theta_{i_3}} & \frac{\partial P_{tip\_x}}{\partial \theta_{i_4}} \\ \frac{\partial P_{tip\_y}}{\partial \theta_{\rho_1}} & \frac{\partial P_{tip\_y}}{\partial \theta_{\rho_2}} & \frac{\partial P_{tip\_y}}{\partial \theta_{\rho_3}} & \frac{\partial P_{tip\_y}}{\partial \theta_{i_1}} & \frac{\partial P_{tip\_y}}{\partial \theta_{i_2}} & \frac{\partial P_{tip\_y}}{\partial \theta_{i_3}} & \frac{\partial P_{tip\_y}}{\partial \theta_{i_4}} \\ \frac{\partial P_{tip\_z}}{\partial \theta_{\rho_1}} & \frac{\partial P_{tip\_z}}{\partial \theta_{\rho_2}} & \frac{\partial P_{tip\_z}}{\partial \theta_{\rho_3}} & \frac{\partial P_{tip\_z}}{\partial \theta_{i_1}} & \frac{\partial P_{tip\_z}}{\partial \theta_{i_2}} & \frac{\partial P_{tip\_z}}{\partial \theta_{i_3}} & \frac{\partial P_{tip\_z}}{\partial \theta_{i_4}} \end{bmatrix} \begin{bmatrix} d_{\theta_{\rho_1}} \\ d_{\theta_{\rho_2}} \\ d_{\theta_{\rho_3}} \\ d_{\theta_{i_1}} \\ d_{\theta_{i_2}} \\ d_{\theta_{i_3}} \\ d_{\theta_{i_4}} \end{bmatrix} \tag{3.14}$$

(3.14)

Where,

$$\frac{\partial P_{tip\_x}}{\partial \theta_{\rho_1}} = 0$$

$$\frac{\partial P_{tip\_x}}{\partial \theta_{\rho_2}} = -L_2 \sin(\theta_{\rho_2} + \theta_{\rho_3}) - L_1 \cos \theta_{\rho_2} - L_3 \cos \theta_{\rho_4} \sin(\theta_{\rho_2} + \theta_{\rho_3}) - L_3 \sin \theta_{\rho_4} \cos(\theta_{\rho_2} + \theta_{\rho_3})$$

$$\frac{\partial P_{tip\_x}}{\partial \theta_{\rho_3}} = -L_2 \sin(\theta_{\rho_2} + \theta_{\rho_3}) - L_3 \cos \theta_{\rho_4} \sin(\theta_{\rho_2} + \theta_{\rho_3}) - L_3 \sin \theta_{\rho_4} \cos(\theta_{\rho_2} + \theta_{\rho_3})$$

$$\frac{\partial P_{tip\_x}}{\partial \theta_{i_1}} = 0$$

$$\frac{\partial P_{tip\_x}}{\partial \theta_{i_2}} = 2d_1 \cos \theta_{i_2} + 2L_5 \sin \theta_{i_2} - L_5 \sin(\theta_{i_2} + \theta_{i_3}) + d_1 \cos \theta_{i_4} \cos(\theta_{i_2} + \theta_{i_3})$$



$$\frac{\partial P_{ip-x}}{\partial \theta_{i3}} = -L_5 \sin(\theta_{i2} + \theta_{i3}) + d_1 \cos \theta_{i4} \cos(\theta_{i2} + \theta_{i3})$$

$$\frac{\partial P_{ip-x}}{\partial \theta_{i4}} = -d_1 \sin \theta_{i4} \sin(\theta_{i2} + \theta_{i3})$$

$$\frac{\partial P_{ip-y}}{\partial \theta_{p1}} = 0$$

$$\frac{\partial P_{ip-y}}{\partial \theta_{p2}} = L_2 \cos(\theta_{p2} + \theta_{p3}) + L_1 \cos \theta_{p2} + L_3 \cos \theta_{p4} \cos(\theta_{p2} + \theta_{p3}) - L_3 \sin \theta_{p4} \sin(\theta_{p2} + \theta_{p3})$$

$$\frac{\partial P_{ip-y}}{\partial \theta_{p3}} = L_2 \cos(\theta_{p2} + \theta_{p3}) + L_3 \cos \theta_{p4} \cos(\theta_{p2} + \theta_{p3}) - L_3 \sin \theta_{p4} \sin(\theta_{p2} + \theta_{p3})$$

$$\begin{aligned} \frac{\partial P_{ip-y}}{\partial \theta_{i1}} = & -d_1 \cos \theta_{i1} \cos \theta_{i4} \cos(\theta_{i2} + \theta_{i3}) + d_1 \sin \theta_{i1} \sin \theta_{i4} - 2L_5 \cos \theta_{i1} \sin \theta_{i2} \\ & - 2d_1 \cos \theta_{i2} \cos \theta_{i1} + L_5 \cos \theta_{i1} \sin(\theta_{i2} + \theta_{i3}) \end{aligned}$$

$$\frac{\partial P_{ip-y}}{\partial \theta_{i2}} = d_1 \sin \theta_{i1} \cos \theta_{i4} \sin(\theta_{i2} + \theta_{i3}) - 2L_5 \cos \theta_{i1} \cos \theta_{i2} + 2d_1 \sin \theta_{i2} \cos \theta_{i1} + L_5 \sin \theta_{i1} \cos(\theta_{i2} + \theta_{i3})$$

$$\frac{\partial P_{ip-y}}{\partial \theta_{i3}} = d_1 \sin \theta_{i1} \cos \theta_{i4} \sin(\theta_{i2} + \theta_{i3}) + L_5 \sin \theta_{i1} \cos(\theta_{i2} + \theta_{i3})$$

$$\frac{\partial P_{ip-y}}{\partial \theta_{i4}} = d_1 \sin \theta_{i1} \sin \theta_{i4} \sin(\theta_{i2} + \theta_{i3}) - d_1 \cos \theta_{i1} \cos \theta_{i4}$$

$$\frac{\partial P_{ip-z}}{\partial \theta_{p1}} = 1, \quad \frac{\partial P_{ip-z}}{\partial \theta_{p2}} = 0, \quad \frac{\partial P_{ip-z}}{\partial \theta_{p3}} = 0$$

$$\begin{aligned} \frac{\partial P_{ip-z}}{\partial \theta_{i1}} = & -d_1 \sin \theta_{i1} \cos \theta_{i4} \cos(\theta_{i2} + \theta_{i3}) - d_1 \cos \theta_{i1} \sin \theta_{i4} - 2L_5 \sin \theta_{i1} \sin \theta_{i2} \\ & - 2d_1 \cos \theta_{i2} \sin \theta_{i1} + L_5 \sin \theta_{i1} \sin(\theta_{i2} + \theta_{i3}) \end{aligned}$$

$$\frac{\partial P_{ip-z}}{\partial \theta_{i2}} = -d_1 \cos \theta_{i1} \cos \theta_{i4} \sin(\theta_{i2} + \theta_{i3}) + 2L_5 \cos \theta_{i1} \cos \theta_{i2} - 2d_1 \sin \theta_{i2} \cos \theta_{i1} - L_5 \cos \theta_{i1} \cos(\theta_{i2} + \theta_{i3})$$

$$\frac{\partial P_{ip-z}}{\partial \theta_{i3}} = -d_1 \cos \theta_{i1} \cos \theta_{i4} \sin(\theta_{i2} + \theta_{i3}) - L_5 \cos \theta_{i1} \cos(\theta_{i2} + \theta_{i3})$$

$$\frac{\partial P_{ip-z}}{\partial \theta_{i4}} = -d_1 \cos \theta_{i1} \sin \theta_{i4} \cos(\theta_{i2} + \theta_{i3}) - d_1 \sin \theta_{i1} \cos \theta_{i4}$$

In the slave manipulator, the redundancy DoFs provide more dexterity for manipulation. However, it also brings about challenges in inverse kinematics computation.

Suppose the position and the orientation of the manipulator are given, the solutions of the inverse kinematics computation are affected by the joint type, boundary constraints and so on.

Many references gave solutions for calculating the inverse kinematics of redundancy manipulator. Since the slave manipulator in this thesis can be divided into two parts: the positioning manipulator and the tool manipulator. The positioning manipulator is just used to transmit the tool manipulator in spatial space. The posture of the distal of manipulator is decided by the tool manipulator. Therefore, in this thesis, the author gives a simple method to calculate the solution of the inverse kinematics. In the calculation of the inverse kinematics, the bending angle in bendable joints can be firstly computed by the posture matrix.

Suppose the position and the orientation matrix of the distal of the manipulator is

$$T_{tip} = \begin{bmatrix} u_x & v_x & w_x & x_{tip} \\ u_y & v_y & w_y & y_{tip} \\ u_z & v_z & w_z & z_{tip} \\ 0 & 0 & 0 & 1 \end{bmatrix} \quad (3.15)$$

By comparing (3.10) and (3.15),

$$tg\theta_{i4} = \frac{v_x}{w_x} \quad (3.16)$$

Since bending angle of each universal joint belongs to  $(-45^\circ, 45^\circ)$ , therefore,  $\theta_4$  can be given

$$\theta_{i4} = \begin{cases} a \tan 2(v_x, w_x) \cdot 180 / \pi & \theta_4 \in (-90^\circ \sim 90^\circ) \\ (a \tan 2(v_x, w_x) + \pi) \cdot 180 / \pi & \theta_4 < -90^\circ \\ (a \tan 2(v_x, w_x) - \pi) \cdot 180 / \pi & \theta_4 > 90^\circ \end{cases} \quad (3.17)$$

From (3.10) and (3.15), we can obtain

$$\cos\theta_{i1} \cdot w_y + \sin\theta_{i1} \cdot w_z = -\sin\theta_{i4} \quad (3.18)$$

Therefore,

$$\theta_{i1} = -a \sin\left(\frac{1}{\sqrt{w_y^2 + w_z^2}} \sin\theta_{i4}\right) - a \tan 2(w_y, w_z) \quad (3.19)$$

Integrated  $p_y$  and  $p_z$  in (3.11),

$$\begin{aligned}
 & L_8 \sin \theta_{i_2} + 2d_1 \cos \theta_{i_2} \\
 & = (p_z - d_1 - \theta_{p1}) \cos \theta_{i_1} - p_y \sin \theta_{i_1} - d_1 \cos \theta_{i_4} \cos(\theta_{i_2} + \theta_{i_3}) + L_5 \sin(\theta_{i_2} + \theta_{i_3})
 \end{aligned} \tag{3.20}$$

Therefore,

$$\theta_{i_2} = a \sin\left(\frac{(p_z - d_1 - \theta_{p1}) \cos \theta_{i_1} - p_y \sin \theta_{i_1} - d_1 \cos \theta_{i_4} \cos(\theta_{i_2} + \theta_{i_3}) + L_5 \sin(\theta_{i_2} + \theta_{i_3})}{\sqrt{(L_8)^2 + (2d_1)^2}}\right) - \varphi \tag{3.21}$$

$$\text{Where, } \varphi = a \sin\left(\frac{2d_1}{\sqrt{(2d_1)^2 + (L_8)^2}}\right)$$

From (3.10) and (3.12), we can obtain

$$u_y = \sin \theta_{i_1} \sin(\theta_{i_2} + \theta_{i_3}) \tag{3.22}$$

Therefore,

$$\theta_{i_2} + \theta_{i_3} = a \sin \frac{u_y}{\sin \theta_{i_1}} \tag{3.23}$$

Substituting (3.21) into (3.23),

$$\theta_{i_3} = a \sin \frac{u_y}{\sin \theta_{i_1}} - a \sin\left(\frac{(p_z - d_1 - \theta_{p1}) \cos \theta_{i_1} - p_y \sin \theta_{i_1} - d_1 \cos \theta_{i_4} \cos(\theta_{i_2} + \theta_{i_3}) + L_5 \sin(\theta_{i_2} + \theta_{i_3})}{\sqrt{(L_8)^2 + (2d_1)^2}}\right) + \varphi \tag{3.24}$$

Due to the bending movement, the distance between the distal and the manipulator will be changed, we introduce a planar function, which is referred to the base panel of the tool manipulator to express the middle plane of the tool manipulator,

$$Ax + By + Cz + D = 0 \tag{3.25}$$

Since the position of point  $B_1$  refer to the base of the tool manipulator is

$$B_1 = (L_5, 0, d_1) \tag{3.26}$$

Therefore, the projection of point  $B_1$  in the middle panel can be described as

$$A(L_5 + \frac{A}{\sqrt{A^2 + B^2 + C^2}} d_1) + B \frac{B}{\sqrt{A^2 + B^2 + C^2}} d_1 + C(d_1 + \theta_{p1} + \frac{C}{\sqrt{A^2 + B^2 + C^2}} d_1) + D = 0 \tag{3.27}$$

Based on (3.12) and (3.25), we can obtain the projection of point  $B_2$  in the middle panel,

$$\begin{aligned}
 & A(x_{iip} - u_x L_5 - w_x d_1 - \frac{A}{\sqrt{A^2 + B^2 + C^2}} d_1) + B(y_{iip} - u_y L_5 - w_y d_1 - \frac{B}{\sqrt{A^2 + B^2 + C^2}} d_1) \\
 & + C(z_{iip} - u_z L_5 - w_z d_1 - \frac{C}{\sqrt{A^2 + B^2 + C^2}} d_1) + D = 0
 \end{aligned} \tag{3.28}$$

Integrated (3.27) and (3.28), obtain

$$\begin{aligned}
 & A(x_{iip} - u_x L_5 - w_x d_1 - L_5) + B(y_{iip} - u_y L_5 - w_y d_1) + \\
 & C(z_{iip} - u_z L_5 - w_z d_1 - \theta_{p1}) - 2\sqrt{A^2 + B^2 + C^2} d_1 = 0
 \end{aligned} \tag{3.29}$$

Since the point  $B_1$  and  $B_2$  are located at the base linkages of the tool manipulator, therefore, the angle between line  $B_1B_2$  and the middle panel of the tool manipulator is given,

$\cos \beta =$

$$\frac{A(x_{iip} - u_x L_5 - w_x d_1 - L_5) + B(y_{iip} - u_y L_5 - w_y d_1) + C(z_{iip} - u_z L_5 - w_z d_1 - d_1 - \theta_{p1})}{\sqrt{A^2 + B^2 + C^2} \sqrt{(x_{iip} - u_x L_5 - w_x d_1 - L_5)^2 + (y_{iip} - u_y L_5 - w_y d_1)^2 + (z_{iip} - u_z L_5 - w_z d_1 - d_1 - \theta_{p1})^2}} \tag{3.30}$$

$$\cos \beta = \frac{L_8}{2d_1} \tag{3.31}$$

Combinating (3.30) and (3.31), achieve the translational displacement

$$\theta_{p1} = z_{iip} - u_z L_5 - w_z d_1 - d_1 \pm \sqrt{4(d_1^2 + L_5^2) - (x_{iip} - u_x L_5 - w_x d_1 - L_5)^2 - (y_{iip} - u_y L_5 - w_y d_1)^2} \tag{3.32}$$

Since in the configuration of slave arm, the positioning manipulator is located near the origin of coordinate frame, therefore, the positive value of  $\theta_{p1}$  will be abandoned.

In session 3.4, substituting (3.6) into (3.7), obtain

$$\begin{aligned}
 x_{p4} &= L_2 \cos(\theta_{p2} + \theta_{p3}) - L_1 \sin \theta_{p2} + L_3 \cos \theta_{p4} \cos(\theta_{p2} + \theta_{p3}) - L_3 \sin \theta_{p4} \sin(\theta_{p2} + \theta_{p3}) \\
 y_{p4} &= L_2 \sin(\theta_{p2} + \theta_{p3}) + L_1 \sin \theta_{p2} + L_3 \cos \theta_{p4} \sin(\theta_{p2} + \theta_{p3}) + L_3 \sin \theta_{p4} \cos(\theta_{p2} + \theta_{p3})
 \end{aligned} \tag{3.33}$$

Where,  $(x_{p4}, y_{p4})$  is the coordinate of point  $B_4$  in the  $xoy$  frame.

From (3.33), the rotary angle of  $\theta_{p2}$  and  $\theta_{p3}$  can be calculated

$$\begin{aligned}
 \theta_{p3} &= a \sin \frac{(x_{p4} - L_3)^2 + y_{p4}^2 - L_1^2 - L_2^2}{2L_1 L_2} \\
 \theta_{p2} &= a \sin \frac{y_{p4}}{\sqrt{(L_1 + L_2 \sin \theta_3)^2 + (L_2 \cos \theta_3)^2}} - \text{atg} \frac{L_2 \sin \theta_3 + L_1}{L_2 \cos \theta_3}
 \end{aligned} \tag{3.34}$$

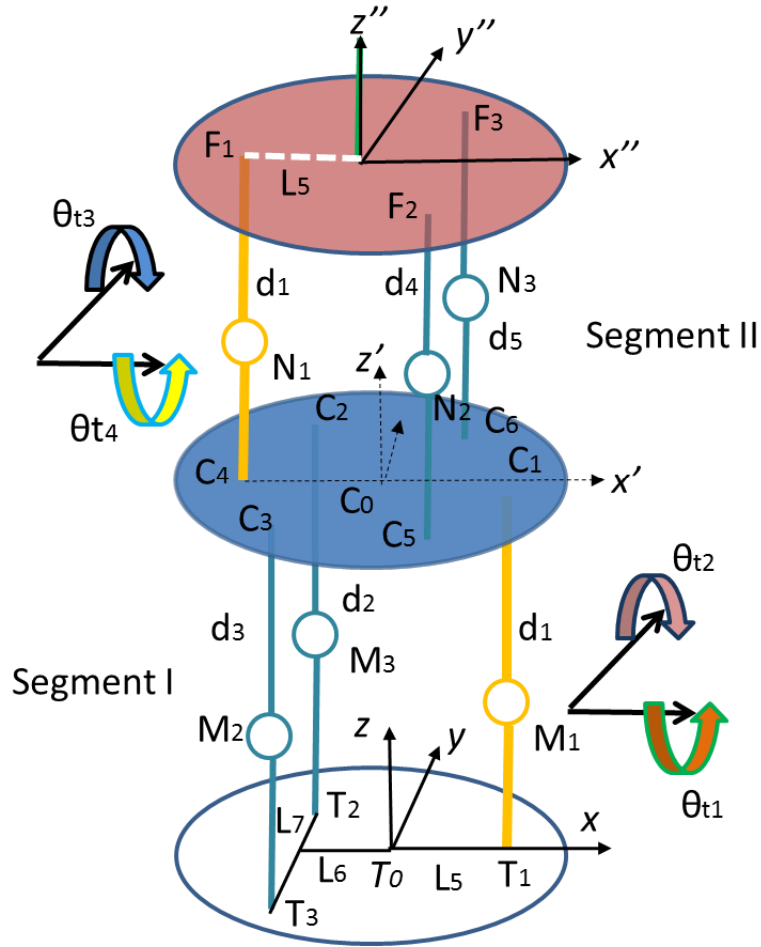


Figure 3. 17 Feature points for rod's length calculation.

### 3.6 Rod's Length Computation

In the tool manipulator, one base linkage and two bending linkages are circumferentially located at a circle. The length deviations of the two bending linkages drive the tool manipulator to rotate along the pivot point of the base linkage. Figure 3.17 shows the feature points in the tool manipulator.

$T_i$  ( $i = 0,1,2,3$ ),  $M_i$  ( $i = 1,2,3$ ),  $C_i$  ( $i = 0,1,2,3,4,5,6$ ),  $N_i$  ( $i = 1,2,3$ ),  $F_i$  ( $i = 1,2,3$ ) are the feature points in the linkages of the tool manipulator. The origin  $T_0$  (0,0,0) of the segment I

### 3. Mechatronics Design of Pediatric Surgical Robot

is located at the center of the base frame  $A_1A_2A_3$ . The coordinate of each feature in segmentI can be calculated

$$T_0 = \begin{bmatrix} 0 \\ 0 \\ 0 \end{bmatrix}, \quad T_1 = \begin{bmatrix} L_5 \\ 0 \\ 0 \end{bmatrix}, \quad T_2 = \begin{bmatrix} -L_6 \\ L_7/2 \\ 0 \end{bmatrix}, \quad T_3 = \begin{bmatrix} -L_6 \\ -L_7/2 \\ 0 \end{bmatrix}$$

$$M_1 = \begin{bmatrix} L_5 \\ 0 \\ d_1 \end{bmatrix}, \quad M_2 = \begin{bmatrix} -L_6 \\ L_7/2 \\ d_2 \end{bmatrix}, \quad M_3 = \begin{bmatrix} -L_6 \\ -L_7/2 \\ d_3 \end{bmatrix}$$

Since the segmentI follows the bending order  $x \rightarrow y$ , therefore, the coordinate transfer is

$$KI_1 = \begin{bmatrix} 1 & 0 & 0 & L_5 \\ 0 & 1 & 0 & 0 \\ 0 & 0 & 1 & d_1 \\ 0 & 0 & 0 & 1 \end{bmatrix}, \quad KI_2 = \begin{bmatrix} 1 & 0 & 0 & 0 \\ 0 & c\theta_{i1} & -s\theta_{i1} & 0 \\ 0 & s\theta_{i1} & c\theta_{i1} & 0 \\ 0 & 0 & 0 & 1 \end{bmatrix}, \quad KI_3 = \begin{bmatrix} c\theta_{i2} & 0 & s\theta_{i2} & 0 \\ 0 & 1 & 0 & 0 \\ -s\theta_{i2} & 0 & c\theta_{i2} & 0 \\ 0 & 0 & 0 & 1 \end{bmatrix},$$

$$KI_{-41} = \begin{bmatrix} 1 & 0 & 0 & 0 \\ 0 & 1 & 0 & 0 \\ 0 & 0 & 1 & d_1 \\ 0 & 0 & 0 & 1 \end{bmatrix}, \quad KI_{-42} = \begin{bmatrix} 1 & 0 & 0 & -(L_5 + L_6) \\ 0 & 1 & 0 & L_7/2 \\ 0 & 0 & 1 & d_1 \\ 0 & 0 & 0 & 1 \end{bmatrix}, \quad KI_{-43} = \begin{bmatrix} 1 & 0 & 0 & -(L_5 + L_6) \\ 0 & 1 & 0 & -L_7/2 \\ 0 & 0 & 1 & d_1 \\ 0 & 0 & 0 & 1 \end{bmatrix}$$

Define,

$$KKI_1 = KI_1 \cdot KI_2 \cdot KI_3 \cdot KI_{-41}$$

$$KKI_2 = KI_1 \cdot KI_2 \cdot KI_3 \cdot KI_{-42}$$

$$KKI_3 = KI_1 \cdot KI_2 \cdot KI_3 \cdot KI_{-43}$$

Therefore, the coordinates of  $C_1, C_2, C_3$  are given

$$C_1 = \begin{bmatrix} KKI_1(1,4) \\ KKI_1(2,4) \\ KKI_1(3,4) \end{bmatrix}, \quad C_2 = \begin{bmatrix} KKI_2(1,4) \\ KKI_2(2,4) \\ KKI_2(3,4) \end{bmatrix}, \quad C_3 = \begin{bmatrix} KKI_3(1,4) \\ KKI_3(2,4) \\ KKI_3(3,4) \end{bmatrix}$$

Since  $|M_1C_1| = d_1, |M_2C_2| = d_2, |M_3C_3| = d_3$ , therefore, the length of bending linkage in segment I is

$$d_2 = \frac{(-L_5 - C_2(1,1))^2 + \left(\frac{L_7}{2} - C_2(1,2)\right)^2 + C_2(1,3)^2}{2C_2(1,3)} \quad (3.35)$$

$$d_3 = \frac{(-L_5 - C_3(1,1))^2 + \left(-\frac{L_7}{2} - C_3(1,2)\right)^2 + C_3(1,3)^2}{2C_3(1,3)}$$

In the segmentII, suppose point  $C_0(0,0,0)$  in the middle frame, then, the coordinate of feature points in segmentII can be given,

$$C_0 = \begin{bmatrix} 0 \\ 0 \\ 0 \end{bmatrix}, \quad C_4 = \begin{bmatrix} -L_5 \\ 0 \\ 0 \end{bmatrix}, \quad C_5 = \begin{bmatrix} L_6 \\ -L_7/2 \\ 0 \end{bmatrix}, \quad C_6 = \begin{bmatrix} L_6 \\ L_7/2 \\ 0 \end{bmatrix}$$

$$N_1 = \begin{bmatrix} -L_5 \\ 0 \\ d_1 \end{bmatrix}, \quad N_2 = \begin{bmatrix} L_6 \\ -L_7/2 \\ d_2 \end{bmatrix}, \quad N_3 = \begin{bmatrix} L_6 \\ L_7/2 \\ d_3 \end{bmatrix}$$

Since the segmentII follows the bending order  $y \rightarrow x$ , therefore, the coordinate transfer is

$$KII_1 = \begin{bmatrix} 1 & 0 & 0 & -L_5 \\ 0 & 1 & 0 & 0 \\ 0 & 0 & 1 & d_1 \\ 0 & 0 & 0 & 1 \end{bmatrix}, \quad KII_2 = \begin{bmatrix} c\theta_{i4} & 0 & s\theta_{i4} & 0 \\ 0 & 1 & 0 & 0 \\ -s\theta_{i4} & 0 & c\theta_{i4} & 0 \\ 0 & 0 & 0 & 1 \end{bmatrix},$$

$$KII_3 = \begin{bmatrix} 1 & 0 & 0 & 0 \\ 0 & c\theta_{i5} & -s\theta_{i5} & 0 \\ 0 & s\theta_{i5} & c\theta_{i5} & 0 \\ 0 & 0 & 0 & 1 \end{bmatrix}, \quad KII_{-41} = \begin{bmatrix} 1 & 0 & 0 & 0 \\ 0 & 1 & 0 & 0 \\ 0 & 0 & 1 & d_1 \\ 0 & 0 & 0 & 1 \end{bmatrix}$$

$$KII_{-42} = \begin{bmatrix} 1 & 0 & 0 & (L_5 + L_6) \\ 0 & 1 & 0 & -L_7/2 \\ 0 & 0 & 1 & d_1 \\ 0 & 0 & 0 & 1 \end{bmatrix}, \quad KII_{-43} = \begin{bmatrix} 1 & 0 & 0 & (L_5 + L_6) \\ 0 & 1 & 0 & L_7/2 \\ 0 & 0 & 1 & d_1 \\ 0 & 0 & 0 & 1 \end{bmatrix}$$

Command,

$$KKII_1 = KII_1 \cdot KII_2 \cdot KII_3 \cdot KII_{-41}$$

$$KKII_2 = KII_1 \cdot KII_2 \cdot KII_3 \cdot KII_{-42}$$

$$KKII_3 = KII_1 \cdot KII_2 \cdot KII_3 \cdot KII_{-43}$$

Therefore, the coordinates of  $F_1, F_2, F_3$  are given

$$F_1 = \begin{bmatrix} KKII_1(1,4) \\ KKII_1(2,4) \\ KKII_1(3,4) \end{bmatrix}, \quad F_2 = \begin{bmatrix} KKII_2(1,4) \\ KKII_2(2,4) \\ KKII_2(3,4) \end{bmatrix}, \quad F_3 = \begin{bmatrix} KKII_3(1,4) \\ KKII_3(2,4) \\ KKII_3(3,4) \end{bmatrix}$$

Since  $|N_1F_1| = d_1, |N_2F_2| = d_4, |N_3F_3| = d_5$ , the length of bending linkage in segmentII is

$$d_4 = \frac{(L_6 - F_2(1,1))^2 + \left(-\frac{L_7}{2} - F_2(1,2)\right)^2 + F_2(1,3)^2}{2F_2(1,3)} \quad (3.36)$$

$$d_5 = \frac{(L_6 - F_3(1,1))^2 + \left(\frac{L_7}{2} - F_3(1,2)\right)^2 + F_3(1,3)^2}{2F_3(1,3)}$$

Since the bending angle of each joint is  $\pm 45^\circ$ , therefore, the relation between rod's length and the bending angle is shown in Fig. 3.18 and Fig. 3.19.

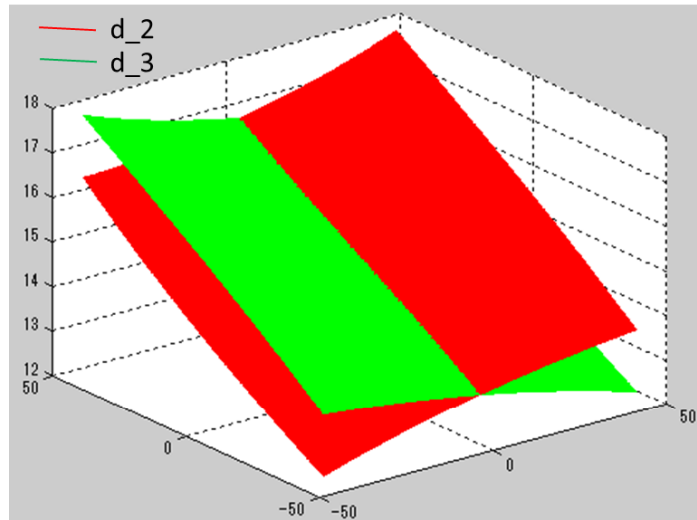


Figure 3. 18 Relation of rod's length and bending angle in segment I.



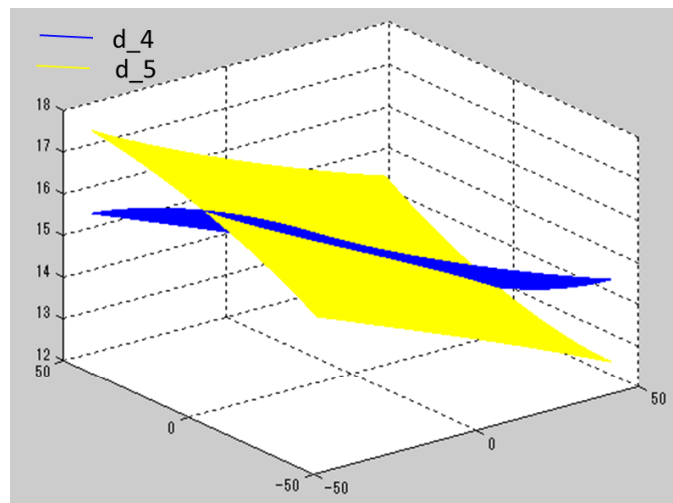


Figure 3.19 Relation of rod's length and bending angle in segment II.

### 3.7 Transmission Medium

In our robot, we use a flexible shaft with 1 m length to connect the driven screw and the corresponding motor. Flexible shaft is made up of several bunches of slim elastic steel wires which twisted with each other. The component of flexible shaft used in the prototype is shown in Fig. 3.20. Due to the elasticity of the flexible shaft, we verified the transmission efficiency of flexible shaft based on the robot structure. Since the surgical manipulator use

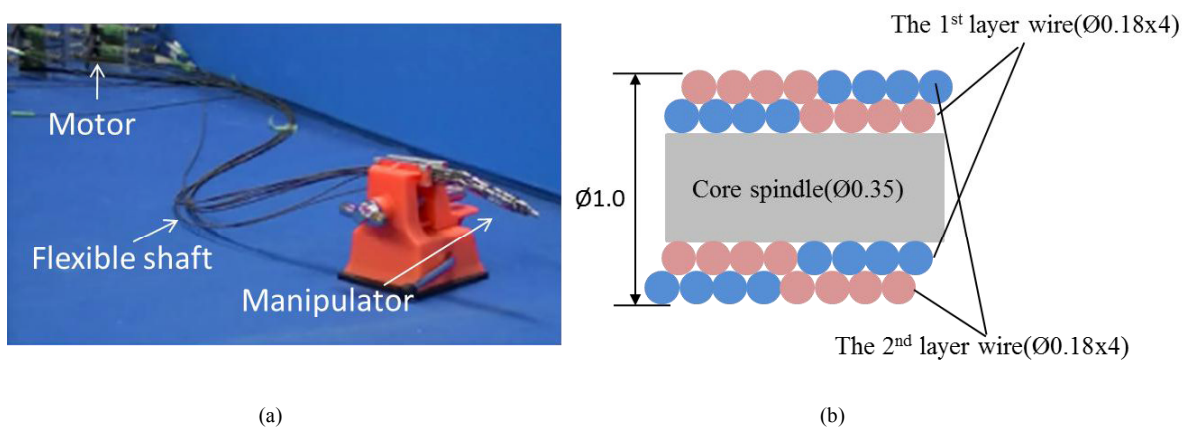


Figure 3. 20 Components of flexible shaft. (a) components of manipulator-driven system; (b) cross section of flexible shaft.

screw-pair driven mode to realize bent motion, therefore, we did experiments to verify the power transmission accuracy that screw drive nut.

The experimental platform is shown in Fig. 3.21. In the experiment, a 3D tracking sensor ( $\Phi 1.0$  mm, Aurora, made by Northern Digital Inc., Canada) [99] was used to tracking the movement of nut.

In our manipulator, the screw pitch is 0.2 mm, and the screw's length of each bendable linkage is 2 mm, therefore, we sent instructions to make motor rotate with a fixed speed ( $2\pi/3$  rad/s) drive the screw-pair mechanism. Corresponding to the screw pitch, thus, the amount of motor output and nut's translational distance meet relation that

$$S = \frac{\theta}{2\pi} L \quad (3.37)$$

Where,  $S$ -translational distance of nut;  $\theta$ -motor rotation angle;  $L$ -lead of screw.

Four different weights (20 g, 50 g, 100 g, 200 g, respectively) were used in this experiment. The experimental data are shown in Fig.3.22. The experimental result demonstrates that there is a linear relation between the input and the moving distance of the weight, therefore, the nut can well tracking the input. Thus, the flexible shaft can satisfy the

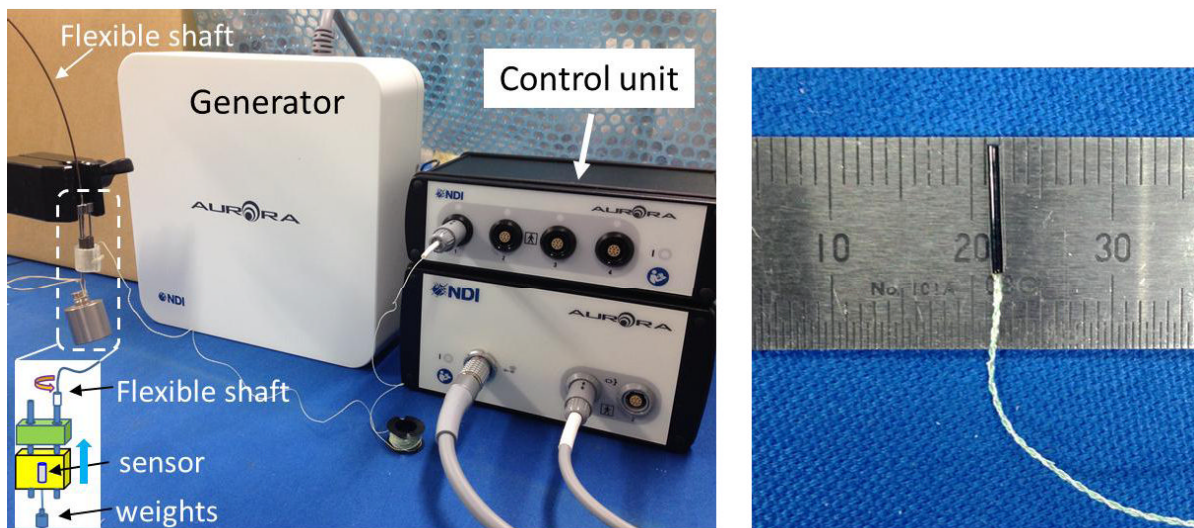


Figure 3. 21 Experimental platform for verifying transimisson accuracy of flexible shaft.  
 (a). experimetal platform; (b) 3D tracking sensor (NDI, Canada).

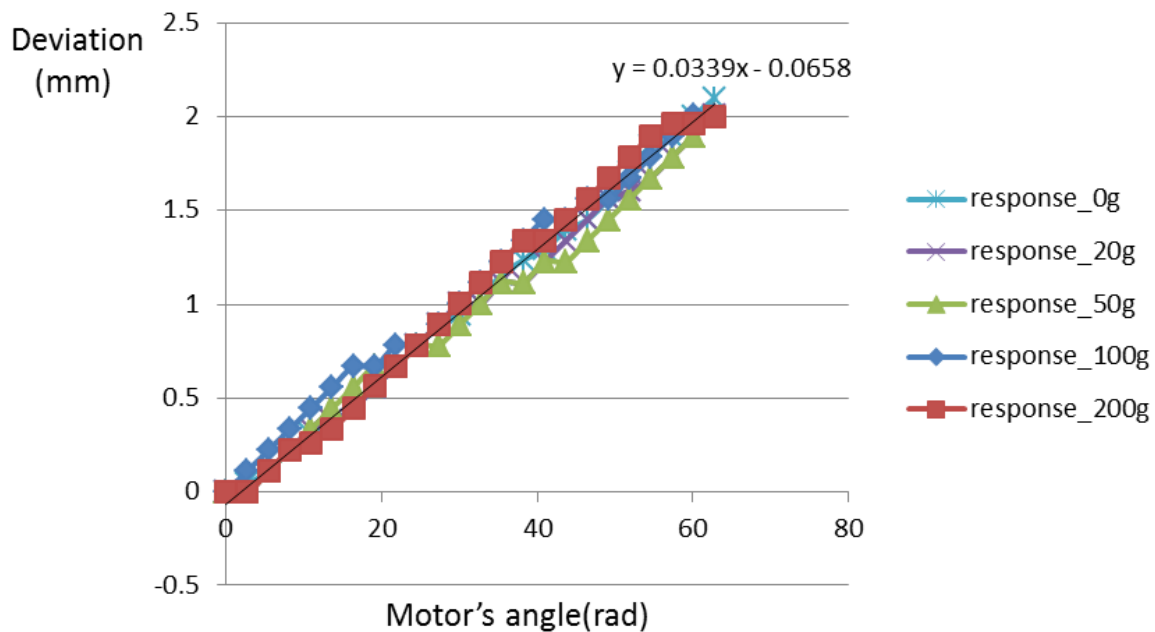


Figure 3. 22 Relation between motor's rotation angle and deviation of screw-nut driven by flexible shaft.

requirement for accurate power transmission when loaded within 2 N.

### 3.8 Discussion

In this chapter, the author illustrates the development of a compact pediatric surgical robot. The surgical robot consists of two surgical manipulators and two visual modules; each surgical manipulator is composed of a positioning manipulator (4 DoFs) and a tool manipulator (5 DoFs + gripper). The positioning manipulator is used to deploy the tool manipulator in the spatial area by integrating a screw pair and a SCARA mechanism. The tool manipulator with an external diameter of 8 mm, consisting of two bendable joints and a rotary gripper, is used to perform tissue intervention. The bendable joint can achieve arbitrary orientational bending motion in spatial zone by using DSD mechanism. The use of two bendable joints in the tool manipulator aims to provide dexterous manipulation. Forward/inverse kinematics of the surgical manipulator are illustrated, the simulation result

### 3. Mechatronics Design of Pediatric Surgical Robot

---

demonstrate the developed surgical robot is competent to work in a 30x30x30 mm narrow workspace. The experiment of rigidity measurement of the flexible shaft demonstrated that the driven distance by flexible shaft is proportional to the input when tip's load is within 2 N. Thus, the position of the tool manipulator's tip can be directly computed by kinematical formation when loaded within 2 N.

## **Chapter 4**

# **Control Strategy of Redundant Robotic Manipulator in Narrow Workspace**

### **4.1 Introduction**

In the preview chapters, the author had already introduced the mechatronics design of the master- slave structure surgical robot. In order to control the slave manipulator to track the instruction of master input, kinematic chain should be constructed between the masters input and the slave manipulators. To our surgical robot, each slave arm has 9 DoFs, therefore, there are redundant DoFs to determine the posture of the distal of the slave manipulator. Although the redundant DoFs could improve the reachable probability and dexterity, however, it also poses big challenge to computer inverse solution that will be used to control robot actuators. Since the slave arm in the proposed surgical robot can be divided into positioning manipulator and tool manipulator, and the positioning manipulator is solely used to achieve translational movement, therefore, the author set the connect point between positioning manipulator and the tool manipulator as the initial coordinate origin. The tool manipulator, having 5 independent DoFs will firstly be consistent with the Phantom Omni by inverse computation

referred in chapter 3. Because the base of the tool manipulator is attached at the distal of the positioning manipulator, thus, the solution of each joint in the positioning manipulator can also be calculated by using the algorithm in chapter 3. We aim to use the surgical robot perform surgery in a 30x30 mm square space, therefore, the surgical manipulator should avoid blocking surgeon's view as small as possible while keeping the distal of the manipulator tracking the instruction of master input. The detailed technical approached to address the engineering challenges mentioned will be provided in this chapter, more specially, they will include 1) initial value of slave manipulator (referred in chapter 3); 2) inverse solutions corresponding to disturbance; 3) visualization in narrow workspace; 4) operability in narrow workspace; 5) integration and motion parameterization.

## 4.2 Inverse Solutions corresponding to Disturbance

### 4.2.1 Inverse Solution Algorithm

In this section, we suppose the distal of the tool manipulator reach a given posture, and apply a disturbance to the redundant DoF of the slave manipulator, build the relation between deviation of each joint and the amount of the given disturbance. As shown in Fig. 4.1, a disturbance is applied at point B3, and the base of the tool manipulator moves from posture (1) to posture (2).

As shown in Fig 4.1, the distal of the tool manipulator is consistent with the posture of the master input, therefore, to a given posture of the master input, the vector of  $\overline{B_1B_2}$  is fixed. Then, the point  $B_3$  can move on a spherical surface and the sphere center located at  $B_2$ . Suppose the current coordination of point  $B_3$  is  $(x_{B_3}, y_{B_3}, z_{B_3})$ , and the deviation in  $x, y$  direction is  $\Delta x$  and  $\Delta y$ , respectively. the spherical equation based on point  $B_2$  can be expressed by,

$$(x - x_{B_2})^2 + (y - y_{B_2})^2 + (z - z_{B_2})^2 = r^2 \quad (4.1)$$

$$\text{Where, } r = \sqrt{(2d_1)^2 + L_8^2}$$

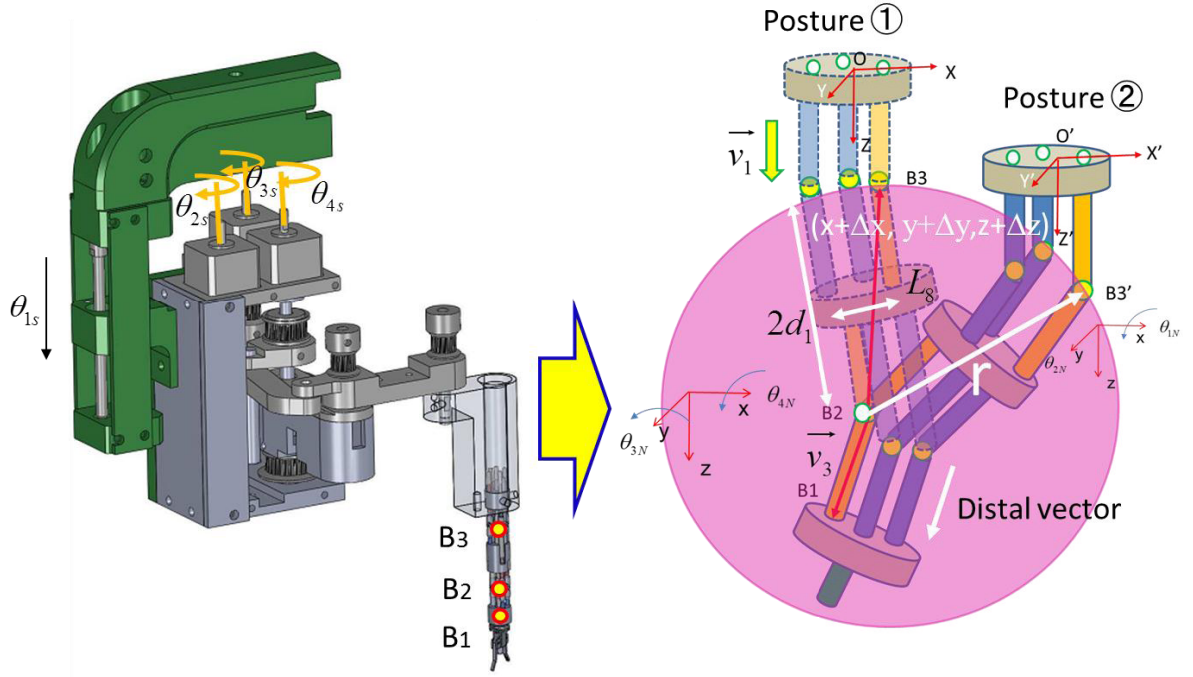


Figure 4. 1 Movement of redundant joint when disturbance at point B3.

Substituting  $x_{B3} + \Delta x$  to  $x$ ,  $y_{B3} + \Delta y$  to  $y$ , the new coordinate  $z'_{B3}$  can be given,

$$z_B = z_{B2} \pm \sqrt{r^2 - (x_{B3} + \Delta x - x_{B2})^2 + (y_{B3} + \Delta y - y_{B2})^2} \quad (4.2)$$

Therefore, the new coordinate of point  $B'_3$  in the world coordinate frame can be expressed

$$(x_{B3} + \Delta x, y_{B3} + \Delta y, z_{B2} \pm \sqrt{r^2 - (x_{B3} + \Delta x - x_{B2})^2 - (y_{B3} + \Delta y - y_{B2})^2}) \quad (4.3)$$

Suppose the bending angles of the bendable joints are  $\theta_{1N}, \theta_{2N}, \theta_{3N}, \theta_{4N}$ , which are shown in Fig 4-1. From (3.8) in chapter III, we can get the new coordinate of point  $B_{2N}$ ,

$$P_{B_{2N}} = [M_{-(1,4)} \quad M_{-(2,4)} \quad M_{-(3,4)}] \quad (4.4)$$

Where,  $M_{-} = {}^0T_1 \cdot {}^1T_2 \cdot {}^2T_3 \cdot {}^3T_4$ .

#### 4. Control Strategy of Redundant Robotic Manipulator in Narrow Workspace

---

Substituting  $\theta_{1N}, \theta_{2N}, \theta_{3N}, \theta_{4N}$  into (4.4), obtain,

$$\begin{aligned}
 P_{B_{2N}_x} &= 2d_1 \sin \theta_{2N} - L_8 \cos \theta_{2N} + L_5 + \Delta x \\
 P_{B_{2N}_y} &= -2d_1 \cos \theta_{2N} \sin \theta_{1N} - L_8 \sin \theta_{1N} \sin \theta_{2N} + \Delta y \\
 P_{B_{2N}_z} &= 2d_1 \cos \theta_{2N} \cos \theta_{1N} + L_8 \cos \theta_{1N} \sin \theta_{2N} + d_1 + z_{B_2} \\
 &\quad - \sqrt{r^2 - (L_5 + \Delta x - x_{B_2})^2 - (\Delta y - y_{B_2})^2}
 \end{aligned} \tag{4.5}$$

From (4.5), the new angle can be calculated,

$$\begin{aligned}
 \theta_{1N} &= a \sin \frac{\Delta y - y_{B_2}}{2d_1 \cos \theta_{2N} + L_8 \sin \theta_{2N}} \\
 \theta_{2N} &= a \sin \frac{x_{B_2} - L_5 - \Delta x}{\sqrt{(2d_1)^2 + (L_8)^2}} + \varphi, \text{ where, } \varphi = a \tan \frac{L_8}{2d_1}
 \end{aligned}$$

Since the point  $B_1$  and  $B_2$  are fixed during disturbance, therefore, the vector  $\overline{B_1 B_2}$  is constant. Suppose  $\overline{B_1 B_2} = (v_{B_2 B_1_x}, v_{B_2 B_1_y}, v_{B_2 B_1_z})$ , based on the (3.8), achieve,

$$\begin{aligned}
 v_{B_2 B_1_x} &= d_1 \cos \theta_{4N} \sin(\theta_{2N} + \theta_{3N}) \\
 v_{B_2 B_1_y} &= -d_1 \cos \theta_{4N} \sin \theta_{1N} \cos(\theta_{2N} + \theta_{3N}) - d_1 \cos \theta_{1N} \sin \theta_{4N} \\
 v_{B_2 B_1_z} &= d_1 \cos \theta_{4N} \cos \theta_{1N} \cos(\theta_{2N} + \theta_{3N}) - d_1 \sin \theta_{1N} \sin \theta_{4N}
 \end{aligned} \tag{4.6}$$

Therefore,

$$\theta_{4N} = -a \sin \frac{v_{B_2 B_1_y} \cos \theta_{1N} + v_{B_2 B_1_z} \sin \theta_{1N}}{d_1} \tag{4.7}$$

$$\theta_{3N} = a \sin \left( \frac{v_{B_2 B_1_x}}{d_1 \cos \theta_{4N}} \right) - \theta_{2N} \tag{4.8}$$

Similar to (3.34), we can obtain the new angles of the positioning manipulator,

$$\theta_{1s} = z'_{B_3} \tag{4.9}$$



$$\theta_{2s} = a \sin \frac{y'_{B3}}{\sqrt{(L_1 + L_2 \sin \theta_3)^2 + (L_2 \cos \theta_3)^2}} - a \tan \frac{L_2 \sin \theta_3 + L_1}{L_2 \cos \theta_3} \quad (4.10)$$

$$\theta_{3s} = a \sin \frac{(x'_{B3} - L_3)^2 + y'_{B3}{}^2 - L_1^2 - L_2^2}{2L_1L_2} \quad (4.11)$$

$$\theta_{4s} = -(z'_{B2} + z'_{B3}) \quad (4.12)$$

### 4.2.2 Algorithm Verification

Based on the mechanism of the surgical robot in chapter III, we build the simplified model of the surgical robot in Adams®, edited by MSC software Corporation [100]. The model is shown in Fig. 4.2.

As shown in Fig. 4.2, point  $O$  the origin of the world frame. Since the left slave arm and the right slave arm are symmetrical, therefore, only the feature points in the left arm are figured out. Point  $P_1, P_2, P_3, P_4, P_5$  are the feature point in the positioning manipulator, Point  $T_1, T_2, T_3, T_4, T_p$  are feature point in the tool manipulator. point  $E_i (i=1....4)$  and  $F_i (i=1....4)$  are feature point in the surgical cavity. Based on the configuration of the surgical robot, the initial coordinate of the feature points are listed below,

Table 4- 1 Coordinate of the feature point in the left arm

<i>Point</i>	<i>Coordinate</i>	<i>Point</i>	<i>Coordinate</i>
$P_1$	(-85,0,0)	$P_2$	(-85,0,145)
$P_3$	(-85,40,145)	$P_4$	(-45,40,145)
$P_5 (T_1)$	(-25,40,145)	$T_2$	(-22.6,40,160)
$T_3$	(-27.4,40,190)	$T_4$	(-27.4,40,205)
$T_p$	(-25,40,205)		

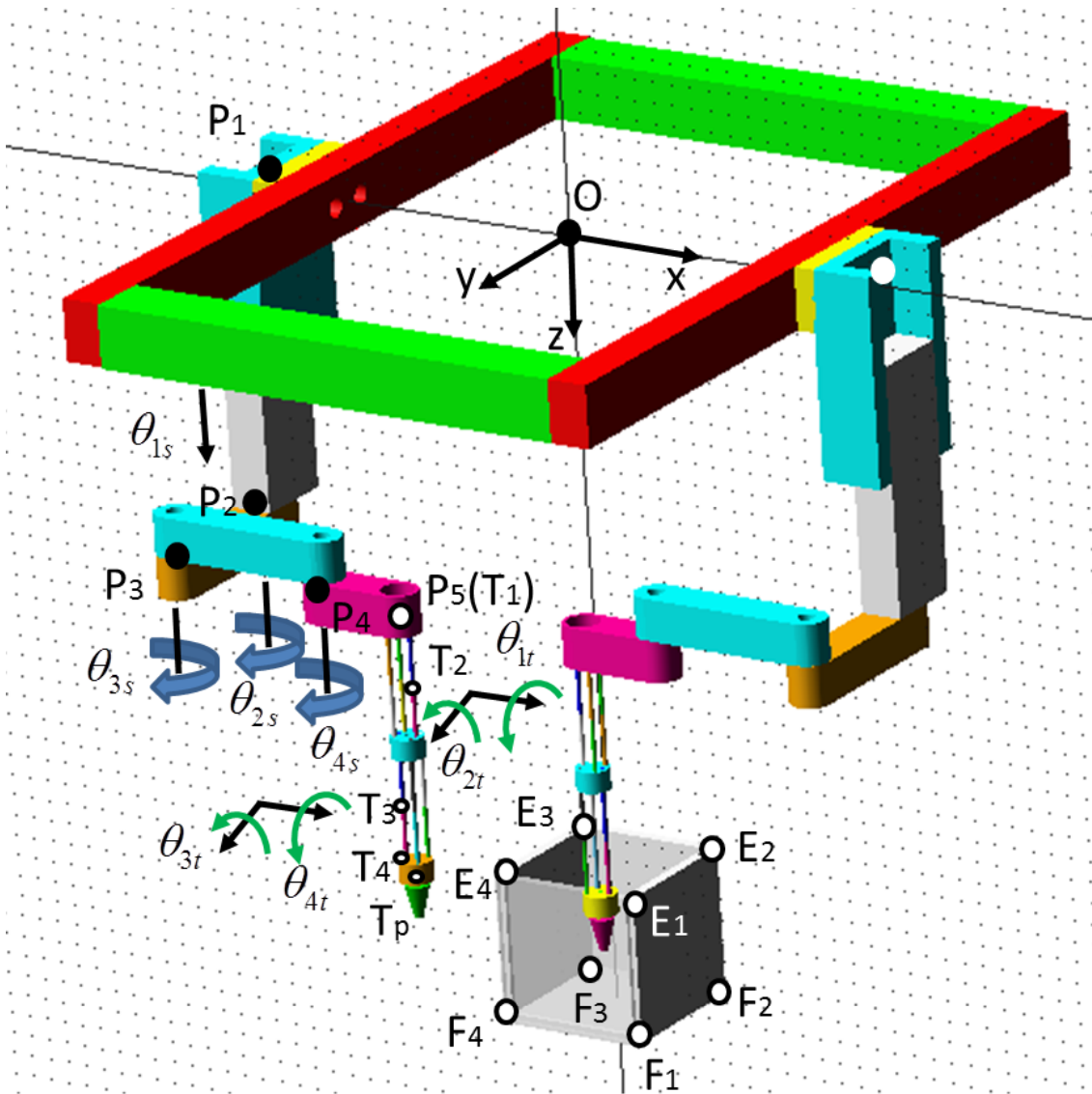


Figure 4. 2 Modeling the surgical robot in Adams.

In order to verify the algorithm, we set a start state for the slave arm by supposing a given master input value, then, give a disturbance at point  $T_2$ , the deviation of each joint can be obtained from the following simulator.

We import the model in Fig. 4.2 into Matlab®, and program the control based on the algorithm of section 4.2.1. The control block in the Matlab is shown in Fig. 4.3. The simulator block consists of 4 parts: the current state (include disturbance), control algorithm, Adams sub, and the scope. The example current value given by the master input is listed in table 4-2,

#### 4. Control Strategy of Redundant Robotic Manipulator in Narrow Workspace

Table 4- 2 The given value mapped from master input to the left arm

<i>Parameter</i>	<i>Value</i>	<i>Parameter</i>	<i>Value</i>
$\theta_{1s}$	0 mm	$\theta_{2s}$	-40°
$\theta_{3s}$	-10°	$\theta_{4s}$	30°
$\theta_{1t}$	10°	$\theta_{2t}$	15°
$\theta_{3t}$	10°	$\theta_{4t}$	15°
$\Delta x$	4sin(t)	$\Delta y$	5sin(t)

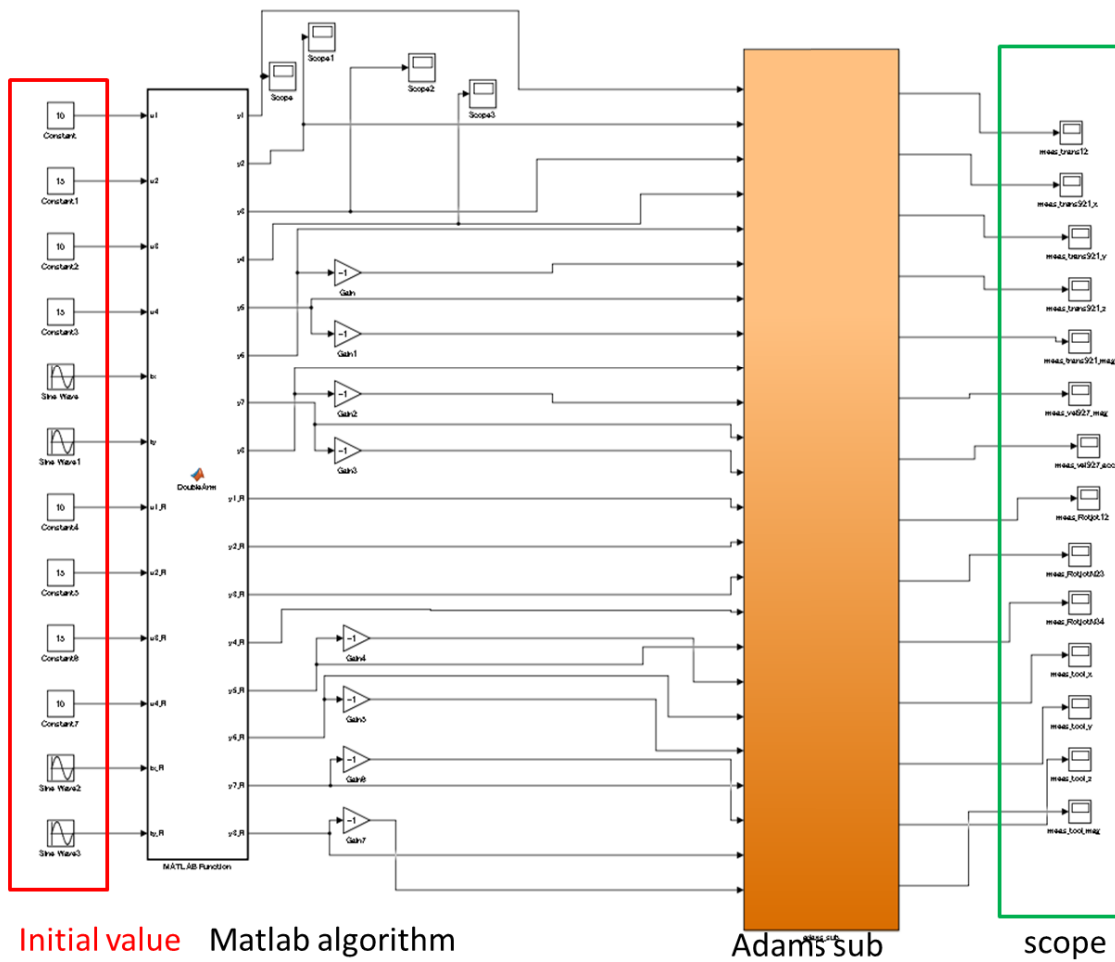


Figure 4. 3 Control diagram of simulator in Matlab.

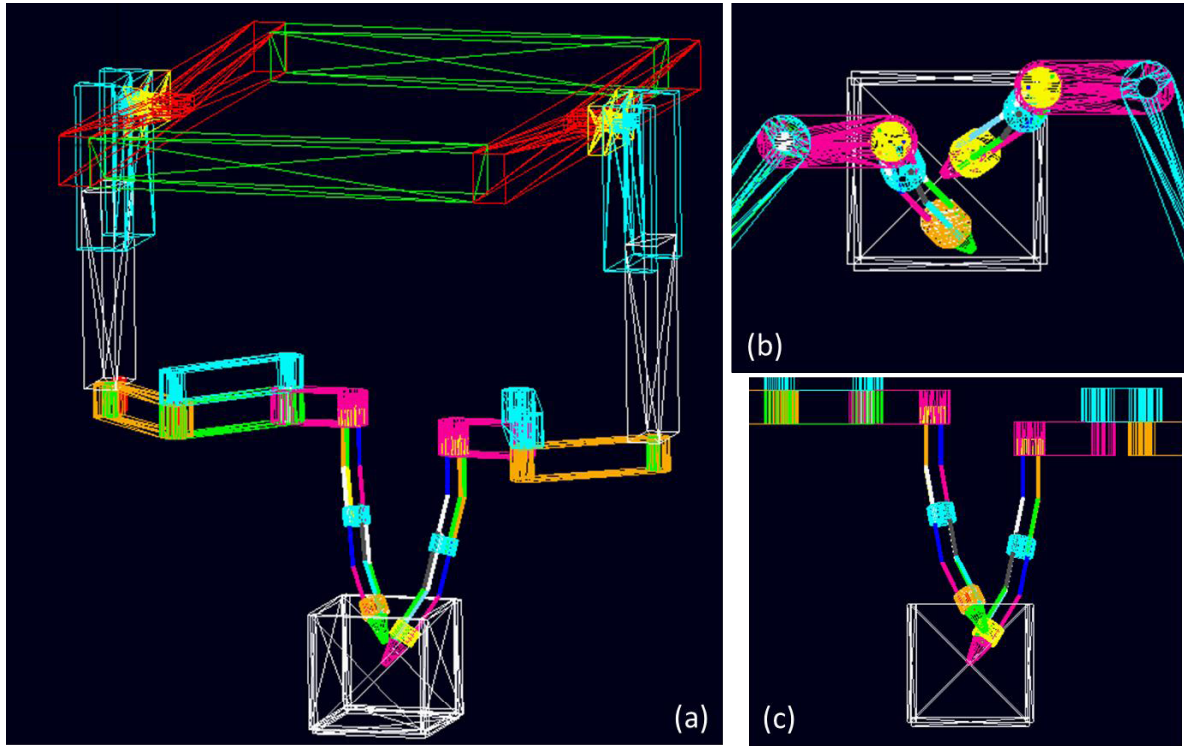


Figure 4. 4 Surgical robot in the simulator.  
 a). isometric view, b) top view, c) front view.

The position and posture of the surgical robot at the given state in the simulator is shown in Fig. 4.4.

According to the disturbance of  $\Delta x, \Delta y$ , the change trends of the joints  $\theta_{1s}, \theta_{2s}, \theta_{3s}, \theta_{4s}$  are illustrated in Fig. 4.5 to Fig. 4.8. The coordinate of the distal of the tool manipulator in the world coordinate frame is shown in Fig. 4.9 to Fig. 4.12.

Comparison between the measurement data in the simulator and the expect data, the robot can well track the input value (tracking error  $\Delta_{simulator} < 0.5mm$ ). Therefore, considering the dynamics effect during joint movement, the result illustrate that the inverse algorithm based on the disturbance is correct.

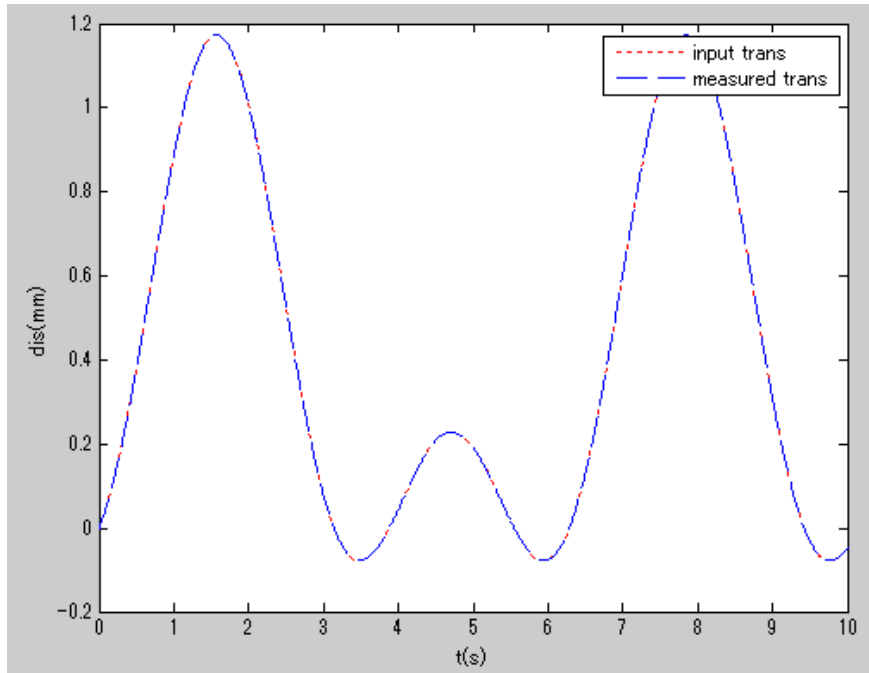


Figure 4. 5 Expect value and the measuredvalue in the simulator of translational joint  $\theta_{1s}$  of the positioning manipulator.

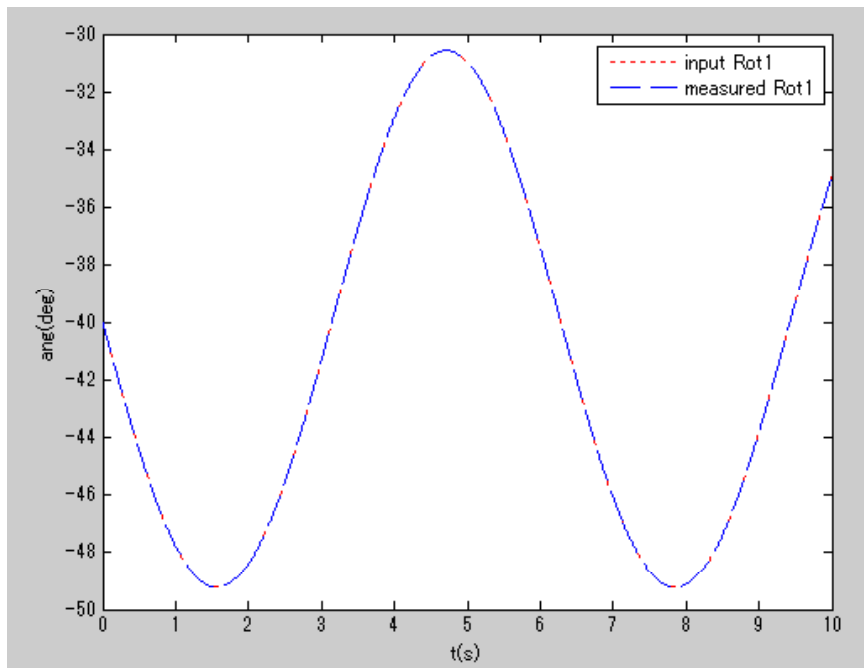


Figure 4. 6 Expect value and the measured value in the simulator of rotary joint  $\theta_{2s}$  of the positioning manipulator.

#### 4. Control Strategy of Redundant Robotic Manipulator in Narrow Workspace

---

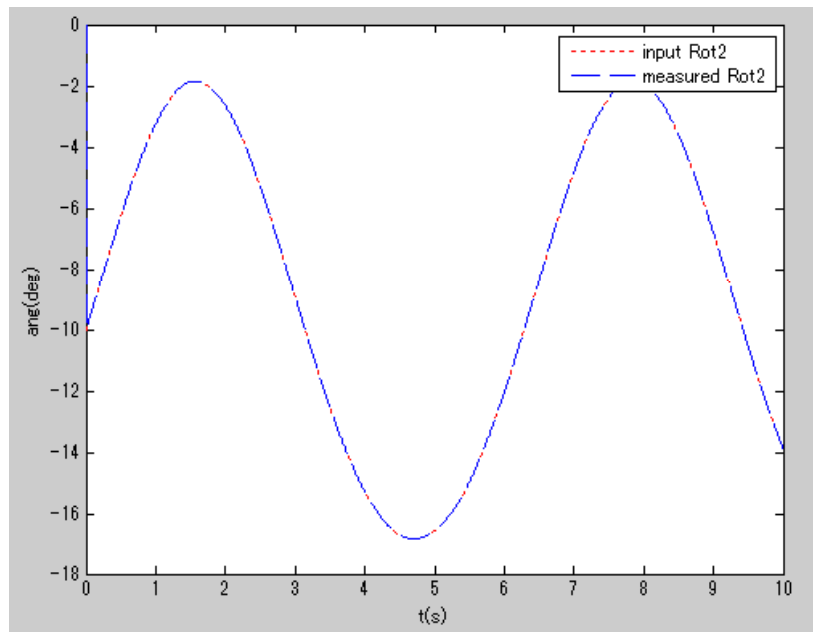


Figure 4.7 Expect value and the measured value in the simulator of rotary joint  $\theta_{3s}$  of the positioning manipulator.

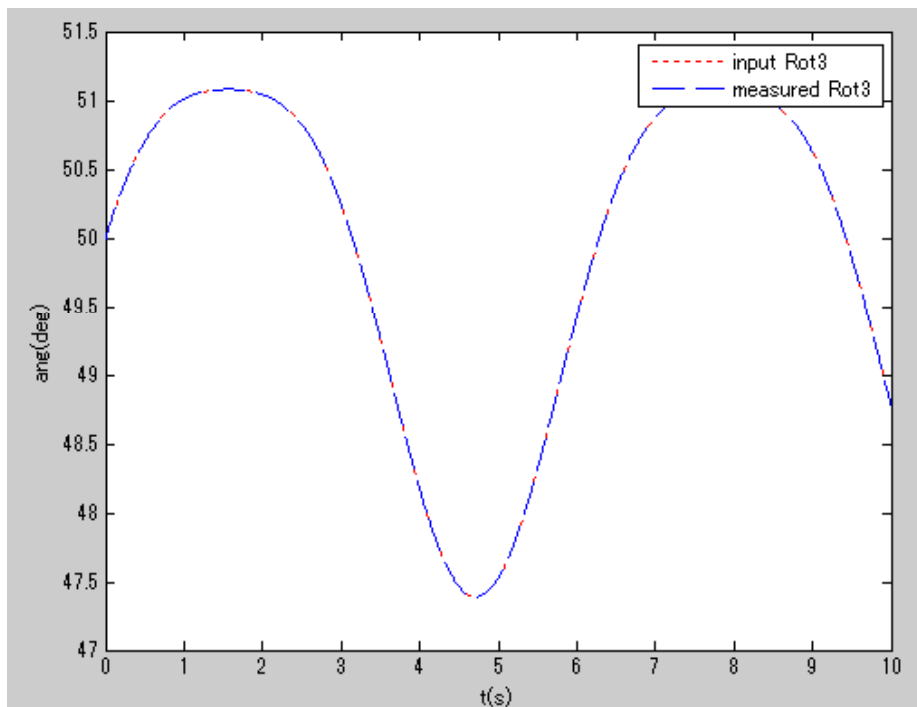


Figure 4.8 Expect value and the measured value in the simulator of rotary joint  $\theta_{4s}$  of the positioning manipulator.

#### 4. Control Strategy of Redundant Robotic Manipulator in Narrow Workspace

---

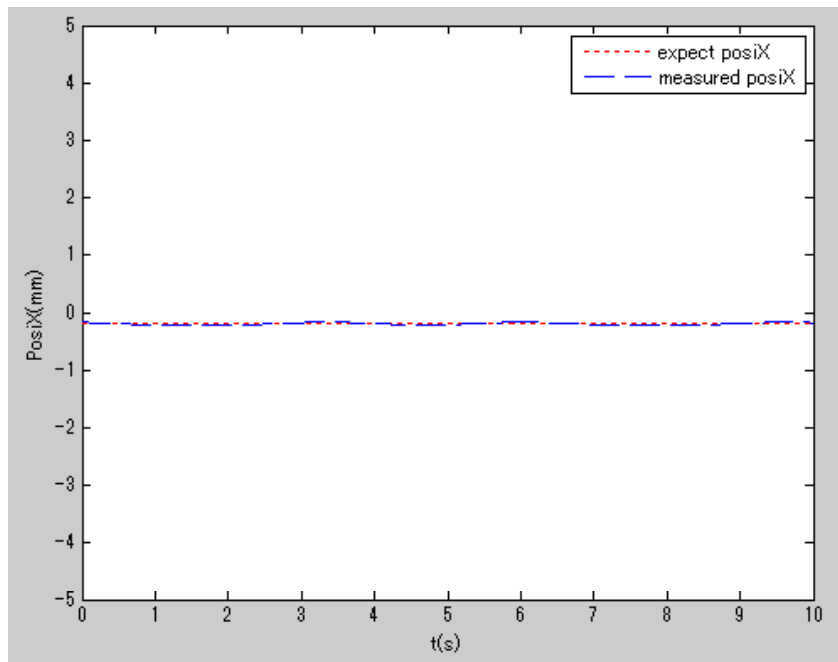


Figure 4.9 Expect x axial position and the measured value in the simulator of the distal of the tool manipulator.

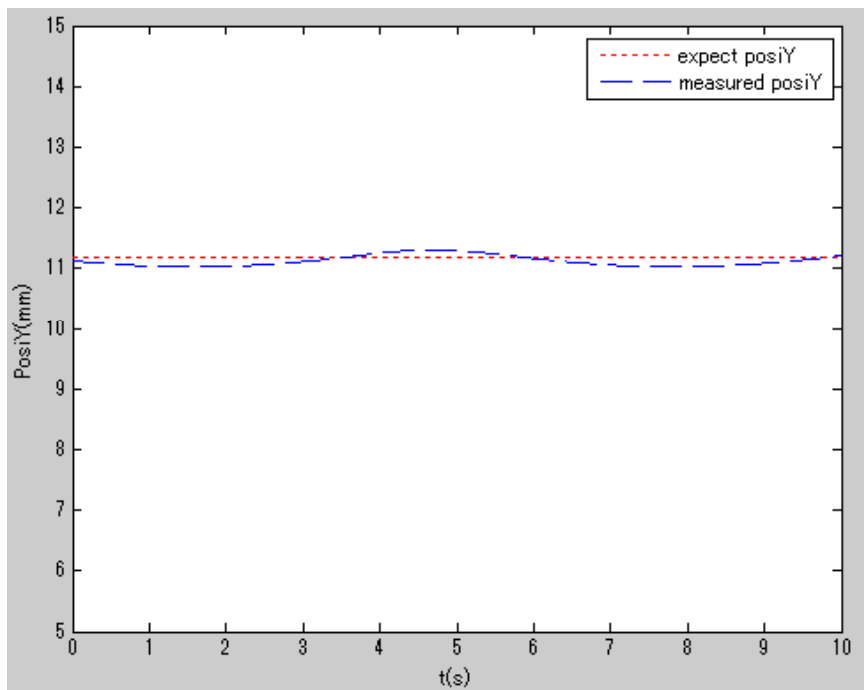


Figure 4.10 Expect y axial position and the measured value in the simulator of the distal of the tool manipulator.

#### 4. Control Strategy of Redundant Robotic Manipulator in Narrow Workspace

---

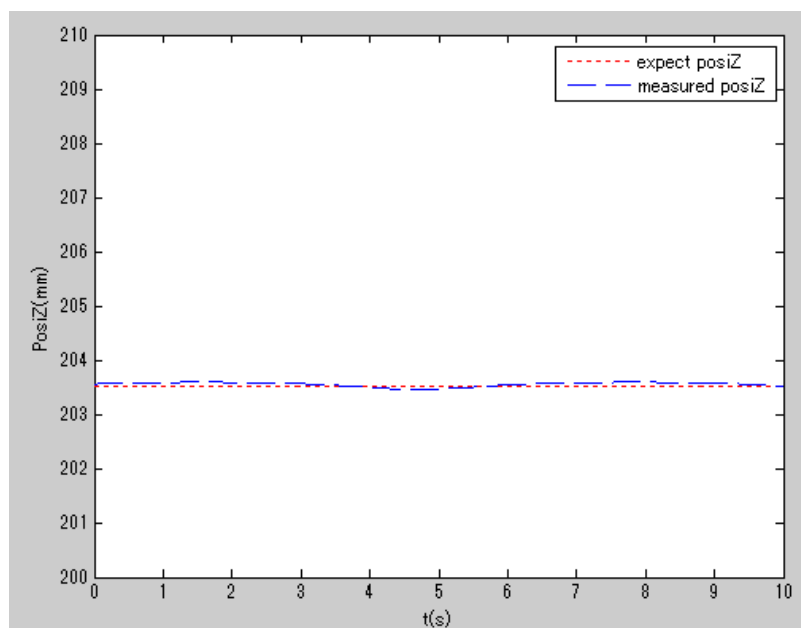


Figure 4.11 Expect z axial position and the measured value in the simulator of the distal of the tool manipulator.

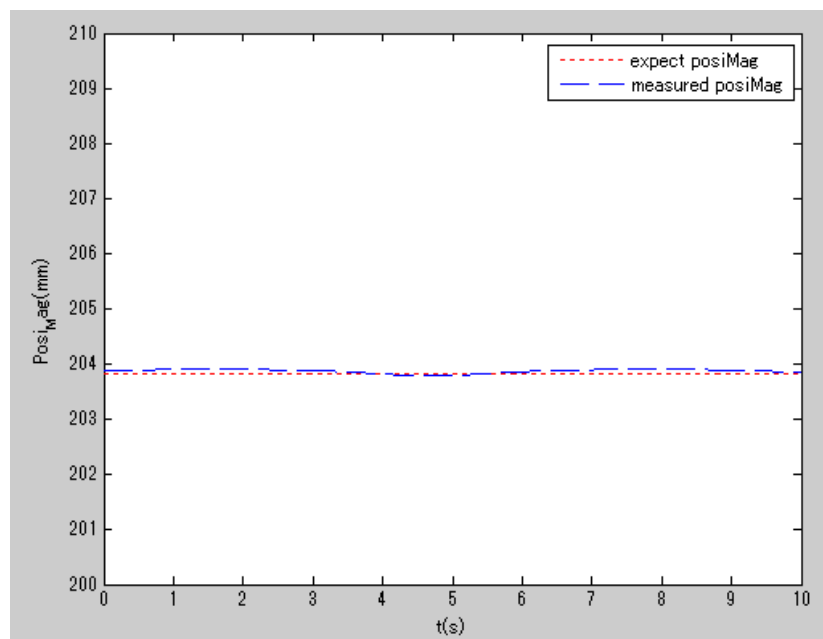


Figure 4.12 Expect Mag position and the measured value in the simulator of the distal of the tool manipulator.



### 4.3 Visualization in Narrow Workspace

In this section, the visualization of the visual feedback will be introduced. During surgery, the distal of the manipulator will be inserted into surgical cavity for surgical intervention. The redundant DoFs of the manipulator should comply with the principle that blocking endoscopic vision as small as possible. Fig. 4.2 shows the relation between the surgical cavity and the surgical robot. By adding into endoscope, the positional relationship between the endoscope and the surgical robot can be illustrated as Fig. 4.13.

In order to analyze the influence of the tool manipulator in the surgical cavity, the boundary of the vision in the surgical cavity should be firstly established.

Supposed the coordinate of the endoscope is  $E_n(x_{E_n}, y_{E_n}, z_{E_n})$  and the vertexes in the upper frame of the surgical cavity are  $E_1(x_{E_1}, y_{E_1}, z_{E_1})$ ,  $E_2(x_{E_2}, y_{E_2}, z_{E_2})$ ,  $E_3(x_{E_3}, y_{E_3}, z_{E_3})$  and  $E_4(x_{E_4}, y_{E_4}, z_{E_4})$  respectively. Since the surgical cavity is 30x30x30mm, therefore, the point  $F_i (i=1...4)$  can be given,

$$F_i = E_i + \begin{bmatrix} 0 & 0 & h \end{bmatrix} \quad (4.13)$$

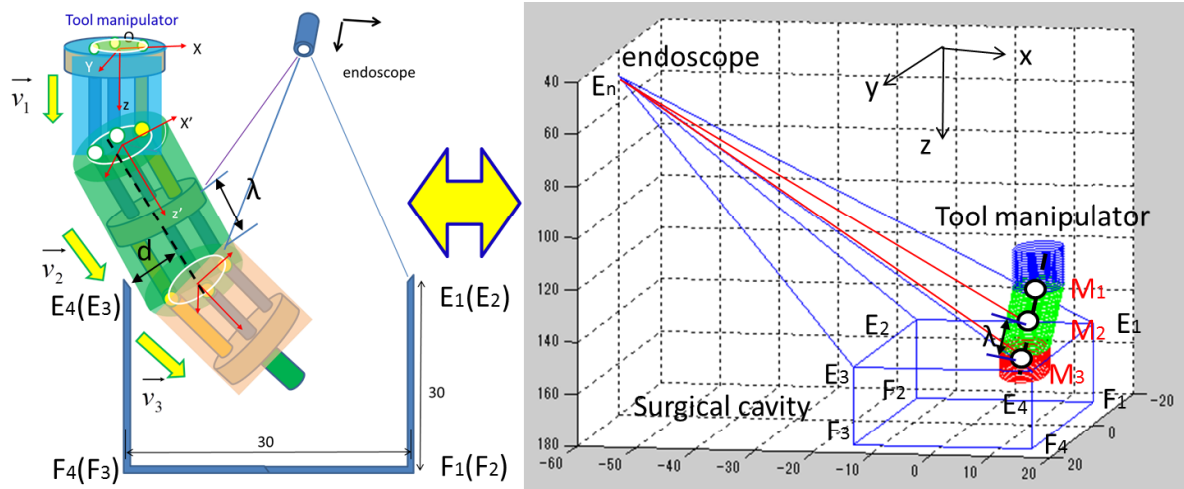


Figure 4. 13 The positional relation between endoscope and surgical cavity.

#### 4. Control Strategy of Redundant Robotic Manipulator in Narrow Workspace

---

Where,  $h = 30$  mm.

Based on the coordinate of point  $E_n, E_1, E_2, E_3, E_4$ , the visual boundary function can be calculated ( $E_n E_1 E_4$  for example). Suppose the plane normal vector is  $\vec{n} = (a, b, c)$ ,

$$\vec{n} = \overrightarrow{E_n E_1} \times \overrightarrow{E_n E_4} = \begin{vmatrix} i & j & k \\ x_{E_1} - x_{E_n} & y_{E_1} - y_{E_n} & z_{E_1} - z_{E_n} \\ x_{E_4} - x_{E_n} & y_{E_2} - y_{E_n} & z_{E_2} - z_{E_n} \end{vmatrix} \quad (4.14)$$

Therefore,

$$\begin{aligned} a &= (y_{E_1} - y_{E_n})(z_{E_2} - z_{E_n}) - (y_{E_2} - y_{E_n})(z_{E_1} - z_{E_n}) \\ b &= (z_{E_1} - z_{E_n})(x_{E_4} - x_{E_n}) - (z_{E_2} - z_{E_n})(x_{E_1} - x_{E_n}) \\ c &= (x_{E_1} - x_{E_n})(y_{E_2} - y_{E_n}) - (y_{E_1} - y_{E_n})(x_{E_4} - x_{E_n}) \end{aligned} \quad (4.15)$$

The plane  $CE_1 E_4$  can be given,

$$a(x - x_{E_n}) + b(y - y_{E_n}) + c(z - z_{E_n}) = 0 \quad (4.16)$$

The distal segment of the tool manipulator will track the instruction of the master input, therefore, the controllable segment is the redundant DoFs to reduce the part that will appear in the vision of the surgical cavity.

From (3-7) and (3-9) in chapter III, the coordinate of  $M_1, M_3$  can be calculated. In order to simplify the expression, we figure  $M_1, M_3$  as  $(x_{M_1}, y_{M_1}, z_{M_1})$  and  $(x_{M_3}, y_{M_3}, z_{M_3})$  respectively.

Therefore the line  $M_1 M_3$  function can be given,

$$\frac{x - x_{M_1}}{x_{M_3} - x_{M_1}} = \frac{y - y_{M_1}}{y_{M_3} - y_{M_1}} = \frac{z - z_{M_1}}{z_{M_3} - z_{M_1}} \quad (4.17)$$

Suppose,

$$\frac{x - x_{M_1}}{x_{M_3} - x_{M_1}} = \frac{y - y_{M_1}}{y_{M_3} - y_{M_1}} = \frac{z - z_{M_1}}{z_{M_3} - z_{M_1}} = t \quad (4.18)$$

Then,

$$\begin{aligned}
 x &= (x_{M3} - x_{M1})t + x_{M1} \\
 y &= (y_{M3} - y_{M1})t + y_{M1} \\
 z &= (z_{M3} - z_{M1})t + z_{M1}
 \end{aligned} \tag{4.19}$$

Substituting (4.18) into (4.16) get,

$$t = -\frac{a \cdot x_{M1} + b \cdot y_{M1} + c \cdot z_{M1} + D}{a \cdot (x_{M3} - x_{M1}) + b \cdot (y_{M3} - y_{M1}) + c \cdot (z_{M3} - z_{M1})} \tag{4.20}$$

Therefore, the intersect point between the plane  $E_n E_l E_4$  and the  $M_1 M_3$  is,

$$M_2 = \begin{bmatrix} (x_{M3} - x_{M1})t + x_{M1} \\ (y_{M3} - y_{M1})t + y_{M1} \\ (z_{M3} - z_{M1})t + z_{M1} \end{bmatrix} \tag{4.21}$$

The distance between point  $M_2$  and  $M_3$  is,

$$Dis_1 = \sqrt{(x_{M3} - x_{M2})^2 + (y_{M3} - y_{M2})^2 + (z_{M3} - z_{M2})^2} \tag{4.22}$$

The distance between point  $M_1$  and  $M_3$  is,

$$Dis_2 = \sqrt{(x_{M1} - x_{M3})^2 + (y_{M1} - y_{M3})^2 + (z_{M1} - z_{M3})^2} = d_2 \tag{4.23}$$

The ratio that visuable part of the tool manipulator under the endsopic vision is,

$$\lambda = \frac{Dis_1}{Dis_2} * 100\% \tag{4.24}$$

Additionally, define parameter  $d$  as the distance between the tool manipulator and the boundary of the surgical cavity. Therefore, the relation between the radius of tool manipulator  $-R-$  and the parameter  $-d-$  can be illustrated,

$$f_{(R,d)} = d - R \tag{4.25}$$

Corresponding to (4.24) and (4.25), user can achieve better visualization when parameter  $\lambda$  and  $f_{(R,d)}$  become smaller.

## 4.4 Operability in Narrow Workspace

This session consists of two indexes: collision detection and eye-hand triangle formation, shown in Fig. 4.14. To our surgical robot, the distal of the tool manipulator will track operator's instructions by master input, while, the redundant DoFs of the manipulator will be displaced to suitable posture based on the disturbance algorithm. Due to the narrow target space, the manipulator must avoid colliding with the surgical cavity for safety control.

### *Avoiding collision:*

The relation between the tool manipulator and the surgical cavity is shown in Fig. 4.15. The central line of the middle segment of the tool manipulator is marked as  $M_1M_3$ . The most possible collision happened at the point, which is closest to the surgical cavity's edge. To the

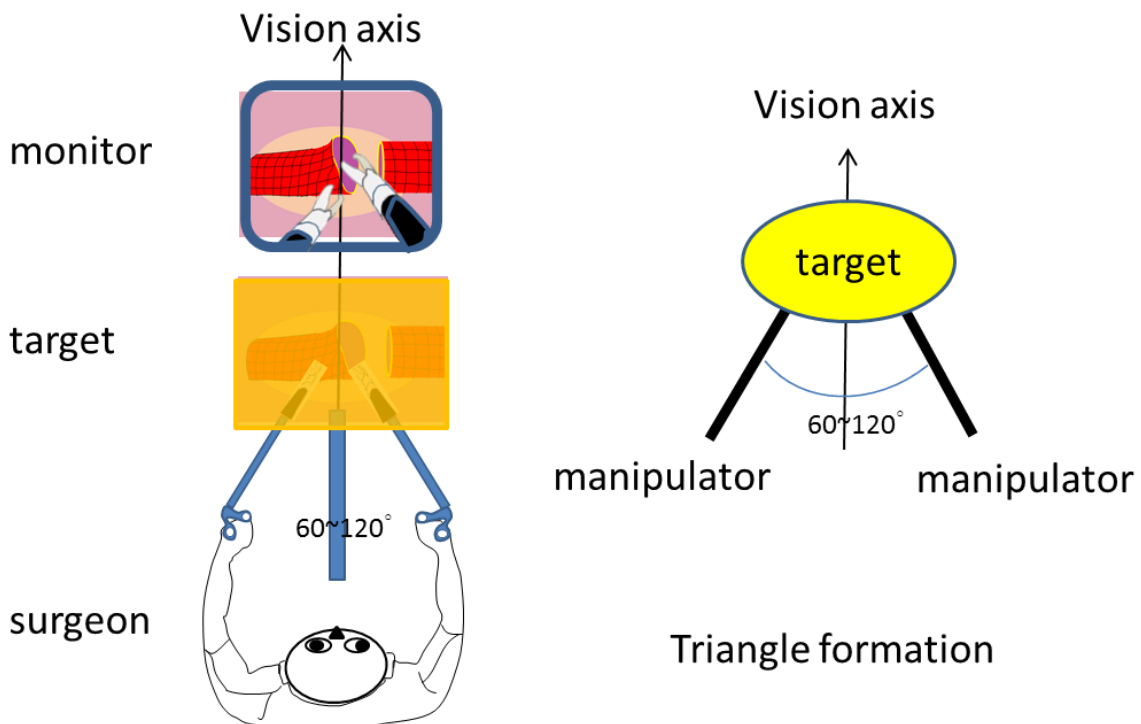


Figure 4. 14 Triangle formation of bimanual surgical operation.

state illustrated in Fig. 4.15, the closest distances between the line  $M_1M_2$  to the neighboring surgical cavity's edge are  $\Delta x$ ,  $\Delta y$  respectively. To the line  $E_3E_4$ , the orientation vector can be given,

$$\vec{v}_{E_3E_4} = (x_{E_4} - x_{E_3}, y_{E_4} - y_{E_3}, z_{E_4} - z_{E_3}) \quad (4.26)$$

Integrated (4.17) and (4.26), the distance between skew line  $M_1M_3$  and  $E_3E_4$  can be calculated,

$$d_{M_1M_3\_E_1E_3} = \frac{\begin{vmatrix} x_{M_1} - x_{E_3} & y_{M_1} - y_{E_3} & z_{M_1} - z_{E_3} \\ x_{M_1} - x_{E_3} & y_{M_1} - y_{E_3} & z_{M_1} - z_{E_3} \\ x_{M_3} - x_{M_1} & y_{M_3} - y_{M_1} & z_{M_3} - z_{M_1} \end{vmatrix}}{\sqrt{\begin{vmatrix} x_{M_1} - x_{E_3} & y_{M_1} - y_{E_3} \\ x_{M_3} - x_{M_1} & y_{M_3} - y_{M_1} \end{vmatrix}^2 + \begin{vmatrix} y_{M_1} - y_{E_3} & z_{M_1} - z_{E_3} \\ y_{M_3} - y_{M_1} & z_{M_3} - z_{M_1} \end{vmatrix}^2 + \begin{vmatrix} z_{M_1} - z_{E_3} & x_{M_1} - x_{E_3} \\ z_{M_3} - z_{M_1} & x_{M_3} - x_{M_1} \end{vmatrix}^2}} \quad (4.27)$$

Similarly, the distance between skew line  $M_1M_3$  and other three edges of the surgical cavity ( $d_{M_1M_3\_E_1E_4}$ ,  $d_{M_1M_3\_E_1E_2}$ ,  $d_{M_1M_3\_E_2E_3}$ ) can be calculated.

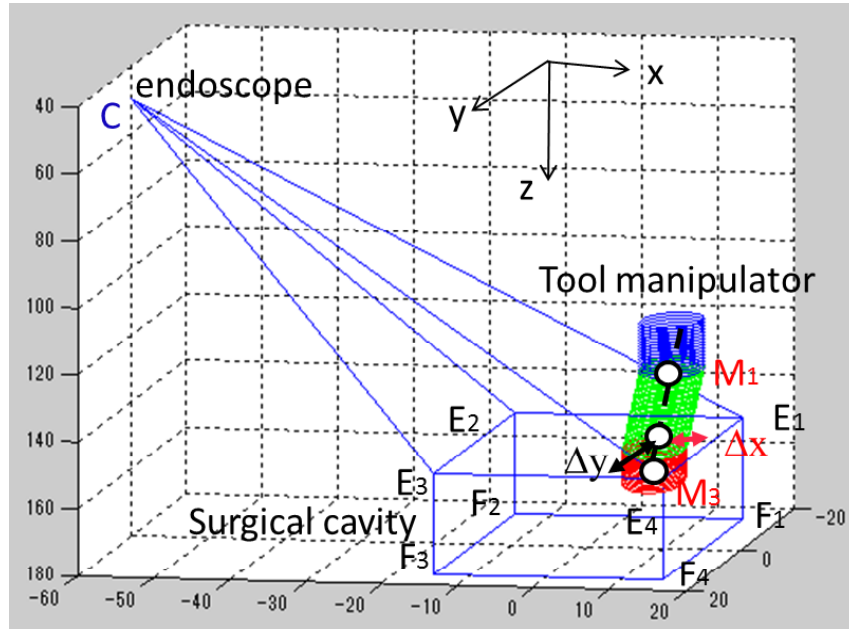


Figure 4. 15 Relation between the tool manipulator and the surgical cavity's edge.

The collision avoidance condition is that

$$d_{[d_{M1M3\_E1E3} \quad d_{M1M3\_E1E4} \quad d_{M1M3\_E1E2} \quad d_{M1M3\_E2E3}]} > Radius \quad (4.28)$$

Where, Radius = 4.

### ***Eye-hand triangle formation:***

In order to naturally perform operation, surgeon would like to perform manipulation as Fig. 4.15.

Mapping to the master-slave robotic manipulation, the slave manipulator should be comply with the triangle formation to provide good operability.

Considering the configuration of endoscope and the slave manipulator, the tilt angle between the tool manipulator and the vision axis should satisfy,

$$\delta |_{M1M3\_Z} \in (30^\circ \sim 60^\circ) \quad (4.29)$$

Where, the recommend angle is  $45^\circ$ .

## **4.5 Motion Modeling and Parameterization**

During operation, a common requirement of tissue intervention is to ensure that the distal of the tool manipulator is fully tracking the instruction of the master input, while the redundant joint would be controlled corresponding to the condition of the operation. In this section, the method to illustrate the control is presented.

### **4.5.1 Nomenclature of Robot Bending**

We presented the articulated robotic manipulator in Chapter 3. In order to exploiting the posture control, we take advantage of Omni-bending configuration to obtain optimal visualization and operability in the narrow workspace. Considered the serial structure of the tool manipulator, we propose a method to model the mathematics from the base to the distal. In this method, user with master input only control the distal of the manipulator. The redundant joints will conform in shape optimization algorithm. We define the bending angle

of the tool manipulator as  $\theta_i$ , where  $i=4$ . As shown in Fig. 3.12, each universal joint comprises two DoFs. Our tool manipulator consists of two bendable segments, therefore, the manipulator is composed of 4 DoFs in the bendable structure.  $\theta_1, \theta_2$  belong to the 1<sup>st</sup> segment and  $\theta_3, \theta_4$  belong to the 2<sup>nd</sup> segment. Since the two DoFs in a single segments are orthogonal with each other, therefore,  $\theta_2, \theta_3$  are parallel to each other when the tool manipulator in the straight state. And  $\theta_1, \theta_4$  are also parallel to each other when the tool manipulator in the straight state. In order to control the shape of the redundant manipulator, we define two parameters  $(q_c, \varphi)$  at the distal of the tool manipulator, which is shown in Fig. 4.16. The distal of the tool manipulator can be actuated to the required posture by change the variable  $(q_c, \varphi)$ . Points  $P_1, P_2, P_3, P_4$  are the feature points in the tool manipulator, where,  $P_1$  locates at the base of the tool manipulator;  $P_4$  locates at the distal of the tool manipulator;  $P_2, P_3$  locates at the rotary center of the bendable joints.

#### 4.5.2 Shape Optimization of Tool Manipulator Configuration

In order to track user's instruction for tissue intervention, robot bending must not block the front vision of the manipulator's tip. According to the section 4.5.1, the search of values  $(q_c, \varphi)$  on operation can be formulated as a circular shape optimization problem. Although many metrics could be used to construct the objective function to shape, we denote that the serial joints are draw to close an arc by the bending configuration.

From (3.7) and (3.8), we can calculate the coordinate of the feature points  $P_1, P_2, P_3, P_4$  in the tool manipulator,

$$\begin{aligned} P_1 &= [0 \ 0 \ 0]^T, \quad P_2 = [0 \ 0 \ d_1]^T, \\ P_3 &= \left[ \sum_{i=0}^3 {}^{i+1}T \cdot \vec{0} \ 1 \right]^T, \quad P_4 = \left[ \sum_{i=0}^6 {}^{i+1}T \cdot \vec{0} \ 1 \right]^T \end{aligned} \quad (4.30)$$

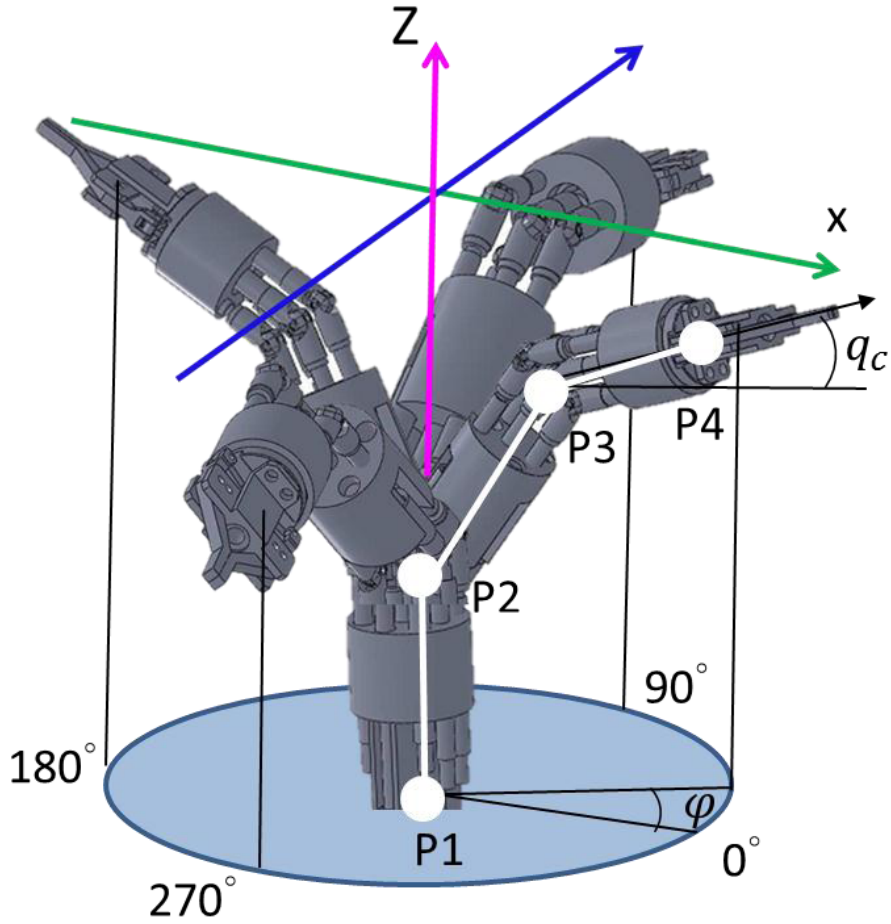


Figure 4. 16 Shape illustration of tool manipulator.

From (4.30), the vector  $\overrightarrow{P_3P_4}$  can be computed,

$$\overrightarrow{P_3P_4} = \begin{bmatrix} d_1 \cos \theta_4 \sin(\theta_2 + \theta_3) \\ d_1(-\cos \theta_1 \sin \theta_4 - \sin \theta_1 \cos \theta_4 \cos(\theta_2 + \theta_3)) \\ d_1(-\sin \theta_1 \sin \theta_4 + \cos \theta_1 \cos \theta_4 \cos(\theta_2 + \theta_3)) \end{bmatrix}^T \quad (4.31)$$

Therefore,

$$\sin q_c = -\sin \theta_1 \sin \theta_4 + \cos \theta_1 \cos \theta_4 \cos(\theta_2 + \theta_3) \quad (4.32)$$

$$\operatorname{tg} \varphi = (-\cos \theta_1 \sin \theta_4 - \sin \theta_1 \cos \theta_4 \cos(\theta_2 + \theta_3)) / (\cos \theta_4 \sin(\theta_2 + \theta_3)) \quad (4.33)$$

To the first bendable segment, we can get

$$\operatorname{tg} \varphi = -\sin \theta_1 \operatorname{ctg} \theta_2 \quad (4.34)$$

From (4.32),



$$\cos(\theta_2 + \theta_3) = (\sin\theta_1 \sin\theta_4 + \sin q_c) / (\cos\theta_1 \cos\theta_4) \quad (4.35)$$

From (4.33),

$$\sin(\theta_2 + \theta_3) = (-\cos\theta_1 \sin\theta_4 - \sin\theta_1 \cos\theta_4 \cos(\theta_2 + \theta_3)) / (tg\varphi \cos\theta_4) \quad (4.36)$$

Square both sides of (4.32) and (4.33), then add left side and right side respectively,

$$\left(\frac{\sin\theta_1 \sin\theta_4 + \sin q_c}{\cos\theta_1 \cos\theta_4}\right)^2 + \left(\frac{-\cos\theta_1 \sin\theta_4 - \sin\theta_1 \cos\theta_4 \cos(\theta_2 + \theta_3)}{tg\varphi \cos\theta_4}\right)^2 = 1 \quad (4.37)$$

Denote an expression  $f(\theta_1, \theta_4)$ ,

$$f_{(\theta_1, \theta_4)} = \left(\frac{\sin\theta_1 \sin\theta_4 + \sin q_c}{\cos\theta_1 \cos\theta_4}\right)^2 + \left(\frac{-\cos\theta_1 \sin\theta_4 - \sin\theta_1 \cos\theta_4 \cos(\theta_2 + \theta_3)}{tg\varphi \cos\theta_4}\right)^2 - 1 \quad (4.38)$$

Define a small error  $\varepsilon$ , make

$$f(\theta_1, \theta_4) \leq \varepsilon \quad (4.39)$$

From (4.30), points  $P_1, P_2, P_3, P_4$  can be known, therefore, the angle  $\angle P_1 P_2 P_3$  and  $\angle P_2 P_3 P_4$  can be calculated by,

$$\begin{aligned} \angle P_1 P_2 P_3 &= a \cos \langle \overrightarrow{P_1 P_2}, \overrightarrow{P_2 P_3} \rangle \\ \angle P_2 P_3 P_4 &= a \cos \langle \overrightarrow{P_2 P_3}, \overrightarrow{P_3 P_4} \rangle \end{aligned} \quad (4.40)$$

The search of values for  $(\hat{\theta}_1, \hat{\theta}_2, \hat{\theta}_3, \hat{\theta}_4)$  of the tool manipulator within the range of optimal bending can be formulated as

$$(\hat{\theta}_1, \hat{\theta}_2, \hat{\theta}_3, \hat{\theta}_4) = \arg \min_{q_c, \varphi} \{ |\angle P_1 P_2 P_3 - \angle P_2 P_3 P_4| \} \quad (4.41)$$

Since, the range of each joint belongs to  $\pm 45^\circ$ , the algorithm for searching the optimal solution can be illustrated by the following pseudo code, shown in Table 4-3.

Base on the optimal algorithm, four example bending shapes in different quadrant are used to illustrate the inverse solutions of bending joints in Fig. 4.17 to Fig. 4.20. Compared with the inverse solutions, a deviation ( $\Delta_{angle\_deviation} < 0.5^\circ$ ) can be selected for shape planning at each state when  $\varepsilon < 0.001$ .

The table 4-4 to table 4-7 show the value of each optimal solution, respectively.

#### 4. Control Strategy of Redundant Robotic Manipulator in Narrow Workspace

Table 4- 3 Steps of shape optimal algorithm for searching bending solutions

Calculate the shape optimal value from the input ( $q_c, \psi$ )	
1.	Input: ( $q_c, \psi$ )
2.	for $\theta_1 = -45, \dots, 45$ <b>do</b>
3.	for $\theta_4 = -45, \dots, 45$ <b>do</b>
4.	if $f(\theta_1, \theta_4) < \varepsilon \rightarrow$ true <b>then</b>
5.	$\theta_2 \leftarrow (4.36)$ ; $\theta_3 \leftarrow (4.37)$ ; $\theta_5 = 0$
6.	$\angle P_1P_2P_3, \angle P_2P_3P_4 \leftarrow \theta_1, \theta_2, \theta_3, \theta_4, \theta_5$
7.	$(\hat{\theta}_1, \hat{\theta}_2, \hat{\theta}_3, \hat{\theta}_4) = \arg \min_{q_c, \varphi} \{ \angle P_1P_2P_3 - \angle P_2P_3P_4 \}$
8.	output: shape optimal solution

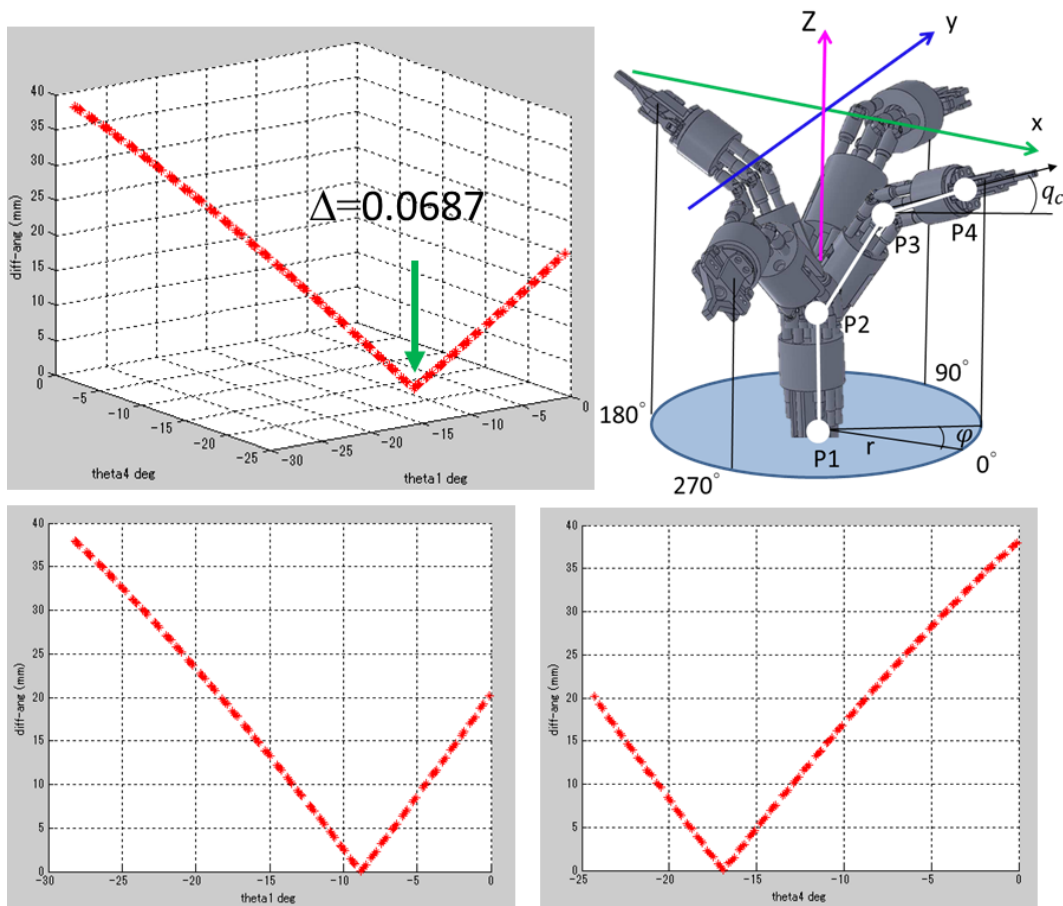


Figure 4. 17 Deviation between  $\angle P1P2P3$  and  $\angle P2P3P4$  within the range for searching optimal bending state in the 1<sup>st</sup> quadrant.

#### 4. Control Strategy of Redundant Robotic Manipulator in Narrow Workspace

Table 4- 4 Inverse solution of bendable joint based on shape optimal algorithm in the 1<sup>st</sup> quadrant

Shape optimization in the 1 <sup>st</sup> quadrant				
$q_c = 50^\circ$ , $\varphi = 40^\circ$ , $\varepsilon = 0.001$				
Solution Number	153			
Optimal solution	$\theta_1(^{\circ})$	$\theta_2(^{\circ})$	$\theta_3(^{\circ})$	$\theta_4(^{\circ})$
	-8.8	10.33	20.66	-16.9
Tip's position of the optimal solution	(12.5074, 10.6491, 55.2861)			

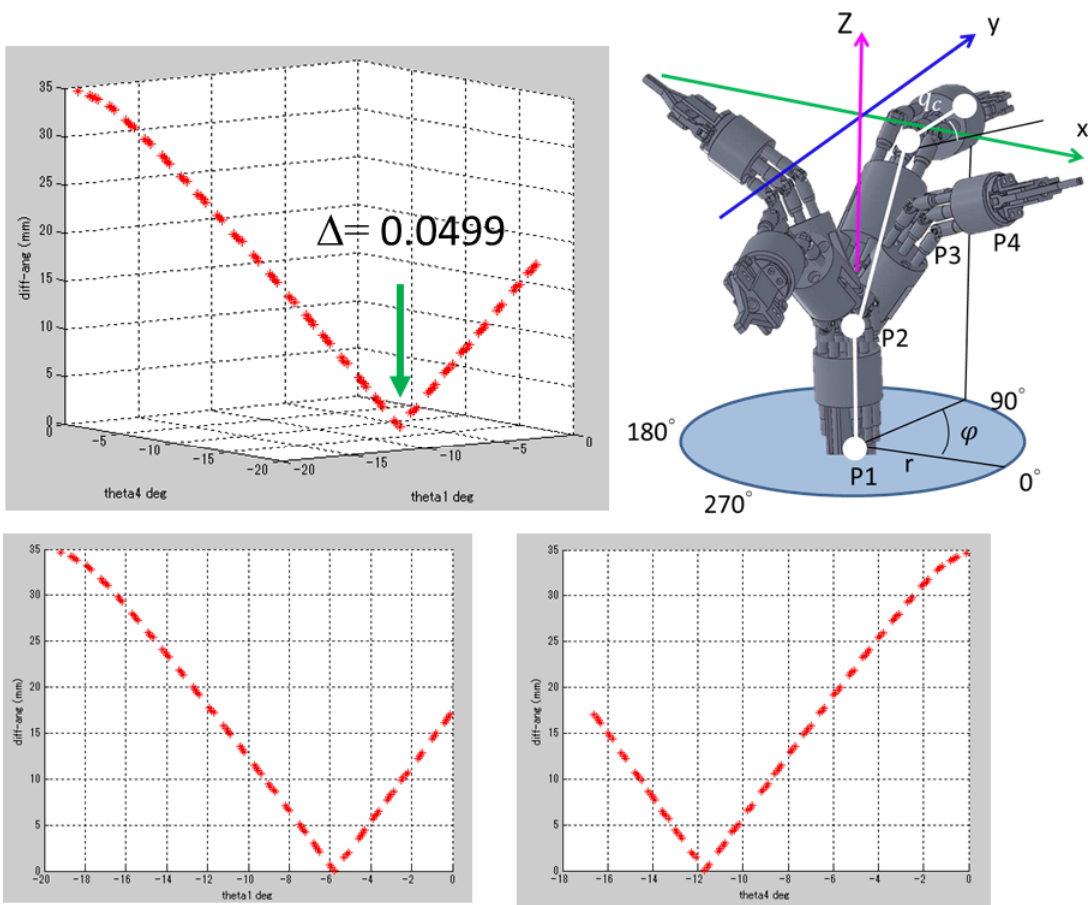


Figure 4. 18 Deviation between  $\angle P1P2P3$  and  $\angle P2P3P4$  within the range for searching optimal bending state in the 2<sup>nd</sup> quadrant.

#### 4. Control Strategy of Redundant Robotic Manipulator in Narrow Workspace

Table 4- 5 Inverse solution of bendable joint based on shape optimal algorithm in the 2<sup>nd</sup> quadrant

Shape optimization in the 2 <sup>nd</sup> quadrant				
$q_c = 55^\circ$ , $\varphi = 150^\circ$ , $\varepsilon = 0.001$				
Solution Number	95			
Optimal solution	$\theta_1(^{\circ})$	$\theta_2(^{\circ})$	$\theta_3(^{\circ})$	$\theta_4(^{\circ})$
	-5.8	-9.93	-20.54	-11.7
Tip's position of the optimal solution	(-12.8808, 7.3312, 57.0743)			

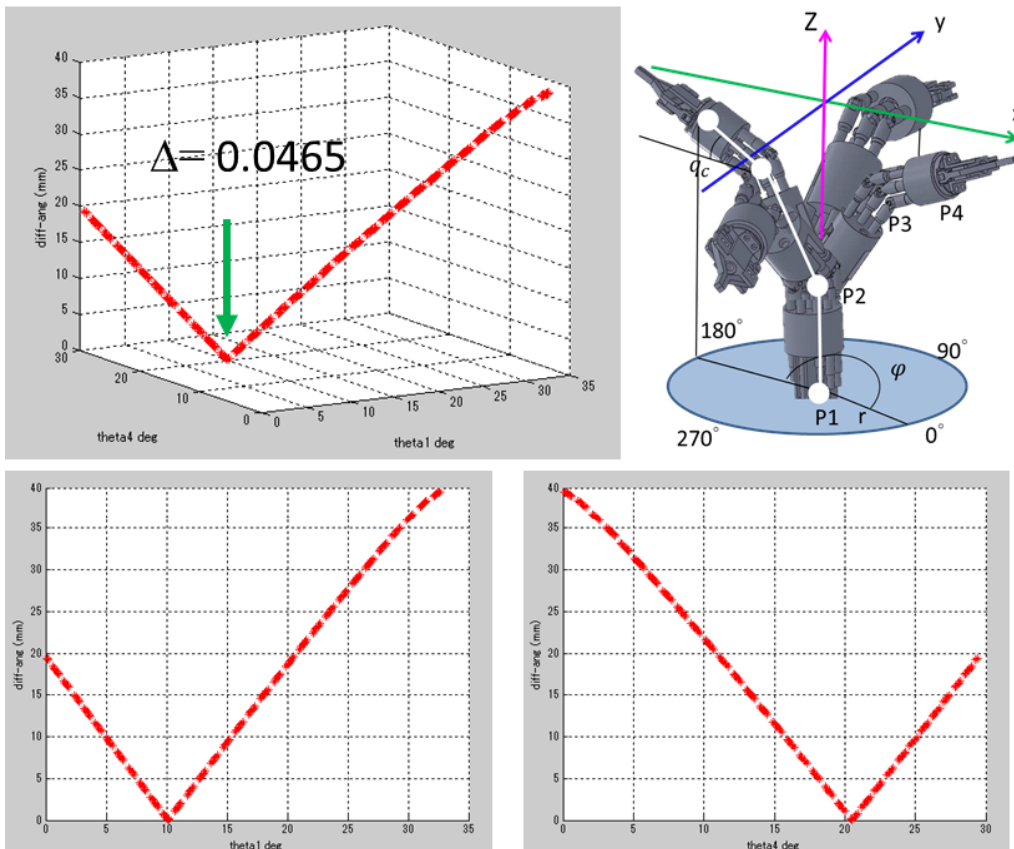


Figure 4. 19 Deviation between  $\angle P1P2P3$  and  $\angle P2P3P4$  within the range for searching optimal bending state in the 3<sup>rd</sup> quadrant.

#### 4. Control Strategy of Redundant Robotic Manipulator in Narrow Workspace

Table 4- 6 Inverse solution of bendable joint based on shape optimal algorithm in the 3<sup>rd</sup> quadrant

Shape optimization in the 3 <sup>rd</sup> quadrant				
$q_c = 50^\circ$ , $\varphi = 230^\circ$ , $\varepsilon = 0.001$				
Solution Number	204			
Optimal solution	$\theta_1(^{\circ})$	$\theta_2(^{\circ})$	$\theta_3(^{\circ})$	$\theta_4(^{\circ})$
	10.1	-8.37	-17.82	20.5
Tip's position of the optimal solution	(-10.7646, -12.6508, 56.0661)			

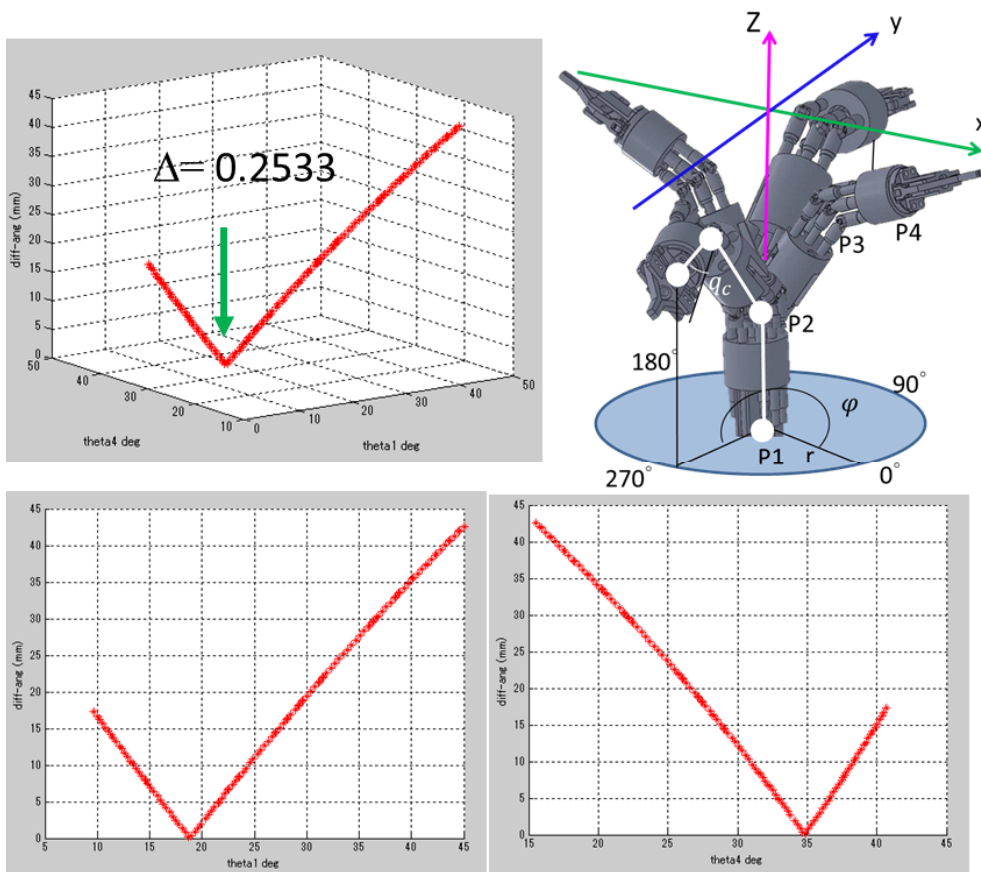


Figure 4. 20 Deviation between  $\angle P1P2P3$  and  $\angle P2P3P4$  within the range for searching optimal bending state in the 4<sup>th</sup> quadrant.

#### 4. Control Strategy of Redundant Robotic Manipulator in Narrow Workspace

Table 4- 7 Inverse solution of bendable joint based on shape optimal algorithm in the 4<sup>th</sup> quadrant

Shape optimization in the 4 <sup>th</sup> quadrant				
$q_c = 20^\circ$ , $\varphi = 310^\circ$ , $\varepsilon = 0.001$				
Solution Number	123			
Optimal solution	$\theta_1(^\circ)$	$\theta_2(^\circ)$	$\theta_3(^\circ)$	$\theta_4(^\circ)$
	18.7	15.06	32.38	34.9
Tip's position of the optimal solution	(16.243, -19.9182, 47.0777)			

#### 4.5.3 Shape Optimization of Slave Arm Configuration

In section 4.5.2, the inverse solutions of the tool manipulator can be calculated by using the shape optimal algorithm, however, in order to decide the position of the distal of the tool manipulator, we should have coordinate input  $P_{4(x,y,z)}$ . Therefore, the input from the master side to the slave arm is  $(q_c, \varphi, x, y, z)$ .

When the slave arm is actuated to perform intervention, because the tool manipulator will conform the shape optimization based on the algorithm in section 4.5.2, therefore, the configuration of redundant manipulator could satisfy the triangle formation of bimanual operation, referred in section 4.3. In order to illustrate the operability referred in section 4.4, we propose that the distal of the tool manipulator moves inside the surgical cavity.

According to the computation in section 4.2, the calculation of the whole slave arm could be divided into two parts: tool manipulator and positioning manipulator. The inverse solution for the tool manipulator can be computed by 2 steps.

##### 1) Shape optimization based on $(q_c, \varphi)$

From section 4.5.2, the shape optimization for calculating the inverse solution of the tool manipulator is presented in (4.43).

##### 2) Collision detection between manipulator and the surgical cavity

From section 4.3, the distance between the manipulator and the surgical cavity could be calculated. Therefore, we define the deviation after collision as  $(\Delta x, \Delta y)$ ,

$$\Delta x_c = \begin{cases} Radius - Dis_{P_2P_3-E_1E_4}, & Dis_{P_2P_3-E_1E_4} < Radius \\ 0, & Dis_{P_2P_3-E_1E_4} \geq Radius \end{cases} \quad (4.42)$$

$$\Delta y_c = \begin{cases} Radius - Dis_{P_2P_3-E_1E_2}, & Dis_{P_2P_3-E_1E_2} < Radius \\ 0, & Dis_{P_2P_3-E_1E_2} \geq Radius \end{cases}$$

Integrated with the disturbance avoidance algorithm in section 4.2, the angle in the bendable joint can be calculated,

$$\left( \prod_{l=1}^m {}^{l-1}T_{T(\theta_{r1}, \theta_{r2}, \theta_{r3}, \theta_{r4}, \theta_{r5})} \right) \cdot \begin{bmatrix} 0 \\ 0 \\ 0 \\ 1 \end{bmatrix} = \left( \prod_{i=1}^n {}^{i-1}T_{T(\hat{\theta}_{r1}, \hat{\theta}_{r2}, \hat{\theta}_{r3}, \hat{\theta}_{r4})} \right) \cdot \begin{bmatrix} 0 \\ 0 \\ 0 \\ 1 \end{bmatrix} + \begin{bmatrix} \Delta x_c \\ \Delta y_c \\ \Delta z_c \\ 1 \end{bmatrix} \quad (4.43)$$

Where,  $m = 5$ ;  $n = 5$ ;

$$(\hat{\theta}_1, \hat{\theta}_2, \hat{\theta}_3, \hat{\theta}_4) = \arg \min_{q_c, \varphi} \{ \angle P_1P_2P_3 - \angle P_2P_3P_4 \};$$

$$\Delta z_c = \pm \sqrt{(d_2^2 + R_2^2)^2 - (P_{2[1,1]} + \Delta x_c - P_{3[1,1]})^2 - (P_{2[1,2]} + \Delta y_c - P_{3[1,2]})^2};$$

Substituting (4.41), (4.42) into (4.43), the current bending angle in the tool manipulator can be computed,

$$\left\{ \begin{array}{l} \theta_{2N} = a \sin \frac{P_{3[1,1]} - R_1 - \Delta x_c}{\sqrt{d_2^2 + (R_2)^2}} + a \tan \frac{R_2}{d_2} \\ \theta_{1N} = a \sin \frac{\Delta y_c - P_{3[1,2]}}{d_2 \cos \theta_{2N} + R_2 \sin \theta_{2N}} \\ \theta_{4N} = -a \sin \frac{\overrightarrow{v_{P_3P_4 [1,2]}} \cos \theta_{1N} + \overrightarrow{v_{P_3P_4 [1,3]}} \sin \theta_{1N}}{d_1} \\ \theta_{3N} = a \sin \left( \frac{\overrightarrow{v_{P_3P_4 [1,1]}}}{d_1 \cos \theta_{4N}} \right) - \theta_{2N} \\ \theta_{5N} = \theta_{Rot} \leftarrow \text{decided by rotary angle of phantom stylus} \end{array} \right. \quad (4.44)$$

We obtain the current bending angle of the tool manipulator from (4.44), and know the distal position from the input  $(q_c, \varphi, x, y, z)$ . Therefore, the inverse solution of the position manipulator can be calculated by 3 steps,

**1) Deviation created by the input  $(q_c, \varphi, x, y, z)$**

$$\Delta_{1(x,y,z)} = P_{(x_2,y_2,z_2)} - P_{(x_1,y_1,z_1)} \quad (4.45)$$

**2) Deviation created by the shape optimization algorithm**

$$\Delta_{2(x,y,z)} = \prod_{i=0}^6 {}^{i+1}T_{(q_c, \varphi)} \begin{bmatrix} \vec{0} & 1 \end{bmatrix}^T - \prod_{i=0}^6 {}^{i+1}T_{(\theta_{1,N}, \dots, \theta_{3,N})} \begin{bmatrix} \vec{0} & 1 \end{bmatrix}^T \quad (4.46)$$

**3) Deviation created by collision avoidance**

$$\Delta_{3(x,y,z)} = \begin{cases} \Delta x_c = \begin{cases} \text{Radius} - \text{Dis}_{P_2P_3-E_1E_4}, & \text{Dis}_{P_2P_3-E_1E_4} < \text{Radius} \\ 0, & \text{Dis}_{P_2P_3-E_1E_4} \geq \text{Radius} \end{cases} \\ \Delta y_c = \begin{cases} \text{Radius} - \text{Dis}_{P_2P_3-E_1E_2}, & \text{Dis}_{P_2P_3-E_1E_2} < \text{Radius} \\ 0, & \text{Dis}_{P_2P_3-E_1E_2} \geq \text{Radius} \end{cases} \\ \Delta z_c = \pm \sqrt{(d_2^2 + R_2^2)^2 - (P_{2[1,1]} + \Delta x_c - P_{3[1,1]})^2 - (P_{2[1,2]} + \Delta y_c - P_{3[1,2]})^2} \end{cases} \quad (4.47)$$

Therefore, the total deviation of the distal of the positioning manipulator is,

$$\Delta(x, y, z) = \Delta_{1(x,y,z)} + \Delta_{2(x,y,z)} + \Delta_{3(x,y,z)} \quad (4.48)$$

Based on the computation of the inverse kinematics in section 3.5 and (4.43), the inverse solution of the positioning manipulator can be expressed as,

$$\left( \prod_{j=1}^k {}^{j-1}T_{P(\theta_{p_1}, \theta_{p_2}, \theta_{p_3}, \theta_{p_4})} \right) \cdot \begin{bmatrix} \vec{0} & 1 \end{bmatrix}^T = \Delta(x, y, z) \quad (4.49)$$

Where,  $k = 4$ ;  $n = 5$ .

Substituting (4.41), (4.48) into (4.49), get the angles in the positioning manipulator,

$$\begin{aligned} \theta_{p_1} &= \Delta(x, y, z)_z \\ \theta_{p_3} &= a \sin \frac{(M_{4[1,1]current} + \Delta(x, y, z)_x - L_3)^2 + (M_{4[1,2]current} + \Delta(x, y, z)_y)^2 - L_1^2 - L_2^2}{2L_1L_2} \\ \theta_{p_2} &= a \sin \frac{M_{4[1,2]current} + \Delta(x, y, z)_y}{\sqrt{(L_1 + L_2 \sin \theta_{p_3})^2 + (L_2 \cos \theta_{p_3})^2}} - a \tan \frac{L_2 \sin \theta_{p_3} + L_1}{L_2 \cos \theta_{p_3}} \\ \theta_{p_4} &= -(\theta_{p_2} + \theta_{p_3}) \end{aligned} \quad (4.50)$$

Based on the illustration of the above computation procedures, the pseudo code for computing the inverse solution of the manipulator can be presented in Table 4-8,



Table 4- 8 Steps for computing the inverse solution of the redundant manipulator

Calculate the inverse solution of the redundant manipulator	
1. Input:	$P4(q_c, \Psi, x, y, z)$
2. for $\theta_1=-45, \dots, 45$	<b>do</b>
3. for $\theta_4=-45, \dots, 45$	<b>do</b>
4.	calculate the deviation expression $f(\theta_1, \theta_4) \leftarrow (4.40)$
5.	if $f(\theta_1, \theta_4) < \varepsilon \rightarrow$ true <b>then</b>
6.	$\theta_2 \leftarrow (4.36); \theta_3 \leftarrow (4.37); \theta_5 = 0$
7.	$\angle P_1P_2P_3, \angle P_2P_3P_4 \leftarrow \theta_1, \theta_2, \theta_3, \theta_4, \theta_5$
8.	$(\hat{\theta}_1, \hat{\theta}_2, \hat{\theta}_3, \hat{\theta}_4) = \arg \min_{q_c, \varphi} \{ \angle P_1P_2P_3 - \angle P_2P_3P_4 \}$
9.	position of bent joint in tool manipulator $P2(x_2, y_2, z_2), P3(x_3, y_3, z_3) \leftarrow (3.8)$
10.	distance (dis) between surgical cavity and tool manipulator $\leftarrow (4.30)$
11.	if (dis < Raduis) $\rightarrow$ true <b>then</b>
12.	new solutions $(\theta_{1N}, \theta_{2N}, \theta_{3N}, \theta_{4N})$ based on $(\Delta x, \Delta y) \leftarrow (4.5), (4.7), (4.8)$
13.	inverse solution of positioning manipulator $(\theta_{p1}, \theta_{p2}, \theta_{p3}, \theta_{p4}) \leftarrow (3.34)$
14. output	

#### 4.5.4 Example Simulation

During surgery, only the distal of the tool manipulator will be inserted into the surgical cavity, and the redundant joint will be planned by the collision avoid algorithm while the distal following the input command .The simulation platform is illustrated in Fig. 4.21. The positions of endoscope and the edge points of the surgical cavity are presented in Table 4-9.

#### 4. Control Strategy of Redundant Robotic Manipulator in Narrow Workspace

Table 4- 9 Nomenclature points and master input

Input instruction ( $q_c, \varphi, x, y, z$ )				
$q_c (^\circ)$	$\varphi (^\circ)$	X (mm)	Y (mm)	Z (mm)
30~60	30	70	0	75
Position of feature points				
$E_1$	$E_2$	$E_3$	$E_4$	$E_n$
(80,15,50)	(80,-15,50)	(50,-15,50)	(50,15,50)	(65,80,-30)
$F_1$	$F_2$	$F_3$	$F_4$	
(80,15,80)	(80,-15,80)	(50,-15,80)	(50,15,80)	

Since ray direction of the example tip point  $P_4$  located at the 1<sup>st</sup> quadrant and the distal segment is directly controlled by master input, hence, the risk that the edges of the surgical cavity would collide with the tool manipulator are edges  $E_2E_3$  and  $E_3E_4$ . Therefore, the distances between the tool manipulator and the edge  $E_2E_3$ ,  $E_3E_4$  should be checked in real time.

From the step 12 in the table 4-8, we can get the new solution corresponding to the deviation ( $\Delta x$ ,  $\Delta y$ ). In this section, three example deviations are presented. In the first two simulations, the deviation in x-axis is different, the change of rod's length are shown in Fig.4.22 to Fig. 4. 25. In the 3<sup>rd</sup> simulation, the redundant joint was forced in both x-axis and y-axis. The changes of rod's length are shown in Fig. 4.26 and Fig. 4.27. The change of rod's length will be analyzed based on the deviation in x-axis and y-axis. Fig. 4.22 to Fig. 4.27 show the inverse solutions of joint angle based on the different deviations listed in table 4-10.

Table 4- 10 Deviation conditions for computing new solutions

No. 1	No. 2	No. 3
$\Delta x = 5; \Delta y = 0$	$\Delta x = 3; \Delta y = 0$	$\Delta x = 3; \Delta y = 3$

#### 4. Control Strategy of Redundant Robotic Manipulator in Narrow Workspace

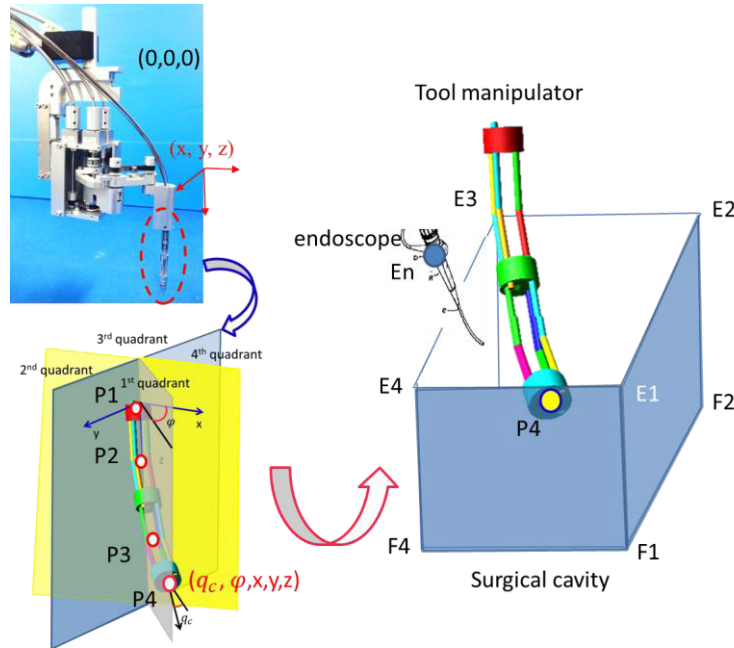


Figure 4.21 Configuration of the robot and the surgical cavity for collision avoidance algorithm.

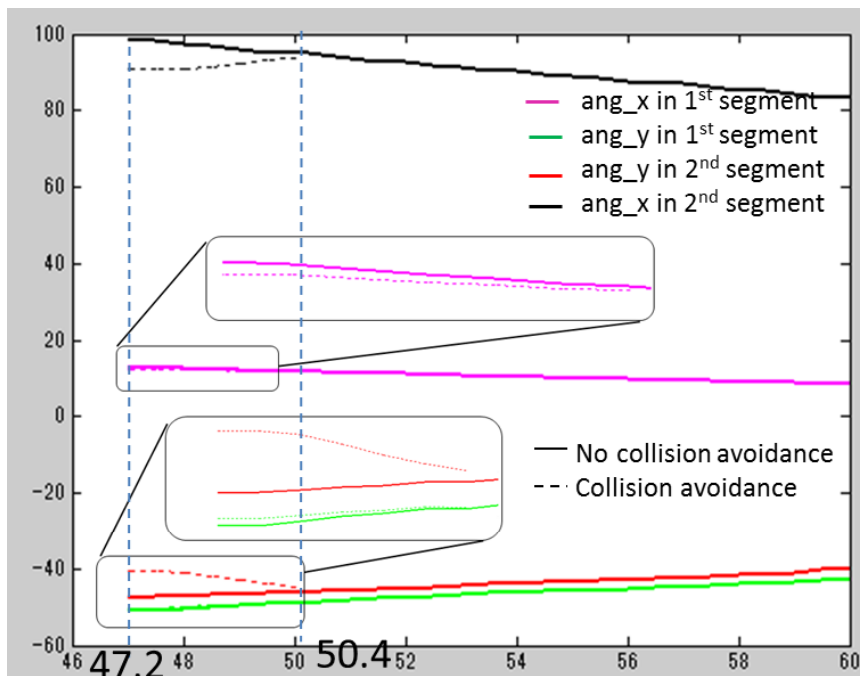


Figure 4.22 Joint value of SCARA manipulator with/without collision avoidance algorithm ( $\Delta x=5, \Delta y=0$ ).

#### 4. Control Strategy of Redundant Robotic Manipulator in Narrow Workspace

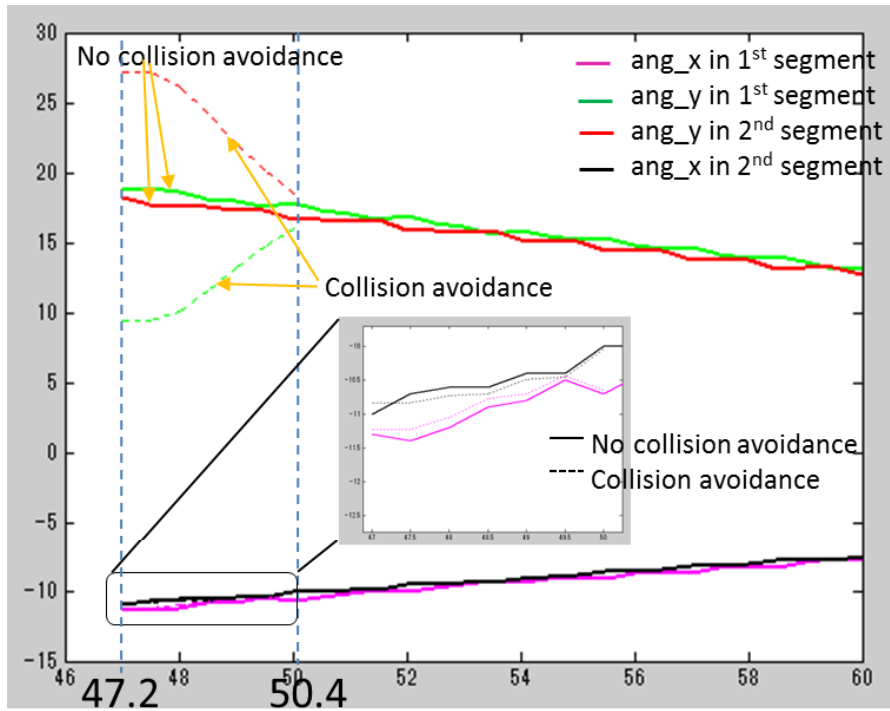


Figure 4.23 Joint value of Tool manipulator with/without collision avoidance algorithm ( $\Delta x=5, \Delta y=0$ ).

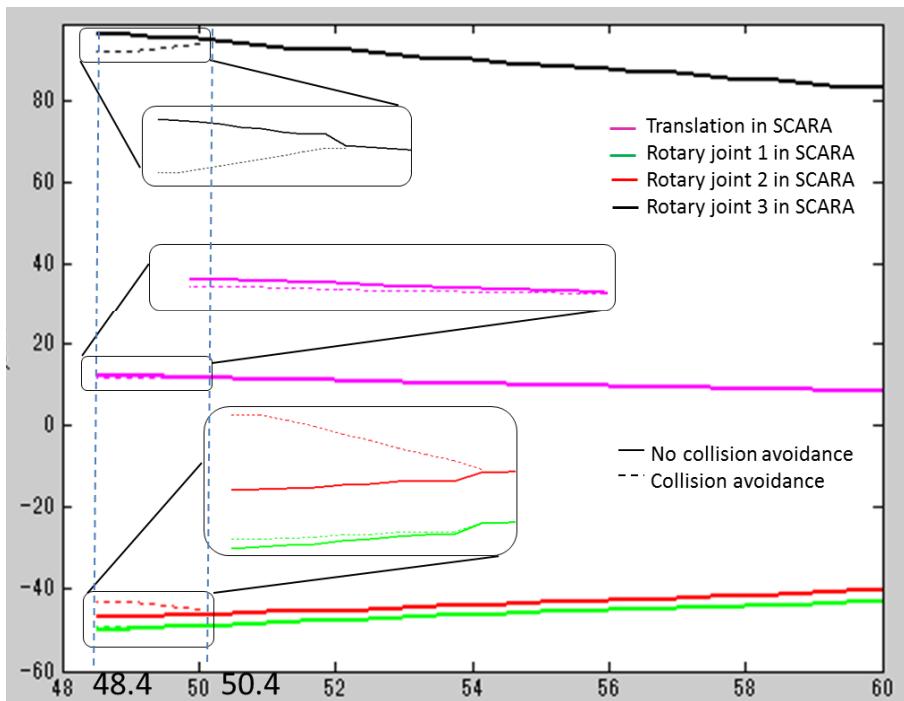


Figure 4.24 Joint value of SCARA manipulator with/without collision avoidance algorithm ( $\Delta x=3, \Delta y=0$ ).

#### 4. Control Strategy of Redundant Robotic Manipulator in Narrow Workspace

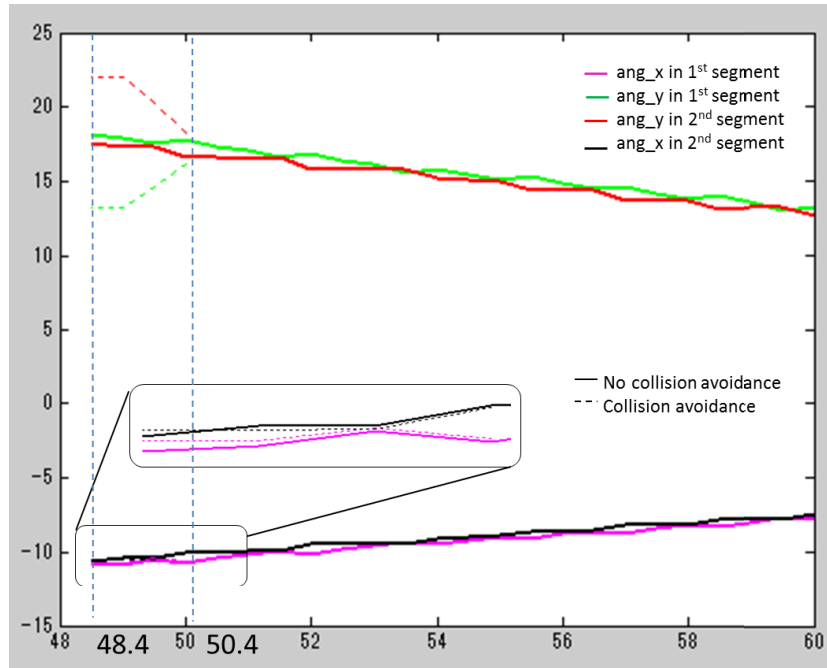


Figure 4.25 Joint value of Tool manipulator with/without collision avoidance algorithm ( $\Delta x=3, \Delta y=0$ ).

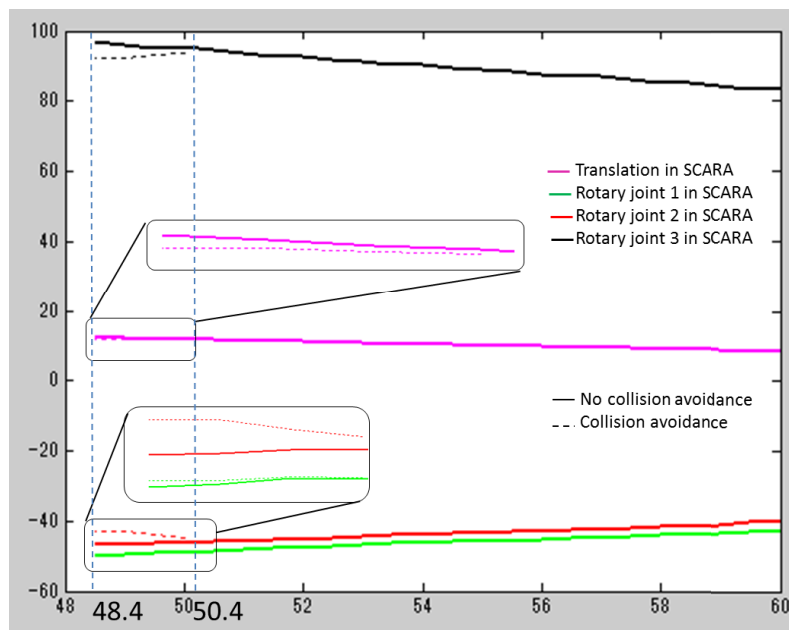


Figure 4.26 Joint value of SCARA manipulator with/without collision avoidance algorithm ( $\Delta x=3, \Delta y=3$ ).

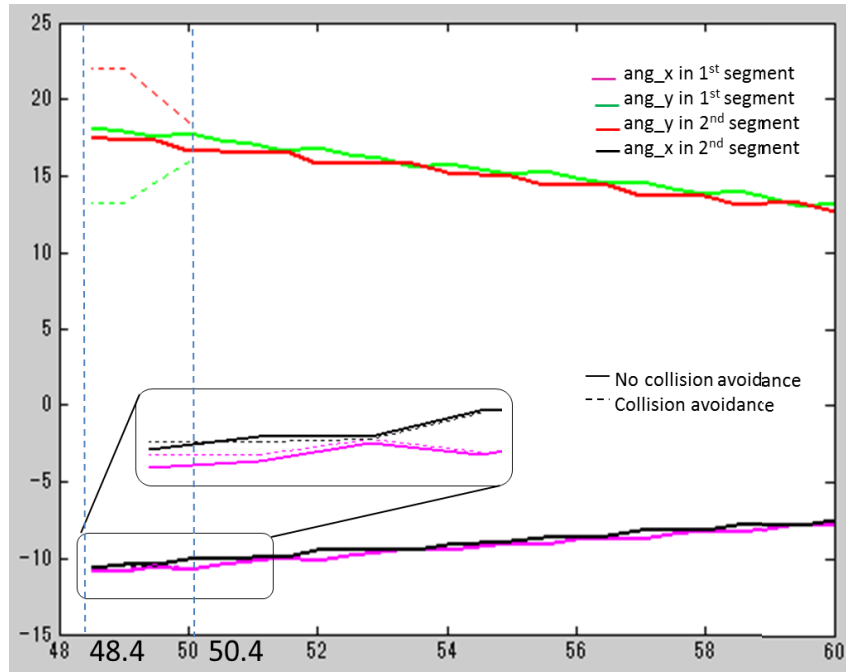


Figure 4.27 Joint value of tool manipulator with/without collision avoidance algorithm ( $\Delta x=3, \Delta y=3$ ).

From Fig. 4.22 to Fig. 4.27, we can know the manipulator follow the normal master-slave control when the bent angle belongs to  $(50.4^\circ \sim 60^\circ)$ . The manipulator would avoid collision with the surgical cavity when the bent angle smaller than  $50.4^\circ$ . Furthermore, the manipulator could reach bigger expansibility when delta value becomes larger (bent range in Fig. 4.24 to Fig. 4.27 is larger than that in Fig. 4.22 and Fig. 4.23). The reason that the value in Fig. 4.26 to Fig. 4.27 is similar to that in Fig. 4.24 and Fig. 4.25 is because the inverse kinematics algorithm considering not only the distance for avoiding collision but also smoothly transmitting during adjacent steps on trajectory.

Referred in section 4.3, the less part of the manipulator under endoscopic vision could reduce the shield area and improve operability. Therefore, the visible ratios of the manipulator during collision avoidance processes are shown in Fig. 4.28 and Fig. 4.29. As shown in Fig. 4.28 and Fig. 4.29, the visible ratio of the tool manipulator continually increases when the tool manipulator bended. Therefore, in order to improve the visualization, the smaller  $\Delta y$  could reduce the shield area created by the tool manipulator.

The visible ratio created by the tool manipulator during bent motion is shown in Fig. 4.30. The influence caused by  $\Delta y$  at fixed  $\Delta x$  is shown in Fig. 4.31. From Fig. 4.31, the

#### 4. Control Strategy of Redundant Robotic Manipulator in Narrow Workspace

incremental is stable. Therefore, in order to reduce the visual part of the tool manipulator, the algorithm will consider  $\Delta_y$  to be zero.

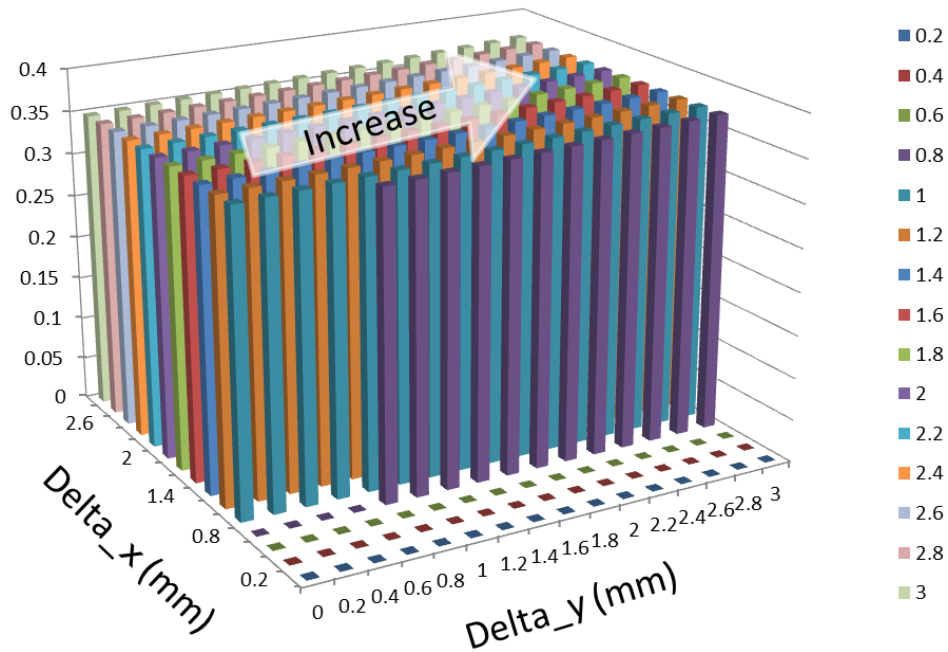


Figure 4.28 The visible ratio of tool manipulator corresponding to different  $\Delta_x$  and  $\Delta_y$  when bent angle =  $50.0^\circ$ .

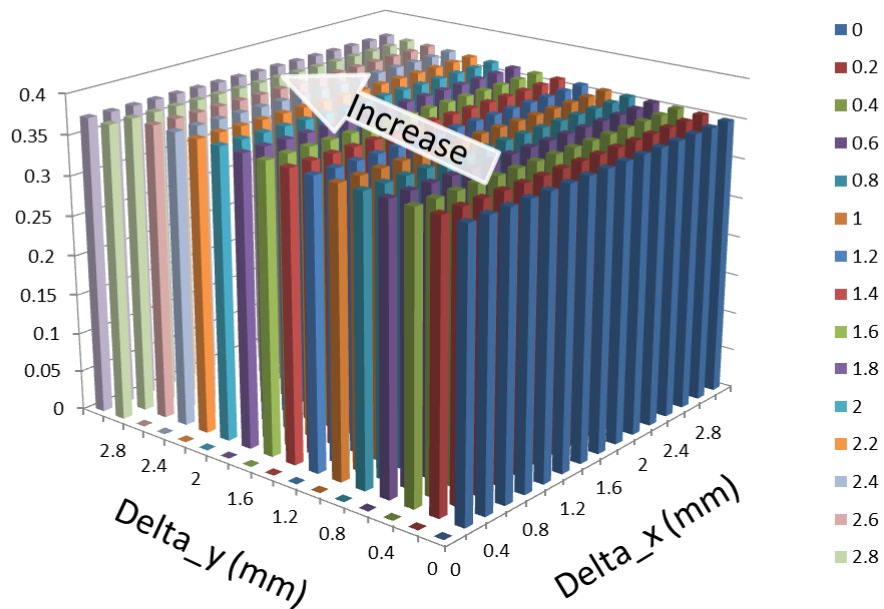


Figure 4.29 The visible ratio of tool manipulator corresponding to different  $\Delta_x$  and  $\Delta_y$  when bent angle =  $50.2^\circ$ .

#### 4. Control Strategy of Redundant Robotic Manipulator in Narrow Workspace

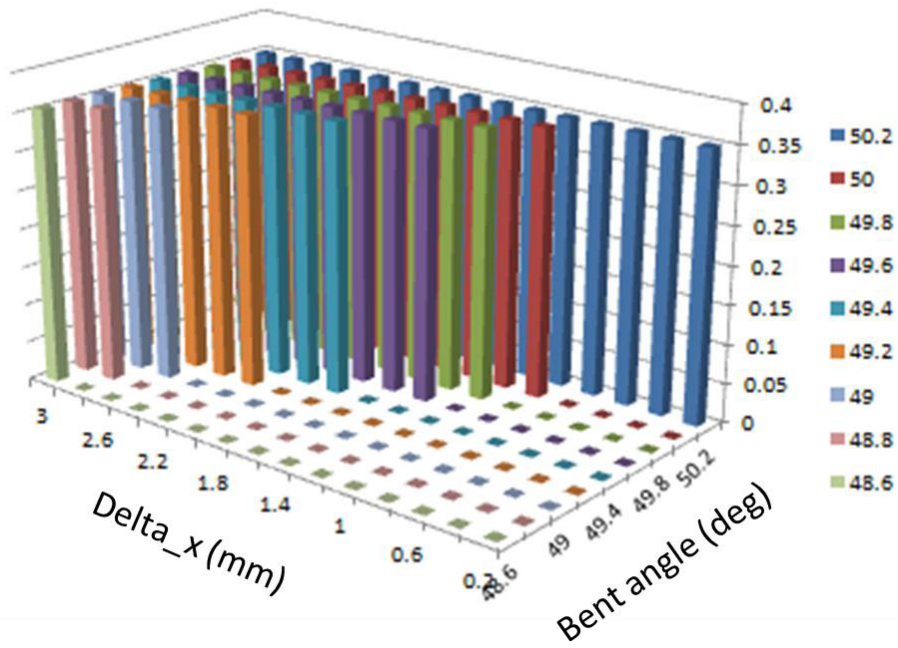


Figure 4.30 Visible ratio of the tool manipulator under collision avoidance algorithm.

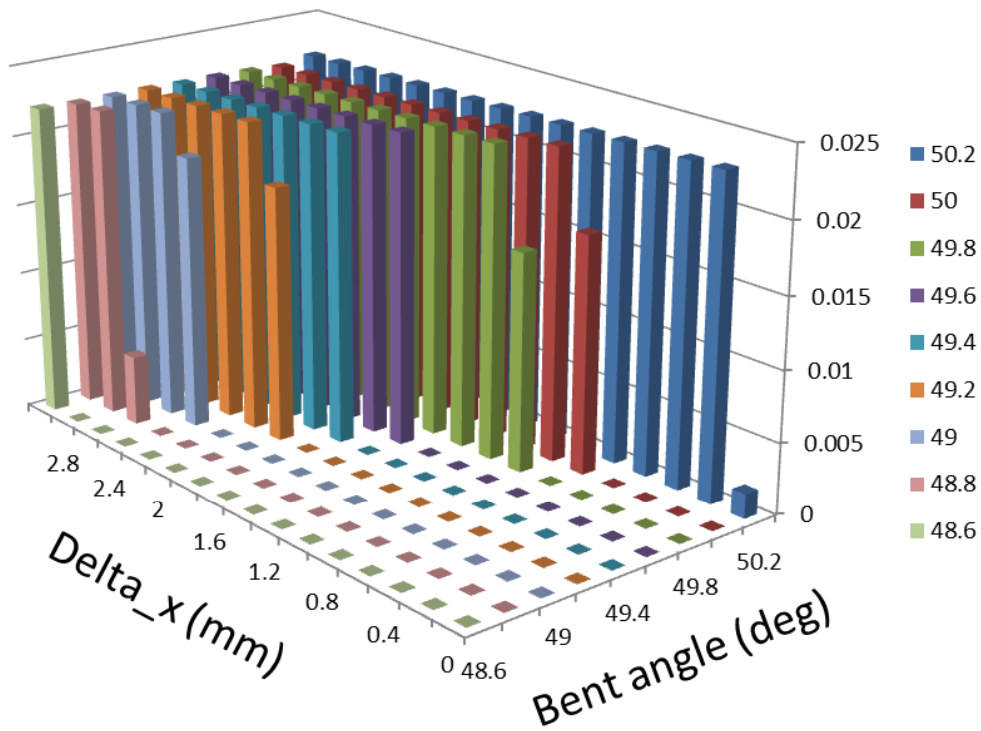


Figure 4.31 Ratio deviation caused by delta\_y corresponding to difference of delta\_x.



## 4.6 Experiments with Pediatric Surgical Robot

### 4.6.1 Accurate Control of Bendable Joints

In our surgical robot, we use “flexible shaft + universal joint” structure for achieving bendable movement. In section 3.7, the rigidity of the flexible shaft had been verified that the deformation of flexible shaft could be neglected when transfer power between motor and driven links. However, corresponding to universal joint in the structure of the bendable joint, the backlash may affect the accuracy of position control.

The experimental platform is shown in Fig. 4.32. Three position sensors (Aurora, NDI<sup>®</sup>) are used to track the movement of bendable joints.

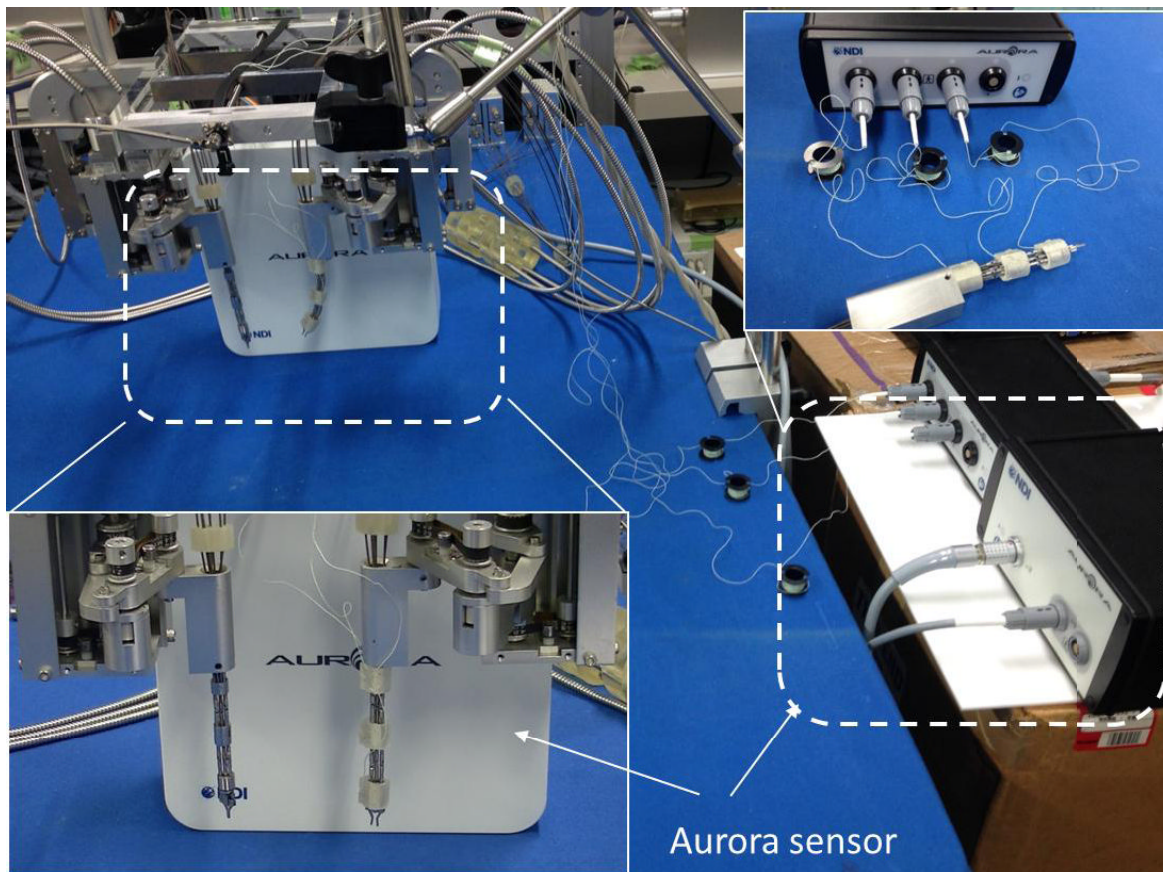


Figure 4. 32 Experimental platform for accuracy verification.

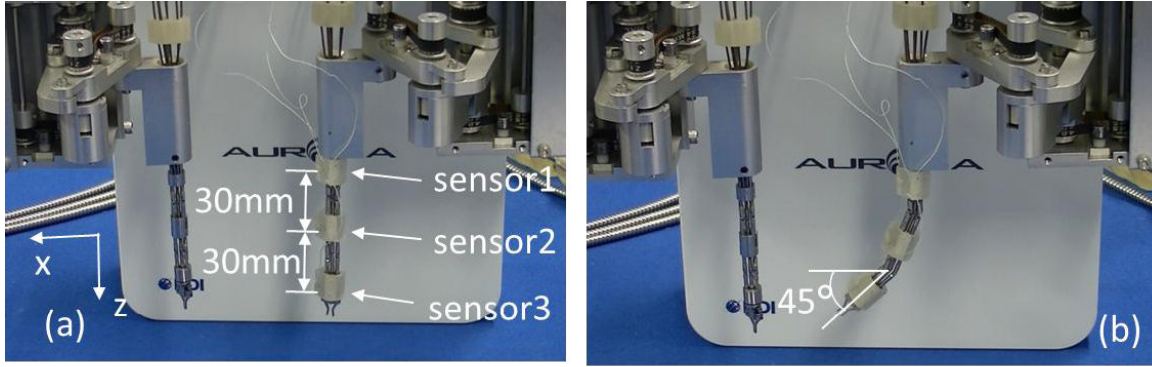


Figure 4. 33 Experiment scene of accuracy during bendable movement. (a) Nonmenclature of sensors configuration; (b) Tool manipulator when bent to 45°.

Fig. 4.33 shows the experimental sence of tool manipulator to achieve bent movement. The part that sensor 1 attached is labled as the reference base; the bent joint that sensor 2 attached is labled as 1<sup>st</sup> bent joint; the bent joint that sensor 3 attached is labled as 2<sup>nd</sup> bent joint. The distance between the adjacent sensors is 30mm. The results that no compensation of backlash in control algorithm are presented in Fig. 4.33. The result shown in Fig.4.34 illustrate that the error in the distal of the bendable joint would continually increase. The reason is that universal joints are used in the bendable joint. Therefore, the backlash in the connector of universal joint will lead to a stable deviation when tool manipulator bent to one direction. The compensation angle caused by the backlash can be computed as,

$$\theta_{com} = \frac{\widehat{L}}{d} \quad (4.51)$$

Where,  $\theta_{com}$  is the compensation angle;  $\widehat{L}$  is the arc length of the distal of the bendable joint; d is the length of bendable joint.

From Fig. 4.34, the deviation in x, z direction is 1.25 mm, 1.25 mm respectively. Therefore, substituting into (4.51), we can get the compensation angle in x, z direction is 0.08rad, 0.12 rad respectively. Thus, in the control algorithm, add the compensation angle in the joint control, the results with compensation algorithm are presented in Fig. 4.35. The experimental results demonstrate that the bendable joint can well track the instruction of controller. The result describe that the error of the distal of the tool manipulator is less than 0.5 mm, which could be used for accurate control. The compensation factor in y direction could be computed use the similar method in the above.

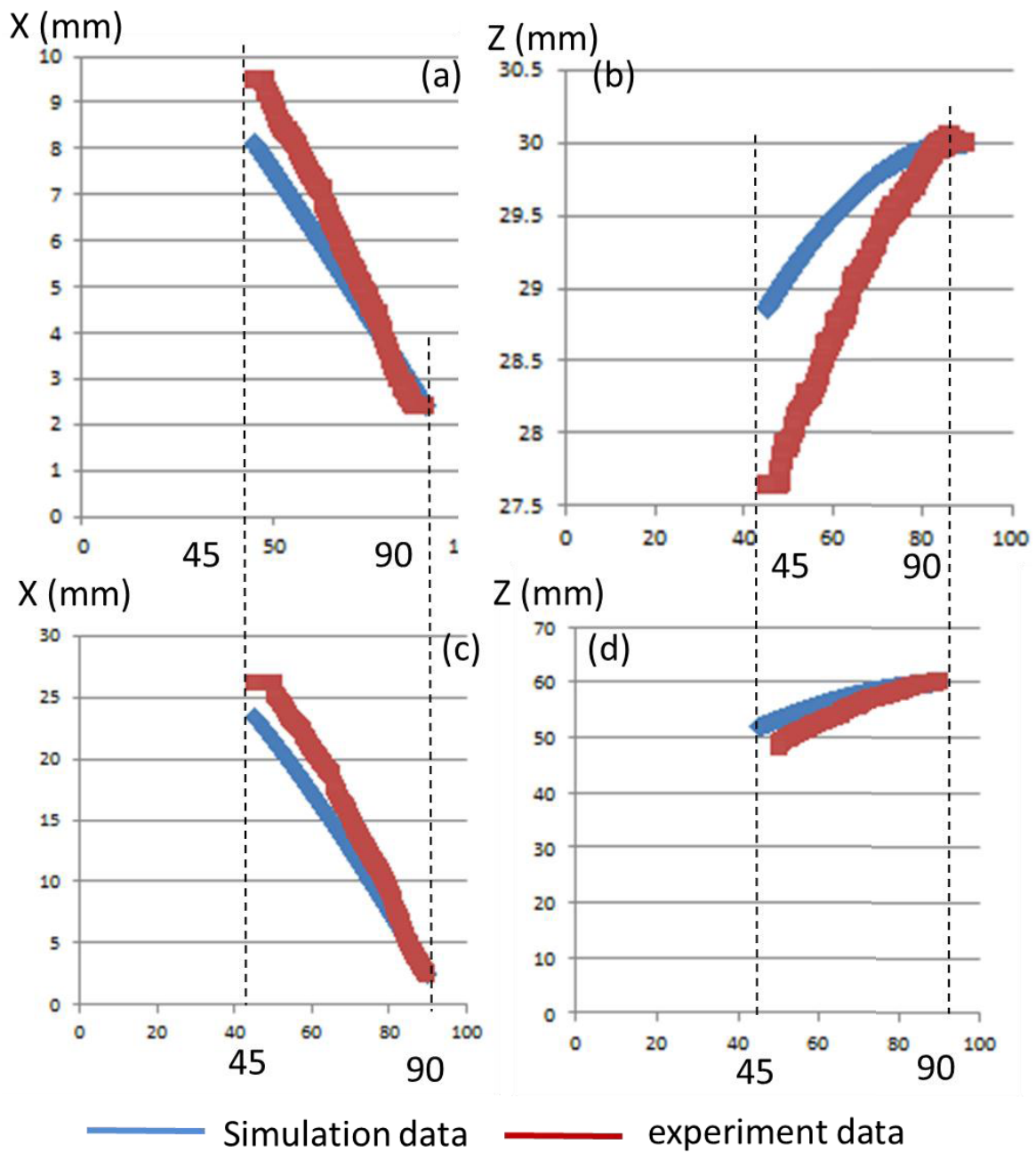


Figure 4. 34 Experimental results without compensation algorithm when the tip bent from 45° to 90°. (a) deviation of 1<sup>st</sup> bendable joint at x direction; (b) deviation of 1<sup>st</sup> bendable joint at z direction; (c) deviation of 2<sup>nd</sup> bendable joint at x direction; (d) deviation of 2<sup>nd</sup> bendable joint at z direction.

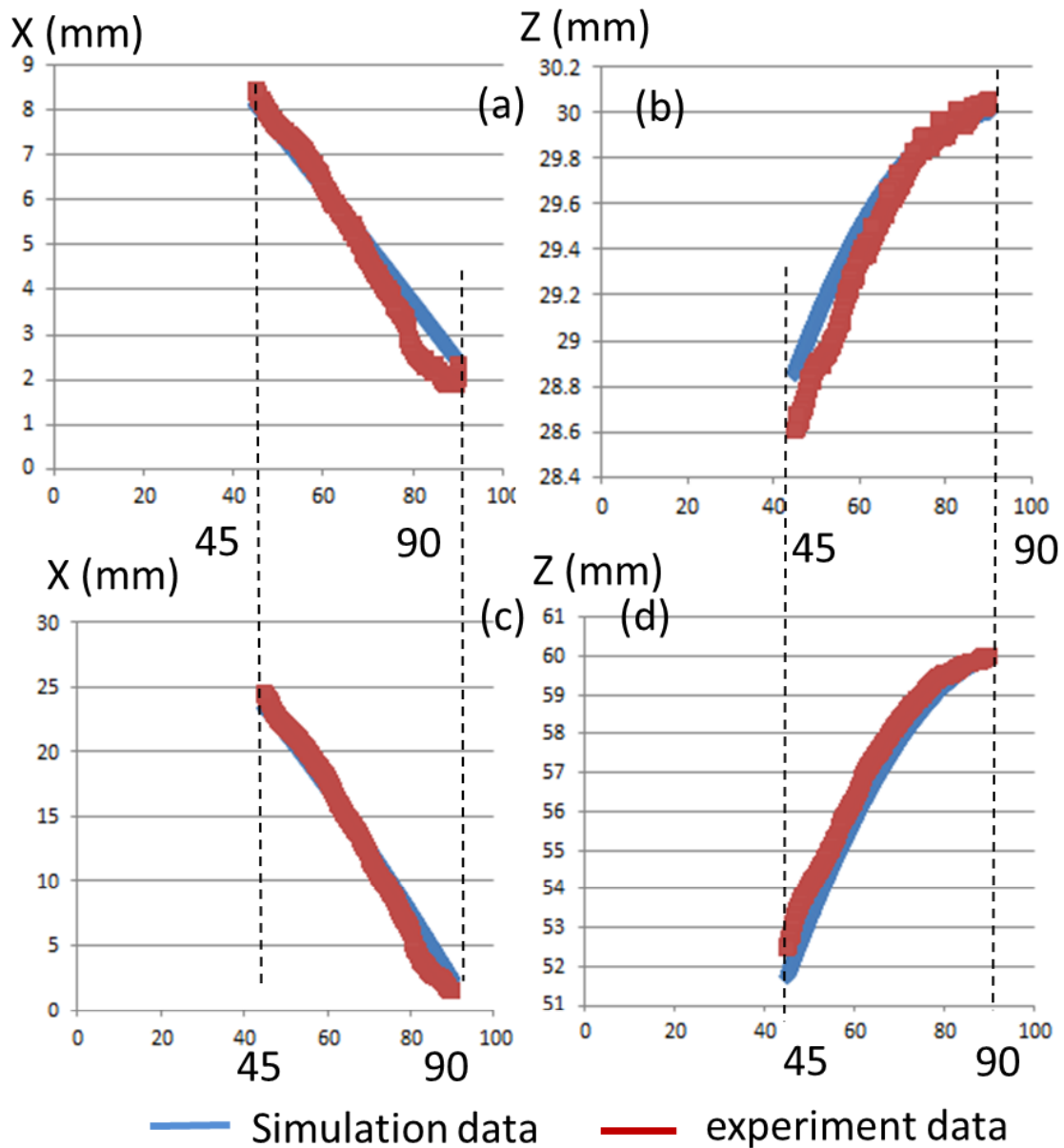


Figure 4. 35 Experimental results with compensation algorithm when the tip bent from  $45^\circ$  to  $90^\circ$ . (a) deviation of 1<sup>st</sup> bendable joint at x direction; (b) deviation of 1<sup>st</sup> bendable joint at z direction; (c) deviation of 2<sup>nd</sup> bendable joint at x direction; (d) deviation of 2<sup>nd</sup> bendable joint at z direction.

In Fig. 4.34 and Fig. 4.35, we compared the tip's accuracy without/with backlash at bent motion. Generally, surgical manipulator would transfer tissue or hold needle for tissue intervention. In order to illustrate the manipulator's performance, we hang a weight at the

distal of the manipulator and drive the tip bent to  $45^\circ$  in xoz plane and bent  $30^\circ$ , rotary  $30^\circ$  in 3D space. The experiment setup is shown in Fig. 4.36.

We attached weights (0g, 10g, 20g, 50g, 100g) at the gripper of the manipulator, respectively. The position trace of the bendable joint will be record by the Aurora sensor (NDI Cor.,). Fig. 4.37 and Fig. 4.38 show the result of position tracking of manipulator's distal in xoz plane. Corresponding to the 30x30x30 mm workspace, the maximum bent angle of the tool manipulator is  $30^\circ$ , therefore, an experiment that the distal of the manipulator's distal bent in xoz plane while synchronized rotated along z axis was carried out. Fig. 4.39 and Fig. 4.40 show the result of position tracking of manipulator's distal in 3D space.

##### 1) Experiment result

The experiment results in Fig. 4.37 and Fig. 4.38 show the tool manipulator could well track the input instruct in 2D plane when load is less than 50 g in the distal (the position error  $\Delta_{position\_error} < 1mm$ ). However, the distal error is up to 2 mm when the distal weight increses to 100 g.

The experiment results in Fig. 4.39 and Fig. 4.40 demonstrate the robot performance while operated in 3D space with load. The tool manipulator can achieve high precision (error is less than 1 mm) when the load in the distal is less than 50 g. When the load weight increase to 100 g, the position error of the distal of the manipulator exceed 2 mm. Fig. 4.40 shows the tip bring the main error is produced in the rotary movement when the load attached at the tip of the manipulator.

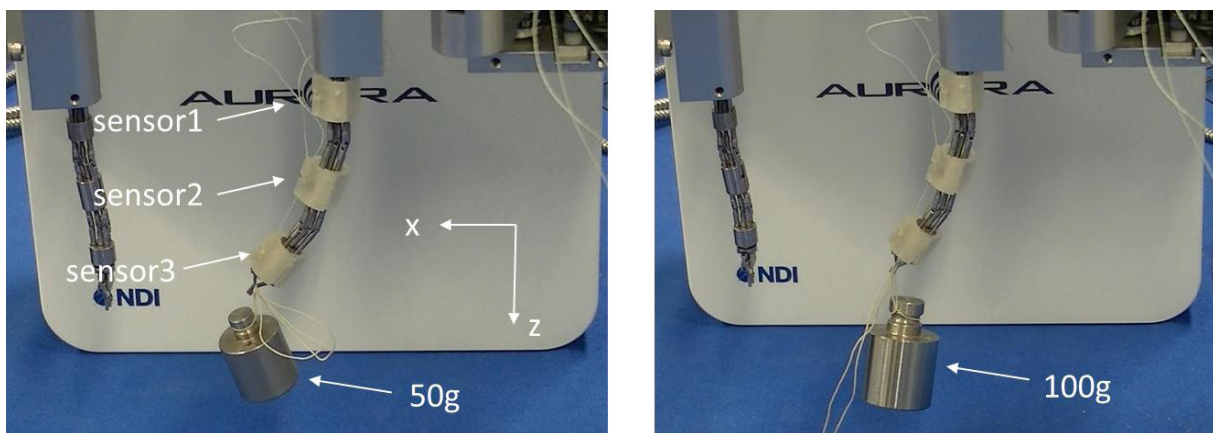


Figure 4. 36 Experiment setup of bent motion with load.

#### 4. Control Strategy of Redundant Robotic Manipulator in Narrow Workspace

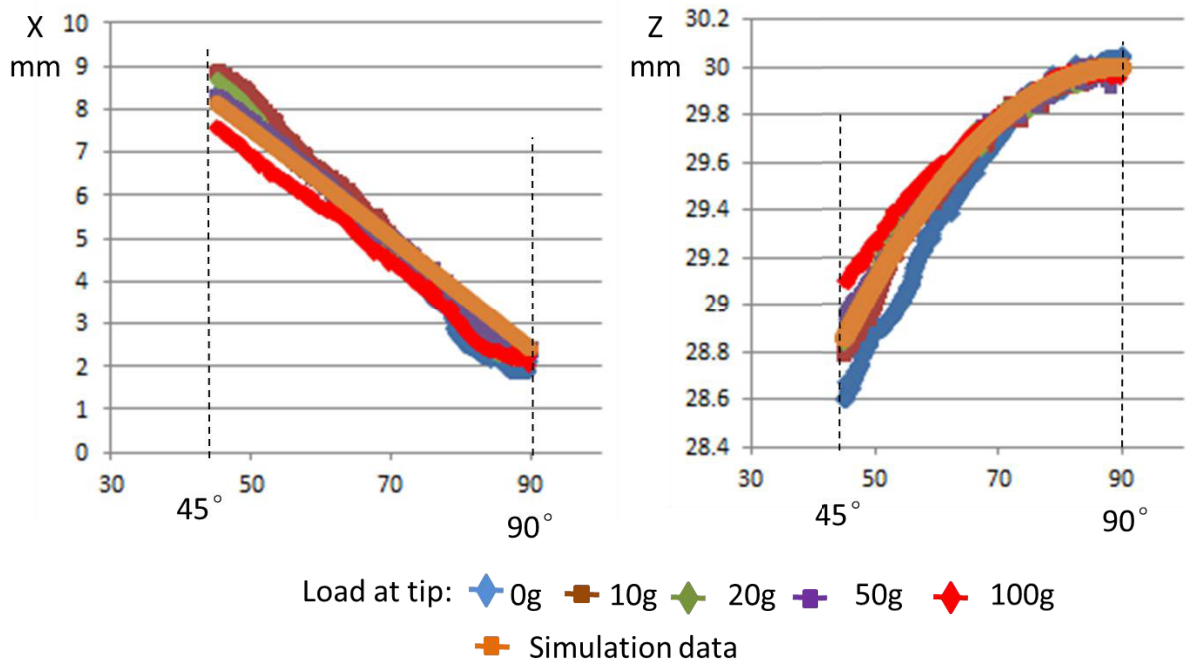


Figure 4.37 Position tracking of sensor 2 at the 1<sup>st</sup> bendable joint in xoz plane.

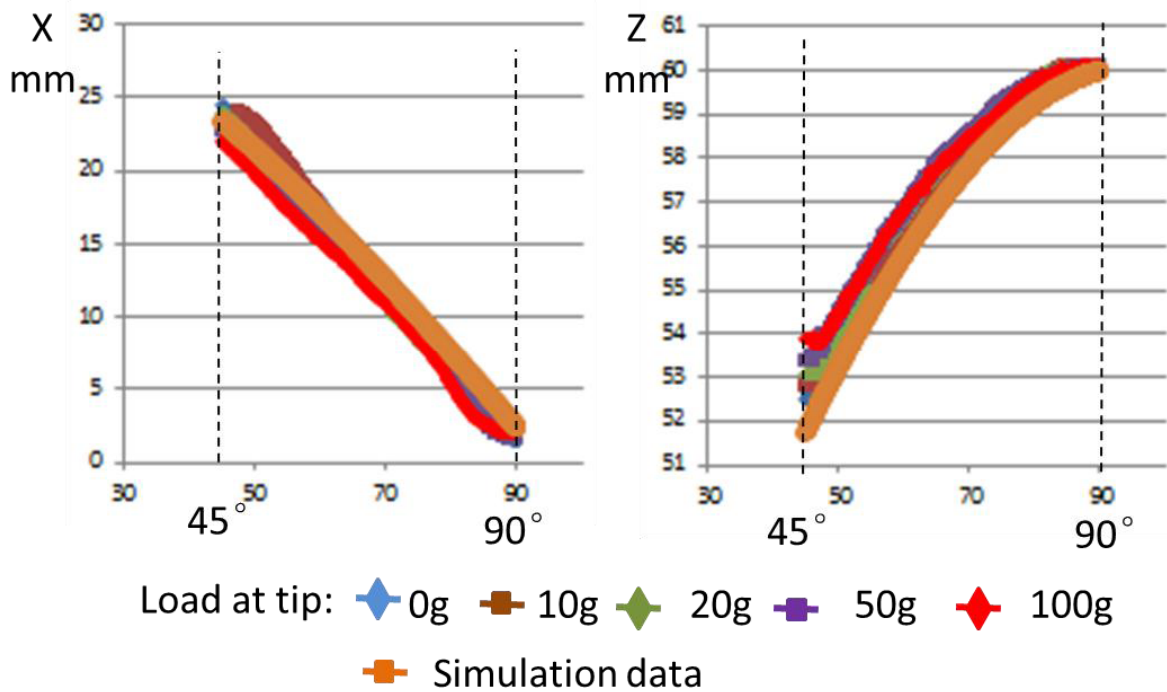


Figure 4.38 Position tracking of sensor 3 at the 2<sup>nd</sup> bendable joint in xoz plane.

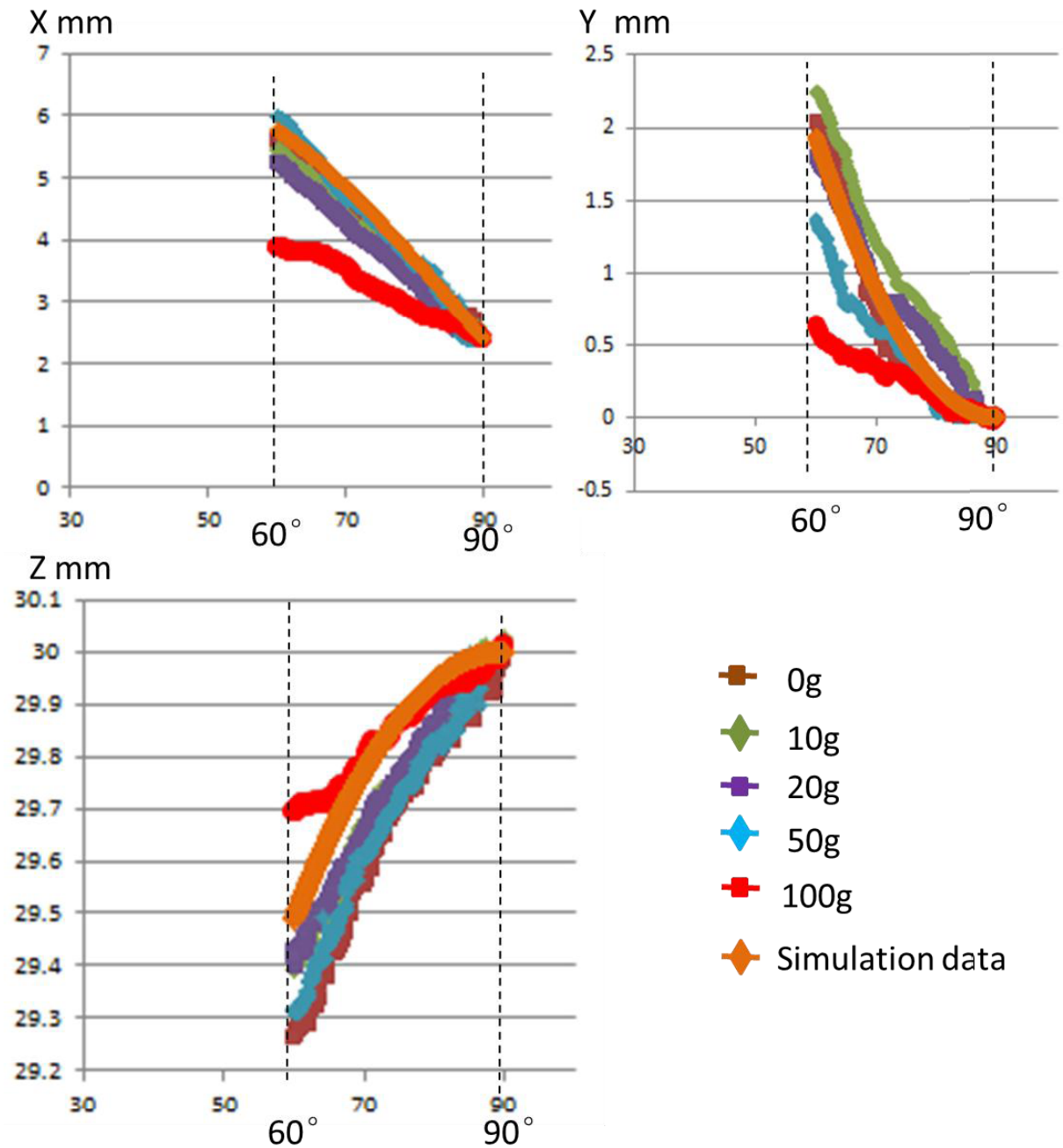


Figure 4. 39 Position tracking of sensor 2 at the 1<sup>st</sup> bendable joint when the manipulator's tip bent 30° and rotated 30° simultaneously in 3D space.

#### 4. Control Strategy of Redundant Robotic Manipulator in Narrow Workspace

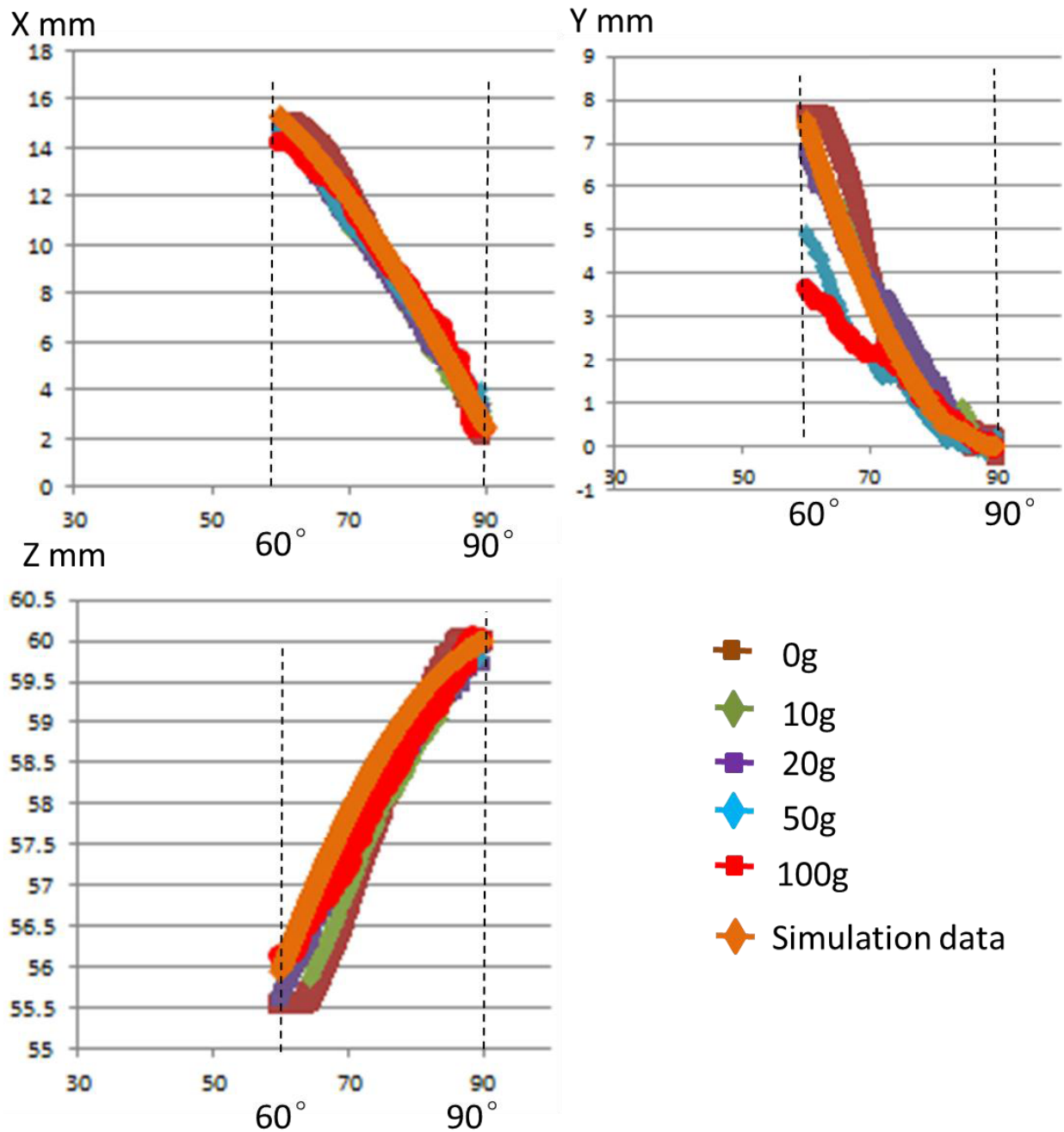


Figure 4. 40 Position tracking of sensor 3 at the 2<sup>nd</sup> bendable joint when the manipulator's tip bent 30° and rotated 30° simultaneously in 3D space.



##### 2) Discussion

Compared the results in Fig. 4.37 to Fig. 4.40, the distal of the manipulator can well track the input even attached 100 g at the tip in xoz plane. When the movement expand to 3D space, the manipulator can follow the input command while the distal load is less than 50 g.

From the experiment results, the main position error is produced when the manipulator carried out a conjunction movement. The reasons are listed the followings:

a) As shown the mechanism structure of the manipulator in Fig. 3.7, the rod's length will stretch or shrink simultaneously when carried bent motion in xoz plane, the load in the distal act as pretension force on universal joint, therefore, the backlash of the universal joint could keep stable during bending movement. The distal of the manipulator can achieve high precision under backlash compensation. However, when the manipulator carried out rotary movement along z axis, the lateral backlash cannot directly compensated by vertical force from weight load, thus, the distal of manipulator get the main position error along y axis.

b) When the rods in the bendable joint stretch or shrink simultaneously, the screws in the single bendable segment synchronously pull or push the nut for bent motion. Therefore, the meshing forces between the screw and the nut in the two bendable linkages are also in the same direction. However, when the manipulator carried out a rotary movement along z-axis, the dual bendable linkages marched on the opposite direction, which increase the burden of driving force on the flexible shaft. Referred in chapter 3, when the load is within 2N, flexible shaft can achieve good rigidity and could be treated as rigid part. However, if the load becomes heavier, flexible shaft will create deformation that leads to position precision loss.

In our surgical assist system, we propose to perform tissue intervention for esophageal repair for pediatric patient. As the diameter of the pediatric esophagus is about 5 mm, therefore, a 8 stitches intervention in the esophageal circumference will be performed, and the suture precision should be under 1 mm along esophageal circumference. We simplify the manipulator just hold needle for 3D motion planning in 30x30x30 mm workspace, thus, the load on the manipulator is within 0.2 N. According to the above analysis, the manipulator can achieve accurate control ( $\Delta_{position\_error} < 1mm$ ) in 3D workspace on operation. Therefore, the pediatric surgical robot satisfies the precision requirement of tissue intervention in pediatric CEA surgery.

### 4.6.2 Trajectory Control in Narrow Workspace

In the narrow workspace surgery, such as the infant congenital esophageal atresia surgery, the workspace for manipulation is about 30x30x30 mm. Therefore, it is a challenge for surgeon to perform tissue intervention. Our motivation is to develop a surgical robot to assist surgical manipulation.

Since the narrow workspace and the slim manipulator, thus, it is difficult to attach sensor in the distal of the tool manipulator. In this section, we carried out the experiment to illustrate the trajectory planning considering the boundary of surgical cavity. The motivation of this experiment is to verify the manipulator's performance working in narrow workspace. The experimental illustration is shown Fig. 4.41. The experimental platform is shown in Fig.4.42.

In this experiment, the process consisted of three stages.

In the first stage, the right arm of the surgical robot move 20 mm along x-axis to the top of the surgical cavity. Only the positioning manipulator would be actuated in the horizon plane. The tool manipulator would keep in its straight posture.

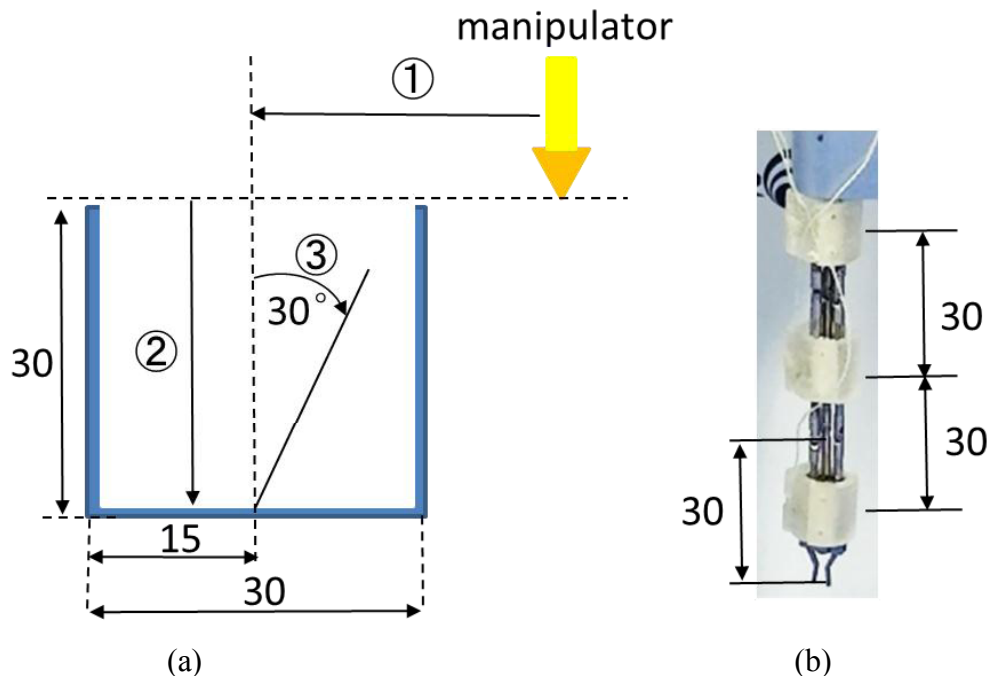


Figure 4. 41 Illustration of experiment 2. (a) steps of control manipulator; (b) geometrical dimension of manipulator.

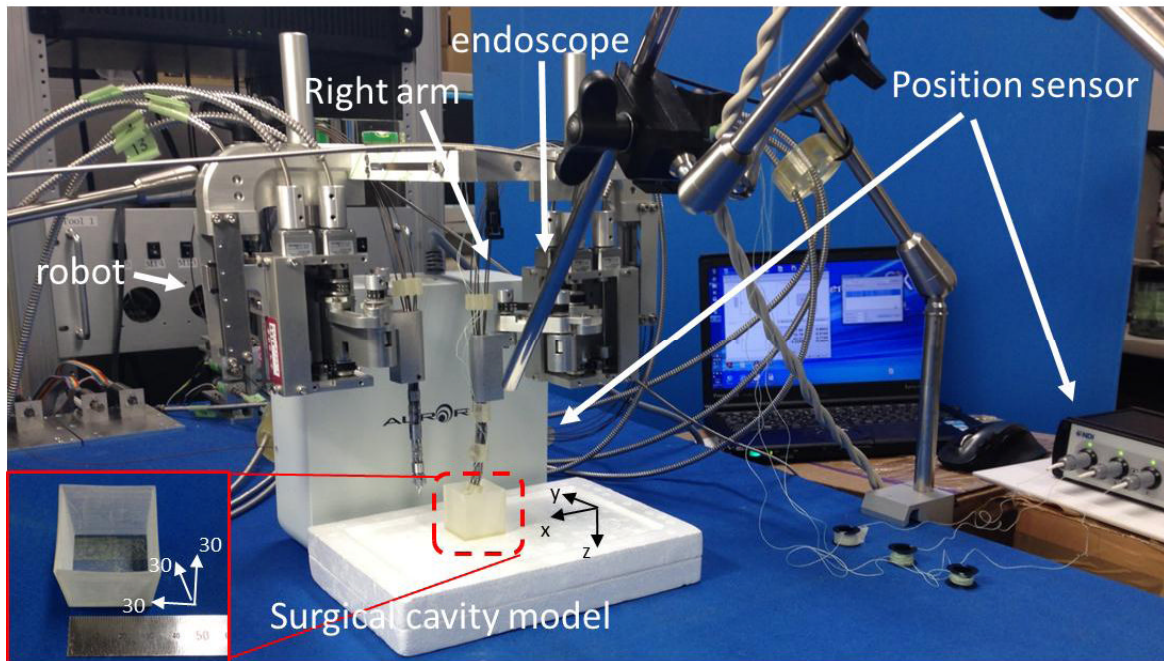


Figure 4.42 Experimental platform for robot trajectory planning.

In the second stage, the distal of the tool manipulator would be driven 20 mm along z-axis to inserted into the surgical cavity. Since the narrow space in the manipulation, therefore, only the last segment of the manipulator would be inserted into the surgical cavity model.

In the third stage, we simulated typical manipulation for surgical intervention. The ideal formation between the endoscope and the dual arms should comply triangle formation to achieve good visualization. Generally, the dual slave arms will mainly charge for its own half surgical zone. Because the length of the distal segment of the tool manipulator is 30mm, therefore, the bent angle of the distal segment is less than 30 degree. We instruct the distal of the tool manipulator would bent from 0 degree to 30 degree while the distal fixed. Since the narrow workspace, therefore, the collision between the surgical tool manipulator and the surgical cavity had been considered for safe operation.

The manipulation sences are shown in Fig. 4.43.

Corresponding to the three control stages, the angle of each joint can be calculated based on the algorithm referred in section 4.4 and section 4.5. We attached three sensors (Aurora, NDI Cor.,) to track the positions of the base, the middle link, the distal of the tool manipulator. Fig. 4.44 to Fig. 4.46 show the results in these sensors.

#### 4. Control Strategy of Redundant Robotic Manipulator in Narrow Workspace

---

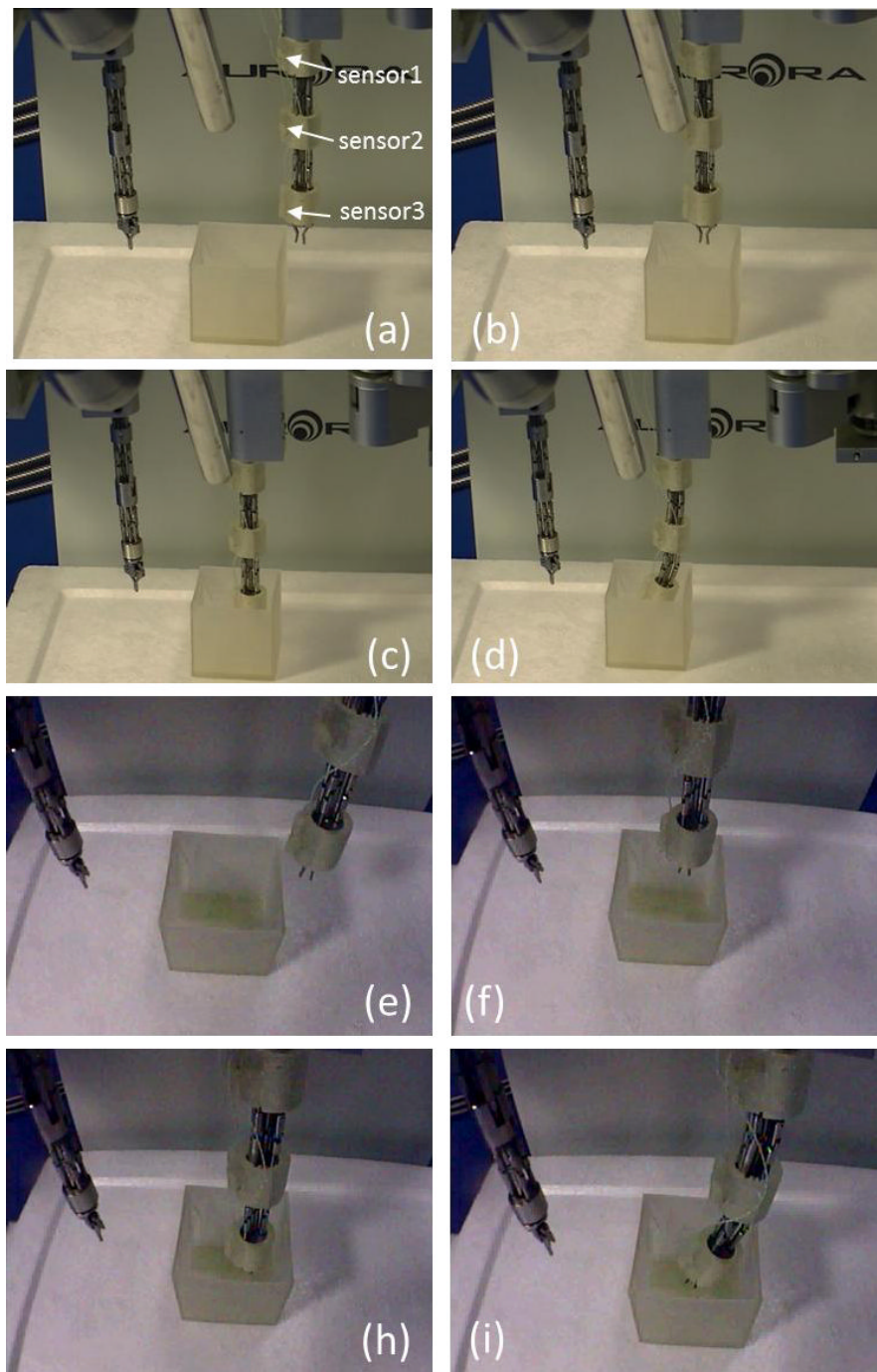


Figure 4. 43 Manipulation sence when the right arm actuated. (a) initial state; (b) move to the top of surgical cavity in the 1<sup>st</sup> stage; (c) move into surgical cavity in the 2<sup>nd</sup> stage; (d) trajectory planning in the 3<sup>rd</sup> stage; (e)~(i) endoscopic images corresponding the stages shown in (a)~(d).

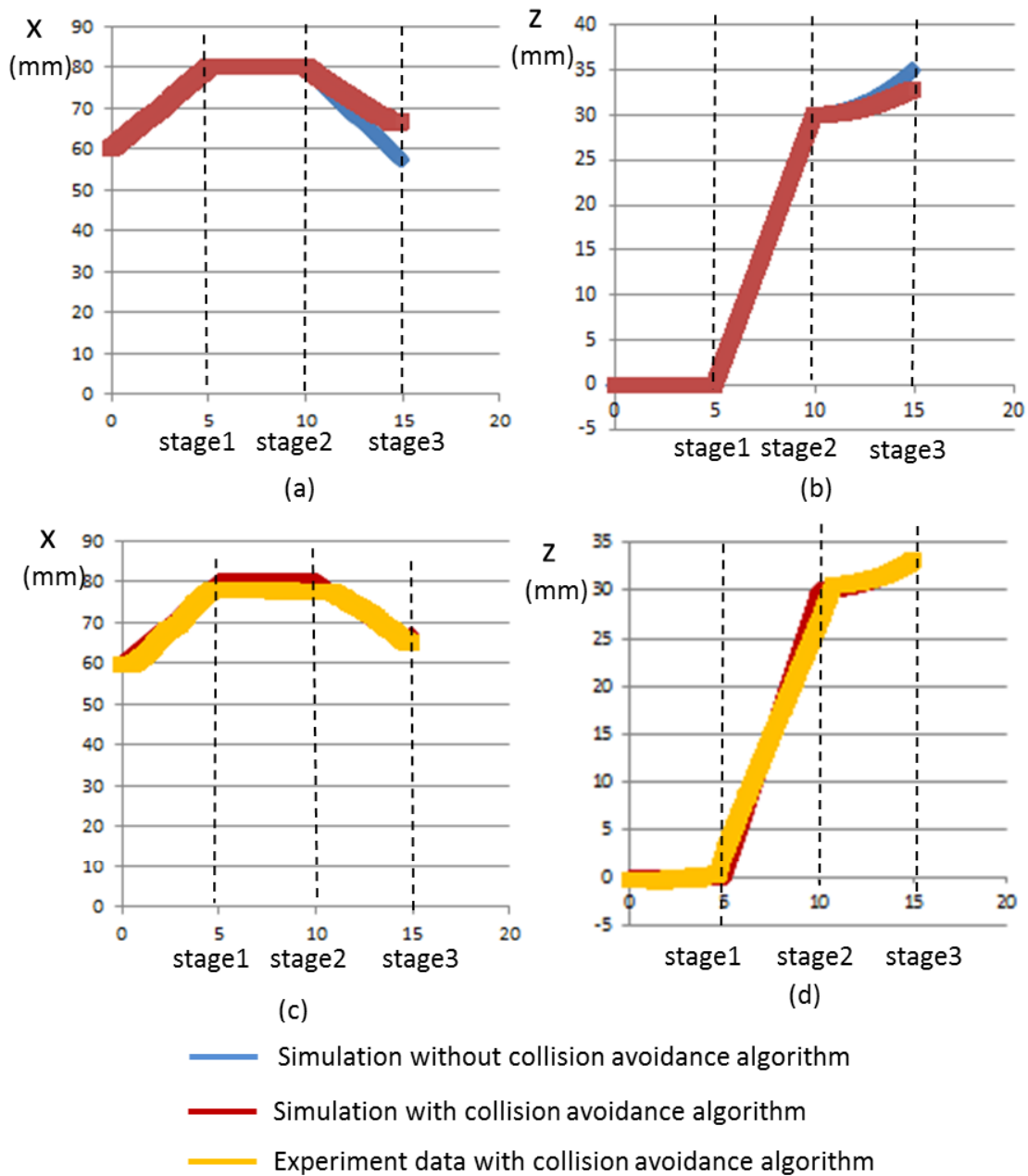


Figure 4.44 Simulation and experimental data in sensor 1. (a) simulation data with/without collision avoidance algorithm in x-axis; (b) simulation data with/without collision avoidance algorithm in z-axis; (c) comparison between simulation and experimental data in x-axis; (d) comparison between simulation and experimental data in z-axis.

#### 4. Control Strategy of Redundant Robotic Manipulator in Narrow Workspace

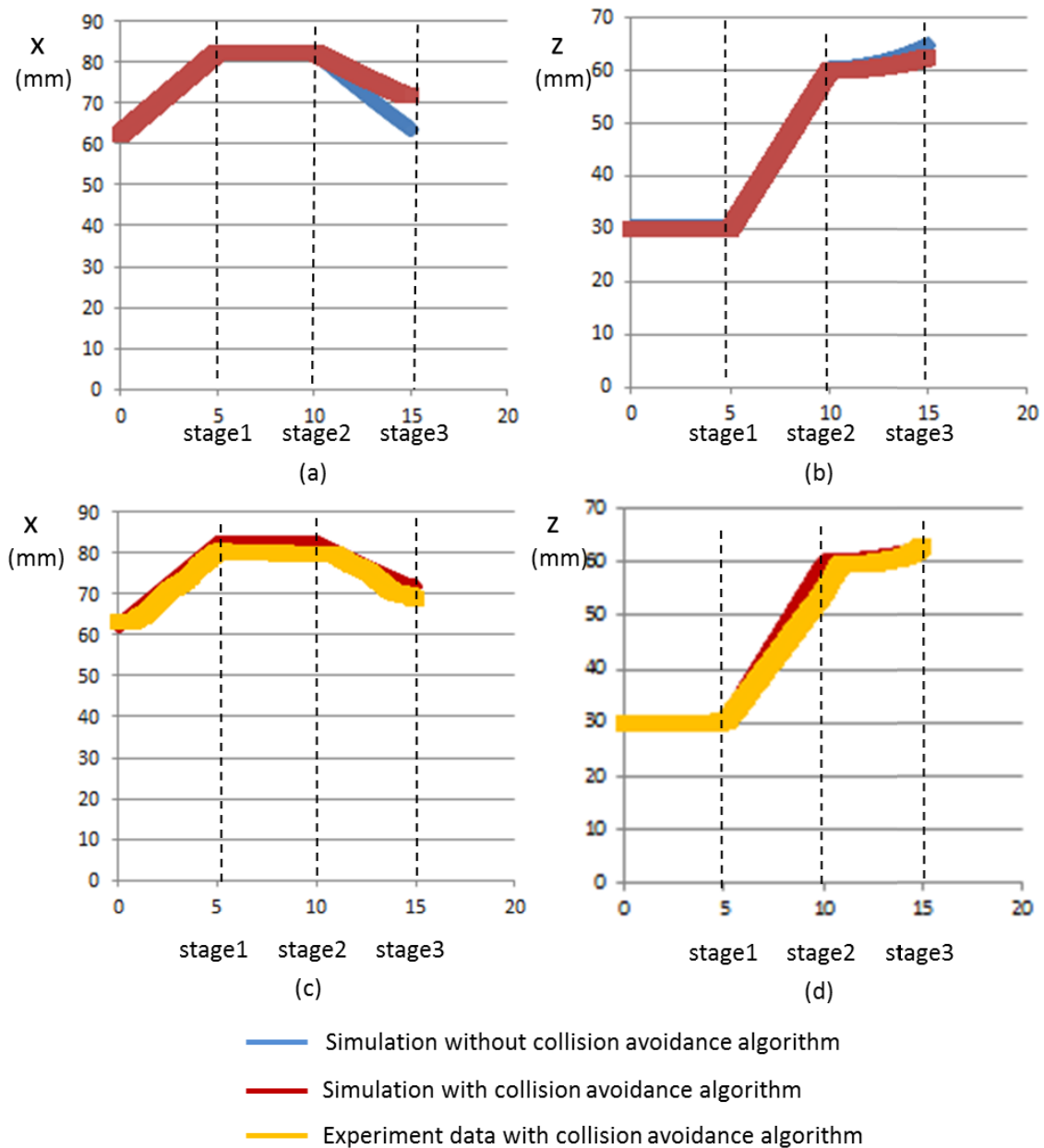


Figure 4.45 Simulation and experimental data in sensor 2. (a) simulation data with/without collision avoidance algorithm in x-axis; (b) simulation data with/without collision avoidance algorithm in z-axis; (c) comparison between simulation and experimental data in x-axis; (d) comparison between simulation and experimental data in z-axis.

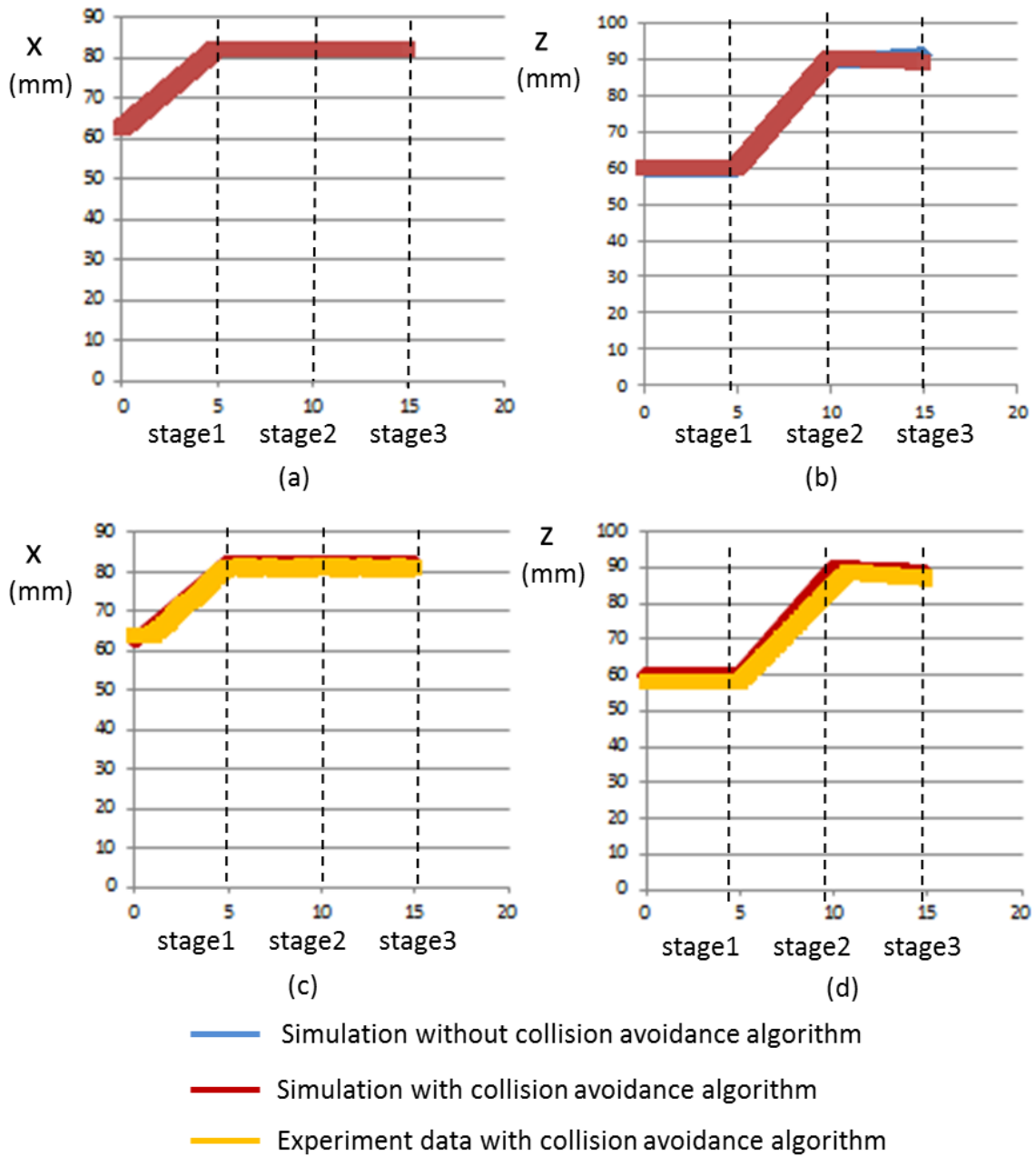


Figure 4. 46 Simulation and experimental data in sensor 3. (a) simulation data with/without collision avoidance algorithm in x-axis; (b) simulation data with/without collision avoidance algorithm in z-axis; (c) comparison between simulation and experimental data in x-axis; (d) comparison between simulation and experimental data in z-axis.

#### 4. Control Strategy of Redundant Robotic Manipulator in Narrow Workspace

---

In our robot system, we use shape optimal algorithm to plan the bent shape of redundant slave manipulator. Since, the core principle of the algorithm is to drive the redundant manipulator convex polygon; therefore, the vision of manipulation zone could be advanced guaranteed.

According to the collision algorithm, the tool manipulator will closest to the boundary of the surgical cavity. From the comparison between simulation and experiment data in Fig. 4.39~4.41, the surgical manipulator could well track the instructions in the control algorithm. Thus, the distance between the surgical manipulator and the boundary of the surgical cavity can be directly calculated by simulation data, the relation between tip's bent angle and the distance between tool manipulator and the surgical cavity is shown in Fig. 4.47. The result illustrate that the tool manipulator would closet to the boundary of surgical cavity even when the redundant manipulator bent to a larger angle.

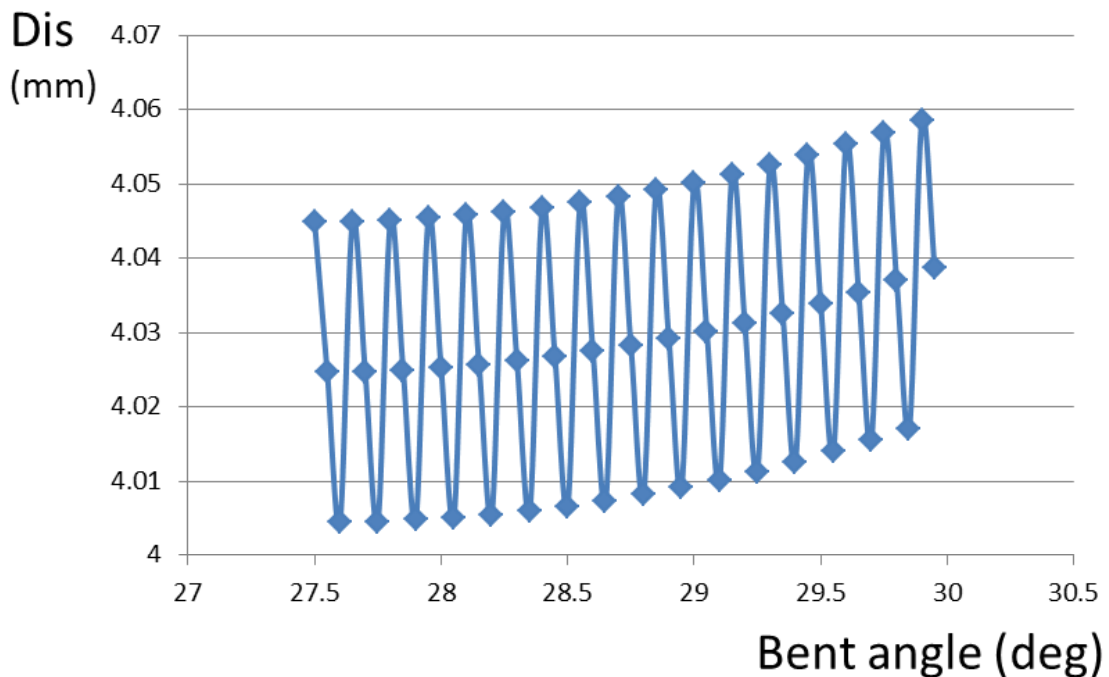


Figure 4. 47 Relation between tip's bent angle and the distance that tool manipulator to the surgical cavity.



### 4.6.3 Manipulation without/with Redundant DoF Control Algorithm

In this section, we perform ring transfer task with/without redundant DoF of the surgical robot. The experimental platform is shown in Fig. 4.48.

Since a single surgical arm consists of a positioning manipulator (4 DoFs) and a tool manipulator (5 DoFs), therefore, it cannot directly control all the joints by a Phantom Omni (6 DoFs). In this experiment, we fixed the 1st bendable joint and set the initial angle of SCARA mechanism in the positioning, thus, the number of a single manipulator's DoF reduces to six. The manipulation scenes are shown in Fig. 4.49.

Since the 1<sup>st</sup> bendable joint is fixed at its straight state, therefore, when the left surgical arm transfer the ring from the proximate pin (pin1 and pin2) to the distal pin (pin3 and pin4), the stem of manipulator will block endoscopic view that navigating user operation. Futhermore, limited by link length of the single bent joint, the SCARA mechanism was driven to move into the endoscopic view, shown in Fig. 4.49(c), which leads to a worse visual feedback.

In order to overcome this drawback, we developed shape optimal algorithm to control

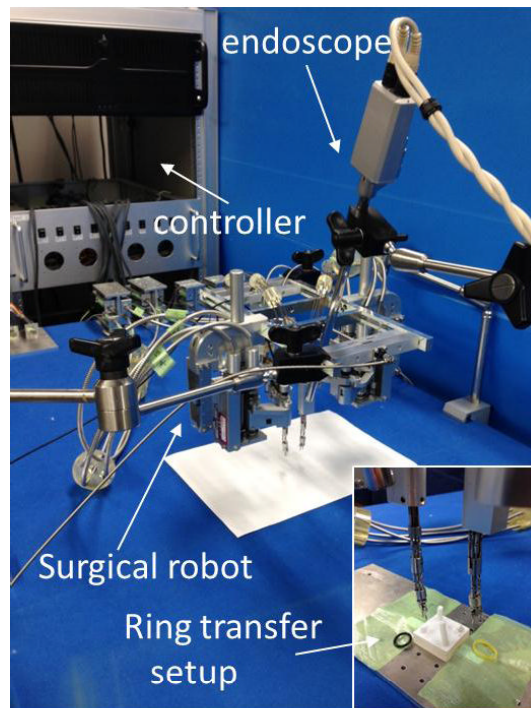


Figure 4. 48 Experimental platform for ring transfer.

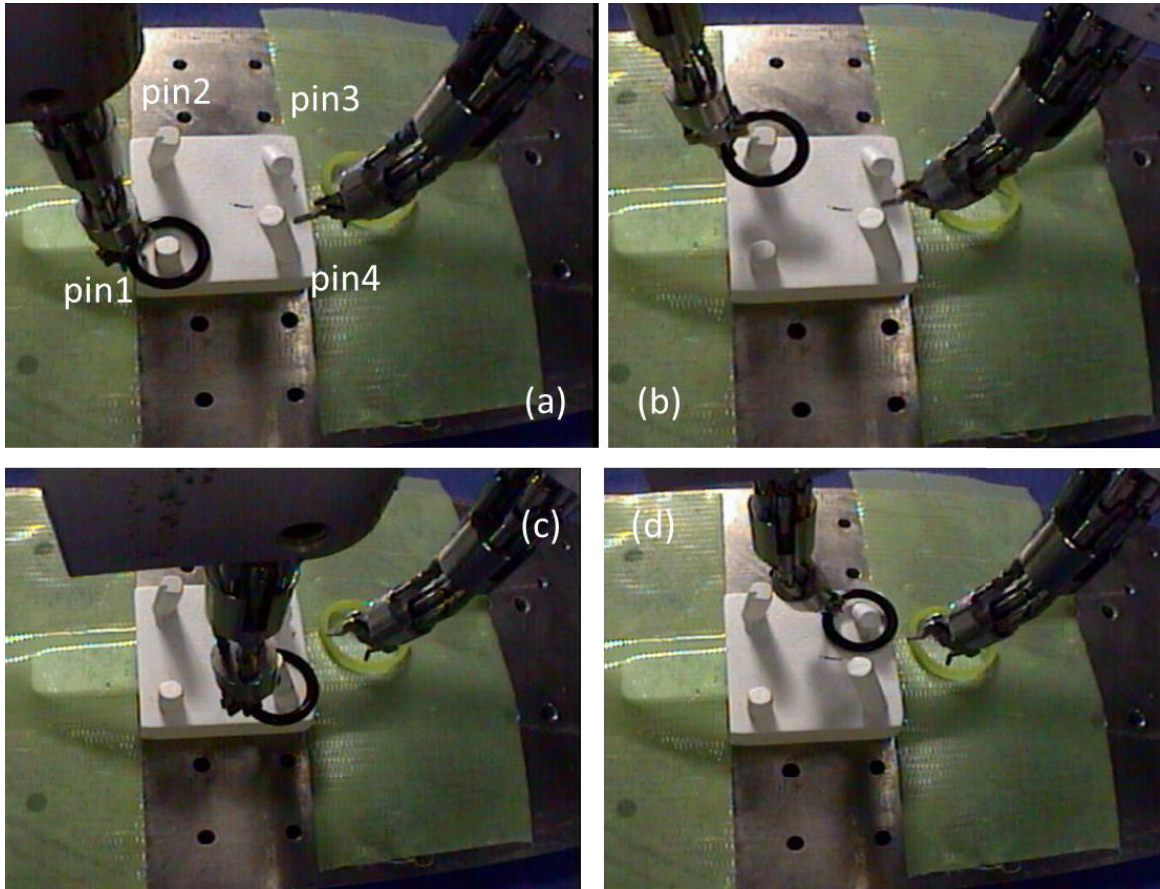


Figure 4.49 Ring transfer task by left surgical manipulator. (a) manipulation at position pin1; (b) manipulation at pin2; (c) manipulation at pin3; (d) manipulation at pin4.

surgical manipulator, the purpose is to maximum the visual feedback for operator. The algorithm is referred in section 4.5.2. The example manipulations are shown in Fig. 4.45.

Fig. 4.50 (a)~(d) show the manipulation scene of surgical robot for transferring a ring between four pins. Fig. 4.50 (e)~(h) show the endoscopic image corresponding to the transfer task in Fig. 4.50 (a)~(d). Fig. 4.51 (a)~(e) are image of ring transfer task by right manipulator; and Fig. 4.47 show the image of ring transfer between two surgical manipulator.

Compared Fig. 4.50 (e)~(h) with Fig. 4.49 (a)~(d), the manipulation without optimal shape algorithm is difficult to drive manipulator avoid blocking endoscopic view (Fig.4.49(c~d)), however, based on the algorithm, operator can achieve good visual feedback

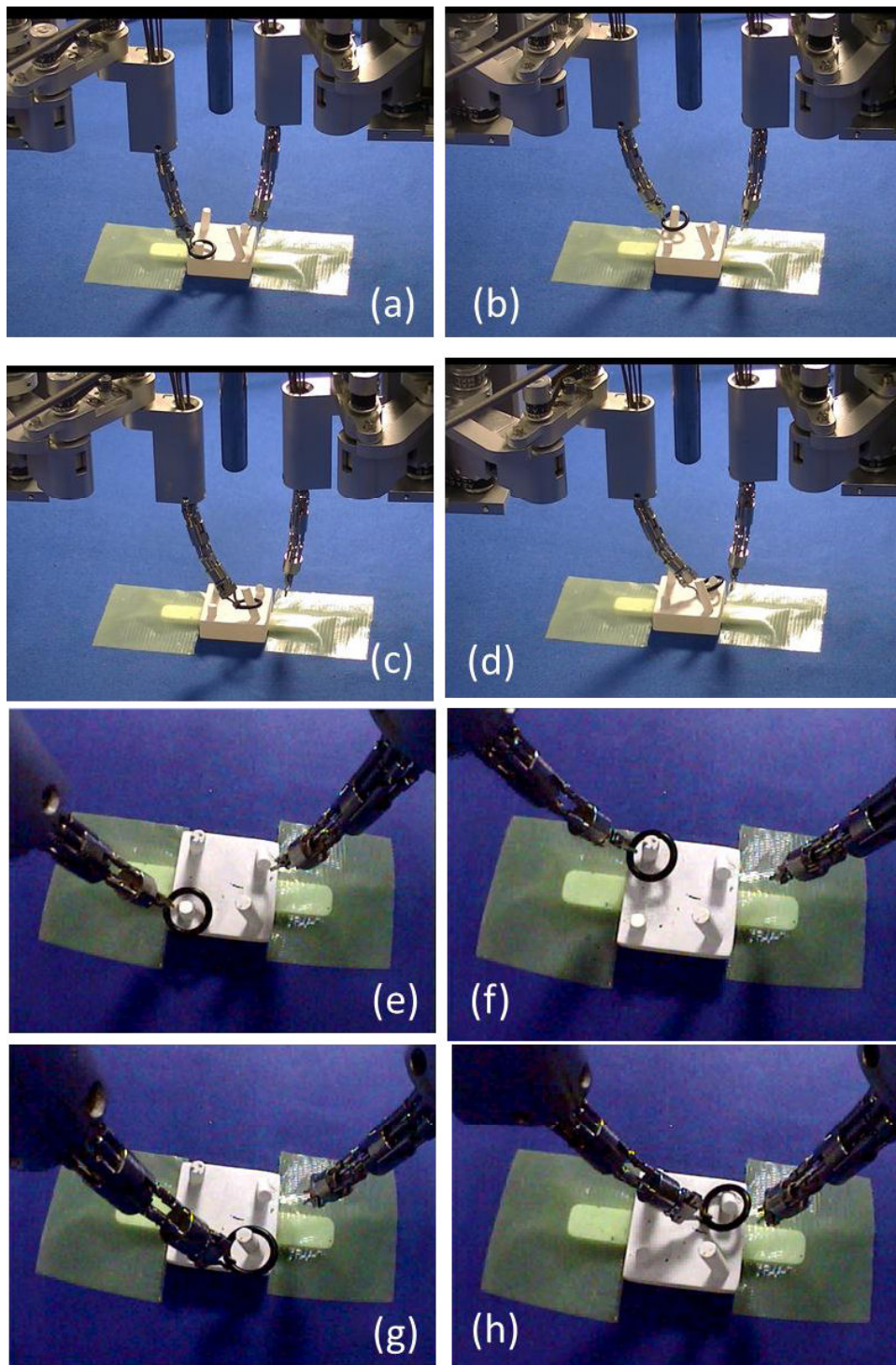


Figure 4. 50 Manipulation scenes with surgical robot for ring transfer task by left surgical manipulator. (a)~(d) ring transfer task between four nails; (e)~(h) endoscopic images corresponding to (a)~(d), respectively.

#### 4. Control Strategy of Redundant Robotic Manipulator in Narrow Workspace

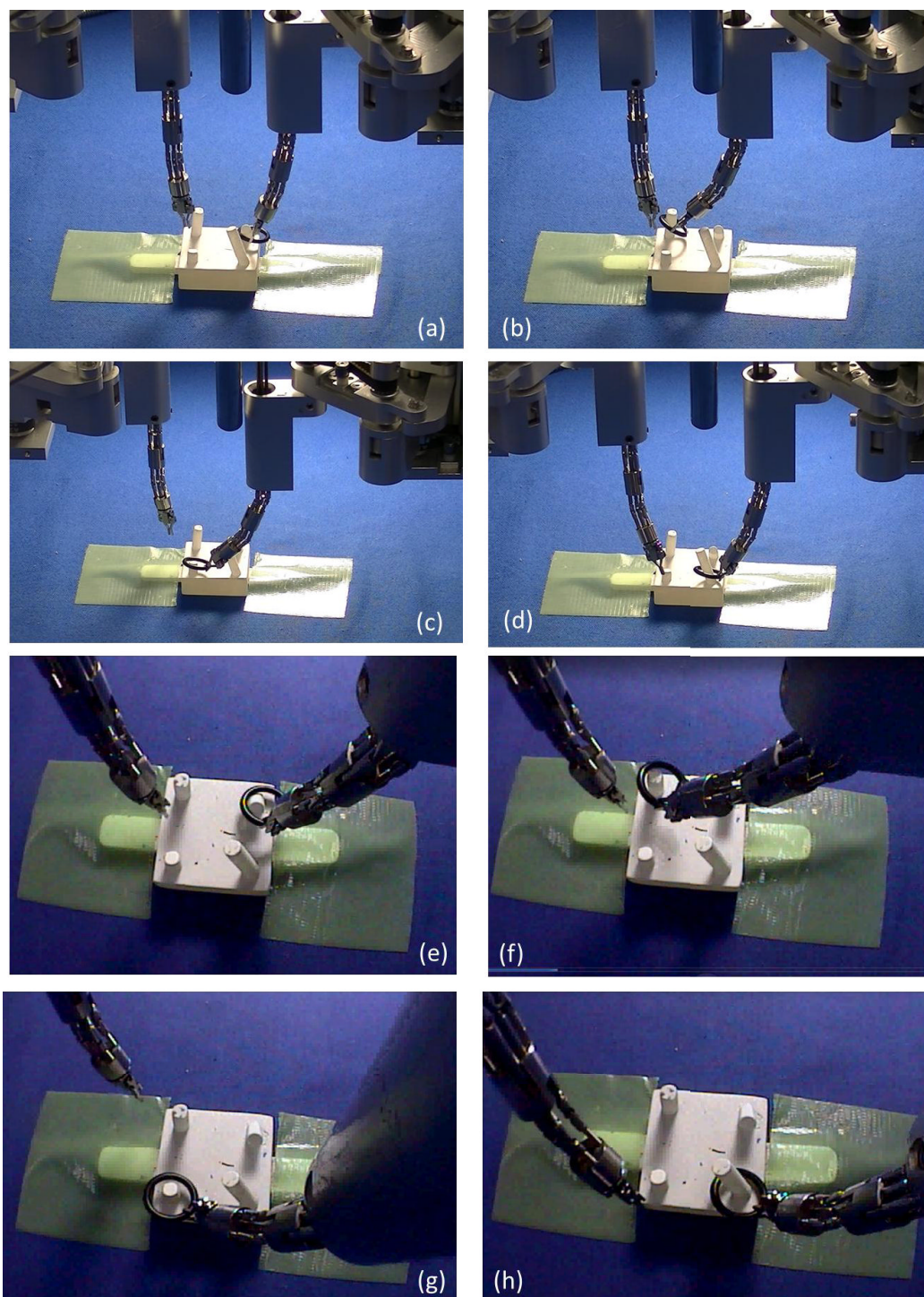


Figure 4. 51 Manipulation scenes with surgical robot for ring transfer task by right surgical manipulator. (a)~(d) ring transfer task between four nails; (e)~(h) endoscopic images corresponding to (a)~(d), respectively.

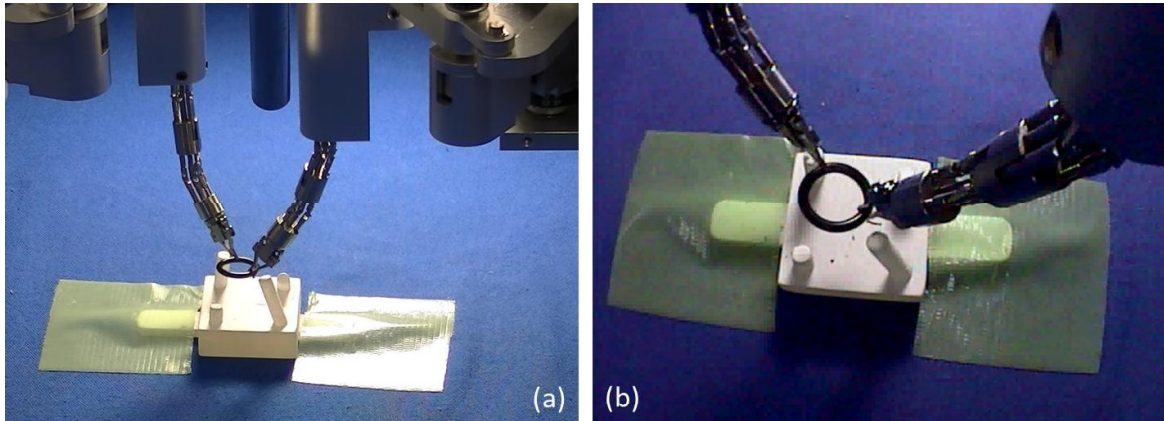


Figure 4. 52 Manipulation scenes with surgical robot for ring transfer task between both hands. (a) Image from external camera; (b) Endoscopic images corresponding to (a).

from endoscope even manipulate ring transfer task in the proximal side of the endoscope (Fig.4.50 (g~h)). Furthermore, according to the optimal shape algorithm, the surgical manipulators and the endoscope could keep ideal triangle formation. Therefore, it reduces the manipulation difficulty to user on operation. The optimal algorithm also benefits the manipulation by right surgical manipulator, shown in Fig. 4.51, and cooperate work by both manipulators, shown in Fig. 4.52.

## 4.7 Discussion

In this chapter, the author presented a control strategy for redundant manipulator. The control strategy consists of clarification of inverse kinematics, shape optimal planning, and constraints consideration. Three experiments were illustrated in this chapter. In the first experiment, the position error of the distal of the tool manipulator is within 1 mm in 2D plane when loaded within 50 g at the tip. The position error of the distal of the tool manipulator is within 1 mm in 3D space when loaded within 20 g at the tip. Since the surgical target is pediatric tissue, the tool manipulator can be simplified as just holding needle in workspace for fine operation, thus, the surgical robot could be used for accurate manipulation in pediatric surgery. In the second experiment, the surgical manipulator was inserted into a 30x30x30 mm workspace, and its distal was driven to bend a 30° in xoz plane. The experiment result show

#### 4. Control Strategy of Redundant Robotic Manipulator in Narrow Workspace

---

the slave manipulator (positioning manipulator + tool manipulator) could well track the input and avoid collision with boundary of surgical cavity by using the proposed algorithm. Therefore, it could improve the operability and safety by controlling the redundant joints in narrow workspace; the third experiment demonstrated that the redundant joints with the proposed algorithm can improve the operability under master-slave control architecture.

## **Chapter 5**

# **Handedness Control with Pediatric Surgical Robot**

### **5.1 Introduction**

Teleoperation, also known as master-slave control, is widely used in robotic surgical systems. It provides beneficial results via taking advantages of less restriction by space in operation room (OR), reduced fatigue of operators because of ergonomic input devices, reduced surgical trauma to patients with dexterous instruments. Most teleoperation robotic surgical systems are composed of a visual module for visual feedback and slave arms for tissue manipulation, while the visual module and the slave arms following a triangle configuration. Guided by the visual feedback, a user manipulates the left input device to control the left slave manipulator, which is shown in the monitor. The correspondence between right input device and right slave manipulator shown in monitor is the same as that of the left side. However, in some surgical procedures, the right-handed operator, suffers from unnatural posture such as holding a needle with the left hand for stitching in suturing task. Therefore, current surgical systems are still restrained by the requirement of comfortable operation. This chapter illustrate the novel eye-hand coordinate for surgical assistance, which can let the user maintain to use their preferred hand to perform important task on surgery.

## 5.2 Handedness Control

### 5.2.1 Handedness

Handedness is a better (faster or more precise) performance or individual preference for use of a hand [101]. Handedness is not a discrete variable (right or left), but a continuous one that can be expressed at levels between strong left and strong right [102] [103] [104].

### 5.2.2 Hypothesis

In the typical teleoperation surgical robotic system, surgeons steer two input devices in a console, the slave manipulators move with a velocity proportional to the user input movement.

Generally, two slave arms are inserted into the surgical site in MIS. The correspondence between user input and slave manipulator is set up before an operation. The dual slave manipulators are assigned different tasks on surgery. However, in narrow workspace such as the esophagus anastomosis in the infant esophageal atresia surgery, it is difficult to perform suturing task in both sides of esophagus, even in open surgery. For example, to a right handed user, a right slave manipulator will be used to hold a needle for stitching movement, and the left slave manipulator will be fitted with a gripper to grasp tissue on a suturing task. However, a cut must be stitched from both sides in a suturing task. Users cannot always use their handedness to do important procedures. Sometimes, the left manipulator is employed to hold the needle to stitch the cut. In this case, the operator should use the unskilled hand for an important task, which increases the risk of surgery accident, shown as Fig. 5.1.

In order to overcome this limitation, two visual modules are introduced for visual feedback. The two visual modules are located at both sides with respect to the plane, which contains both slave arms, as shown in Fig. 5.2.

Fig. 5.2 shows a right-handed operator performs a right stitching task by using his/her left hand to catch a needle, and positioning the tissue controlled by his/her right hand.



however, at the current state, the user expect the correspondence between the master input and the slave manipulator could be exchanged, therefore, he/she can still use the preferred hand to catch the needle for performing surgical intervention.

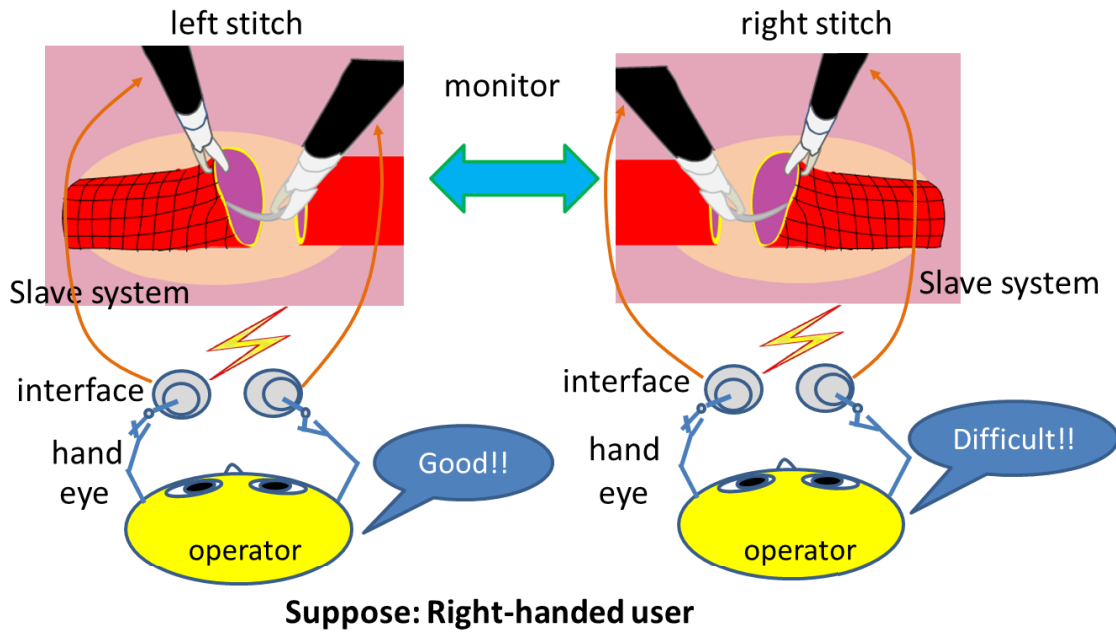


Figure 5. 1 Correspondence between master input and the slave manipulator in the master-slave robotic system.

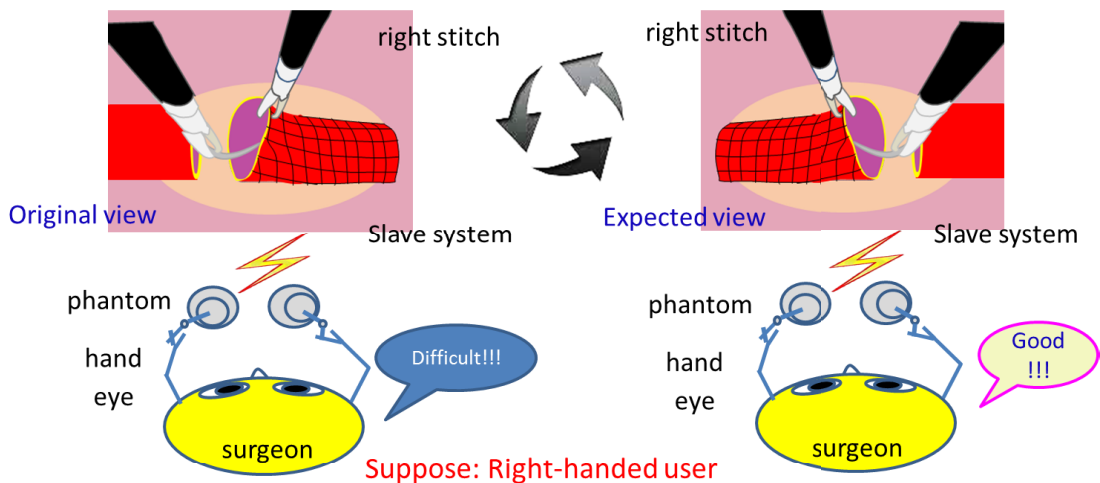


Figure 5. 2 Expected manipulation manner at unnatural work task.

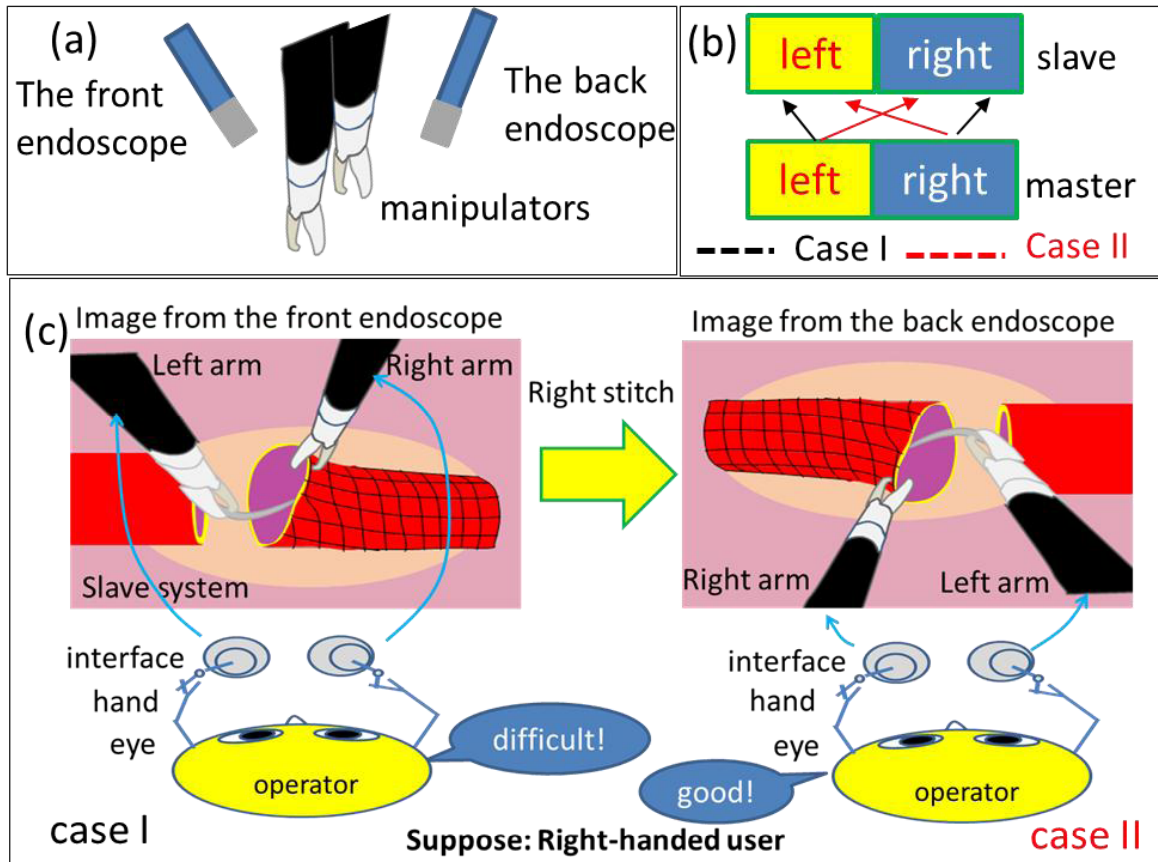


Figure 5.3 Mode switch when working at unnatural state. a). configuration between endoscope and the slave manipulators; b). correspondence between master input and the slave manipulators; c). dialogarm of hand's correspondence and visual module exchange.

### 5.2.3 User Interface and System Control

In order to overcome this limitation, two visual modules are introduced for visual feedback. The two visual modules are located at both sides with respect to the plane, which contains both slave arms, as shown in Fig. 5.3.

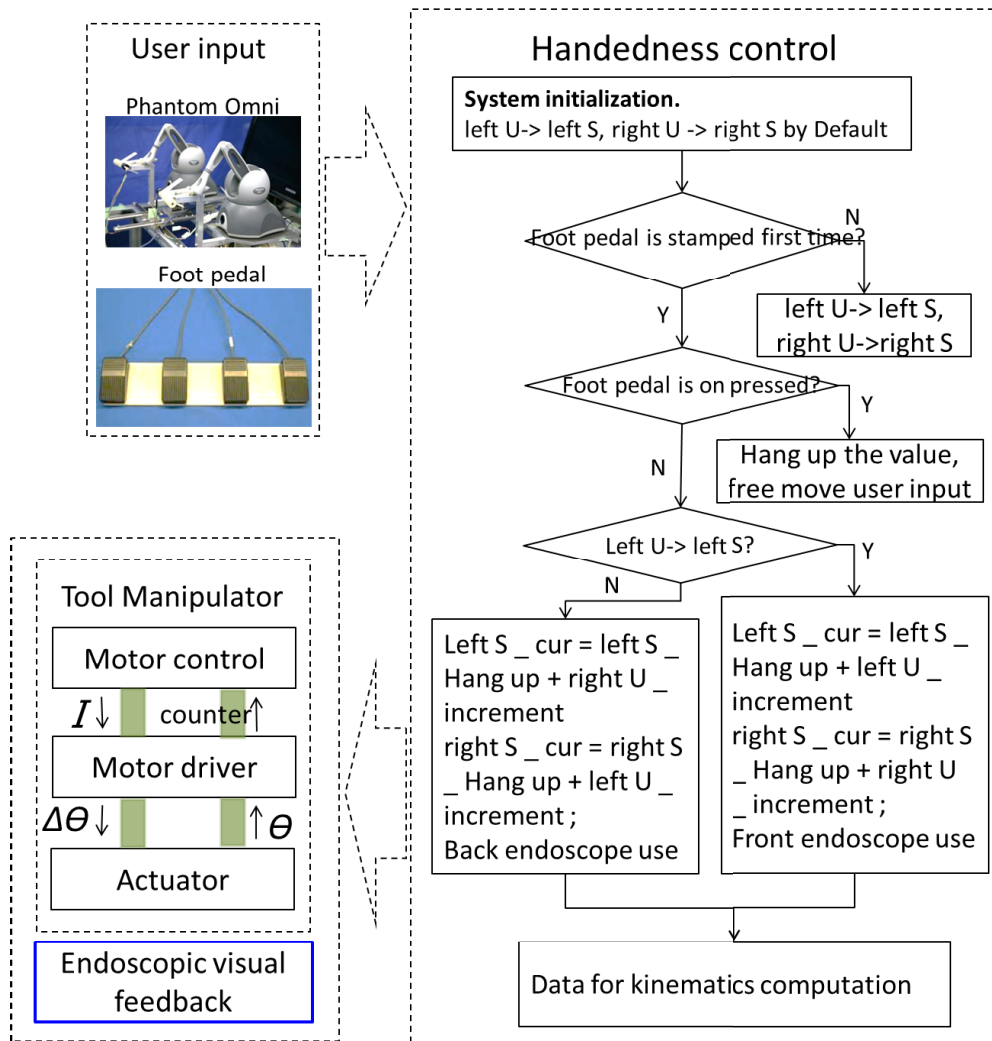


Figure 5. 4 Control frame for handedness control with surgical robot. left U: left user input; right U: right user input; left S: left slave manipulator; right S: right slave manipulator.

As shown in Fig. 5.3, the slave manipulators with the front camera or the back camera provide different triangle configurations. Therefore, when the right handed operator has to use the left hand for important tasks under the visual feedback from the front camera, the control system will switch to the back camera for visual feedback and exchange the correspondence between the master user input devices and the slave manipulators. Based on this conversion, the operator could always use his or her preferred hand for important tasks even while performing a task with an unnatural configuration. The control architecture is shown in Fig.5.4.

## 5.3 Handedness Control Experiment with Pediatric Surgical Robot

### 5.3.1 Handedness Control for Ring Transfer Task

In this session, we performed experiment to verify the feasibility of exchange of correspondence between master input and slave manipulator. The experimental setup of robotic platform is shown in Fig. 5.5. Operator bimanual two Phantom Omni (SensAble Tech, USA) [105] to telecontrol the slave manipulator while guided by visual feedback from endoscope.

The function of the four foot pedals (No.1~4) correspond to emergency, normal, exchange, start command respectively. The surgical robot will be driven to transfer a ring between four pins. The configuration of the task is illustrated in Fig. 5.6.

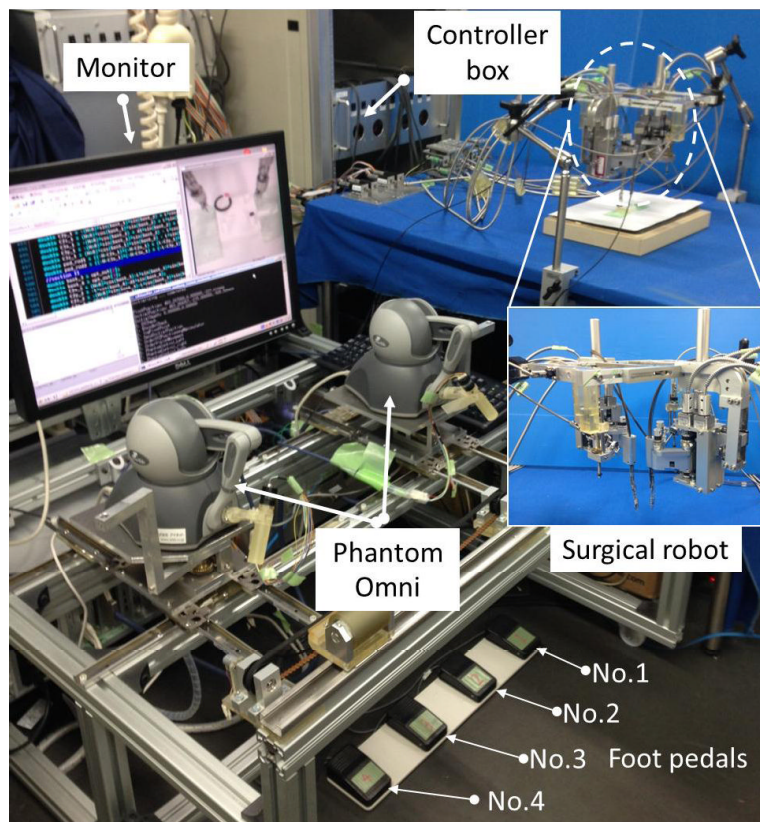


Figure 5. 5 Experiment setup.

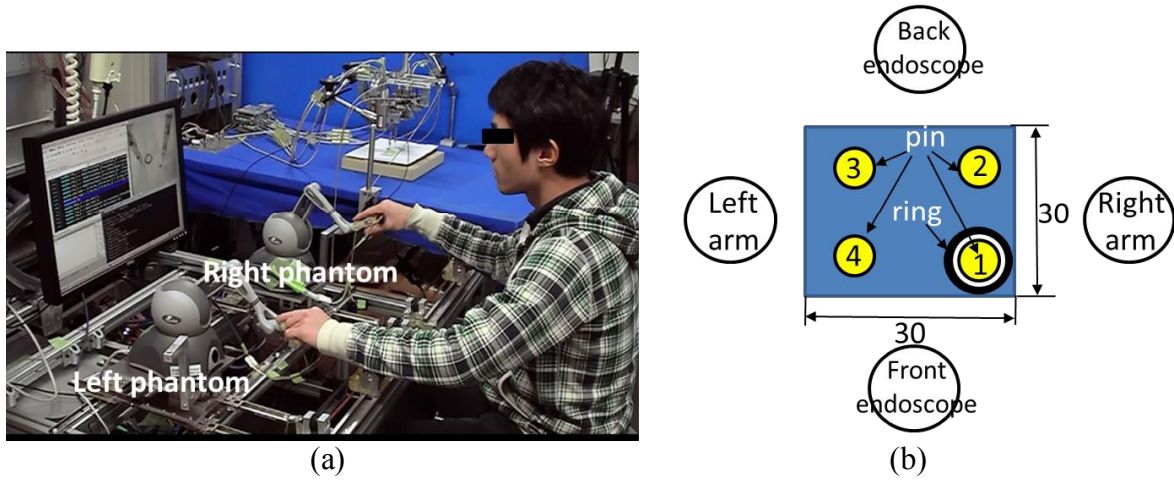


Figure 5.6 Configuration of ring transferring task with handedness control.(a) operation scene; (b) location between slave arm, endoscope, and pin.

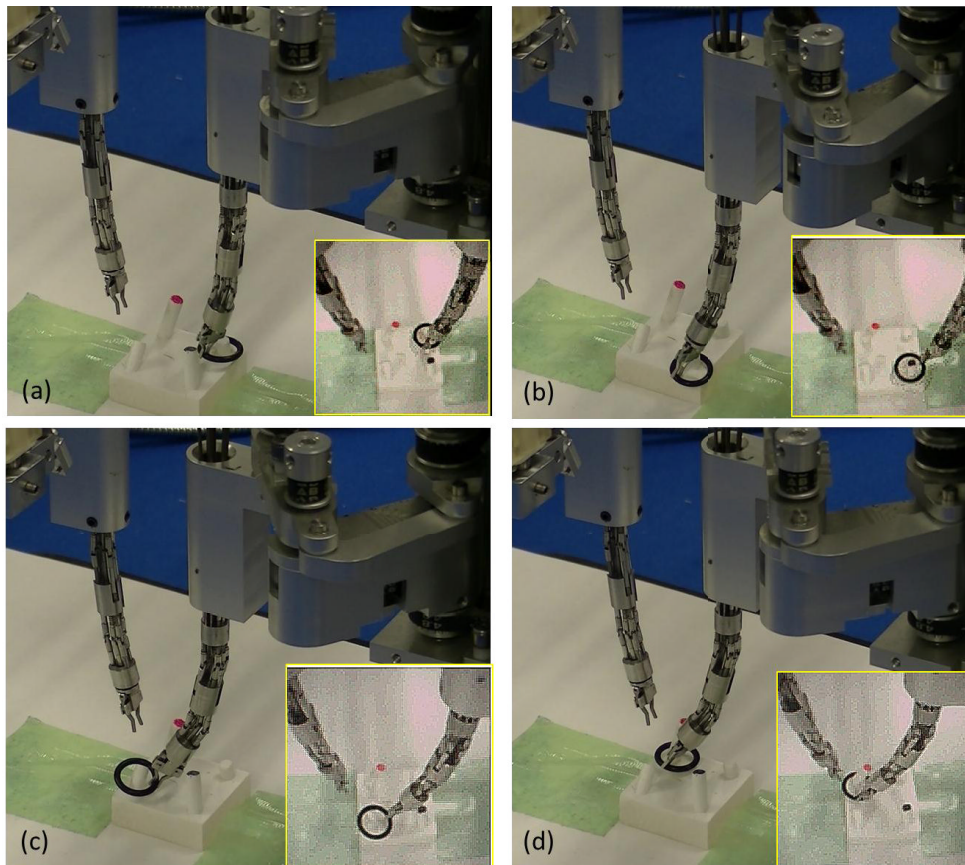


Figure 5.7 Image of ring transfer task by user's preferred hand (yellow frames are endoscopic view).(a) operation at pin 1; (b) operation at pin 2; (c) operation at pin 3; (d) operation at pin 4.

## 5. Handedness Control with Pediatric Surgical Robot

---

In this experiment, a right-handed user was asked to transfer a ring among four pins with his preferred hand. The scene image and the endoscopic image are shown in Fig. 5.7.

When the operator uses his preferred hand to operate right slave manipulator to transfer ring between pin 1 and pin 2, the distal of the driven manipulator is always located at the same side as the configuration of body's hand (Fig. 5.7(a-b)). However, when transfer ring between pin 3 and pin 4, the operator should drive the manipulator to the oppsite side for manipulation (right side to left side in this experiment) or must use left hand to do task (Fig.5.7 (c-d)). The large span manipulation leads to the worse visual feedback of surgical sence which shielded by the manipulator. Therefore, when the task is not in user's preferred side, the user could exchange the correspondence between the master, the slave and visual module referred in section 5.2.3. Therefore, the operator can always use his preferred hand for operation. The result is shown in Fig. 5.8.

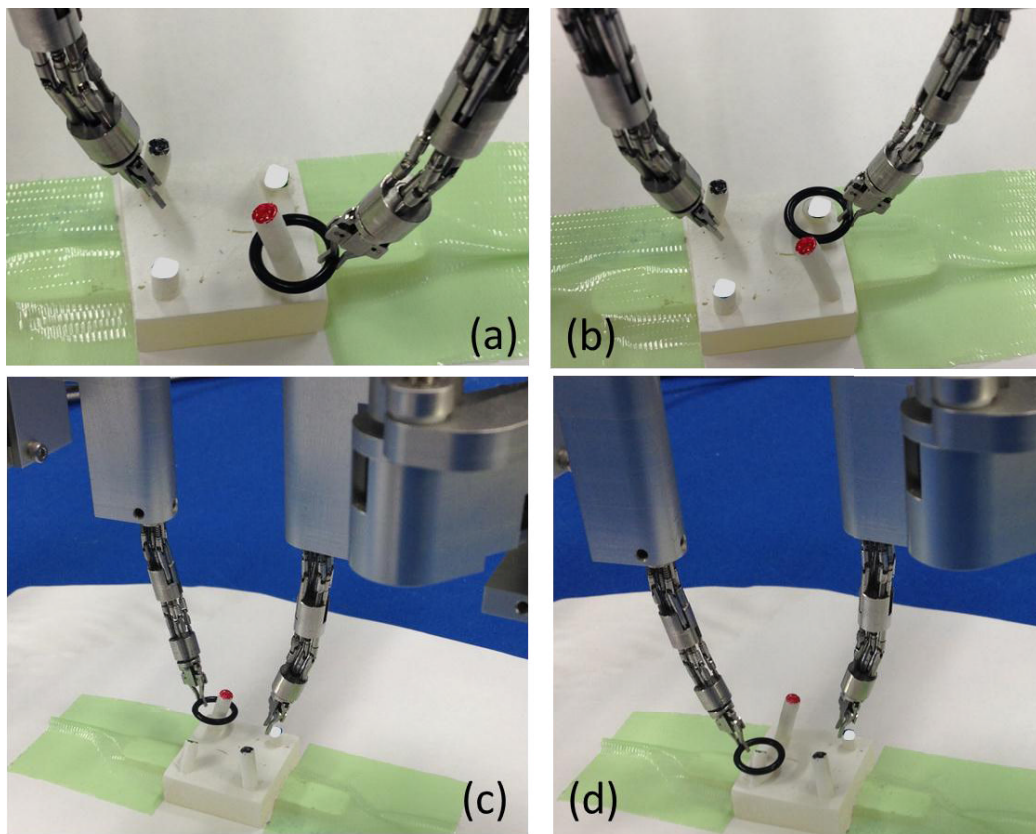


Figure 5. 8 Manipulation sence after exchange of the correspondence between the master, the slave and visual modules. (a)-(b) endoscopic view of operation at pin 3 and pin4; (c)-(d) manipulation sence at pin 3 and pin 4.

In Fig. 5.8, the ring was still transferred between pin 3 and pin 4. However, the left slave manipulator was driven to finish this task. According to the exchanged correspondence, the operator still use his/her right hand to manipulate right phantom, and the right slave manipulator was working in the monitor.

We divide the task into three segments: first, transfer the ring in the preferred side by operator's dexterous hand control (pin 1 and pin 2); second, transfer the ring in the oppsite side by operator's unskilled hand control (pin3 and pin 4); third, transfer the ring in the oppsite side by operator's dexterous hand control (pin 3 and pin 4). In the first and the second task, the master input and the slave manipulator are with normal normal correspondence (left master input corresponds to left slave manipulator; right master input correspond to right slave manipulator). In the third task, the master input and the slave manipulator are with exchanged correspondence (left master input corresponds to right slave manipulator, right master input corresponds to left slave manipulator). Each task was performed by five trails. The time taken to complete the transfer tasks is shown in Fig. 5.9. The experimental result

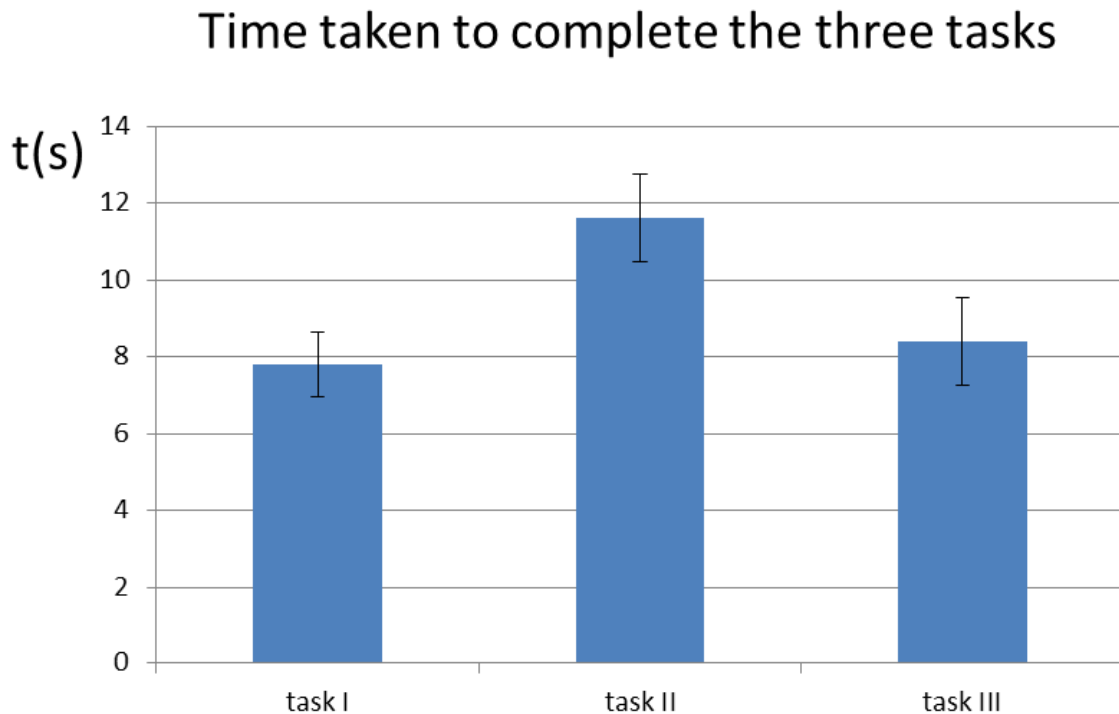


Figure 5. 9 Time taken to complete the three tasks by five trails.

demonstrated that user's performance are almost same in task I and task III, and the average time taken in these two tasks are obviously shorter than that in task II.

### 5.3.2 Handedness Suture Manipulation in Narrow Workspace

In the surgical intervention for ICEA surgery, surgeon should perform stitching work on both sides of the separated esophagus in a 30x30x30 mm narrow workspace. Generally, people have preferred hand use between their both hands. Therefore, when a surgeon hold needle to suture the separated esophagus, he/she should stand on both operation table in turn if keep using preferred hand, otherwise, he/she should use the unskilled hand to hold needle for stitching. In order to provide surgeon a comfortable operation manner during surgery, the author proposed a robotic system with handedness control to assist surgeon.

Fig. 5.10 shows the platform of robotic system working on a 30x30x30 mm narrow

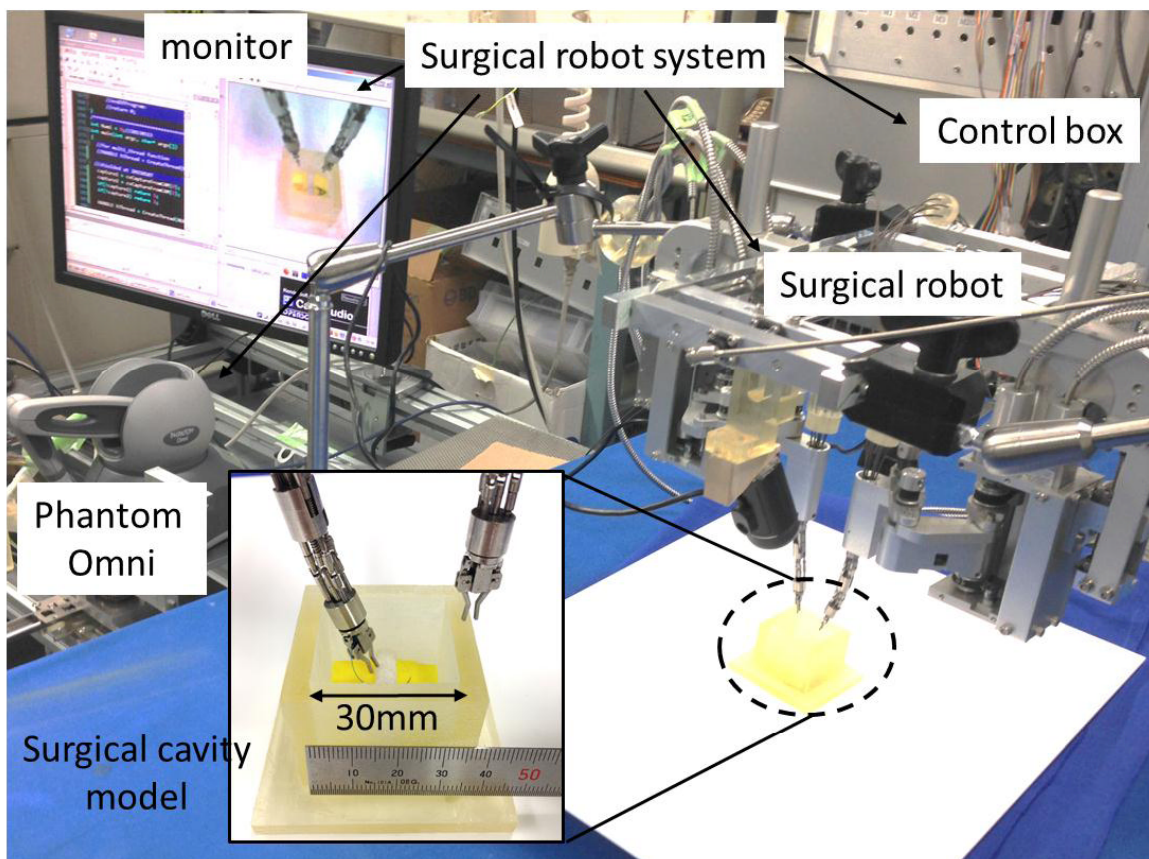


Figure 5. 10 Experimental setup of handedness control for suture task.



space model.

A right-handed engineering student without any medical background will operate the pediatric assist surgical robot to complete suture task on an esophageal model. When the user suturing on the right side of esophageal model, the master input and the slave manipulator of the robotic system is under normal correspondence. Therefore, the image in monitor will show the right slave manipulator hold needle for stitching while the operator use his right hand to

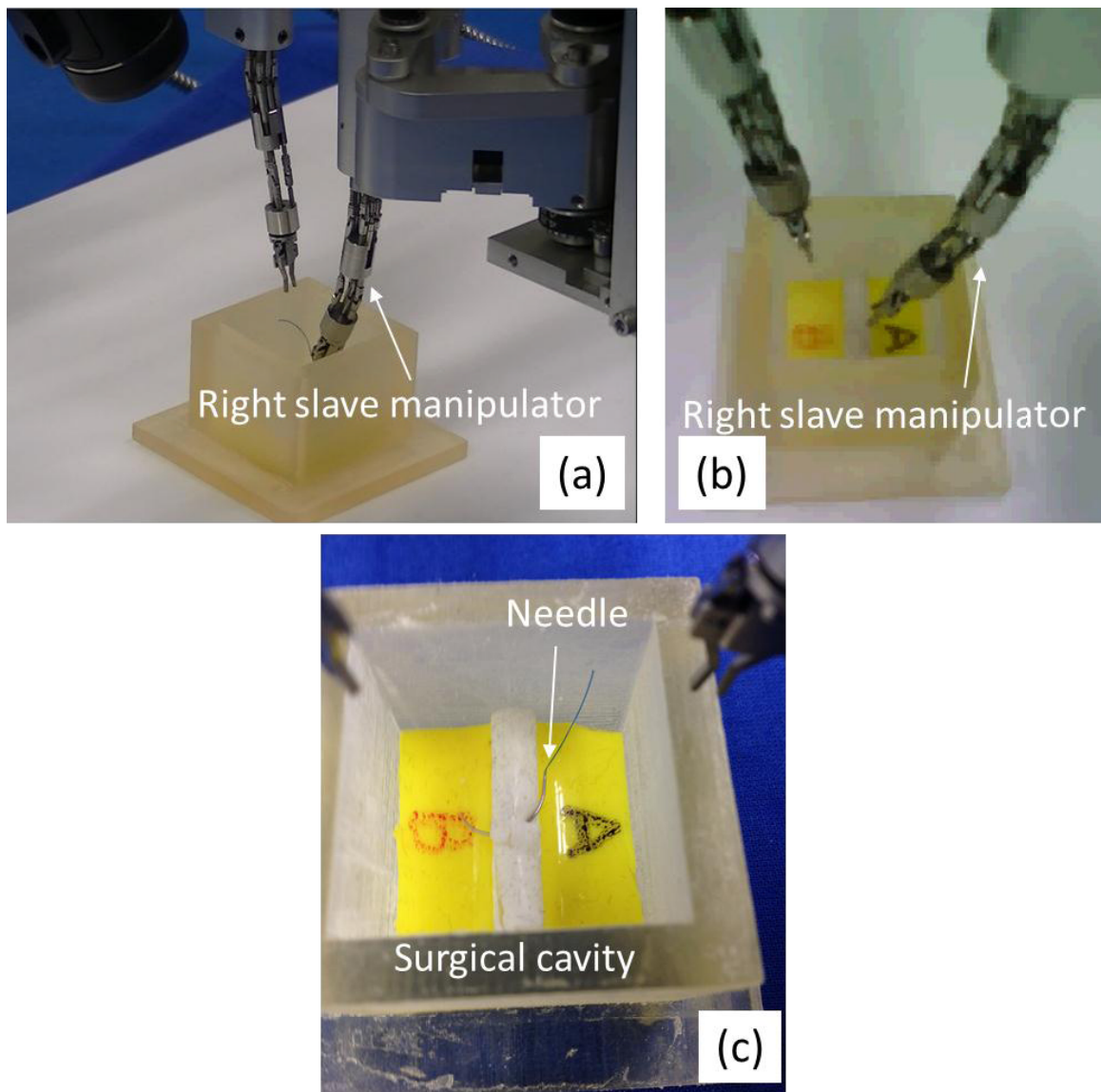


Figure 5. 11 Suture manipulation on the right side by right slave manipulator with right Phantom Omni. (a) manipulation scene from external camera; (b) visual feedback from endoscope; (c) suture result on the esophageal model by right slave manipulator.

manipulate the right master input. The manipulation on the model is shown in Fig. 5.11.

When suturing on the opposite side of the separated esophagus, the operator would like to use his preferred hand (right hand) to hold needle for stitching. As shown in Fig. 5.4, by stepping foot pedals 2 and foot pedals 3, the correspondence will be converted between the normal and the exchanged manner. Therefore, the operator can always use his preferred hand to hold needle to suture on both sides of the separated esophagus. The operation scenes are shown in Fig. 5.12. The suture result by the left slave manipulator is shown in Fig. 5.13.

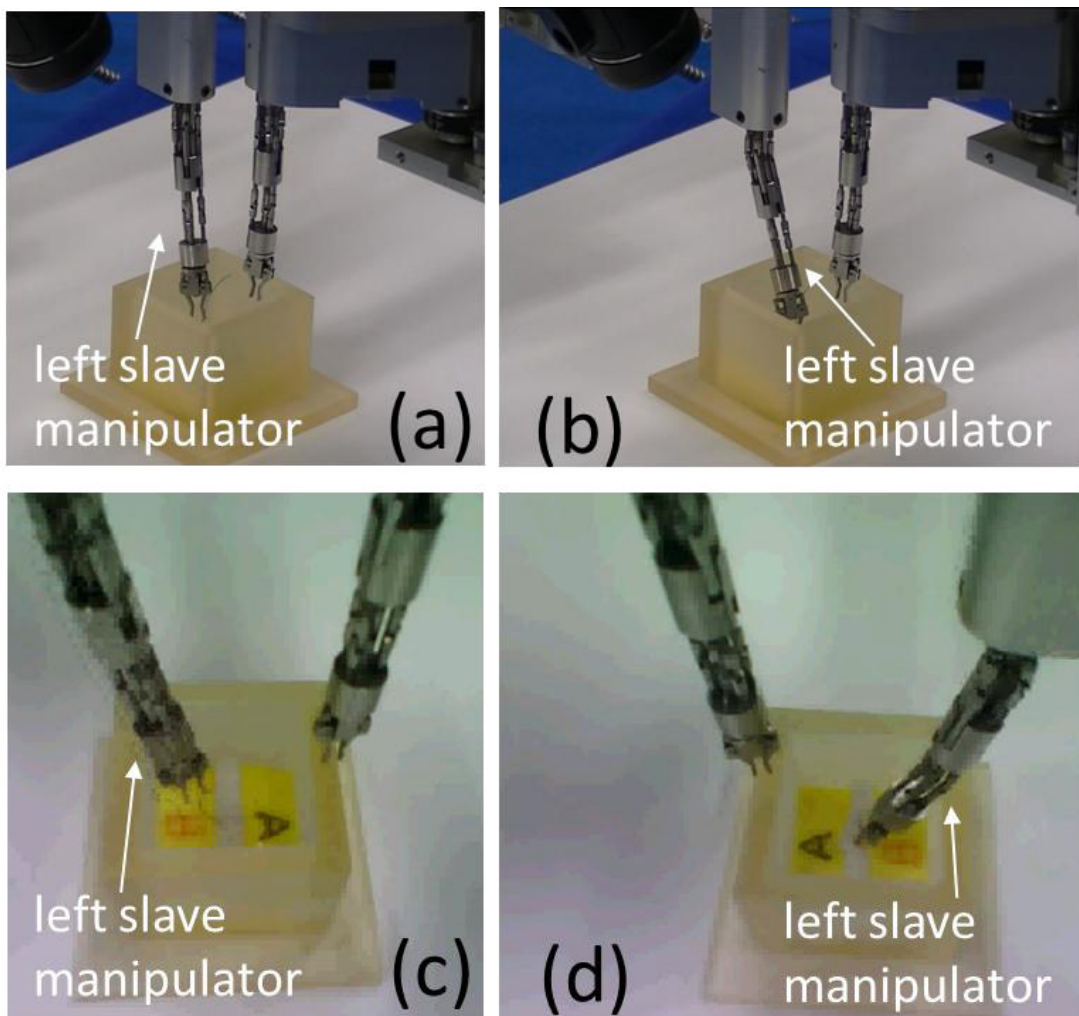


Figure 5. 12 Suture manipulation on the left side by left slave manipulator with right Phantom Omni. (a) sense of left Phantom Omni manipulate left slave manipulator; (b) sense of right Phantom omni manipulate left slave manipulator; (c) visual feedback of endoscope in (a); (d) visual feedback of endoscope in (b).

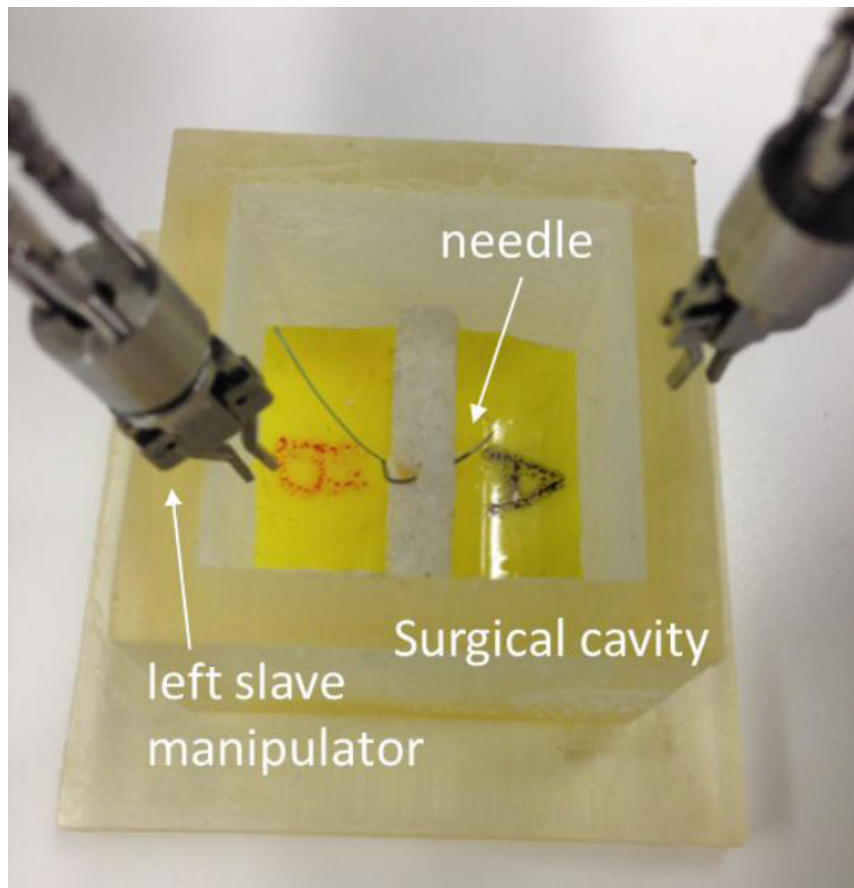


Figure 5.13 Suture result on the esophageal model by the left slave manipulator.

## 5.4 Discussion

In this chapter, the author illustrated robot user's operation manner under master-slave control architecture. Considering the difference of proficiency between human's both hands, the author proposed a novel application to release robot operator's burden. In the control system, we developed an algorithm that the correspondence between the master input and the slave manipulator can be exchanged based on the priority of hand's proficiency. Therefore, it guarantees the robot user can always manipulate surgical intervention with preferred hand on operation.

Two experiments are presented in this chapter, in the first experiment, operator control the pediatric surgical robot to transfer ring between nails on a 30x30 mm square model. By

## 5. Handedness Control with Pediatric Surgical Robot

---

comparing the time taken to complete the three tasks, the handedness control mode could save operation time by using preferred hand to manipulate the opposite transfer task.

In the second experiment, a suture manipulation was performed in a 30x30x30 mm narrow workspace by using the pediatric surgical robot under handedness control. The experiment result demonstrated that robot operator could always use his/her preferred hand to do important task at suture intervention.

# Chapter 6

## Conclusion and Future Work

### 6.1 Conclusion

In this research, our goal is to develop a surgical robot system, which can assist surgeon perform tissue intervention in narrow workspace. For the final goal, firstly, the author presents the detailed mechanism design of the pediatric surgical robot, and illustrates the kinematics and inverse kinematics computation. Subsequently, the author proposes an algorithm for optimizing the inverse solution for redundant manipulator. Finally, corresponding to the visualization and operability of master-slave control architecture, the author presents a novel application for reducing operation difficulty in bimanual manipulation under master-slave control system.

#### 6.1.1 Master-slave Pediatric Surgical Robot for Narrow Workspace

In chapter 3, the author presented a surgical robot to assist surgeon perform tissue intervention in narrow workspace for pediatric surgery. The surgical robot consists of two main parts: two slave arms and two visual modules. Each slave arm is composed of a positioning manipulator and a tool manipulator. The positioning manipulator, having 4 DoFs in total, consists of a SCARA (Selective Compliance Assembly Robot Arm) and a screw-pair mechanism. It can achieve three translational movements in 3D space. The positioning

manipulator is held at the distal of the SCARA mechanism. The use of the SCARA mechanism make the serial joint can be independently controlled. The tool manipulator, with an external diameter of 8 mm, having 5 DoFs in total, consists of two bendable segments (2 DOFs for each) and a rotatable gripper. Each bendable joint including “double screw drive (DSD) + universal joint” structure is used to realize two bending movements, which are orthogonal with each other. The combination of two bendable joints guarantee the distal of the tool manipulator can achieve dexterous arbitrary orientational bending motion. The two visual modules located at both sides of the work frame, where the slave arms located. There are two combinations between the visual modules and the slave arms, alternative selection ensure surgical robot user can perform handedness manipulation.

### **6.1.2 Control Strategy of Redundant Manipulator in Narrow Workspace**

The author computed forward/inverse kinematics of the redundant surgical manipulator. The simulation results demonstrate the surgical robot can cover a 30x30x30mm space, which is created for pediatric surgery. Corresponding to the geometric dimension of pediatric surgical robot, the author built a co-simulator in Adams/Matlab. Since the surgical robot aims to be operated in narrow workspace (30x30x30 mm), therefore, the collision between the surgical manipulator and the boundary of surgical cavity should be avoided during operation. The changes of robot's joints during the tool manipulator performing obstacle avoidance were analyzed in co-simulation, the simulation results indicate that each robot's joint can be smoothly controlled when imposing a disturbance on the redundant joint. Combining visualization and operability, a shape optimal algorithm for controlling the redundant manipulator is developed, which drive the dual arms and the endoscope to satisfy eye-hand triangle formation during manipulation. Three experiments are performed to verify the performance of pediatric surgical robot. In the 1<sup>st</sup> experiment, the tool manipulator was driven to bend 45°, while the positioning manipulator was fixed. Since the utility of universal joint in the bendable joint, therefore, the max error of the tip of the manipulator is up to 3 mm. By compensating the backlash of the universal joint, the tool manipulator can reach positioning precision within 1mm. In the 2<sup>nd</sup> experiment, the surgical manipulator was driven into a 30x30x30 mm surgical cavity, and the tip was forced to bent 30° in order to satisfy eye-

hand triangle formation, the experiment data show that combination of positioning manipulator and the tool manipulator can well track the master's instruction. In the 3<sup>rd</sup> experiment, the author manipulate pediatric surgical robot without/with redundant DoF control algorithm. The visual feedback demonstrates that utility of redundant DoF control algorithm can get better visual field and closest to eye-hand triangle formation.

### 6.1.3 Handedness Control with Pediatric Surgical Robot

Considering the proficiency of hand use for surgeon, a novel method to offer surgeon for an easy operation with skilled hand was presented in chapter 5. Corresponding to the configuration of the master-slave surgical robot system, a control algorithm that can alternatively match the correspondence between the master input, the slave arms and the visual module depending on the surgical task was illustrated. The goal aims to guarantee the robot user could maintain preferred hand use for important task even at the moment that the unskilled hand should be used for operation in normal correspondence of robot system. The experiment result with pediatric surgical robot verified the effectiveness of the proposed control system.

## 6.2 Future Work

In this overall research, the author developed a surgical robot to assist surgeon to perform tissue manipulation in narrow workspace for pediatric surgery, and proposed a control strategy to map the trajectory of the slave manipulator. As the future work, the pediatric surgical robot still have improvements in the following points:

1. Construct the power transmission model to compensate the precision loss of the bendable joints in 3D bent motion when loaded at the distal of the tool manipulator.

In this thesis, the author developed a tool manipulator with external diameter of 8 mm. The tool manipulator includes two segments of bendable joints, which consists of two bending linkages and one base linkage. The bending linkage, connected with motor by a flexible shaft, is composed of a left-handed screw, a universal joint and a right-handed screw.

By rotating the bending linkage, the left-handed screws and the right-handed screw will “bite” into or “retreat” from the nut simultaneously, which will drive the distal of the manipulator bend based on the base linkage. Currently, the author use experiment to verify the manipulator could obtain high position accuracy in 3D bent motion when loaded within 20g at the tip. When the load suspases 20 g, the flexible shaft will be deformed due to the stall torque created by the friction in screw pair.

In order to fit heavier load for accuracy position control, the power transmission model should be constructed. By modeling the power transmission path, the controller sends out appropriate compensation signals to the corresponding motors.

2. Image processing for smooth transition when the visual module exchanged in handedness control.

In the handedness control system, two visual modules are located at both sides with respect to the plane, which includes the two tool manipulators. When the correspondence between the master Phantom Omni and the slave manipulator changed, the visual module capturing surgical sence image for visual feedback will directly be exchanged corresponding to the master/slave match. In order to reduce the visual mutation for surgeon, image processing for smooth transiting the image in monitor when the visual modules exchanged will be considered.

3. Evaluate pediatric surgical robot by *in vivo* experiment.

The surgical robot system should be performed in the *in vivo* experiment to verify the benefits of dexterous manipulation and the function of the handedness control.

4. Spread the control strategy and the handedness control for other surgical robot systems.



# Appendix A

## Aurora System (Aurora V3, NDI)

### A.1 Description

Aurora V3 is manufactured by Northern Digital Inc.(NDI), Ontario, Canada. NDI is a global measurement technology systems, with over 45,000 installations worldwide. Today, the Polaris® optical measurement system, Aurora® and 3D Guidance® electromagnetic tracking systems are trusted by the industry's top medical equipment manufactures.

### A.2 Important Feature

- Geometric dimension (in mm):  $\phi 1.8 \times 9$
- Degree of Freedom: 6
- Measurement rate:  $\leq 40Hz$
- Metal resistance: cobalt-chrome alloy, steel DIN 1.441, titanium (TiA16V4), 300 series stainless steel

## A.3 System Component

- Field Generator
- System Control Unit (SCU)
- Sensor Interface Unit (SIU)

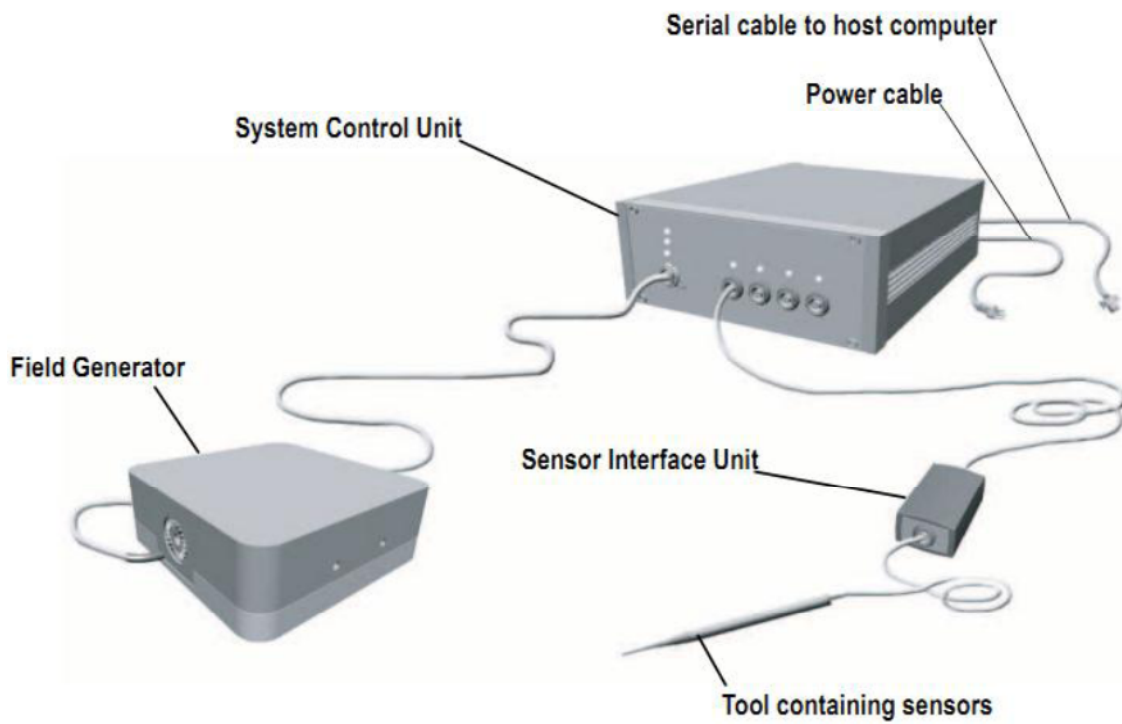


Figure A. 1 Aurora system.

## A.4 Measurement Volume

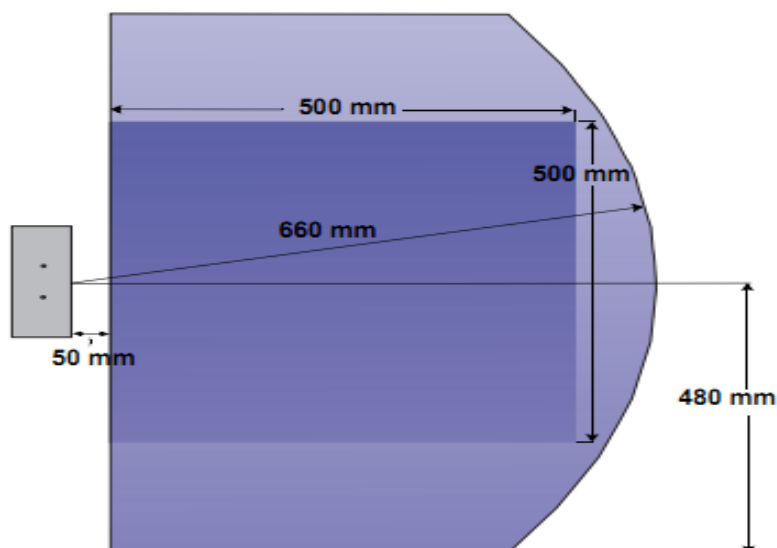


Figure A. 2 Aurora system measurement volumes.

## A.5 Aurora System Accuracy

Table A- 2 Cube volume- position errors

Position Errors	5DOF		6DOF	
	RMS (mm)	95% CI (mm)	RMS (mm)	95% CI (mm)
Position Accuracy	1.4	2.6	0.9	1.8
Position Precision	1.1	2.1	0.7	1.4
Position Trueness	1.0	1.9	0.7	1.2

Table A- 1 Cube volume- orientation errors

Orientation Errors	5DOF		6DOF	
	RMS (°)	95% CI (°)	RMS (°)	95% CI (°)
Orientation Accuracy	0.3	0.5	0.4	0.6
Orientation Precision	0.1	0.2	0.2	0.4
Orientation Trueness	0.3	0.5	0.4	0.6

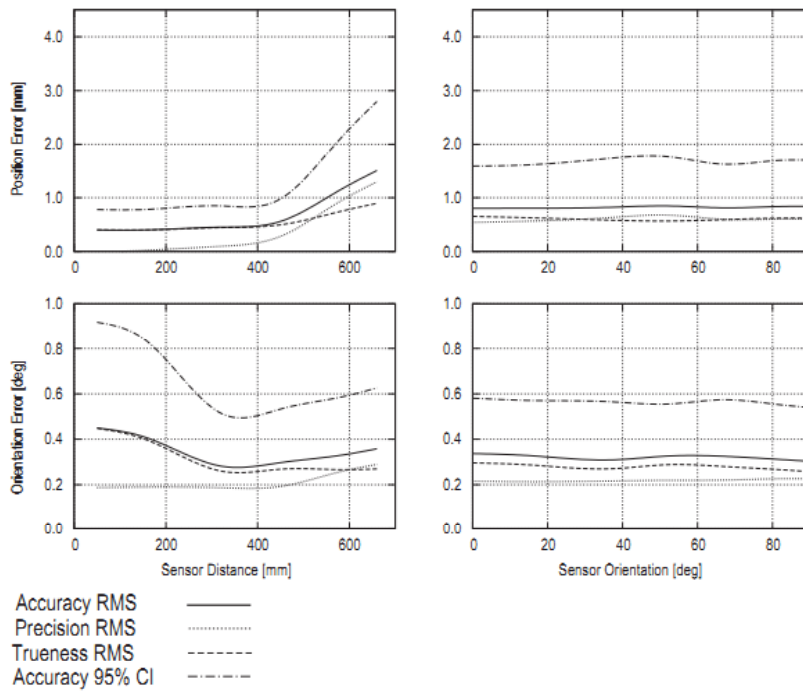


Figure A. 3 System accuracy (6DoF sensor)

## **Appendix B**

# **Super Extra Fine 2.9mm Industrial Video Borescope (HNL-2.9CAM, SPI ENG Co., Ltd)**

### **B.1 Description**

SPI ENGINEERING Co., Ltd, specializes in industrial video endoscopes by using CMOS camera and image processing technologies.

### **B.2 Main Feature**

- Geometric dimension (in mm):  $\phi 2.9$
- Pixels: 160,000
- 2 High-Intensity white LEDs

## B.3 Specification

Table B- 1 Specification of HNL-2.9 CAM

Camera	
Model	HNL-2.9CAM
Sensor	1/10" CMOS Sensor
Resolutions	400 × 400
Light Source	2 White LEDs (Adjustable LED intensity)
Camera probe diameter	2.9mm
Angle of view	35 degrees
Focal Distance	Approximately 0.19" (5mm)
Probe Length	3.28ft (1m) *Extendable up to 9.84ft (3m)
Tube	None (PVC electric cable)

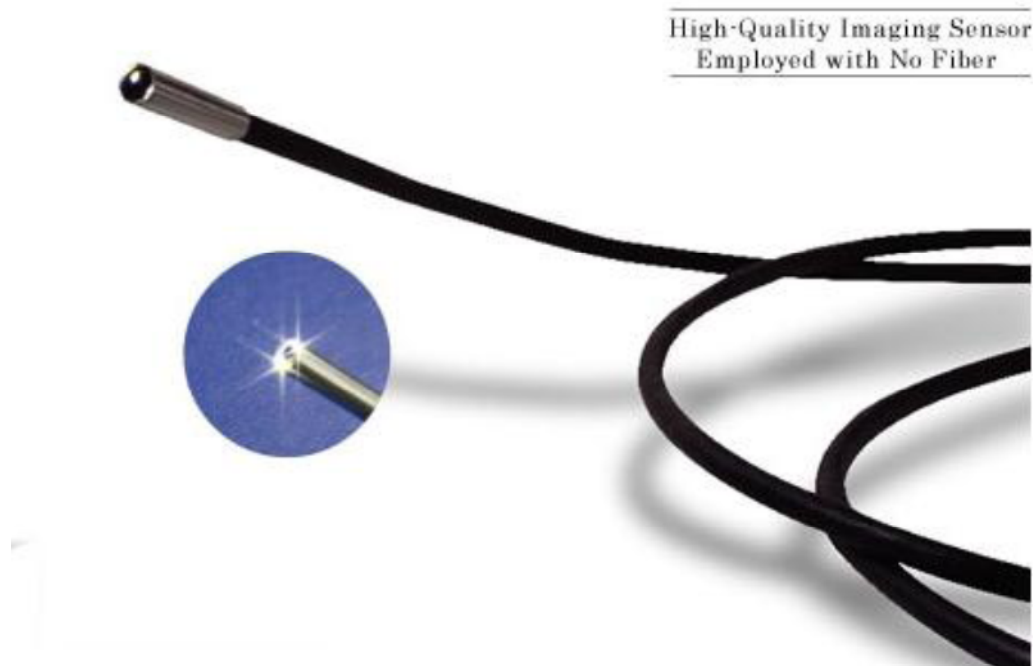


Figure B. 1 Super extra fine 2.9 mm industrial video borescope.

## **Appendix C**

# **PHANTOM Omni (SensAble Technologies, Inc., USA)**

### **C.1 Description**

The Sensible Technologies PHANTOM product line of haptic devices makes it possible for users to touch and manipulate virtual objects. The PHANTOM Omni mode is the most cost-effective haptic device available today. Portable design, compact footprint, and IEEE-1394a FireWire port interface ensure quick installation and ease-of-use.

### **C.2 Highlighted Feature**

- Six degree-of-freedom positional sensing
- Portable design and compact footprint for workplace flexibility
- Stylus-docking inkwell for automatic workspace calibration

## C.3 Specification

Table C- 1 Specifications of Phantom Omni

<b>Nominal Position Resolution</b>	> 450 dpi	~0.055 mm
<b>Workspace</b>	~6.4 w x 4.8 h x 2.8 d in	> 160 w x 120 h x 70 d mm
<b>Backdrive Friction</b>	< 1 oz	< 0.26 N
<b>Maximum Exertable Force</b>	0.75 lbf	3.3 N
<b>Continuous Exertable Force (24 hrs)</b>	> 0.2 lbf	> 0.88 N
<b>Stiffness</b>	X axis > 7.3 lbs./in Y axis > 13.4 lbs./in Z axis > 5.9 lbs./in	X axis > 1.26 N/ mm Y axis > 2.31 N/mm Z axis > 1.02 N/mm
<b>Inertia (apparent mass at tip)</b>	~ 0.101 lbm	~ 45 g
<b>Footprint</b>	~ 6 5/8 w x 8 d in	~ 168 w x 203 d mm
<b>Weight*</b>	3 lbs 15 oz	~1.47 kg
<b>Operating Temperature</b>	50° to 95°F	10° to 35°C
<b>Storage Temperature</b>	-40° to 149°F	-40° to 65°C
<b>Relative Humidity</b>	20% to 80% (noncondensing)	
<b>Force Feedback</b>	3 degrees of freedom (x, y, z)	
<b>Position Sensing</b>	x, y, z (digital encoders)	
	Pitch, roll, yaw ( $\pm$ 5% linearity potentiometers)	
<b>Interface</b>	IEEE-1394 FireWire® port	
<b>Input Voltage</b>	100-240 VAC (Use supplied power supply only AD-740-1180)	
<b>Input Frequency</b>	50-60 Hz	
<b>Input Current</b>	1 A	
<b>Warranty</b>	Three months	

\* Does not include power supply or cables.



# Reference

- [1] Jaffray. B. "Minimally invasive surgery," *Arch Dis Child*, Vol. 90, pp.537-542, 2004.
- [2] Horgan S., Vanuno D., "Robots in laparoscopic surgery," *J Laparoendosc Adv Surg Tech A*, Vol. 11, pp. 415-419, 2001.
- [3] Hatzinger M., Kwon ST., Langbein S., Kamp S., Hacker A., Alken P., "Hans Christian Hacobaeus: Inventor of human laparoscopy and thoracoscopy", *J. Endourol.*, Vol.20, pp.848-850.
- [4] Tarasconi J.C. "Endoscopic salpingectomy", *J. Reprod Med*, Vol.26, pp.541-545, 1981.
- [5] Laparoscopic surgery history, [Online], <http://www.news-medical.net/health/Laparoscopic-Surgery-History.aspx> (Accessed October 2014).
- [6] Fibroid treatments, [Online], <http://www.misforwomen.com/service/medical-library/treatments/fibroid-treatments/> (Accessed October 2014).

- [7] Fitzgibbons R.J., Camps J., Cornet D.A., Nguyen N.X., Litke B.S., Annibali R., and Salerno G.M., "Laparoscopic inguinal herniorrhaphy. Results of a multicenter trial", *Ann. Surg.* Vol.221, pp.3-13, 1995.
- [8] Arregui M.E., Fitzgibbons R.J., Katkhouda N., McKernan J.B., Reich H. eds. "Principles of Laparoscopic Surgery: Basic and Advanced Techniques", *New York: Springer Verlag*; 1995.
- [9] Michael B.L., Langer H.C., Quasebarth M.A., Whitman E.D., "Comparative analysis of laparoscopic versus open splenectomy", *Am. J. Surg.*, Vol.172, pp.596-601, 1996.
- [10] Isolauro J., Luostarinen M., Viljakka M., "Long-term comparison of antireflux surgery versus conservative therapy for reflux esophagitis", *Ann Surg.* Vol.225, pp.295-299, 1997.
- [11] Peters J.H., Heimbucher J., Kauer W.K., Incarbone R., Bremner C.G., DeMeester T.R., "Clinical and physiologic comparison of laparoscopic and open Nissen fundoplication", *Journal of the American College of Surgeons*, Vol.180, pp.385-393, 1995.
- [12] Bais J.E., Bartelsman J.F.W.M., Bonjer H.J., Cuesta M.A., Go P.M.N.Y.H., Klinkenberg-Knol E.C., Lanschot J.J.B.van, Badorp J.H.S.M., Smout A.J.P.M., Graaf Y.van der., Gooszen H.G., *The Lancet*, Vol.355, pp.170-174, 2000.
- [13] Mattioli G., Esposito C., Pini Prato A., Doldo P. Castagnetti M., Barabino A., Gandullia P., Staiano A.M., Settini A., Cucchiara S., Montobbio G., Jasonni V., "Results of the laparoscopic Heller-Dor procedure for pediatric esophageal achalasia", *Surg Endosc* Vol.17, pp.1650-1652, 2003.
- [14] Fujimoto B.T., Lane G.J., Segawa O., Esaki S., and Miyano T., "Laparoscope extramucosal pyloromy versus open pyloromyotomy for infantile hypertrophic pyloric stenosis: which is better?", *Journal of Pediatric Surgery*, Vol.34, pp.370-372, 1999.
- [15] Sisten E., Bax N.M. van der Zee D.C., "Is laparoscopic pyloromyotomy superior to open surgery?", *Surg Endosc.*, Vol.12, pp.813-815, 1998.

- 
- [16] Greason K.L., Thompson W.R., Downey E.C., Lo Sasso B., “Laparoscopic pyloromyotomy for infantile hypertrophic stenosis: report of 11 cases”, *J Pediatr Surg.*, Vol.30, pp.1571-1574, 1995
- [17] Kim P.C.W., Wesson D., Superina R., and Filler R.,” Laparoscopic cholecystectomy versus open cholecystectomy in children: which is better?” *Journal of Pediatric Surgery*, Vol.30, pp.971-973, 1995
- [18] Park A., Marcaccio M., Sternbach M., Witzke D., Fitzgerald P., “laparoscopic vs open splenectomy”, *Arch Surg.*, Vol.134, pp.1263-1269, 1999
- [19] Chen M.K, Schropp K.P., and Lobe T.E., “Complications of Minimal access surgery in children”, *Journal of Pediatric Surgery*, Vol.31, pp.1161-1166, 1996
- [20] Cohan S., “ROBODOC achieves pinless registration”, *Industrial robot: An International Journal*, Vol.28, pp.381-386, 2001.
- [21] <http://www.robodoc.com/> (Accessed October 2014).
- [22] Sugiya N., Genma F., Nakajima Y., and Mitsuishi M., “Adaptive controlled milling robot for orthopedic surgery”, *Proceedings of the 2007 IEEE International Conference on Robotics&Automation (ICRA)*, pp.605-610, 2007
- [23] First surgical procedures for Renishaw’s neuro|mate® robot in nice, France [Online] <http://www.renishaw.com/en/first-surgical-procedures-for-renishaws-neuromate-robot-in-nice-france--19414>, (Accessed October 2014).
- [24] Finlay P.A., "PathFinder image guided robot for neurosurgery", *Industrial robot*, Vol.30, pp.30-34, 2003.
- [25] Koseki Y., Koyachi N., Arai T., and Chinzei K., “Remote actuation mechanism for MR compatible manipulator using leverage and parallelogram”, *Proceedings of the 2003 IEEE International Conference on Robotics&Automation (ICRA)*, pp.652-657, 2003

- [26] Masamune K., Kobayashi E., Masutani Y., Suzuki M., Dohi T., Iseki H., Takakura K., “Development of an MRI-compatible needle insertion manipulator for stereotactic neurosurgery”, *J Image Guid Surg.*, Vol.1, pp.242-248, 1995
- [27] Krieger A., Susil R.C., Menard C., Coleman J.A., Fichtinger G., Atalar E., Whitcomb L.L., “Design of a novel MRI compatible manipulator for image guided prostate interventions”, *IEEE Trans Biomed Eng.*, Vol.52, pp.306-313, 2005
- [28] Larson B.T., Erdman A.G., Tsekos N.V., Yacoub E., Tsekos P.V., Koutlas I.G., “Design of an MRI-compatible robotic stereotactic device for minimally invasive interventions in the breast”, *J Biomech Eng.* Vol.126, pp.458-465, 2004.
- [29] Tajima F., Kishi k., Nishizawa K., Kan K., Ishii H., Sudo K., Fujie M.G., and Dohi T., "A prototype master-slave system consisting of two MR-compatible manipulators with interchangeable surgical tools", *Proceedings of the 2004 IEEE ICRA*, pp.2505-2510, 2004.
- [30] Tsekos N.V., Ozcan A., Christoforou E., "A prototype manipulator for magnetic resonance-guided interventions inside standard cylindrical magnetic resonance imaging scanners", *J. Biomech Eng.*, Vol.127, pp.972-980, 2005.
- [31] Marescaux J., Leroy J., Gagner M., Rubino F., Mutter D., Vix M., Butner S.E., Smith M.K., “Transatlantic robot-assisted telesurgery”, *Nature*, Vol.413, pp.379-380, 2001
- [32] Frequently asked questions, [Online] [http://www.intuitivesurgical.com/products/products\\_faq.html#12](http://www.intuitivesurgical.com/products/products_faq.html#12), (Accessed October, 2014)
- [33] Xu K., Simaan N., “ Acutation compensation for flexible surgical snake-like robots with redundant remote actuation”, *Proceedings of the 2006 IEEE International Conference on Robotics&Automation (ICRA)*, pp.4148-4154,2006
- [34] Dupont P. E., Lock J., Itkowitz B., and Butler E., “Design and control of concentric-tube robots”, *IEEE Transactions on robotics*, Vol.26, pp.209-225, 2010

- 
- [35] Shang J., Noonan D.P., Payne C., Clark L., Sodergren M.H., Darzi A., and Yang G.Z. “An articulated universal joint based flexible access robot for minimally invasive surgery”, *Proceedings of the 2010 IEEE International Conference on Robotics&Automation (ICRA)*, pp.1147-1152,2010.
- [36] Clark J., Sodergren M., Noonan D.P., Darzi A., and yang G.Z, “The natural Orifice simulated surgical environment (NoSsE): exploring the challenges of NOTES without the animal model”, *Journal of Laparoendoscopic & Advanced Surgical Techniques*, Vol.19, pp.211-214, 2009.
- [37] Xu K., Goldman R.E., Ding J.N., Allen P.K., Fowler D.L., and Simaan N., “System Design of an insertable robotic effector platform for single port access (SPA) surgery”, *Proceedings of the 2009 IEEE International Conference on Robotics&Automation (ICRA)*, pp.5546-5552,2009.
- [38] Shang J.Z., Payne C.J., Clark J., Noonan D.P., Kwok K.W., Darzi A., and Yang G.Z., “Design of a multitasking robotic platform with flexible arms and articulated head for minimally head for minimally invasive surgery”, *Proceedings of the 2012 IEEE International Conference on Robotics&Automation (ICRA)*, pp.1988-1993,2012
- [39] Usgi medical®, [Online] <http://www.usgimedical.com/> (Accessed October, 2014).
- [40] Simaan N., Taylor R., Flint P., “A dexterous system for laryngeal surgery”, 2004 *IEEE ICRA*, pp.351-357, 2004.
- [41] Mahvash M., Zenati M., “Toward a hybrid snake robot for single-port surgery”, *IEEE EMBS*, pp.5372-5375, 2011.
- [42] Su H., Cardona D.C., Shang W., Camilo A., Cole G.A., Rucher D.C., Webster R.J., and Fischer G.S., “A MRI-guided concentric tube continuum robot with piezoelectric actuation: a feasibility study”, *Proceedings of the 2012 IEEE International Conference on Robotics&Automation (ICRA)*, pp.1939-1945, 2012
- [43] Alqahtani A., Albassam A., Zamakhshary M., Shoukri A., Altohkais T., Alzahim A.,

## Reference

---

- Mallik M., Alshehri A., “Robot-assisted pediatric surgery: how far can we go?”, *World J Surg.*, Vol.5, pp.975-978, 2010.
- [44] Russell W., David L., Thomas M.K., Craiq A., “Robot-assisted pediatric surgery”, *The American Journal of Surgery*, Vol.188, pp.27-37, 2004.
- [45] Hollands C.M., Dixey L.N., Torma M.J., “Technical assessment of porcine enteroenterostomy performed with ZEUS robotic technology”, *J Pediatr. Surg.*, Vol.36, pp.1231-1233, 2001.
- [46] Heller K., Cutt C., Schaeff B., Beyer P.A., Markus B., “Use of the robot system da Vinci for laparoscopic repair of gastroesophageal reflux in children”, *Eur J Pediatr Surg*, Vol 12, pp.239-242, 2002.
- [47] Ballantne G.H., Moll F.,”The da Vinci telerobotic surgical system: the virtual operative field and telepresence surgery”, *Surg Clin North Am*, Vol.83, pp.1293-1304, 2003.
- [48] Goedeke van H., Susan L., Winifred H., “pediatric robotic surgery: early assessment”, *Pediatrics*, Vol.124, pp.1642-1649, 2009.
- [49] Lanfranco AR, Castellanos AE, Desai JP, Mayers WC. Robotic surgery: a current perspective. *Ann Surg*, Vol.239,pp.14–21, 2004.
- [50] Yee D.S. Shanberg A.M., Duel B.P., Rodriguez E., Eichel L., Rajpoot D., “Initial comparison of robotic-assisted laparoscopic versus open pyeloplasty in children”, *Urology*, Vol.67, pp.599-602, 2006.
- [51] Jacob B.P., Gagner M., “Robotics and general surgery”, *Surg Clin North Am*, Vol.83, pp.1405-1419, 2003.
- [52] Menon M., Shrivastava A., Tewari A., “Laparoscopic and robot assisted radical prostatectomy: establishment of a structured program and preliminary analysis of outcomes”, *J Urol*, Vol.168, pp.945-949, 2002.

- 
- [53] Lee R.S., Retik A.B., Borer J.G., Peters C.A., “Pediatric robot assisted laparoscopic dismembered pyeloplasty: comparison with a cohort of open surgery”, *J Urology*, Vol.175, pp.683-687, 2006.
- [54] Lehnet M., Richter B., Beyer P.A., Heller K., “A prospective study comparing operative time in conventional laparoscopic and robotically assisted that semifundoplication in children”, *J Pediatr Surg.*, Vol.41, pp.1392-1396, 2006.
- [55] Franco I., Dyer L.L., Zelkovic P., “Laparoscopic pyeloplasty in the pediatric patient: hand sewn anastomosis versus robotic assisted anastomosis-is there a difference?”, *J Urology*, Vol.178, pp.1483-1486, 2007.
- [56] Todd D., Carlos G., James A., “Pediatric applications of robotic surgery”, *Pediatric Endosurgery & Innovative Techniques*, Vol.7, pp. 377-384, 2003.
- [57] Volfson I.A., Munver R., Esposito M., Dakwar G., Hanna M., Stock J.A., “Robot-assisted urologic surgery: safety and feasibility in the pediatric population”, *J Endourol*, Vol.21, pp.1315-1318, 2007.
- [58] Clark D.C., “Esophageal atresia and tracheoesophageal fistula”, *Am Fam Physician*, Vol.59, pp.910-916, 1999.
- [59] Kunisaki S.M., Foker J.E., "Surgical advances in the fetus and neonate: esophageal atresia", *Clinics in perinatology*, Vol.39, pp. 349-361, 2012.
- [60] Seitz G., Warmann S.W., Schaefer J., Poets C.F., Fuchs J., “Primary repair of esophageal atresia in extremely low birth weight infants: a single-center experience and review of the literature”, *Biol Neonate*, Vol.90, pp.247-251, 2006.
- [61] Castilloux J., Noble A.J., Faure C., “Risk factors for short and long-term morbidity in children with esophageal atresia”, *J of Pediatric*, Vol.156, pp.755-760, 2010
- [62] Seo J., Kim D.Y., Kim A.R., Kim D.Y., Kim S.C., Kim I.K., Kim K.S., Yoon C.H., Pi S.Y., “An 18-year experience of tracheoesophageal fistula and esophageal atresia”,

- Korean J. Pediatr.*, Vol.53, pp.705-710, 2010.
- [63]Huelke D.F., “An overview of anatomical considerations of infants and children in the adult world of automobile safety design”, *Annu Proc Assoc Adv Automot Med.*, Vol.42, pp.93-113, 1998.
- [64]Pinheiro P.F., Silva A.C.S., Pereira, “Current knowledge on esophageal atresia”, *W J of Gastr.*, pp.3662-3672, 2012.
- [65]Atkins H.J.B., “Peraxillary approach to the stellate and upper thoracic ganglia”, *Lancet*, vol.2, pp.1152, 1949.
- [66]Siciliano B., “Kinematic control of redundant robot manipulators: a tutorial”, *Journal of Intelligent and Robotic Systems*, Vol.3, pp.201-212,1990.
- [67]Maciejewski A.A., Klein C.A., “Obstacle avoidance for kinematically redundant manipulators in dynamically varying environments”, *the International Journal of Robotics Research*, Vol.4,pp.109-116, 1985.
- [68]Baillieul J., “Kinematic programming alternatives for redundant manipulators”, *Proceedings of the 1985 IEEE International Conference on Robotics&Automation (ICRA)*, pp.722-728,1985
- [69]Mayorga R.V., “A singularities avoidance approach for the optimal local path generation of redundant manipulators”, *Proceedings of the 1988 IEEE International Conference on Robotics&Automation (ICRA)*, pp.49-54,1988.
- [70]Chevallereau C., Khalil W., “A new method for the solution of the inverse kinematics of redundant robots”, *Proceedings of the 1988 IEEE International Conference on Robotics&Automation (ICRA)*, pp.37-42,1988.
- [71]LIEGEOIS A., “Automatic supervisory control of the configuration and behavior of multibody mechanisms”, *IEEE Transactions of System, Man, and Cybernetics*, Vol.12, pp.868-871,1977.



- 
- [72]Dubey R.V., Euler J.A., Babcock S.M., “An efficient gradient projection optimization scheme for a seven-degree of freedom redundant robot with spherical wrist”, *Proceedings of the 1988 IEEE International Conference on Robotics&Automation (ICRA)*, pp.28-36,1988.
- [73]Hsu P., Hauser J., Sastry S., “Dynamic control of redundant manipulator”, *Proceedings of the 1988 IEEE International Conference on Robotics&Automation (ICRA)*, pp.183-187,1988.
- [74]Siciliano B., “Kinematic control of redundant robot manipulators: a tutorial”, *Journal of Intelligent and Robotic Systems*, Vol.3, pp.201-212, 1990.
- [75]Sciavicco L., Siciliano B., “A dynamic solution to the inverse kinematic problem for redundant manipulators”, *Proceedings of the 1987 IEEE International Conference on Robotics&Automation (ICRA)*, pp.1081-1087,1987.
- [76]Nakamura Y., Hanafusa H., Yoshikawa T., “Task-priority based redundancy control of robot manipulators”, *the International Journal of Robotics Research*, Vol.6, pp.3-15, 1987.
- [77]Baillieul J., “Avoiding obstacle and resolving kinematics redundancy”, *Proceedings of the 1986 IEEE International Conference on Robotics&Automation (ICRA)*, pp.1698-1704, 1986.
- [78]Ren J., Patel R.V., McIsaac K.A., Guiraudon G., Peters T.M., “Dynamic 3-D virtual fixtures for minimally invasive beating heart procedures”, *IEEE transactions on medical image*, Vol.27,pp.1061-1070,2008.
- [79]Gilbert E.G., Johnson D.W., Keerthi S.S., “A fast procedure for computing the distance between complex objects in three –dimensional space”, *IEEE Journal of robotics and automation*, Vol.4, pp.193-203, 1988.
- [80]Mirtich B., “V-clip: fast and robust polyhedral collision detection”, *ACM Trans. Graph.*, Vol.17, pp.177-208.

- [81] Kwok K.W., Tsoi K.H., Vitiello V., Clart J., Chow G.C.T., Luk W., Yang G.Z., “Dimensionality reduction in controlling articulated snake robot for endoscopy under dynamic active constraints”, *IEEE transactions on robotics*, Vol.29, pp.15-31, 2013.
- [82] Chakraborty N., Peng J.F., Akella S., Mitchell J.E., “Proximity queries between convex objects: an interior point approach for implicit surfaces”, *IEEE transactions on robotics*, Vol.24, pp.211-220, 2008.
- [83] Hashizume M., “Fundamental training for safe endoscopic surgery”, pp.95-98, 2005.
- [84] “The standard operations in pediatric surgery”, Medical view Co., Ltd.
- [85] Liu Q.Q., Kobayashi Y., Zhang B., Noguchi T., Takahashi Y., Nishio Y., Cao Y., Ieiri S., Toyoda K., Uemura M., Tomikawa M., Hashizume M., Fujie M.G., “Development of a smart surgical robot with bended forceps for infant congenital esophageal atresia surgery”, *Proceedings of the 2014 IEEE International Conference on Robotics & Automation (ICRA)*, pp.2430-2435, 2014.
- [86] Robot type [on line], <http://machinedesign.com/robotics/kinematics-and-dynamics-non-cartesian-actuators-and-robotics> (Accessed October, 2014)
- [87] Robot type [on line], <http://machinedesign.com/motion-control/difference-between-cartesian-six-axis-and-scara-robots> (Accessed December, 2014)
- [88] Robot type [on line], [http://www.robotics.org/content-detail.cfm/Industrial-Robotics-Industry-Insights/Scara-vs-Cartesian-Robots-Selecting-the-Right-Type-for-Your-Applications/content\\_id/1001](http://www.robotics.org/content-detail.cfm/Industrial-Robotics-Industry-Insights/Scara-vs-Cartesian-Robots-Selecting-the-Right-Type-for-Your-Applications/content_id/1001) (Accessed December, 2014)
- [89] Robot type [on line], <http://www.used-robots.com/articles/viewing/the-advantages-and-disadvantages-of-scara-material-handling-robots> (Accessed December, 2014)
- [90] Maxon motor [on line], <http://www.maxonjapan.co.jp/maxon/view/content/brushless-dc-motors-overview> (Accessed November, 2014)

- [91] Harmonic reduction [on line], [https://www.mekasys.jp/detail.php?sid=CS\\_0002&type=maker&tab=UL-54760000&page=1&grp=&narrow=&#spec](https://www.mekasys.jp/detail.php?sid=CS_0002&type=maker&tab=UL-54760000&page=1&grp=&narrow=&#spec) (Accessed November, 2014)
- [92] Liu Q.Q., Kobayashi Y., Noguchi T., Inko E., Sekiguchi Y., Zhang B., Ye J., Toyoda K., Hashizume M., Fujie M.G., “Development of a 6-DOF manipulator driven by flexible shaft for minimally invasive surgical application”, *35<sup>th</sup> Annual International Conference of the IEEE EMBS*, pp.6261-6264, 2013.
- [93] Kobayashi Y., Sekiguchi Y., Noguchi T., Takahashi Y., Liu Q.Q., Susumu O., Toyoda K., Uemura M., Ieiri S., Tomikawa M., Ohdaira T., Hashizume M., Fujie M.G., “Development of a robotic system with six-degrees-of-freedom robotic tool manipulators for single-port surgery”, *The International Journal of Medical Robotics and Computer Assisted Surgery*, DOI:10.1002/rxs.1600, 2014.
- [94] Liu Q.Q., Kobayashi Y., Zhang B., Fujie M.G., “A novel smart surgical robotic system with eye-hand coordination for surgical assistance”, *IEEE international conference on system, man, and cybernetics (SMC)*, pp.1175-1180, 2014.
- [95] Kobayashi Y., Tomono Y., Sekiguchi Y., Watanabe H., Toyoda K., Konishi K., Tomikawa M., Ieiri S., Tanoue K., hashizume M., and Fujie M.G., “A surgical robot with vision field control for single port endoscopic surgery”, *Int. J. Med. Robotics Compute Assist Surg.*, Vol.6, pp.454-464, 2010.
- [96] Ishii C., Kobayashi K., “Development of a new bending mechanism and its application to robotic forceps manipulator”, *Proceedings of the IEEE International Conference on Robotics&Automation (ICRA)*, pp.238-243, 2007.
- [97] Sekiguchi Y., Kobayashi Y., Tomono Y., Watanabe H., Toyoda K., Konishi K., Tomikawa M., Ieiri S., Tanoue K., Hashizume M., Fujie M.G., “Development of a tool manipulator driven by a flexible for single port endoscopic surgery”, *Proceedings of the IEEE RAS&EMBS*, pp.120-125, 2010.

## Reference

---

- [98] Craig J.J., “Introduction to robotics: mechanics and control (3<sup>rd</sup> edition)”, Prentice Hall, 2004.
- [99] <http://www.ndigital.com/ndi-introduces-the-aurora-v3-electromagnetic-tracking-system/> (Accessed December, 2014).
- [100] Adams software [on line], <http://www.mscsoftware.com/ja/product/adams> (Accessed December, 2014)
- [101] Holder, M.K. What does Handedness have to do with Brain Lateralization (and who cares?). (Accessed December, 2014)
- [102] Annett M., “Handedness and Brain Asymmetry”, 2002.
- [103] “Why are more people right-handed?” <http://www.scientificamerican.com/article/why-are-more-people-right/> (Accessed September, 2014).
- [104] Chris M.. “Right Hand, Left Hand”. *Phoenix Paperbacks*, 2003.
- [105] <http://www.dentsable.com/haptic-phantom-omni.htm>. (Accessed September, 2014).

# Research Achievement

種別	題名	発表・発行掲載誌名	発表・発行年月	連名者
論文 (主著) ○	A Novel Smart Surgical Robotic System with Eye-hand Coordination for Surgical Assistance	2014 IEEE <i>International Conference on System, Man, and Cybernetics (SMC)</i> , pp.1175-1180.	2014年10月	<b><u>Q. Liu</u></b> , Y. Kobayashi, B. Zhang, M. G. Fujie
○	Development of a Smart Surgical Robot with Bended Forceps for Infant Congenital Esophageal Atresia Surgery	2014 IEEE <i>International Conference on Robotics and Automation (ICRA)</i> , pp. 2430-2435.	2014年5月	<b><u>Q. Liu</u></b> , Y. Kobayashi, B. Zhang, T. Noguchi, Y. Takahashi, Y. Cao, S. Ieiri, K. Toyoda, M. Uemura, M. Tomikawa, M. Hashizume, M.G. Fujie
	Design of an Insertable Surgical Robot with Multi-Level Endoscopic Control for Single Port Access Surgery	2013 IEEE <i>International Conference on Robotics and Biomimetics (ROBIO)</i> , pp.750-755.	2013年12月	<b><u>Q. Liu</u></b> , Y. Kobayashi, B. Zhang, J. Ye, E. Inko, Y. Cao, Y. Sekiguchi, Q. Cao, M. Hashizume, M. G. Fujie

Research Achievement

種別	題名	発表・発行掲載誌名	発表・発行年月	連名者
論文 (共著)	A Dexterous Manipulator for Single Port Access Surgery	<i>Proceeding of 9<sup>th</sup> Asian Conference on Computer Aided Surgery (ACCAS), 2013,</i> pp.102-103.	2013年9月	<b>Q.Liu,</b> Y. Kobayashi, B. Zhang, Y. Cao, J. Ye, Y. Sekiguchi, Q. Cao, M. Hashizume, M. G. Fujie
	Development of a 6-DOF Manipulator Driven by Flexible Shaft for Minimally Invasive Surgical Application	<i>2013 Annual International Conference of the IEEE EMBS,</i> pp. 6261-6264.	2013年7月	<b>Q. Liu,</b> Y. Kobayashi, T. Noguchi, E. Inko, Y. Sekiguchi, B. Zhang, J. Ye, K. Toyoda, M. Hashizume, M. G. Fujie
	Development of a Robotics System with Six Degrees of Freedom Robotic Tool Manipulators for Single Port Surgery	<i>The International Journal of Medical Robotics and Computer Assisted Surgery (IJMRCAS),</i> 2014, DOI:10.1002/rcs.1600	2014年5月	Y. Kobayashi, Y. Sekiguchi, T. Noguchi, Y. Takahashi, <b>Q. Liu,</b> S. Oguri, K. Toyoda, M. Uemura, S. Ieiri, M. Tomikawa, T. Ohdaira, m. Hashizume, M. G. Fujie
	Development of Endoscope Manipulator Control System Based on Movement of Pupils for Single Port Surgery Assist Robot	<i>The 14<sup>th</sup> SICE System Integration Division Annual Conference (SI),</i> pp.2275-2279.	2013年11月	Y. Cao, S. Miura, <b>Q. Liu,</b> y. Nishio, Y. Koreeda, Y. kobayashi, K. Kawamura, M.G. Fujie

種類別	題名	発表・発行掲載誌名	発表・発行年月	連名者
講演	Development of a Novel Gait Rehabilitation System Based on FES and Treadmill-Walk for Convalescent Hemiplegic Stroke Survivors	2013 <i>IEEE/RSJ International Conference on Intelligent Robots and Systems (IROS)</i> , pp.977-982.	2013年11月	J. Ye, Y. Nakashima, T. Watanabe, M. Seki, B. Zhang, <u>Q. Liu</u> , Y. Yokoo, Y. Kobayashi, Q. Cao, M. G. Fujie
	Development of a Novel FES Control System Based on Treadmill Motor current Variation for Gait Rehabilitation of Hemiplegic Patients after Stroke	2013 <i>13<sup>th</sup> International Conference on Control, Automation and System (ICCAS)</i> , pp.635-640.	2013年10月	J. Ye, Y. Nakashima, T. Watanabe, M. Seki, B. Zhang, <u>Q. Liu</u> , Y. Yokoo, Y. Kobayashi, Q. Cao, M. G. Fujie
	Research of the Minimally Invasive Surgical Robot System for Infant Congenital Esophageal Atresia	2012 <i>International Symposium on Micro-nano Systems for the Interaction of Young Researchers</i>	2012年11月	<u>Q. Liu</u> , Y. Kobayashi, M.G. Fujie
	Experience-based Surgical Training System	2012 <i>GMSI-GSISH International Winter School on Biomedical Engineering</i>	2012年3月	<u>Q. Liu</u> , Y. Kobayashi, M.G. Fujie

